frontiers | Research Topics

Bone metastasis in the milieu of osteoimmunology

Edited by
Jawed A. Siddiqui and Marco Ponzetti

Published in
Frontiers in Immunology
Frontiers in Oncology

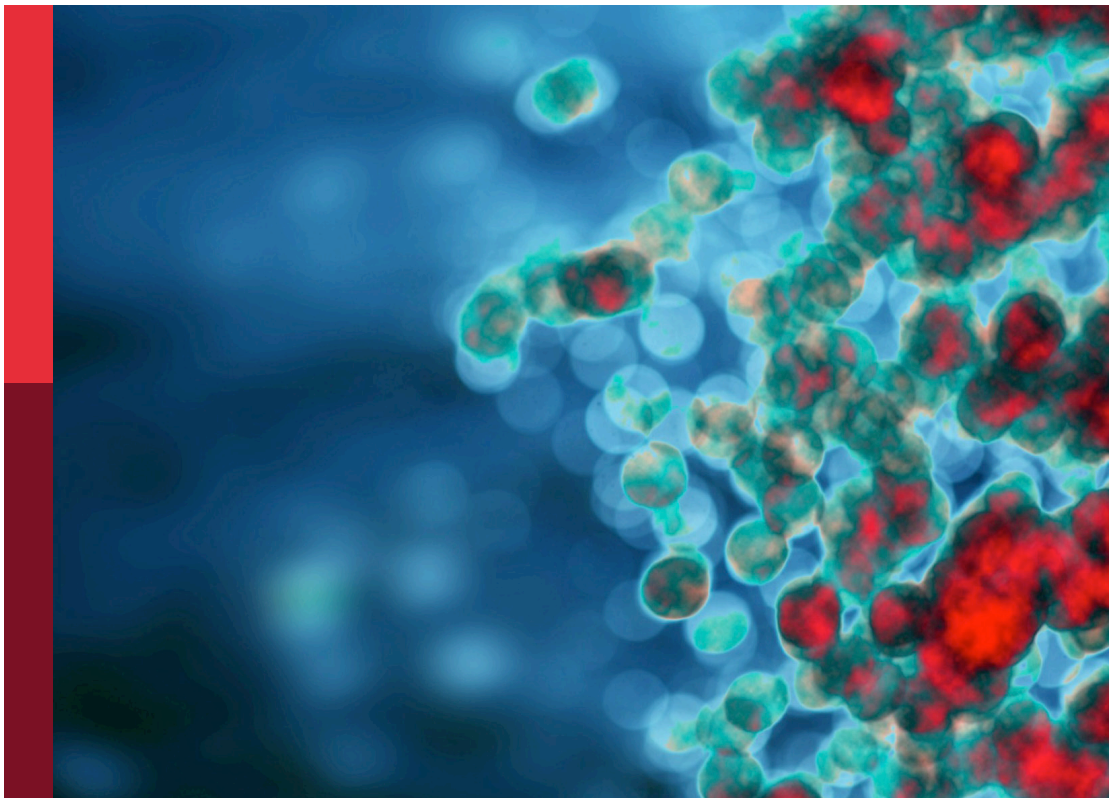

ISSN 1664-8714
ISBN 978-2-8325-3289-8
DOI 10.3389/978-2-8325-3289-8

About Frontiers

Frontiers is more than just an open access publisher of scholarly articles: it is a pioneering approach to the world of academia, radically improving the way scholarly research is managed. The grand vision of Frontiers is a world where all people have an equal opportunity to seek, share and generate knowledge. Frontiers provides immediate and permanent online open access to all its publications, but this alone is not enough to realize our grand goals.

Frontiers journal series

The Frontiers journal series is a multi-tier and interdisciplinary set of open-access, online journals, promising a paradigm shift from the current review, selection and dissemination processes in academic publishing. All Frontiers journals are driven by researchers for researchers; therefore, they constitute a service to the scholarly community. At the same time, the *Frontiers journal series* operates on a revolutionary invention, the tiered publishing system, initially addressing specific communities of scholars, and gradually climbing up to broader public understanding, thus serving the interests of the lay society, too.

Dedication to quality

Each Frontiers article is a landmark of the highest quality, thanks to genuinely collaborative interactions between authors and review editors, who include some of the world's best academicians. Research must be certified by peers before entering a stream of knowledge that may eventually reach the public - and shape society; therefore, Frontiers only applies the most rigorous and unbiased reviews. Frontiers revolutionizes research publishing by freely delivering the most outstanding research, evaluated with no bias from both the academic and social point of view. By applying the most advanced information technologies, Frontiers is catapulting scholarly publishing into a new generation.

What are Frontiers Research Topics?

Frontiers Research Topics are very popular trademarks of the *Frontiers journals series*: they are collections of at least ten articles, all centered on a particular subject. With their unique mix of varied contributions from Original Research to Review Articles, Frontiers Research Topics unify the most influential researchers, the latest key findings and historical advances in a hot research area.

Find out more on how to host your own Frontiers Research Topic or contribute to one as an author by contacting the Frontiers editorial office: frontiersin.org/about/contact

Bone metastasis in the milieu of osteoimmunology

Topic editors

Jawed A. Siddiqui — University of Nebraska Medical Center, United States

Marco Ponzetti — University of L'Aquila, Italy

Citation

Siddiqui, J. A., Ponzetti, M., eds. (2023). *Bone metastasis in the milieu of osteoimmunology*. Lausanne: Frontiers Media SA. doi: 10.3389/978-2-8325-3289-8

Table of contents

frontiers | Frontiers in Immunology

TYPE Editorial
PUBLISHED 07 August 2023
DOI 10.3389/fimmu.2023.1265434

OPEN ACCESS

EDITED AND REVIEWED BY
Dominique Heymann,
Institut de Cancérologie de l'Ouest, France

*CORRESPONDENCE
Jawed A. Siddiqui
jawed.siddiqui@unmc.edu

RECEIVED 22 July 2023
ACCEPTED 26 July 2023
PUBLISHED 07 August 2023

CITATION
Sharma G, Ponzetti M and Siddiqui JA (2023) Editorial: Bone metastasis in the milieu of osteoimmunology. *Front. Immunol.* 14:1265434. doi: 10.3389/fimmu.2023.1265434

Editorial: Bone metastasis in the milieu of osteoimmunology

Gunjan Sharma[1], Marco Ponzetti[2] and Jawed A. Siddiqui[1,3]*

[1]Department of Biochemistry and Molecular Biology, University of Nebraska Medical Center, Omaha, NE, United States, [2]Department of Biotechnological and Applied Clinical Sciences, University of L'Aquila, L'Aquila, Italy, [3]Fred and Pamela Buffett Cancer Center, University of Nebraska Medical Center, Omaha, NE, United States

KEYWORDS

bone metastasis, osteoimmunology, immune checkpoint inhibitor, osteosarcoma, tumor microenvironment (TME)

Editorial on the Research Topic
Bone metastasis in the milieu of osteoimmunology

Bone metastasis severely hampers the survival of advanced cancer patients, and the nature of treatments is generally restricted to primary tumors. The mechanisms causing this discrepancy between therapy effectiveness in the different sites depend on several factors, a crucial one being the microenvironment. In particular, a pivotal role of the immune system has emerged in the last few years. However, despite great advances in the field, there is still much to be done to understand and exploit the immunological side of bone metastases to fight cancer. This prompted us to initiate this Research Topic entitled "*Bone metastasis in the milieu of Osteoimmunology*" to understand more about cancer and various immune aspects in the bone microenvironment (Figure 1). A total of nine articles were published in this Research Topic, including five original research papers (Talbot et al., Li et al., Yang et al., Guo et al., and Chang et al.), three review articles (Yu et al., Tong et al., and Kähkönen et al.), and one case report (Asano et al.). One original research and one review article containing B7-H3-CAR T Cells, Cuproptosis-related lncRNA, cancer stem cell-related genes, and chemoresistance in turn of immune modulation in osteosarcoma (OS). One research and one review article deal with the drug repurposing and interleukin-1 family in prostate cancer bone metastases. Two more articles, one original research, and one case report, have been included in the topic; both studies are associated with immunotherapy in bone-metastatic patients with advanced non-small cell lung cancer and renal cell carcinoma.

Innovative technologies and ideas are leveraging the advancement of our knowledge, specifically cancer and osteoimmunological aspects in the bone microenvironment. Talbot et al. study equipped with a novel orthotopic (tibial osteotomy) implantation procedure for OS cells where B7-H3, an immune regulatory protein, crucially participates in spontaneous metastasis. B7-H3 targeted Chimeric antigen receptor-T (CAR-T) cells (injected via tail vein) therapy reduces the tumor burden and metastatic spread to the lungs, thenceforth enhancing the survival of NOD scid gamma mouse (NSG) mice. Another original research by Yang et al. included in this Research Topic is based on the long noncoding (lnc) RNA link to novel copper-mediated cell death (cuproptosis) in the prognosis of OS. This article aims to correlate the status of cuproptosis-related lncRNAs (CRLncs) with the survival outcomes of OS patients. Analysis of OS transcriptome and clinical dataset from The

Cancer Genome Atlas (TCGA) revealed three high-risk CRLncs and three low-risk CRLncs involved in OS prognosis and immune microenvironment. In a drug-sensitive study, authors found four potent drugs: AUY922, bortezomib, and Z.LLNle.CHO is sensitive to low-risk and lenalidomide for the high-risk OS group.

Furthermore, Guo et al., by using consensus clustering analysis, identified 25 cancer stem cell-related genes and classified OS into three (CSC cluster A, B, and C) molecular subtypes. Among 25 CSC-related genes, authors emphasized MEF2C as a significant player in immune infiltration and tumor cell stemness which correlated with patient survival. A recent study in bladder cancer also revealed MEF2C as a prognostic factor and putative role in immune modulation (1). Moreover, the authors established a unique CSC scoring system that could be beneficial in assessing tumor-microenvironment (TME) immune infiltration and for personalized immunotherapy of OS patients.

The role of chemokines and cytokines is highly correlated with tissue-specific tropism, niche formation, and colonization of cancer cells (2). However, interleukins (ILs) are well known for the inflammatory response in various diseases and tumor microenvironments. Tong et al. highlight the pivotal role of the IL-1 family in prostate cancer (PCa) progression and bone metastasis. As PCa exhibits the highest incidence of bone metastasis, authors attractively connect IL-1 family-mediated inflammation with PCa bone metastasis progression. They have covered several ILs' functions as anti- and pro-tumorigenic activity. Additionally, the authors provide a glimpse of ILs' diverse role in colonization, dormancy, reactivation, angiogenesis, and bone remodeling. In a transcriptome-based multiplex drug repurposing study, Chang et al. validated a new scheme to screen specific candidate compounds to prevent bone metastasis of castration resistance prostate cancer (CRPC) patients. After a battery of

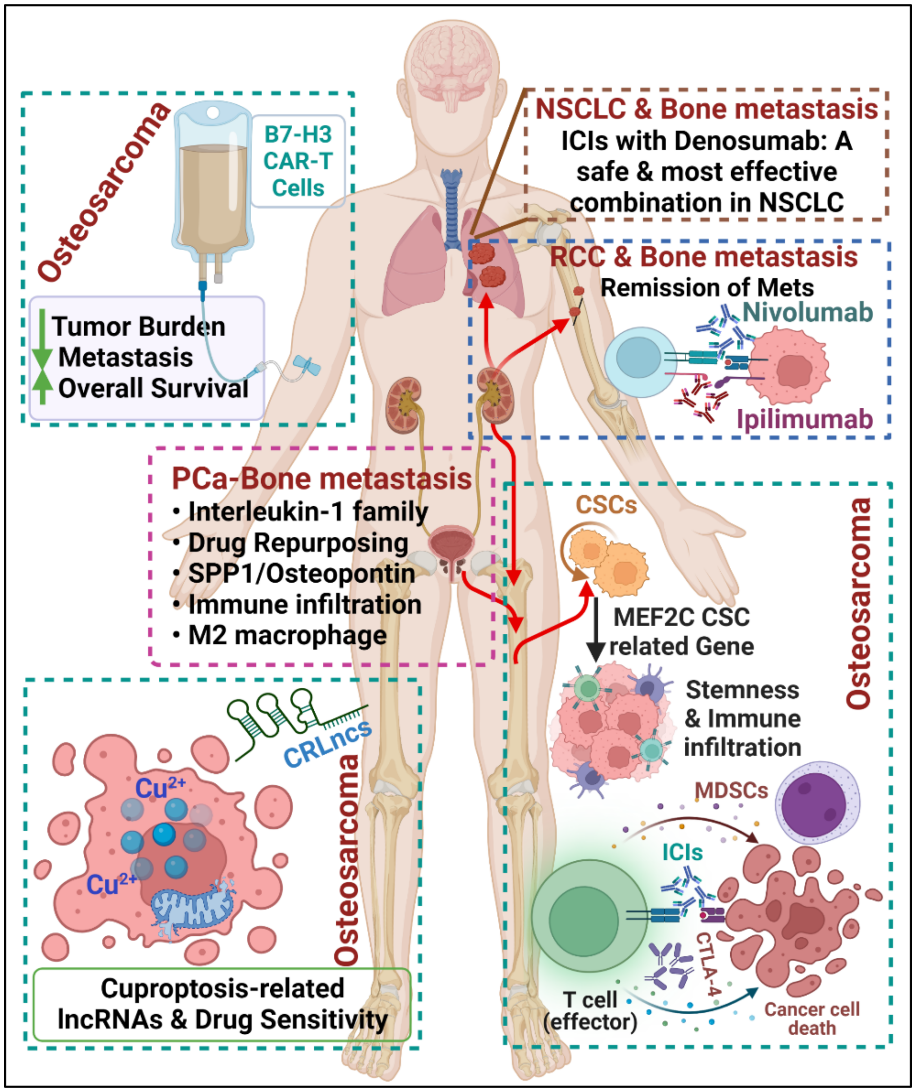

FIGURE 1
Cartoon summarizing the contributions submitted to the Research Topic, including osteosarcoma and bone metastasis in PCa, NSCLC, and RCC, showing a multidisciplinary approach, attractive osteoimmunological targets, and therapeutic outcomes in preclinical and clinical settings. (Created with biorender.com).

comprehensive analysis, two compounds, namely CID 190453/mulberroside C and CID 78177919/terrestrosin D, show selective and potent binding with Secreted phosphoprotein 1 (SPP1), also known as Osteopontin, that can regulate the M2 macrophage-associated PCa-bone metastatic genes. Elevated expression of SPP1 is highly correlated with immune cell infiltration and poor survival in various cancers (3).

Li et al. performed a study on 171 non-small cell lung cancer (NSCLC)-bone metastatic patients and categorized them into four groups. Among all groups, DI, i.e., patients receiving a combination of denosumab with immune checkpoint inhibitors (ICIs), reveals safe, highest drug efficacy and survival of bone metastatic NSCLC patients with minimal side effects. Recently, in a clinical trial, dostarlimab, an anti–PD-1 monoclonal antibody, showed complete remission in all advanced rectal carcinoma patients (4).

In a series of therapeutic efficacy of ICIs against bone metastasis, Yu et al. summarize the recent studies on various mechanisms of chemoresistance and vulnerable targets, including myeloid-derived suppressor cells (MDSCs). In this review, authors emphasize the status of different immunotherapeutic targets such as programmed death-ligands/receptors (PD-1/PD-L1) and cytotoxic T lymphocyte-associated protein 4 (CTLA-4) and clinical trials of ICIs for OS patients. Similarly, a case report by Asano et al. demonstrates that the combination of neutralizing antibodies (nivolumab for PD-1 and ipilimumab for CTLA-4) attenuates bone metastasis in a renal cell carcinoma (RCC) patient. A fracture in the humerus diaphysis with osteolytic changes due to bone metastasis and lung metastasis. No sign of tumor or metastasis in the histopathological examination after four courses of ICIs treatment.

As a primary goal of this Research Topic to improve knowledge and significant advancement of bone metastasis in osteoimmunology, Kähkönen et al. summarize and short-listed 24 anti-bone metastatic therapies by utilizing a novel 1stOncology database based on osteoimmuno-oncology (OIO) concept. This OIO approach deals with the interaction patterns between cancer, bone, and immune cells. Twenty drugs were short-listed from 1498 for breast cancer and 746 for prostate cancer. The authors provide an innovative approach and robust platform to identify therapies for immune activation and prevention or attenuation of bone metastasis in breast and prostate cancer.

Simultaneously, the collection of articles in this Research Topic splendidly adds novel procedures, attractive targets, and ideas to combat bone metastasis in the milieu of Osteoimmunology. Indeed, this Research Topic will improve our knowledge of bone metastasis and related events in various cancers.

Author contributions

JS: Funding acquisition, Supervision, Writing – original draft, Writing – review & editing. GS: Writing – original draft, Writing – review & editing. MP: Writing – review & editing.

Funding

This work and the authors are, in part, supported by grants from the U.S. Department of Defense (DOD) through the Prostate Cancer Research Program under Award No. W81XWH-21-1-0640 and Fred & Pamela Buffett Cancer Center (FPBCC) Support Grant (P30 CA036727) to JS.

Conflict of interest

Author MP is employed by the company Novo Nordisk.

The remaining authors declare that the research was conducted in the absence of any commercial or financial relationships that could be construed as a potential conflict of interest.

The authors declared that they were an editorial board member of Frontiers, at the time of submission. This had no impact on the peer review process and the final decision.

Publisher's note

References

1. Zhu J, Wang H, Ma T, He Y, Shen M, Song W, et al. Identification of immune-related genes as prognostic factors in bladder cancer. *Sci Rep* (2020) 10(1):19695. doi: 10.1038/s41598-020-76688-w

2. Sharma G, Pothuraju R, Kanchan RK, Batra SK, Siddiqui JA. Chemokines network in bone metastasis: Vital regulators of seeding and soiling. *Semin Cancer Biol* (2022) 86(Pt 3):457–72. doi: 10.1016/j.semcancer.2022.02.003

3. Wei T, Bi G, Bian Y, Ruan S, Yuan G, Xie H, et al. The significance of secreted phosphoprotein 1 in multiple human cancers. *Front Mol Biosci* (2020) 7:565383. doi: 10.3389/fmolb.2020.565383

4. Cercek A, Lumish M, Sinopoli J, Weiss J, Shia J, Lamendola-Essel M, et al. PD-1 blockade in mismatch repair-deficient, locally advanced rectal cancer. *N Engl J Med* (2022) 386(25):2363–76. doi: 10.1056/NEJMoa2201445

frontiers in Immunology

ORIGINAL RESEARCH
published: 15 June 2021
doi: 10.3389/fimmu.2021.691741

A Novel Orthotopic Implantation Technique for Osteosarcoma Produces Spontaneous Metastases and Illustrates Dose-Dependent Efficacy of B7-H3-CAR T Cells

Lindsay Jones Talbot[1], Ashley Chabot[1], Amy Funk[2], Phuong Nguyen[3], Jessica Wagner[3], Aaron Ross[4], Heather Tillman[5], Andrew Davidoff[1], Stephen Gottschalk[3] and Christopher DeRenzo[3]*

[1] Department of Surgery, St. Jude Children's Research Hospital, Memphis, TN, United States, [2] Department of Veterinary Medicine, St. Jude Children's Research Hospital, Memphis, TN, United States, [3] Department of Bone Marrow Transplant and Cellular Therapy, St. Jude Children's Research Hospital, Memphis, TN, United States, [4] University of Tennessee Health Sciences School of Medicine, Memphis, TN, United States, [5] Department of Pathology, St. Jude Children's Research Hospital, Memphis, TN, United States

OPEN ACCESS

Edited by:
Manel Juan, Hospital Clínic de Barcelona, Spain

Reviewed by:
Cristina Eguizabal, Biocruces Bizkaia Health Research Institute, Spain
Marta Maria Alonso, University Clinic of Navarra, Spain

***Correspondence:**
Lindsay Jones Talbot
lindsay.talbot@stjude.org

Specialty section:
This article was submitted to Cancer Immunity and Immunotherapy, a section of the journal Frontiers in Immunology

Received: *07 April 2021*
Accepted: *24 May 2021*
Published: *15 June 2021*

Citation:
Talbot LJ, Chabot A, Funk A, Nguyen P, Wagner J, Ross A, Tillman H, Davidoff A, Gottschalk S and DeRenzo C (2021) A Novel Orthotopic Implantation Technique for Osteosarcoma Produces Spontaneous Metastases and Illustrates Dose-Dependent Efficacy of B7-H3-CAR T Cells. Front. Immunol. 12:691741. doi: 10.3389/fimmu.2021.691741

The outcome for metastatic pediatric osteosarcoma (OS) remains poor. Thus, there is an urgent need to develop novel therapies, and immunotherapy with CAR T cells has the potential to meet this challenge. However, there is a lack of preclinical models that mimic salient features of human disease including reliable development of metastatic disease post orthotopic OS cell injection. To overcome this roadblock, and also enable real-time imaging of metastatic disease, we took advantage of LM7 OS cells expressing firefly luciferase (LM7.ffLuc). LM7.ffLuc were implanted in a collagen mesh into the tibia of mice, and mice reliably developed orthotopic tumors and lung metastases as judged by bioluminescence imaging and histopathological analysis. Intratibial implantation also enabled surgical removal by lower leg amputation and monitoring for metastases development post-surgery. We then used this model to evaluate the antitumor activity of CAR T cells targeting B7-H3, an antigen that is expressed in a broad range of solid tumors including OS. B7-H3-CAR T cells had potent antitumor activity in a dose-dependent manner and inhibited the development of pulmonary metastases resulting in a significant survival advantage. In contrast T cells expressing an inactive B7-H3-CAR had no antitumor activity. Using unmodified LM7 cells also enabled us to demonstrate that B7-H3-CAR T cells traffic to orthotopic tumor sites. Hence, we have developed an orthotopic, spontaneously metastasizing OS model. This model may improve our ability not only to predict the safety and efficacy of current and next generation CAR T cell therapies but also other treatment modalities for metastatic OS.

Keywords: osteosarcoma, orthotopic, model, CAR, T cell therapy, B7-H3

INTRODUCTION

Osteosarcoma (OS) is the most common tumor of bone in children and adolescents, and the third most common solid tumor encountered in this age group. While great success has been achieved with local control modalities over the last thirty years, resulting in a survival rate from primary OS of approximately 60 – 75% depending on histologic response, the treatment of recurrent and metastatic disease remains less effective (1–3). This is in part due to a lack of highly relevant pre-clinical models (4), prohibiting the realistic screening and modeling of therapeutic approaches.

Current preclinical orthotopic models of OS have varying success in reproducing clinically relevant metastatic processes, which include escape from the primary tumor, navigation of stromal interactions, bloodstream entry, vascular arrest, extravasation, and establishment of a pro-tumorigenic microenvironment in the metastatic niche (5–7). Limitations of current models include a low rate of systemic or pulmonary metastasis in subcutaneous and fragment-implantation models, and inadvertent seeding of the pulmonary vasculature with tumor cells after marrow-cavity orthotopic injections. These models, while contributing substantially to the preclinical literature in OS, either do not reliably recapitulate the clinical metastatic process or have lower rates of metastasis that hamper feasibility of use.

Here, we developed a novel spontaneously metastasizing orthotopic OS model and explored its utility to evaluate the efficacy of chimeric antigen receptor (CAR) T cells. CAR T cell therapy has shown considerable preclinical promise in pediatric sarcoma models (8–12). However, while early clinical trials have demonstrated feasibility and safety, clinical responses have thus far been disappointing, highlighting the need to ensure that preclinical models mimic the clinical setting while maintaining feasibility (12–14).

We show that collagen-tumor cell scaffolds surgically implanted into the tibia of mice reliably produced local and systemic metastatic OS. Likewise, we demonstrate that CAR T cells targeting B7-H3, a tumor antigen that is expressed in a high percent of OS (15–17), have antitumor activity in a dose dependent fashion against primary and metastatic OS. Thus, the described model should be highly relevant for the preclinical evaluation and optimization of cell-based immunotherapies.

MATERIALS AND METHODS

Cell Lines

The OS cell line LM7, a derivative of SaOS-2, was kindly provided by Dr. Eugenie Kleinerman (MD Anderson Cancer Center, Houston, TX, USA) (18). LM7 cells expressing green fluorescent protein (GFP) and firefly luciferase (ffluc) (LM7.ffluc) previously generated in our laboratory were used for all experiments (15). LM7 was grown in DMEM (GE Healthcare, Marlborough, MA, USA) supplemented with 10% fetal bovine serum (GE Healthcare) and 1% Glutamax (Thermo Fisher Scientific, Waltham, MA, USA). Cell subculture was performed by detaching adherent cells using 0.05% trypsin-EDTA (Thermo Fisher Scientific). BV173 leukemic cells (German Collection of Microorganisms and Cell Cultures, Braunschweig, Germany) were cultured in RPMI (GE Healthcare) supplemented with 10% fetal bovine serum and 1% Glutamax. All cells were maintained at 37°C in 5% CO_2. Cell lines were authenticated by STR profiling and checked routinely while in culture for mycoplasma using the MycoAlert mycoplasma detection kit (Lonza).

Generation of B7-H3-CAR and Control Lentiviral Vectors

The lentiviral vectors encoding B7-H3.CD8α.CD28ζ and B7-H3.CD8α.Δ (nonsignaling control) CARs were previously described (15). VSVG-pseudotyped lentiviral particles were produced by St. Jude Children's Research Hospital Vector Core as previously described (19).

Generation of B7-H3-CAR and Control CAR T Cells

Human peripheral blood mononuclear cells (PBMCs) were obtained from whole blood of healthy donors under an Institutional Review Board (IRB)-approved protocol at St. Jude Children's Research Hospital after informed written consent was obtained in accordance with the Declaration of Helsinki. The generation of CAR T cells was previously described (15). Briefly PBMCs were isolated by Lymphoprep (Abbott Laboratories, Abbott Park, IL, USA) gradient centrifugation. On day -1, CD4+ and CD8+ T cells were enriched from PBMCs by immunomagnetic separation using CD4 and CD8 microbeads (Miltenyi, Germany), an LS column (Miltenyi), and a MidiMACS separator (Miltenyi). Enriched T cells were resuspended at 1 x 10^6 cells/mL in RPMI 1640 (GE Healthcare) supplemented with 10% FBS (GE Healthcare), 1% GlutaMAX (Thermo Fisher Scientific), and cytokines IL7 and IL15 (10 ng/mL each) (Biological Resources Branch, National Cancer Institute, Frederick, MD, USA, and PeproTech, Rocky Hill, NJ, USA) and stimulated overnight on 24-well non-tissue-culture treated plates that were precoated with CD3 and CD28 antibodies (Miltenyi). Transduction was performed on day 0 by adding LV particles at an MOI of 50 TU/cell and protamine sulfate at 4 μg/mL. On day 3, T cells were transferred into new 24-well tissue culture treated plates and subsequently expanded with IL7 and IL15 (10 ng/mL each). All experiments were performed 7 – 14 days post-transduction. Biological replicates were performed using PBMCs from different healthy donors.

Flow Cytometry

A FACSCanto II (BD Biosciences) instrument was used to acquire flow cytometry data, which was analyzed using FlowJo v10.7 (BD Biosciences). For surface staining, samples were washed with and stained in PBS (Lonza) with 1% FBS (GE Healthcare). For all experiments, matched isotypes or known negatives (e.g. nontransduced T cells or B7-H3-negative cell lines) served as gating controls. CAR detection was performed

using F(ab')$_2$ fragment-specific antibody (polyclonal, Jackson ImmunoResearch, West Grove, PA, USA). T cells were stained with fluorochrome-conjugated antibodies using combinations of the following markers: CD4 (clone SK3, BD Biosciences), CD8 (clone SK1, BD Biosciences), CCR7 (clone G043H7, BioLegend, San Diego, CA, USA), and CD45RO (clone UCHL1, BD Biosciences). LM7 and the negative control leukemia cell line BV173 were evaluated for expression of B7-H3 using B7-H3 antibody (clone 7-517, BD Biosciences, or clone FM276, Miltenyi). Cells were additionally stained with DAPI (BD Biosciences) to gate for live cells.

Analysis of Cytokine Production

T cells were cultured alone or with LM7 tumor cells at a 1:1 effector to target ratio without the provision of exogenous cytokines. Approximately 24 hours after coculture initiation, supernatant was collected and frozen for later analysis. Production of IFNγ and IL2 was measured using a quantitative ELISA per the manufacturer's instructions (R&D Systems, Minneapolis, MN, USA).

Antigen-Stimulated Expansion Assay

T cells were cultured alone or with LM7 tumor cells at a 1:1 effector to target ratio without the provision of exogenous cytokines. Approximately 72 hours after coculture initiation, T cells were removed from coculture and replated in fresh complete media. Following 4 additional days of culture, T cells were counted and fold change from baseline was calculated.

Cytotoxicity Assay

The xCELLigence real-time cell analyzer (RTCA) MP instrument (Agilent Technologies, Santa Clara, CA, USA) was used to assess CAR T cell cytotoxicity. All assays were performed in triplicate and without the addition of exogenous cytokines. First, 30,000 LM7 cells in complete RPMI were added to each well of a 96-well E-plate (Agilent). After LM7 cells adhered to the E-plate for approximately 24 hours and reached a cell index (relative cell impedance) plateau, 150,000 T cells in complete RPMI were added. LM7 cells alone served as a tumor only control and LM7 cells in DMSO served as a full lysis control. The cell index was monitored every 15 minutes for 24 hours and normalized to the maximum cell index value immediately prior to T cell plating. Percent cytotoxicity was calculated using the RTCA Software Pro immunotherapy module (Agilent) (20).

Orthotopic Modeling Technique

Mice

Eight-week-old, female, NSG (NOD.*Cg-PrkdcscidIl2rgtm1Wjl*/SzJ) mice were purchased from The Jackson Laboratory (Bar Harbor, ME, USA), with all animal procedures reviewed and approved by the St. Jude Children's Research Hospital Institutional Animal Care and Use Committee. Mice underwent orthotopic tibial implantation as described below and were followed by weekly bioluminescence. They underwent hindlimb amputation when they reached a humane endpoint that included lameness, large tumor burden interfering with the animal's ability to reach food or water, significant tumor ulceration, guarding behavior, or upon becoming moribund. After hindlimb amputation, mice were followed with weekly bioluminescence imaging until they reached a total body bioluminescent flux of 1 x 10^{10} photons or if other endpoints were seen such as persistent poor grooming or lethargy; > 20% body weight loss post-amputation, respiratory difficulty or upon becoming moribund.

Tibial Implants

LM7.ffluc cells were harvested at confluence and pelleted by centrifugation. 5X collagen neutralization buffer was prepared by mixing 2.5 g minimum essential media (MEM) alpha powder without nucleosides (Thermo Fisher Scientific, Waltham, MA) and 2% wt/vol $NaHCO_3$ in 45 ml demineralized water, adding 5 ml of 1 M HEPES (Thermo Fisher Scientific, Waltham, MA), and filtering through a 0.22 μm filter. Neutralized high-concentration type I rat-tail collagen was prepared fresh by mixing high-concentration rat tail collagen I (Corning, New York, USA; concentration range 8 – 11 mg/ml) and 5X collagen neutralization buffer in a 5:1 vol/vol ratio on ice. LM7 cells were then resuspended in neutralized high-concentration collagen at 1 x 10^6 cells per 10 μL collagen, taking care to maintain reagents and pelleted cells on ice during resuspension process and pipetting using wide-bore pipette tips. Once resuspended, cell mixture was pulse-vortexed and pulse-centrifuged for < 5 seconds to disrupt bubbling in mixture. Cells were then plated for individual implants at 10 μL cell mixture per well in a 96-well ultra-low-attachment round-bottom plate (Corning, NY, USA) and allowed to solidify at 37°C in 5% CO_2 for 20 minutes. DMEM supplemented with 10% fetal bovine serum and 1% Glutamax was then added and implants allowed to mature overnight at 37°C in 5% CO_2. The collagen preparation and neutralization protocol described above is as that previously described (21).

Orthotopic Implantation

Prior to beginning the implantation procedure, mice are anesthetized using inhaled isoflurane at a MAC of 2, depilated, and the right hindlimb prepped from the inguinal area to the paw using 70% alcohol and chlorhexidine solution. Multimodal analgesia was administered both preemptively with meloxicam 5 mg/mL (Boehringer Ingelheim, St. Joseph, MO), subcutaneously at 1 mg/kg and post-operatively with buprenorphine 0.03 mg/mL (Patterson Veterinary, Greeley, CO), subcutaneously at 0.1 mg/kg. The mouse is placed in dorsal recumbency with the right hindfoot gently grasped while flexing the knee. A 5 mm skin incision is made proximal to the patella (**Figure 1A**) and retracted using gentle traction below the patella to expose the proximal anterior tibia (**Figure 1B**). The musculature and soft tissue are gently dissected away from the anterior tibia using a fine hemostat (**Figure 1C**; Fine Science Tools, Foster City, CA, USA). Once cleared of soft tissue, a 2 mm fragment of anterior tibial cortical bone is removed using a 2 mm sharp Rongeur (**Figures 1D, E**; Fine Science Tools). Care is taken to avoid the inferior patellar tendon and to avoid significant entry into the marrow cavity or tibial fracture. An LM7 collagen implant (**Figure 1F**) is then grasped with forceps and placed gently into the cavity left at the

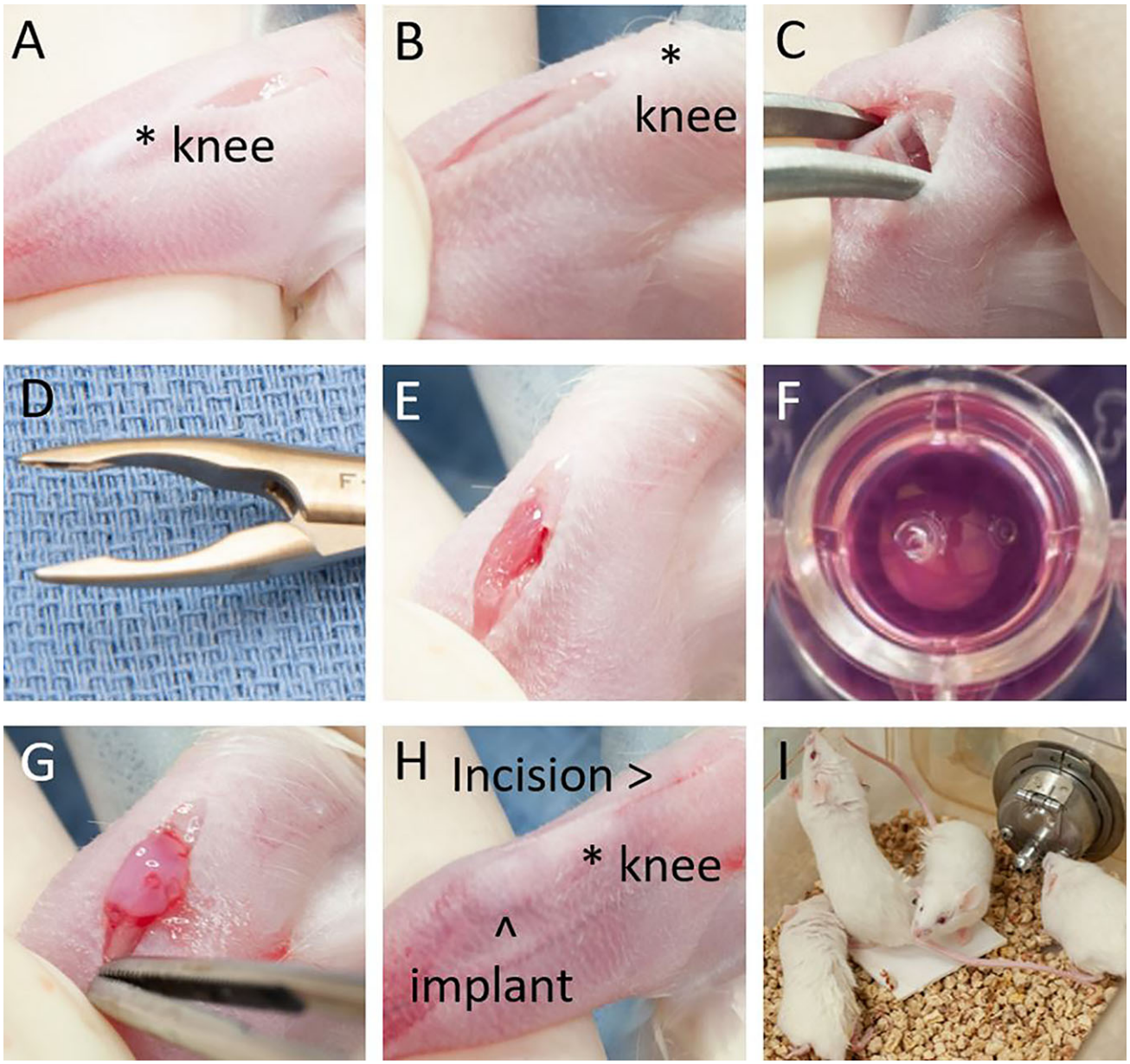

FIGURE 1 | Tibial osteotomy implantation procedure. **(A)** Incision is made over distal femur. **(B)** Incision retracted distally to expose anterior tibia. **(C)** Soft tissue dissected away from anterior tibia. **(D)** 2 mm tip Rongeur used for osteotomy. **(E)** Tibial osteotomy. **(F)** LM7-collagen implant. **(G)** Implant in place over osteotomy. **(H)** Final position of implant and incision. **(I)** Mice demonstrating exploration and weight bearing behavior minutes after anesthesia emergence.

osteotomy site (**Figure 1G**). The distal aspect of the skin incision is then gently raised over the implant and the incision allowed to recoil back to its original position proximal to the patella, leaving the implant secured in place by intact skin (**Figure 1H**). Gentle pressure is applied to ensure hemostasis and implant adherence to the bony surface. The skin incision is closed with Vetbond® surgical glue (3M Animal Care Products, St. Paul, MN). Mice are monitored through until completely recovered from anesthesia (**Figure 1I**), with the entire procedure from incision to closure taking 2 – 5 minutes to perform.

Hindlimb Amputation

Mice are anesthetized with surgical prep performed from the right hindlimb to the umbilicus. Preemptive analgesia is administered as described above and a 1 mL bolus of sterile saline is administered subcutaneously. The surgical area is

draped with the hindlimb extended and secured in place with a sterile adhesive bandage.

A skin incision is made in an elliptical fashion along the inguinal canal from the rostral dorsal iliac spine to the level of the pubic ramus. Gentle blunt dissection with a cotton tipped applicator is used to push the peritoneum and abdominal musculature rostrally to expose the proximal aspect of the femoral neurovascular bundle (artery, vein, and nerve). The bundle is carefully dissected with a fine hemostat and controlled proximally and distally with 5-0 Vicryl® (Ethicon Inc, Somerville, NJ) braided absorbable suture ties. Axonotmesis is performed on the femoral nerve as the bundle is divided with sharp fine scissors. The musculature overlying the femur is gently divided using sharp dissection and the femur grasped distally using toothed forceps. A heavy scissor is used to divide the femur at the mid-shaft. The distal femur is elevated, allowing visualization of the caudal musculature, which is sharply divided. Axonotmesis is performed on the sciatic nerve as it is visualized caudally using smooth forceps 3 mm proximal to the division site and then ligated. The remaining soft tissue is sharply divided, and the skin incision completed to remove the hindlimb. Care is taken to leave a sufficient posterior muscle flap to cover the proximal femur stump.

After removal of the hindlimb from the field, gentle pressure is used to ensure hemostasis. A single figure of eight suture is used to cover the proximal femur stump with the caudal muscle flap. Skin edges are adhered with an intradermal suture pattern using 5-0 Vicryl® suture. Vetbond® surgical glue is applied. The animal is maintained on heat throughout the surgery and during anesthetic recovery with continuous monitoring. The entire procedure from incision to closure lasts 15 – 25 minutes. Amoxicillin 400 mg/50 mls (Sandoz, Princeton, NJ) is added to a 350 ml water bottle at a dosage of 50 mg/kg for one week. Mice are monitored closely at least twice a day, in addition to regular health checks following surgery for 7-10 days by experienced veterinary technologists.

Xenograft *In Vivo* Antitumor Model

For the B7-H3-CAR dose escalation experiment, mice underwent orthotopic LM7 implantation as described above and were monitored for engraftment and growth by weekly bioluminescent imaging. Each mouse was imaged from the ventral aspect both with and without lower extremity shielding to allow for assessment for pulmonary metastases. At day 47 post-implantation, based on bioluminescent flux of 10^8 – 10^9 photons/second (p/s) and visible tumor masses, mice were injected *via* tail vein with either B7-H3-CAR T cells at $3x10^5$, $1x10^6$, $3x10^6$, or $1x10^7$ T cells per mouse, or control T cells at 3 x 10^6 per mouse. Only mice with demonstrably engrafted tumors on bioluminescent imaging were treated, leaving groups of 4 – 5 mice each. Mice were then monitored weekly using bioluminescence imaging. At reaching physical endpoints as described above, mice underwent hindlimb amputation with harvest of tumor tissue and ongoing bioluminescence imaging. Mice subsequently underwent ongoing imaging and sacrifice at physical humane endpoints or when systemic metastatic spread was consistently present in multiple organ systems and for at least 2 consecutive weeks. The right lung of each euthanized animal was reserved for dissociation and flow cytometry, and the left lung submitted for pathologic analysis.

Xenograft *In Vivo* CAR T Cell Trafficking Model

For the *in vivo* CAR T cell trafficking assay, mice underwent orthotopic unlabeled LM7 implantation as described above. On day 28 post implantation, mice were injected *via* tail vein with $3x10^6$ B7-H3-CAR T cells or control T cells labelled with ffluc. Mice were then followed by daily bioluminescence imaging for 5 days, followed by 2 times per week for a total of 14 days.

Bioluminescent Imaging

Mice were injected i.p. with 150 mg/kg of d-luciferin 5 minutes before imaging, anesthetized with isoflurane (1.5% - 2% delivered in 100% oxygen at 1 L/min), and imaged with an *in vivo* imaging system (IVIS 200; PerkinElmer, Waltham, MA, USA). The photons emitted from the luciferase-expressing cells were quantified using Living Image software (PerkinElmer). Mice were imaged once per week to track tumor burden, and once per day to track T cell trafficking.

Histopathological Examination

All mice, either upon sacrifice or upon reaching the end of the study, underwent necropsy. The primary tumor site, the left lung of each mouse, and any sites of obvious extrapulmonary metastatic disease were harvested and fixed in 10% neutral-buffered formalin, embedded in paraffin, sectioned at 4 μm, and stained with hematoxylin and eosin (HE). Bony tissues were decalcified in 10% formic acid. Stained sections were visually reviewed using a Nikon Eclipse Ni upright microscope (Nikon Instruments Inc., Melville, NY) by a board-certified veterinary pathologist.

Immunohistochemistry

All formalin-fixed, paraffin-embedded (FFPE) tissues were sectioned at 4 μm, mounted on positively charged glass slides (Superfrost Plus; Thermo Fisher Scientific, Waltham, MA), and dried at 60°C for 20 min. The following antibodies and procedures were used to detect immunohistochemical markers. CD276 (Clone RBT-B7-H3, Rabbit Monoclonal, IgG) and GFP (Clone JL8, Clontech, #632381,1:2000) were separately detected using HIER with cell conditioning media 1 (CC1, 950-224, Ventana Medical Systems, Tucson, AZ) for 32 minutes at 37°C followed by visualization with DISCOVERY OmniMap anti-Rb HRP (760-4311; Ventana Medical Systems, Tucson, AZ), and DISCOVERY ChromoMap DAB kit (760-159; Ventana Medical Systems, Tucson, AZ) or DISCOVERY ChromoMap Purple kit (760-229; Ventana Medical Systems, Tucson, AZ), respectively. Positive and negative tissue controls and isotype controls for monoclonal antibodies were used to assess the specificity of immunostaining.

Flow Cytometric Assessment for Primary and Pulmonary Metastatic Lesions

At necropsy, half of any residual primary tumor and the right lung of each mouse was harvested and dissociated manually. Dissociated tissue was passed through a 70 μm cell strainer and washed. Cells were resuspended in PBS with 1% FBS. Flow cytometry was performed as detailed in section 2.4. Tumor cells were detected by GFP fluorescence and the percent of GFP-positive cells in each lung specimen was quantified.

Statistical Analysis

For comparison of 3 or more groups with a single independent variable, statistical significance was determined by one-way ANOVA with a Tukey's multiple comparison test. For comparison of three or more groups with two or more independent variables, statistical significance was determined by two-way ANOVA with Sidak's multiple comparison test. Cumulative incidence and survival curves were plotted using the Kaplan-Meier method. Statistical significance between survival curves was determined using the long-rank (Mantel-Cox) test. For curves generated over time (cytotoxicity, bioluminescence over time), where appropriate, area under the curve was determined for each subject. Mean AUC was compared between groups using either two-tailed student's t test for two group analyses or one-way ANOVA for three or more groups with a single independent variable.

RESULTS

B7-H3-CAR T Cells Exhibit Anti-Osteosarcoma Activity *Ex Vivo*

To establish CAR T cell activity against OS in our novel spontaneously metastasizing orthotopic model (**Figures 1A–I**), we first evaluated their function *ex vivo*. We chose to target B7-H3 in these studies because B7-H3 i) is highly expressed in a majority of OS samples (15–17), ii) is associated with OS progression/metastasis (22), and iii) has limited expression in normal human tissues (15, 16, 23, 24). Likewise, the LM7 OS cell line (25) we used to develop this model expresses high levels of B7-H3 (**Figure 2A**). We chose LM7 for this model given its development as a lung metastatic derivative of the well-characterized SaOS OS cell line (18).

B7-H3-CAR T cells or T cells expressing a nonsignaling version of the B7-H3-CAR (Control (Ctrl)-CAR T cells) were generated by lentiviral transduction as previously described (15), with resultant high level CAR expression (**Figure 2B**). Phenotyping of CAR-positive cells demonstrated comparable CD4:CD8 ratios and a predominance of T cells with a memory phenotype (CD45RO+/CCR7+ or CD45RO+/CCR7-) (**Figures 2C, D**). To evaluate their effector function, CAR T cells were incubated with LM7 tumor cells and supernatant was collected 24 hours later to measure cytokine production. B7-H3-CAR T cells secreted significantly greater IFNγ and IL-2 compared to Ctrl CAR T cells (**Figures 2E, F**; N = 7 donors; $p < 0.0001$ for IFNγ; $p < 0.05$ for IL-2). No significant cytokine production was observed by T cells in the absence of tumor cells, confirming that cytokine production occurred due to CAR recognition of the tumor cells. B7-H3-CAR T cells also expanded in the presence of LM7 cells in contrast to Ctrl-CAR T cells (**Figure 2G**; N= 4-5 donors; $p < 0.05$). This expansion was antigen specific since no significant difference was observed in the absence of tumor cells between B7-H3- and Ctrl-CAR T cell populations. -CAR T cell cytotoxicity was measured using an xCELLigence impedance-based assay. B7-H3-CAR T cells rapidly killed LM7 OS cells, reaching > 95% cytolysis 5 hours post co-culture (**Figure 2H**). In contrast, Ctrl CAR T cells exhibited minimal antitumor activity (N = 4 donors, statistical analysis by AUC and one-way ANOVA; *$p < 0.05$; **$p < 0.01$; ****$p < 0.0001$).

B7-H3-CAR T Cells Exhibit Dose-Dependent Antitumor Activity in the Established Orthotopic Spontaneously Metastasizing Xenograft Model

Twenty-five 8-week old NSG mice were implanted with collagen-embedded LM7.GFP.ffluc in the anterior tibial crest according to the procedure described in the Material and Methods section and shown in **Figures 1A–I**. All mice survived general anesthesia and were weight-bearing, grooming, and had normal cage exploration behaviors within 10 minutes of anesthetic recovery. There were no perioperative complications such as wound dehiscence, infection, bleeding, intractable pain, or evidence of osteomyelitis. A perioperative analgesic regimen of daily meloxicam and buprenorphine for 5 – 7 days resulted in satisfactory pain control after tibial osteotomy. Out of 25 implanted mice, 22 (88%) developed robust tibial tumors detectable by bioluminescent imaging and visual inspection and were used for further studies.

Four escalating doses of B7-H3-CAR T cells derived from a single healthy donor were injected by tail vein (iv) ($3x10^5$, $1x10^6$, $3x10^6$, or $1x10^7$ cells/mouse) 48 days post tumor implantation. In addition, Ctrl-CAR T cells were injected iv at $3x10^6$ cells per mouse. Post injection, B7-H3-CAR T cells exhibited antitumor activity in a dose-dependent manner (**Figures 3A, B**). All Ctrl- and low-dose B7-H3-CAR ($3x10^5$) T cell treated mice had progressive primary disease and required hindlimb amputation by day 100. Overall, 14 mice achieved baseline primary tumor control with CAR T cell therapy. All mice in the intermediate ($1x10^6$), intermediate-high ($3x10^6$), and high ($1x10^7$) dose groups initially had complete primary tumor response to CAR T cell treatment (**Figures 3A, B**). However, 2 mice in the intermediate dose group recurred at the primary site and required amputation at day 135. At intermediate-high and high doses, primary tumors responded completely to B7-H3-CAR T cell treatment and none required amputation, demonstrating robust CAR T cell antitumor activity (**Figures 3A, B**). At study completion, mice in the intermediate-high and high dose treatment groups were euthanized and pathologic examination of the tibial implantation sites revealed no tumor cells, confirming the complete responses determined by bioluminescence imaging.

As one of the major goals of this study was to evaluate systemic metastatic disease, amputation was performed to enable survival,

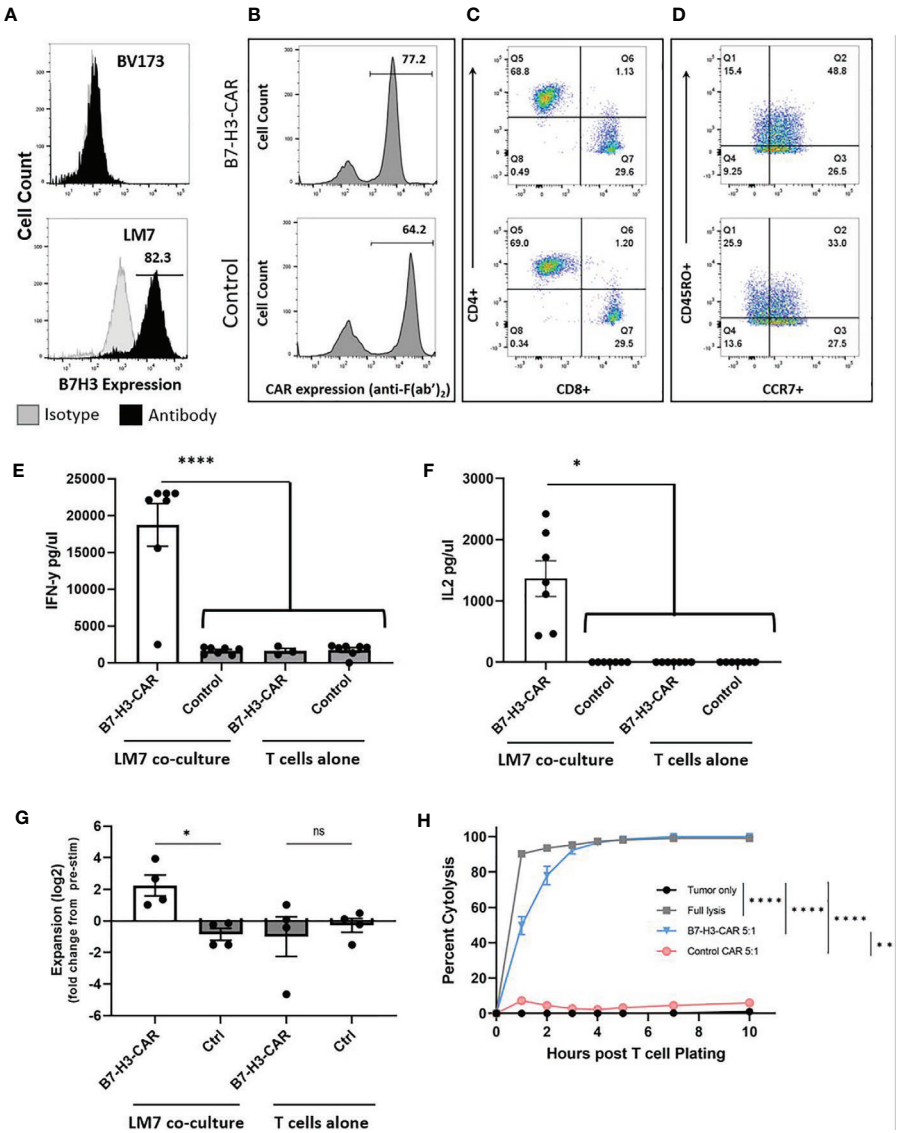

FIGURE 2 | LM7 OS B7-H3 expression, CAR T cell transduction, phenotype, and *in vitro* effector function. **(A)** The LM7 OS cell line was evaluated by flow cytometry for surface B7-H3 expression and shows robust expression. BV173 cells served as known negative controls. Activated T cells were transduced with lentiviral particles encoding B7-H3.CD28ζ CARs or a control CAR (B7-H3.CD8α.Δ). B-D) Representative flow plots of transduced T cells. **(B)** Percent transduction of B7-H3-CAR and control CAR T cells. **(C)** CAR T cell CD4+/CD8+ phenotype. **(D)** CAR T cell CD45RO+/CCR7+ memory phenotypes. E-F) CAR T cells were placed in coculture with LM7 tumor cells or plated alone at a 1:1 effector:target ratio. After 24 hours, supernatant was removed and assessed by ELISA for cytokine production. B7-H3-CAR T cells demonstrated robust **(E)** IFN-γ ($p < 0.0001$) and **(F)** IL-2 ($p < 0.05$) production. N = 7 donors; performed in duplicate. Statistical analysis by one-way ANOVA. **(G)** CAR T cells were placed in coculture with LM7 tumor cells or plated alone and fold change from baseline quantified as described in the text (N = 4 donors; performed in duplicate; $p < 0.05$; statistical analysis by one-way ANOVA). **(H)** Impedance-based cytotoxicity assay (xCELLigence) using LM7 cells as targets demonstrated robust cytotoxicity of B7-H3-CAR T cells compared to controls (N = 4 donors; E:T ratio = 5:1; statistical analysis by AUC and one-way ANOVA; *$p < 0.05$; **$p < 0.01$; ****$p < 0.0001$). ns, not significant.

and not to prevent disease spread. Development of imaging-defined systemic metastasis was defined as two consecutive weeks of extra-tibial bioluminescent signal above flux of 1 x 10^6 p/s. Our orthotopic implantation method resulted in a high propensity for spontaneous OS metastasis. All Ctrl- and low dose B7-H3-CAR T cell treated mice developed systemic metastatic disease despite hind limb amputation (**Figures 3B, C**). Notably, two mice in the control group had evidence of metastatic disease prior to hindlimb amputation performed on day 100 (**Figure 3B**). At the intermediate dose two mice developed metastatic disease despite showing a complete response at the primary tumor site without amputation (**Figures 3B, C**), and 2 mice in the intermediate-high dose group developed metastatic disease despite B7-H3-CAR T cell control of the primary tumor. No

mice in the high dose treatment group developed systemic metastasis detectable by bioluminescent imaging. At 6 months, there was a clear and statistically significant dose-dependent difference in metastasis development (**Figure 3C**) and survival advantage for B7-H3-CAR T cell treated mice (**Figure 3D**). In total, 8 mice remained long-term survivors: 1/5 in the intermediate dose group, 3/5 in the intermediate-high dose group, and 4/4 in the high dose group.

These data demonstrate utility of this model for evaluating CAR T cell activity and demonstrate that B7-H3-CAR T cells control local OS and prevent metastatic disease in a dose-dependent fashion.

Established Orthotopic Spontaneously Metastasizing Xenograft Model Allows Non-Invasive Monitoring of B7-H3-CAR T Cell Trafficking to Tumors

We next explored if the orthotopic implant OS model could be used to monitor T cell trafficking and expansion at the primary tumor site. Ten mice were implanted with collagen-embedded LM7 cells, and twenty-eight days later, $3x10^6$ ffluc-expressing B7-H3- or Ctrl-CAR T cells were injected *via* tail vein into 9 surviving mice (one mouse unexpectedly died before treatment). Bioluminescent imaging was performed daily for 5 days, followed by 2 times per week to track T cells *in vivo*. After exiting the pulmonary vasculature, B7-H3-CAR T cells trafficked to engrafted right tibial tumors beginning on day 3 post implantation and exhibited significantly (**Figures 4A–C**; $p < 0.01$) greater tibial expansion on day 4 post-injection compared to Ctrl-CAR T cells. In addition, B7-H3-CAR T cells persisted at the primary tumor site through 14 days post-injection. In contrast, Ctrl-CAR T cells, while exhibiting similar early trafficking to right tibial tumors, did not expand and had minimal persistence beyond 7 days post-injection (**Figures 4A, B**).

Orthotopic LM7 Tumor Implantation Produces Robust Primary and Metastatic Disease and Tumors Have Essential Characteristics of OS

All mice in the dose-escalation CAR T cell treatment experiment underwent tissue harvest at hindlimb amputation, and necropsy

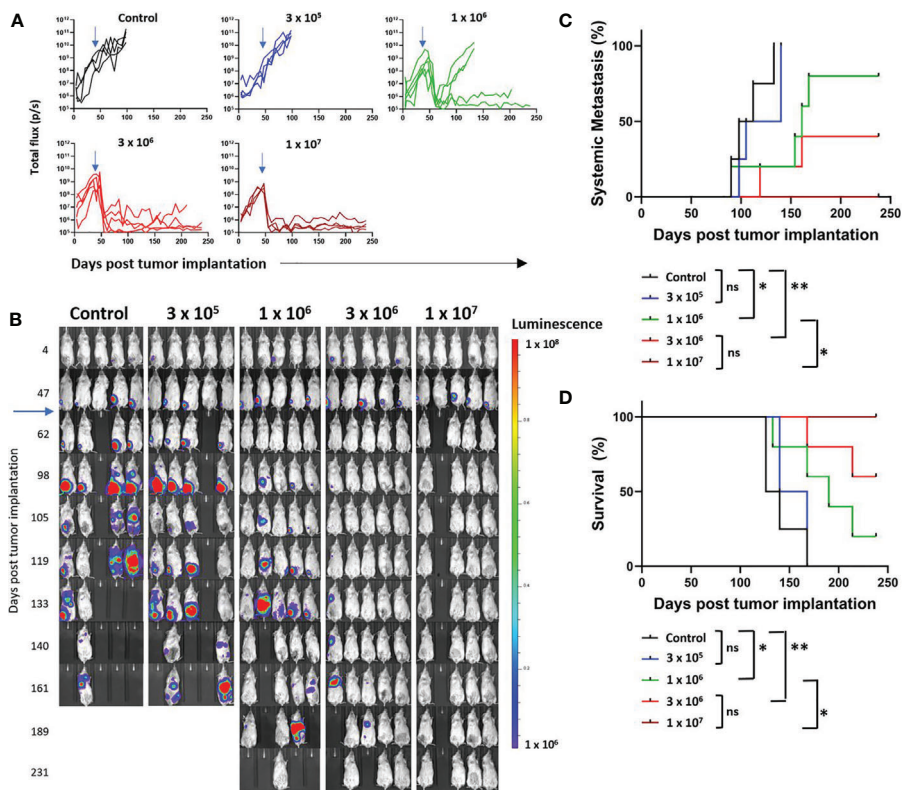

FIGURE 3 | Growth and metastasis of LM7 OS cells in orthotopic model. LM7 OS cells expressing firefly luciferase were embedded in highly-viscous collagen and implanted into the tibia of NSG mice on Day 0. On day 48, CAR T cells were injected by tail vein at indicated doses (blue arrows). Mice were followed by serial bioluminescence imaging and underwent hindlimb amputation or sacrifice as described in the text. **(A)** Quantified growth of OS tumors after implantation (total flux (p/s) per ROI). **(B)** Serial imaging of implanted mice over time. **(C)** Cumulative incidence curve indicating development of systemic disease as determined by non-tibial bioluminescent signal appearance in two consecutive images. **(D)** Kaplan-Meier curve indicating overall survival of mice. N = 4-5 mice/group, 1 healthy T cell donor. Statistical analysis performed by log-rank testing. *$p < 0.05$; **$p < 0.01$. ns, not significant.

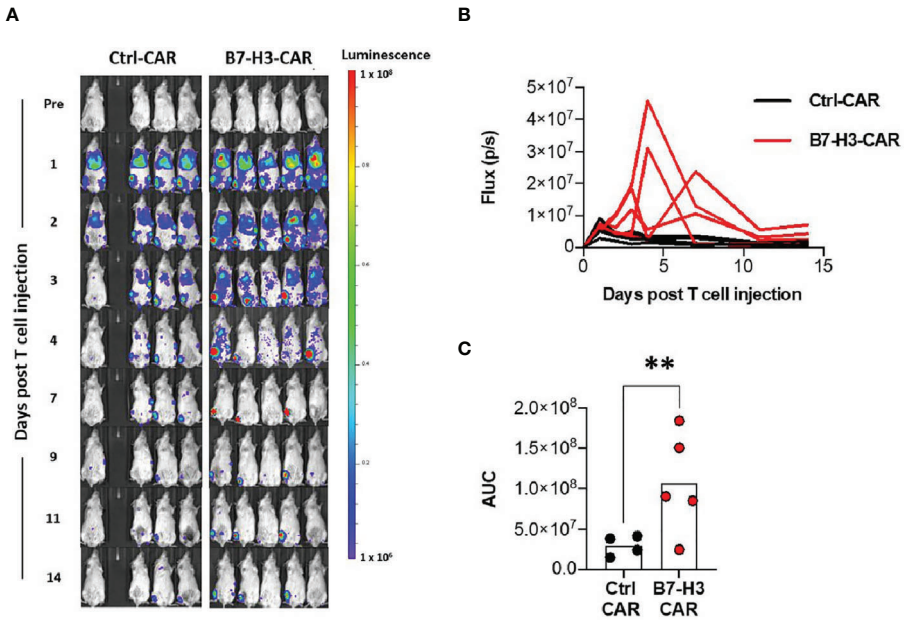

FIGURE 4 | CAR T cell trafficking to orthotopic tumors. LM7 OS cells were embedded in highly-viscous collagen implanted into the tibia of NSG mice on Day 0. On day 28, B7-H3-CAR T cells expressing firefly luciferase were injected *via* tail vein. Mice were then imaged with serial bioluminescence over the following 14 days. **(A)** Serial imaging of implanted mice over time. **(B)** Quantification of tibial implant site bioluminescence (total flux (p/s) per ROI) over time. **(C)** AUC calculation for B7-H3-CAR (N = 5) and Ctrl-CAR (N = 4) treated mice. One healthy T cell donor. Statistical analysis performed by student's t test. **p < 0.01.

was performed at terminal endpoints to allow pathologic evaluation of tumor and lung tissues. Extrapulmonary sites of metastasis were quantified at necropsy and selectively sampled for further studies. Engrafted tumors demonstrated cortical disruption and intramedullary extension of tumor burden. **Figure 5A** demonstrates a representative coronal section through the proximal tibia, showing both the distal femur and proximal tibia, the associated joint space, and surrounding soft tissue. Engrafted OS disrupted the cortical surface, extends into the medullary cavity, and established on both the anterior surface of the tibia and extended posteriorly into the soft tissue of the thigh and calf. All engrafted primary tumors exhibited pleomorphic spindle-shaped cells with a high mitotic index and nuclear pleomorphism. In addition, deposition of malignant osteoid was observed, consistent with OS (**Figure 5A**). Additionally, all engrafted tumors exhibited strong B7-H3 immunostaining, consistent with expression of B7-H3 in the LM7 cell line (**Figure 5B**).

Of the 8 mice in the control and low dose treatment groups, 6 had evidence of pulmonary metastasis on lung H&E sections. Five of these exhibited multifocal nodular metastases, and 1 in the low dose group exhibited multifocal neoplastic emboli without established metastasis. Of the 6 mice in the intermediate- and intermediate-high treatment groups that were euthanized due to progression of systemic metastasis, 4 showed evidence of micro-metastasis on H&E. Nodular lung metastases exhibited similar characteristics to the primary tumor site, with high nuclear pleomorphism, high mitotic rates, and malignant osteoid deposition (**Figure 5C**). Pulmonary lesions also stained positive for B7-H3 (**Figure 5D**). Primary and pulmonary specimens were additionally assessed for surface B7-H3 expression and evidence of metastatic spread to the lungs by evaluating GFP and B7-H3 positive cells within the primary tumor and pulmonary tissue. Fragments of primary tumor tissue and the right lung of each mouse were made into single-cell suspension and evaluated by flow cytometry for B7-H3 and GFP expression (**Figure 5E**). GFP expression was detected in all persistent primary tumors and in all pulmonary specimens from mice that did not achieve long-term survival, indicating presence of GFP-positive tumor cell spread to the lungs in these mice even in cases where metastasis was not demonstrated by H&E. Additionally, all primary and metastatic tumors exhibited ongoing B7-H3 expression (**Figure 5E**). Finally, extrapulmonary metastatic spread was noted in all mice examined by H&E. The primary extrapulmonary metastatic sites included liver, adrenal glands, kidney, axial bony sites, mesenteric and serosal surfaces including presence of carcinomatosis, and others (**Figure 5F**).

DISCUSSION

In this study, we describe a novel spontaneously metastasizing orthotopic model of OS with several advantages over existing methodologies. These include i) a high rate of spontaneous pulmonary and extrapulmonary systemic metastases, ii) lack of

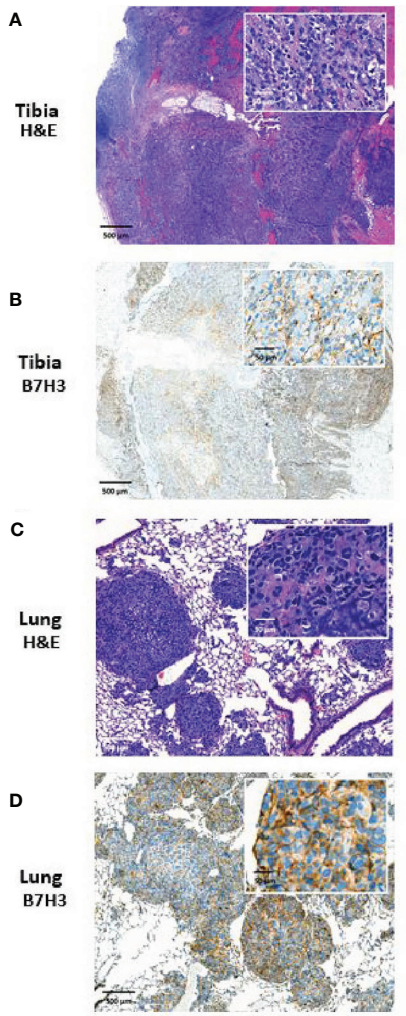

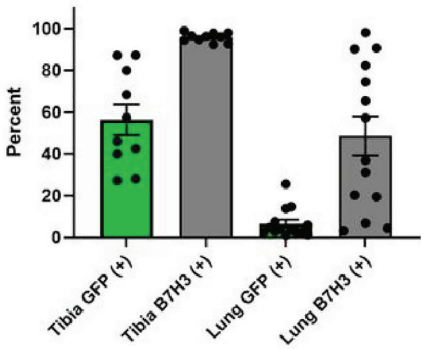

F

Histologic Findings	% (H&E)	% (Flow)
Primary engraftment	88.0	88.0
Pulmonary metastases *	64.2	100
Extrapulmonary metastases *	100	100
Liver	79	NP
Adrenal	29	NP
Bone	29	NP
Subcutaneous/ mammary	21	NP
Other **	7-14	NP

* sacrificed animals; includes all treatment groups
** "other" includes kidney, peritoneal implants/carcinomatosis, mesenteric, ovarian, brain, cardiac, and splenic sites. Flow cytometry not performed for these lesions.
NP = not performed

FIGURE 5 | Characterization of primary and metastatic lesions. Primary tibial osteosarcoma lesions are characterized by **(A)** H&E and B) B7H3 immunohistochemical staining, demonstrating formation of lesions with the appearance of malignant osteoid and invasion of the cortex and marrow cavity as well as B7H3 expression. Pulmonary metastases are characterized by **(C)** H&E and **(D)** B7-H3 immunohistochemical staining, demonstrating consistency of metastatic lesions with osteosarcoma lesions and persistent B7-H3 after metastasis. For **(A–D)**, scale indicated is 500 μm for low power images and 50 μm for high power inserts. **(E)** Percent of tumor cells (GFP+) and B7-H3 expression on tumor cells (B7-H3+) as assessed by flow cytometry. Primary tumor sites contained high percentages of human tumor cells as assessed by GFP fluorescence (mean 56.5%, SE 7.3%). Tumor cells were additionally detected in all right lungs of mice not achieving long-term survival (mean 6.6%, SE 1.9%). B7-H3 expression was additionally demonstrated in all primary lesions (mean 95.8%, SE 2.2%) and pulmonary metastatic lesions (mean 48.7%, SE 9.4%). **(F)** Percent of animals with primary site engraftment, pulmonary metastases, and other distant hematogenous metastases on post-mortem histology and/or post-mortem flow cytometry (as applicable) on recovered tissue.

immediate pulmonary seeding *via* marrow injection, iii) easily accessible site for implantation and subsequent primary tumor amputation, and iv) ability to use modified or suspension cellular material, such as ffluc-modified tumor cells for noninvasive bioluminescent imaging, without resorting to intramedullary injection. The model resulted in primary tumor engraftment in 88% of mice in this study, with 58% and 100% of CAR T cell non-responders developing pulmonary metastasis by H&E and flow cytometry respectively, and 100% of non-responders developing extrapulmonary metastatic disease. Considering these advantages and the high rate of systemic metastasis, this model fills a gap in the currently available methodology for studying OS in orthotopic and metastatic settings. A comparison of our model with currently available orthotopic models is summarized in **Table 1** and discussed in further detail below.

Using our model, we demonstrated here that B7-H3-CAR T cells exhibit antitumor activity against primary and metastatic OS in a dose-dependent fashion. In mice treated with intermediate-high and high CAR T cell doses, we have achieved complete response and long-term survival of > 6 months from treatment.

TABLE 1 | Comparison of murine orthotopic osteosarcoma models.

Model	Characteristics						
	Modified or selected cells	Whole tissue fragments	Inoculum spread controlled	Direct pulm seeding	Spont pulm mets	Ease of access	
						Implantation & imaging	Amputation
This study							
Tibial osteotomy with collagen implant or fragment transplantation	Y	Y	Y	N	Y	Y	Y
Previous studies							
Periosteal activation with cell injection or fragment transplantation (26)	Y	Y	N	N	Y	Y*	Y*
Intraosseous cell injection (27)	Y	N	Y	Y	N	Y*	Y*
Femoral fragment transplantation (28)	N	Y	Y	N	Y	N	N

*Spont, spontaneous; pulm, pulmonary; mets, metastasis; *, tibial site only.*

We have shown that different CAR T cell doses result in different patterns of primary tumor response and subsequent metastasis development in a way that mimics clinical surveillance of human patients and their outcomes.

Despite considerable preclinical promise for CAR T cell therapies in sarcomas, including osteosarcoma, rhabdomyosarcoma, synovial sarcoma, and Ewing sarcoma, clinical efficacy has remained elusive. A single phase I/II clinical trial for pediatric sarcoma has been reported (12), although several are now actively recruiting (NCT00902044, NCT02107963, NCT01953900, NCT03635632, NCT04483778, NCT03618381), and clinical trials have been reported for pediatric patients with glioblastoma (29) and neuroblastoma (30, 31). However, these clinical trials have not demonstrated robust antitumor activity in humans. The failure in clinical trials has been due to either lack of response, with patients exhibiting disease progression after CAR T cell therapy, or partial responses that progress after treatment. Very few complete responses have been noted. These failures raise concerns that preclinical models available for pediatric sarcomas, specifically OS, are not of sufficiently high-fidelity to allow adequate preclinical vetting of antitumor efficacy. Preclinical modeling for CAR T cell therapy in bone tumors, including OS and Ewing sarcoma, has relied on several strategies to assess *in vivo* efficacy. For primary tumor modeling, these have included periosteal injection (26, 32), intratibial injection (11, 33–35), an intraperitoneal loco-regional model (13, 36), and subcutaneous injection (34, 37–41). Other investigators have used an orthotopic OS model to evaluate T cells expressing an MGA271 scFv-based B7-H3-CAR with a 41BB costimulatory domain (26). Based on our previous publication, which demonstrated improved antitumor activity of MGA271 scFv-based B7-H3-CAR with a CD28 versus a 41BB costimulatory domain (15), we selected a CAR with a CD28 costimulatory domain for this study. Clearly, future studies should focus on directly comparing MGA271 scFv-based B7-H3-CARs with different costimulatory domains, including CD28, 41BB, and others, in this model to fully understand the different tumor control capacities of these CARs.

We performed a half-log dose de-escalation study in our model evaluating a dose range of 1 x $10^7$to 3 x 10^5 CAR T cells per mouse. We chose a starting cell dose of 1 x 10^7CAR T cells because 1 – 2 x 10^7 CAR T cells per mouse is a routinely accepted maximum cell dose in preclinical CAR T cell xenograft models. For the Ctrl CAR T cell group, we evaluated a cell dose of 3 x 10^6 CAR T cells per mouse, which approximated our maximum B7-H3-CAR T cell dose. Based on our results at this cell dose (no antitumor activity of Ctrl-CAR T cells; excellent antitumor activity with long-term survival of > 100 days post infusion of B7-H3-CAR T cells), we felt that it was not justified to perform additional animal experiments at lower Ctrl-CAR T cell doses.

The most common orthotopic method of OS inoculation involves intratibial injection of single cell suspensions using a heavy gauge needle (27). This model system has been extensively used for chemotherapeutic investigation, metabolic research, and immunotherapy in osteosarcoma in primary and metastatic settings (11, 42–52). A similar protocol has been described for intra-femoral injection (53–55). This injection method results in robust primary orthotopic tumor engraftment, and indeed, has been used to demonstrate antitumor activity of CAR T cells against bone tumors (11, 14, 33, 35, 37). However, direct injection of OS cells into murine femurs or tibias has been shown to result in direct pulmonary seeding due to venous outflow from the medullary cavity, making it suboptimal as a model of osteosarcoma metastasis (56, 57). While this may be avoided by using extremely low cell inoculums or attempting low-pressure injection (58), such strategies may not be feasible for all model systems or reliably reproducible between technicians. Our method avoids this problem while maintaining robust orthotopic engraftment by confining the tumor cells within a collagen scaffold, thereby avoiding direct medullary injection and venous dissemination while providing a high rate of spontaneous metastasis.

Two groups have reported using a periosteal injection strategy to establish primary orthotopic OS tumors without intramedullary injection for assessing CAR T cell therapy. In the first, periosteal injection of OS cells resulted in successful engraftment of primary OS tumors with rapid growth (26). The second group utilized the

highly aggressive 143B OS cell line in a periosteal injection method to assess primary tumor growth (32). This method produces cortical OS and does not result in immediate pulmonary seeding. It can also be applied to both implantable fragments and single cell suspensions, provided the injected cells remain in apposition to the scored periosteum. However, this method can result in soft tissue or periosteal inoculation as a result of imprecise localization of the injected cells, thereby not reliably achieving cortical and intramedullary OS engraftment (59, 60). Finally, the metastatic rate of models using this method is relatively low, and the injection of single cell suspensions into the paracortical position can result in less control over the spread of the suspension into the soft tissue than placement of a tumor fragment or implant as we have described here (60–62). Subcutaneous and intraperitoneal locoregional models of OS, which are the other major methodologies employed in murine CAR T cell preclinical models, do not recapitulate the microenvironment of skeletal OS and are known to have inferior metastasis rates compared to orthotopic implantation (63).

Metastatic OS models for CAR T cell evaluation have included IV injection of OS cells (35, 36, 40), resulting in immediate seeding but allowing for evaluation of stabilization and growth in the pulmonary niche, and in two cases assessment of either number of pulmonary metastases at endpoint by histology or overall survival after hindlimb amputation (14, 26), which is imputed to treatment of metastatic sites. While IV injection of tumor cells results in reliable pulmonary OS seeding, it does not allow for high-fidelity recapitulation of the metastatic process, as it avoids the steps of primary tumor escape, vascular entry, and metastatic site extravasation.

An additional option for orthotopic investigation of OS, not yet described in CAR T cell preclinical studies, involves surgical exposure of the distal femur of the mouse, resection of the lateral femoral condyle, and implantation of a fragment of fresh tumor tissue (28). This method has the advantage of providing an orthotopic implantation site without injection of tumor cells and allows implantation of fresh fragments of tumor, which is valuable for applications requiring intact tumor-stroma connections. It also does not result in direct seeding of the pulmonary metastatic site. However, it does not provide a method for orthotopic implantation of single cell suspensions, and therefore is limited in terms of the ability to use bioluminescence or fluorescent noninvasive monitoring of primary tumor growth without first establishing xenograft donor tumors (i.e., by subcutaneous injection and subsequent harvest). In addition, the site itself is buried within the lateral musculature of the animal's hindlimb, making direct visual monitoring of the tumor site difficult and hindlimb amputation for long-term tumor studies technically challenging. The presence of proximal tumor and/or intramedullary extension throughout the femoral medullary canal means that amputation must be performed near or through the acetabular/glenoid junction, leading to technical difficulty related to adequate dissection of the joint capsule and avoidance of the femoral artery and vein at an anatomic site of close apposition to the joint capsule. These technical difficulties may limit the performance of hindlimb amputation to more highly trained technicians or researchers.

Two groups of investigators have described intratibial implantation of histologically intact fresh tumor tissue into the tibia of mice (64, 65). Both models closely resemble that described in this report, but do not allow the use of modified cells or single cell suspensions for noninvasive tumor growth and imaging applications. They also do not allow the use of specialized cell line variants, such as serially passaged lines with high metastatic capability (66) or gene-edited cell lines. Our model addresses this problem by additionally incorporating embedding of the tumor cells within a collagen scaffold.

This model is technically feasible. The mice used in this methodology do well after implantation. Mice are recovered from anesthesia, weight-bearing, and exploring surroundings within five minutes of awakening from general anesthesia. There is no evidence that pretreatment with buprenorphine and meloxicam affects the tumor growth in this model (67). The method is technically straightforward and easily teachable for nonsurgical personnel, and the subsequent hindlimb amputations are rendered significantly easier by use of a tibial rather than a femoral implantation site. These considerations increase the feasibility of use of this model.

Limitations of this method may include the need to acquire specialized surgical tools including the fine Rongeur used for creating the tibial osteotomy and the need to train technicians in the surgical technique. In addition, the impact of the collagen scaffold on tumor cells has not been established. We do not anticipate the collagen matrix to significantly change tumor biology and have demonstrated that this technique results in histology consistent with osteosarcoma. In addition, the use of scaffolding material such as Matrigel® (Corning, Arizona, USA) is extremely common in tumor cell injection and implantation techniques, and therefore this strategy is not overly divergent from common practice. Finally, while the pulmonary metastatic potential of this model is a major advantage, the frequency and burden of the extrapulmonary systemic metastatic sites differs from the pattern of osteosarcoma metastasis in humans (68, 69). This may be due to different tumor tropism for osteosarcoma in murine systems, and indeed, extrapulmonary metastases have been reported in previous orthotopic models (61). While this metastatic pattern does differ from the clinical pattern in humans, it still allows rigorous evaluation of the metastatic process.

In summary, the orthotopic implantation technique detailed in this study, in which tumor cells are first embedded into a collagen scaffold implant and then implanted surgically into the anterior tibia of mice, results in robust primary tumor engraftment and systemic metastasis as determined by H&E and flow cytometry. We additionally describe effective antitumor activity of B7-H3-CAR T cell therapy in a dose dependent fashion using this model and show its efficacy in distinguishing primary tumor control from subsequent systematic metastasis. Thus, our model is a valuable addition to the field and should enable the realistic modeling not only of cell therapies but other therapeutics for primary and metastatic OS.

DATA AVAILABILITY STATEMENT

The raw data supporting the conclusions of this article will be made available by the authors, without undue reservation.

ETHICS STATEMENT

The animal study was reviewed and approved by St. Jude Children's Research Hospital Institutional Animal Care and Use Committee.

AUTHOR CONTRIBUTIONS

Conception and design: LT, SG, CD. Development of surgical orthotopic implantation model: LT, AD, AF. Development of nonsurgical methodology: LT, AC, PN, JW. Acquisition of data: LT, AC, PN, JW, HT. Analysis and interpretation of data: LT, AC, HT, AR, SG, CD. Writing, review, and revision of manuscript: all authors. Study supervision: AD, SG, CD. All authors contributed to the article and approved the submitted version.

FUNDING

This work was supported by the Assisi Foundation of Memphis, the American Lebanese Syrian Associated Charities, and the Rally Foundation for Childhood Cancer Research Young Investigator grant program (grant 20YIN44). Animal imaging was performed by the St. Jude Center for In Vivo Imaging and Therapeutics, which is supported in part by NIH grants P01CA096832 and R50CA211481. The content is solely the responsibility of the authors and does not necessarily represent the official views of the National Institutes of Health.

ACKNOWLEDGMENTS

We thank Deanna Langfitt for her brilliance, advice, and technical support for flow cytometry experiments. We thank Cara Goodrem, Amanda George, Randi Rooney, Krista Millican, Angie Hammond, and Jenna McCommon for their enthusiastic and knowledgeable support in peri- and intra-operative monitoring and assessment of mouse subject health and comfort.

REFERENCES

1. Khanna C, Fan TM, Gorlick R, Helman LJ, Kleinerman ES, Adamson PC, et al. Toward a Drug Development Path That Targets Metastatic Progression in Osteosarcoma. *Clin Cancer Res* (2014) 20(16):4200–9. doi: 10.1158/1078-0432.CCR-13-2574
2. Ebb D, Meyers P, Grier H, Bernstein M, Gorlick R, Lipshultz SE, et al. Phase II Trial of Trastuzumab in Combination With Cytotoxic Chemotherapy for Treatment of Metastatic Osteosarcoma With Human Epidermal Growth Factor Receptor 2 Overexpression: A Report From the Children's Oncology Group. *J Clin Oncol* (2012) 30(20):2545–51. doi: 10.1200/JCO.2011.37.4546
3. Gok Durnali A, Paksoy Turkoz F, Ardic Yukruk F, Tokluoglu S, Yazici OK, Demirci A, et al. Outcomes of Adolescent and Adult Patients With Lung Metastatic Osteosarcoma and Comparison of Synchronous and Metachronous Lung Metastatic Groups. *PloS One* (2016) 11(5):e0152621. doi: 10.1371/journal.pone.0152621
4. Roberts RD, Lizardo MM, Reed DR, Hingorani P, Glover J, Allen-Rhoades W, et al. Provocative Questions in Osteosarcoma Basic and Translational Biology: A Report From the Children's Oncology Group. *Cancer* (2019) 125(20):3514–25. doi: 10.1002/cncr.32351
5. Popper H. Primary Tumor and Metastasis-Sectioning the Different Steps of the Metastatic Cascade. *Transl Lung Cancer Res* (2020) 9(5):2277–300. doi: 10.21037/tlcr-20-175
6. Hanahan D, Weinberg RA. Hallmarks of Cancer: The Next Generation. *Cell* (2011) 144(5):646–74. doi: 10.1016/j.cell.2011.02.013
7. Heymann MF, Lezot F, Heymann D. The Contribution of Immune Infiltrates and the Local Microenvironment in the Pathogenesis of Osteosarcoma. *Cell Immunol* (2019) 343:103711. doi: 10.1016/j.cellimm.2017.10.011
8. Chulanetra M, Morchang A, Sayour E, Eldjerou L, Milner R, Lagmay J, et al. GD2 Chimeric Antigen Receptor Modified T Cells in Synergy With Sub-Toxic Level of Doxorubicin Targeting Osteosarcomas. *Am J Cancer Res* (2020) 10(2):674–87.
9. Thanindratarn P, Dean DC, Nelson SD, Hornicek FJ, Duan Z. Chimeric Antigen Receptor T (Car-T) Cell Immunotherapy for Sarcomas: From Mechanisms to Potential Clinical Applications. *Cancer Treat Rev* (2020) 82:101934. doi: 10.1016/j.ctrv.2019.101934
10. Merker M, Pfirrmann V, Oelsner S, Fulda S, Klingebiel T, Wels WS, et al. Generation and Characterization of ErbB2-CAR-engineered Cytokine-Induced Killer Cells for the Treatment of High-Risk Soft Tissue Sarcoma in Children. *Oncotarget* (2017) 8(39):66137–53. doi: 10.18632/oncotarget.19821
11. Fernandez L, Metais JY, Escudero A, Vela M, Valentin J, Vallcorba I, et al. Memory T Cells Expressing an NKG2D-CAR Efficiently Target Osteosarcoma Cells. *Clin Cancer Res* (2017) 23(19):5824–35. doi: 10.1158/1078-0432.CCR-17-0075
12. Ahmed N, Brawley VS, Hegde M, Robertson C, Ghazi A, Gerken C, et al. Human Epidermal Growth Factor Receptor 2 (Her2) -Specific Chimeric Antigen Receptor-Modified T Cells for the Immunotherapy of HER2-Positive Sarcoma. *J Clin Oncol* (2015) 33(15):1688–96. doi: 10.1200/JCO.2014.58.0225
13. Ahmed N, Salsman VS, Yvon E, Louis CU, Perlaky L, Wels WS, et al. Immunotherapy for Osteosarcoma: Genetic Modification of T Cells Overcomes Low Levels of Tumor Antigen Expression. *Mol Ther* (2009) 17 (10):1779–87. doi: 10.1038/mt.2009.133
14. Rainusso N, Brawley VS, Ghazi A, Hicks MJ, Gottschalk S, Rosen JM, et al. Immunotherapy Targeting HER2 With Genetically Modified T Cells Eliminates Tumor-Initiating Cells in Osteosarcoma. *Cancer Gene Ther* (2012) 19(3):212–7. doi: 10.1038/cgt.2011.83
15. Nguyen P, Okeke E, Clay M, Haydar D, Justice J, O'Reilly C, et al. Route of 41BB/41BBL Costimulation Determines Effector Function of B7-H3-CAR.CD28zeta T Cells. *Mol Ther Oncolytics* (2020) 18:202–14. doi: 10.1016/j.omto.2020.06.018
16. Modak S, Kramer K, Gultekin SH, Guo HF, Cheung NK. Monoclonal Antibody 8H9 Targets a Novel Cell Surface Antigen Expressed by a Wide Spectrum of Human Solid Tumors. *Cancer Res* (2001) 61(10):4048–54.
17. Kendsersky NM, Lindsay JM, Kolb EA, Smith MA, Teicher BA, Erickson S, et al. The B7-H3-targeting Antibody-Drug Conjugate M276-SL-PBD is Potently Effective Against Pediatric Cancer Preclinical Solid Tumor Models. *Clin Cancer Res* (2021) 27(10):2938–46. doi: 10.1158/1078-0432.CCR-20-4221
18. Jia SF, Worth LL, Kleinerman ES. A Nude Mouse Model of Human Osteosarcoma Lung Metastases for Evaluating New Therapeutic Strategies. *Clin Exp Metastasis* (1999) 17(6):501–6. doi: 10.1023/a:1006623001465
19. Bauler M, Roberts JK, Wu CC, Fan B, Ferrara F, Yip BH, et al. Production of Lentiviral Vectors Using Suspension Cells Grown in Serum-free Media. *Mol Ther Methods Clin Dev* (2020) 17:58–68. doi: 10.1016/j.omtm.2019.11.011
20. Cerignoli F, Abassi YA, Lamarche BJ, Guenther G, Santa Ana D, Guimet D, et al. In Vitro Immunotherapy Potency Assays Using Real-Time Cell Analysis. *PloS One* (2018) 13(3):e0193498. doi: 10.1371/journal.pone.0193498
21. Fumagalli A, Suijkerbuijk SJE, Begthel H, Beerling E, Oost KC, Snippert HJ, et al. A Surgical Orthotopic Organoid Transplantation Approach in Mice to Visualize and Study Colorectal Cancer Progression. *Nat Protoc* (2018) 13 (2):235–47. doi: 10.1038/nprot.2017.137

22. Wang L, Zhang Q, Chen W, Shan B, Ding Y, Zhang G, et al. B7-H3 is Overexpressed in Patients Suffering Osteosarcoma and Associated With Tumor Aggressiveness and Metastasis. *PloS One* (2013) 8(8):e70689. doi: 10.1371/journal.pone.0070689
23. Seaman S, Zhu Z, Saha S, Zhang XM, Yang MY, Hilton MB, et al. Eradication of Tumors Through Simultaneous Ablation of CD276/B7-H3-Positive Tumor Cells and Tumor Vasculature. *Cancer Cell* (2017) 31(4):501–15.e8. doi: 10.1016/j.ccell.2017.03.005
24. Du H, Hirabayashi K, Ahn S, Kren NP, Montgomery SA, Wang X, et al. Antitumor Responses in the Absence of Toxicity in Solid Tumors by Targeting B7-H3 Via Chimeric Antigen Receptor T Cells. *Cancer Cell* (2019) 35(2):221–37 e8. doi: 10.1016/j.ccell.2019.01.002
25. Duan X, Jia SF, Zhou Z, Langley RR, Bolontrade MF, Kleinerman ES. Association of Alphavbeta3 Integrin Expression With the Metastatic Potential and Migratory and Chemotactic Ability of Human Osteosarcoma Cells. *Clin Exp Metastasis* (2004) 21(8):747–53. doi: 10.1007/s10585-005-0599-6
26. Majzner RG, Theruvath JL, Nellan A, Heitzeneder S, Cui Y, Mount CW, et al. Car T Cells Targeting B7-H3, a Pan-Cancer Antigen, Demonstrate Potent Preclinical Activity Against Pediatric Solid Tumors and Brain Tumors. *Clin Cancer Res* (2019) 25(8):2560–74. doi: 10.1158/1078-0432.CCR-18-0432
27. Yuan J, Ossendorf C, Szatkowski JP, Bronk JT, Maran A, Yaszemski M, et al. Osteoblastic and Osteolytic Human Osteosarcomas can be Studied With a New Xenograft Mouse Model Producing Spontaneous Metastases. *Cancer Invest* (2009) 27(4):435–42. doi: 10.1080/07357900802491477
28. Higuchi T, Sugisawa N, Yamamoto J, Oshiro H, Han Q, Yamamoto N, et al. The Combination of Oral-Recombinant Methioninase and Azacitidine Arrests a Chemotherapy-Resistant Osteosarcoma Patient-Derived Orthotopic Xenograft Mouse Model. *Cancer Chemother Pharmacol* (2020) 85(2):285–91. doi: 10.1007/s00280-019-03986-0
29. Ahmed N, Brawley V, Hegde M, Bielamowicz K, Kalra M, Landi D, et al. Her2-Specific Chimeric Antigen Receptor-Modified Virus-Specific T Cells for Progressive Glioblastoma: A Phase 1 Dose-Escalation Trial. *JAMA Oncol* (2017) 3(8):1094–101. doi: 10.1001/jamaoncol.2017.0184
30. Louis CU, Savoldo B, Dotti G, Pule M, Yvon E, Myers GD, et al. Antitumor Activity and Long-Term Fate of Chimeric Antigen Receptor-Positive T Cells in Patients With Neuroblastoma. *Blood* (2011) 118(23):6050–6. doi: 10.1182/blood-2011-05-354449
31. Park JR, Digiusto DL, Slovak M, Wright C, Naranjo A, Wagner J, et al. Adoptive Transfer of Chimeric Antigen Receptor Re-Directed Cytolytic T Lymphocyte Clones in Patients With Neuroblastoma. *Mol Ther* (2007) 15 (4):825–33. doi: 10.1038/sj.mt.6300104
32. Long AH, Highfill SL, Cui Y, Smith JP, Walker AJ, Ramakrishna S, et al. Reduction of MDSCs With All-trans Retinoic Acid Improves CAR Therapy Efficacy for Sarcomas. *Cancer Immunol Res* (2016) 4(10):869–80. doi: 10.1158/2326-6066.CIR-15-0230
33. Huang G, Yu L, Cooper LJ, Hollomon M, Huls H, Kleinerman ES. Genetically Modified T Cells Targeting interleukin-11 Receptor Alpha-Chain Kill Human Osteosarcoma Cells and Induce the Regression of Established Osteosarcoma Lung Metastases. *Cancer Res* (2012) 72(1):271–81. doi: 10.1158/0008-5472.CAN-11-2778
34. Wang Y, Yu W, Zhu J, Wang J, Xia K, Liang C, et al. Anti-CD166/4-1BB Chimeric Antigen Receptor T Cell Therapy for the Treatment of Osteosarcoma. *J Exp Clin Cancer Res* (2019) 38(1):168. doi: 10.1186/s13046-019-1147-6
35. Charan M, Dravid P, Cam M, Audino A, Gross AC, Arnold MA, et al. GD2-Directed CAR-T Cells in Combination With HGF-targeted Neutralizing Antibody (AMG102) Prevent Primary Tumor Growth and Metastasis in Ewing Sarcoma. *Int J Cancer* (2020) 146(11):3184–95. doi: 10.1002/ijc.32743
36. Huang X, Park H, Greene J, Pao J, Mulvey E, Zhou SX, et al. IGF1R- and ROR1-Specific Car T Cells as a Potential Therapy for High Risk Sarcomas. *PloS One* (2015) 10(7):e0133152. doi: 10.1371/journal.pone.0133152
37. Wang LC, Lo A, Scholler J, Sun J, Majumdar RS, Kapoor V, et al. Targeting Fibroblast Activation Protein in Tumor Stroma With Chimeric Antigen Receptor T Cells can Inhibit Tumor Growth and Augment Host Immunity Without Severe Toxicity. *Cancer Immunol Res* (2014) 2(2):154–66. doi: 10.1158/2326-6066.CIR-13-0027
38. Xiao W, Wang J, Wen X, Xu B, Que Y, Yu K, et al. Chimeric Antigen Receptor-Modified T-cell Therapy for Platelet-Derived Growth Factor Receptor Alpha-Positive Rhabdomyosarcoma. *Cancer* (2020) 126 Suppl 9:2093–100. doi: 10.1002/cncr.32764
39. Leuci V, Casucci GM, Grignani G, Rotolo R, Rossotti U, Vigna E, et al. CD44v6 as Innovative Sarcoma Target for CAR-redirected CIK Cells. *Oncoimmunology* (2018) 7(5):e1423167. doi: 10.1080/2162402X.2017.1423167
40. Hsu K, Middlemiss S, Saletta F, Gottschalk S, McCowage GB, Kramer B. Chimeric Antigen Receptor-Modified T Cells Targeting EphA2 for the Immunotherapy of Paediatric Bone Tumours. *Cancer Gene Ther* (2020) 106 (6):1123–33. doi: 10.1038/s41417-020-00221-4
41. Kailayangiri S, Altvater B, Meltzer J, Pscherer S, Luecke A, Dierkes C, et al. The Ganglioside Antigen G(D2) is Surface-Expressed in Ewing Sarcoma and Allows for MHC-independent Immune Targeting. *Br J Cancer* (2012) 106 (6):1123–33. doi: 10.1038/bjc.2012.57
42. Arlt MJ, Kuzmanov A, Snedeker JG, Fuchs B, Silvan U, Sabile AA. Fascin-1 Enhances Experimental Osteosarcoma Tumor Formation and Metastasis and Is Related to Poor Patient Outcome. *BMC Cancer* (2019) 19(1):83. doi: 10.1186/s12885-019-5303-3
43. Wang W, Li J, Ding Z, Li Y, Wang J, Chen S, et al. Tanshinone I Inhibits the Growth and Metastasis of Osteosarcoma Via Suppressing JAK/STAT3 Signalling Pathway. *J Cell Mol Med* (2019) 23(9):6454–65. doi: 10.1111/jcmm.14539
44. Yu P, Wen J, Wang J, Liang J, Shen Y, Zhang W. Establishment and Characterization of a Novel Human Osteosarcoma Cell Line for Spontaneous Pulmonary Metastasis Research In Vivo. *Ann Transl Med* (2019) 7(20):573. doi: 10.21037/atm.2019.09.23
45. Baglio SR, Lagerweij T, Perez-Lanzon M, Ho XD, Leveille N, Melo SA, et al. Blocking Tumor-Educated Msc Paracrine Activity Halts Osteosarcoma Progression. *Clin Cancer Res* (2017) 23(14):3721–33. doi: 10.1158/1078-0432.CCR-16-2726
46. Luu HH, Kang Q, Park JK, Si W, Luo Q, Jiang W, et al. An Orthotopic Model of Human Osteosarcoma Growth and Spontaneous Pulmonary Metastasis. *Clin Exp Metastasis* (2005) 22(4):319–29. doi: 10.1007/s10585-005-0365-9
47. Igarashi K, Yamamoto N, Hayashi K, Takeuchi A, Kimura H, Miwa S, et al. Non-Toxic Efficacy of the Combination of Caffeine and Valproic Acid on Human Osteosarcoma Cells in Vitro and in Orthotopic Nude-Mouse Models. *Anticancer Res* (2016) 36(9):4477–82. doi: 10.21873/anticanres.10992
48. Ren K, Zhang J, Gu X, Wu S, Shi X, Ni Y, et al. Migration-Inducing Gene-7 Independently Predicts Poor Prognosis of Human Osteosarcoma and Is Associated With Vasculogenic Mimicry. *Exp Cell Res* (2018) 369(1):80–9. doi: 10.1016/j.yexcr.2018.05.008
49. Kim EH, Kim MS, Lee KH, Sai S, Jeong YK, Koh JS, et al. Effect of Low- and High-Linear Energy Transfer Radiation on In Vitro and Orthotopic In Vivo Models of Osteosarcoma by Activation of Caspase-3 and -9. *Int J Oncol* (2017) 51(4):1124–34. doi: 10.3892/ijo.2017.4102
50. Collantes M, Martinez-Velez N, Zalacain M, Marrodan L, Ecay M, Garcia-Velloso MJ, et al. Assessment of Metabolic Patterns and New Antitumoral Treatment in Osteosarcoma Xenograft Models by [(18)F]FDG and Sodium [(18)F]Fluoride PET. *BMC Cancer* (2018) 18(1):1193. doi: 10.1186/s12885-018-5122-y
51. He X, Lin H, Yuan L, Li B. Combination Therapy With L-arginine and alpha-PD-L1 Antibody Boosts Immune Response Against Osteosarcoma in Immunocompetent Mice. *Cancer Biol Ther* (2017) 18(2):94–100. doi: 10.1080/15384047.2016.1276136
52. Comstock KE, Hall CL, Daignault S, Mandlebaum SA, Yu C, Keller ET. A Bioluminescent Orthotopic Mouse Model of Human Osteosarcoma That Allows Sensitive and Rapid Evaluation of New Therapeutic Agents In Vivo. *In Vivo* (2009) 23(5):661–8.
53. Vormoor B, Knizia HK, Batey MA, Almeida GS, Wilson I, Dildey P, et al. Development of a Preclinical Orthotopic Xenograft Model of Ewing Sarcoma and Other Human Malignant Bone Disease Using Advanced In Vivo Imaging. *PloS One* (2014) 9(1):e85128. doi: 10.1371/journal.pone.0085128
54. Sasaki H, Iyer SV, Sasaki K, Tawfik OW, Iwakuma T. An Improved Intrafemoral Injection With Minimized Leakage as an Orthotopic Mouse Model of Osteosarcoma. *Anal Biochem* (2015) 486:70–4. doi: 10.1016/j.ab.2015.06.030
55. Miretti S, Roato I, Taulli R, Ponzetto C, Cilli M, Olivero M, et al. A Mouse Model of Pulmonary Metastasis From Spontaneous Osteosarcoma Monitored In Vivo by Luciferase Imaging. *PloS One* (2008) 3(3):e1828. doi: 10.1371/journal.pone.0001828
56. Maloney C, Edelman MC, Kallis MP, Soffer SZ, Symons M, Steinberg BM. Intratibial Injection Causes Direct Pulmonary Seeding of Osteosarcoma Cells and Is Not a Spontaneous Model of Metastasis: A Mouse Osteosarcoma Model. *Clin Orthop Relat Res* (2018) 476(7):1514–22. doi: 10.1007/s11999.0000000000000291

57. Zhang L, Ye Y, Yang D, Lin J. Survivin and Vascular Endothelial Growth Factor are Associated With Spontaneous Pulmonary Metastasis of Osteosarcoma: Development of an Orthotopic Mouse Model. *Oncol Lett* (2014) 8(6):2577–80. doi: 10.3892/ol.2014.2556
58. Berlin O, Samid D, Donthineni-Rao R, Akeson W, Amiel D, Woods VL Jr. Development of a Novel Spontaneous Metastasis Model of Human Osteosarcoma Transplanted Orthotopically Into Bone of Athymic Mice. *Cancer Res* (1993) 53(20):4890–5.
59. Yang SY, Yu H, Krygier JE, Wooley PH, Mott MP. High VEGF With Rapid Growth and Early Metastasis in a Mouse Osteosarcoma Model. *Sarcoma* (2007) 2007:95628. doi: 10.1155/2007/95628
60. Marques da Costa ME, Daudigeos-Dubus E, Gomez-Brouchet A, Bawa O, Rouffiac V, Serra M, et al. Establishment and Characterization of In Vivo Orthotopic Bioluminescent Xenograft Models From Human Osteosarcoma Cell Lines in Swiss Nude and NSG Mice. *Cancer Med* (2018) 7(3):665–76. doi: 10.1002/cam4.1346
61. Goldstein SD, Hayashi M, Albert CM, Jackson KW, Loeb DM. An Orthotopic Xenograft Model With Survival Hindlimb Amputation Allows Investigation of the Effect of Tumor Microenvironment on Sarcoma Metastasis. *Clin Exp Metastasis* (2015) 32(7):703–15. doi: 10.1007/s10585-015-9738-x
62. Fourman MS, Mahjoub A, Mandell JB, Yu S, Tebbets JC, Crasto JA, et al. Quantitative Primary Tumor Indocyanine Green Measurements Predict Osteosarcoma Metastatic Lung Burden in a Mouse Model. *Clin Orthop Relat Res* (2018) 476(3):479–87. doi: 10.1007/s11999.0000000000000003
63. Jaroensong T, Endo Y, Lee SJ, Kamida A, Mochizuki M, Nishimura R, et al. Effects of Transplantation Sites on Tumour Growth, Pulmonary Metastasis and Ezrin Expression of Canine Osteosarcoma Cell Lines in Nude Mice. *Vet Comp Oncol* (2012) 10(4):274–82. doi: 10.1111/j.1476-5829.2011.00294.x
64. Crnalic S, Hakansson I, Boquist L, Lofvenberg R, Brostrom LA. A Novel Spontaneous Metastasis Model of Human Osteosarcoma Developed Using Orthotopic Transplantation of Intact Tumor Tissue Into Tibia of Nude Mice. *Clin Exp Metastasis* (1997) 15(2):164–72. doi: 10.1023/A:1018456911823
65. Blattmann C, Thiemann M, Stenzinger A, Roth EK, Dittmar A, Witt H, et al. Establishment of a Patient-Derived Orthotopic Osteosarcoma Mouse Model. *J Transl Med* (2015) 13:136. doi: 10.1186/s12967-015-0497-x
66. Tome Y, Kimura H, Maehara H, Sugimoto N, Bouvet M, Tsuchiya H, et al. High Lung-Metastatic Variant of Human Osteosarcoma Cells, Selected by Passage of Lung Metastasis in Nude Mice, Is Associated With Increased Expression of Alpha(V)Beta(3) Integrin. *Anticancer Res* (2013) 33 (9):3623–7.
67. Husmann K, Arlt MJ, Jirkof P, Arras M, Born W, Fuchs B. Primary Tumour Growth in an Orthotopic Osteosarcoma Mouse Model Is Not Influenced by Analgesic Treatment With Buprenorphine and Meloxicam. *Lab Anim* (2015) 49(4):284–93. doi: 10.1177/0023677215570989
68. Giuliano AE, Feig S, Eilber FR. Changing Metastatic Patterns of Osteosarcoma. *Cancer* (1984) 54(10):2160–4. doi: 10.1002/1097-0142 (19841115)54:10<2160::AID-CNCR2820541016>3.0.CO;2-P
69. Jeffree GM, Price CH, Sissons HA. The Metastatic Patterns of Osteosarcoma. *Br J Cancer* (1975) 32(1):87–107. doi: 10.1038/bjc.1975.136

Disclaimer: The content is solely the responsibility of the authors and does not necessarily represent the official views of the National Institutes of Health.

Conflict of Interest: SG and CD have patent and patent applications in the field of cell and gene therapy for cancer, including a patent application for B7-H3-CAR T cells. SG consults for Catamaran Bio, Nektar Therapeutics, TESSA Therapeutics, is on the Scientific Advisory Board of Tidal, and is a DSMB member of Immatics.

The remaining authors declare that the research was conducted in the absence of any commercial or financial relationships that could be construed as a potential conflict of interest.

frontiers | Frontiers in Immunology

TYPE Original Research
PUBLISHED 29 July 2022
DOI 10.3389/fimmu.2022.919231

OPEN ACCESS

EDITED BY
Keqiang Chen,
National Cancer Institute at Frederick (NIH), United States

REVIEWED BY
Yafeng He,
National Heart, Lung, and Blood Institute (NIH), United States
Feng Jiang,
Fudan University, China

*CORRESPONDENCE
Peng Xu
sousou369@163.com

SPECIALTY SECTION
This article was submitted to Cancer Immunity and Immunotherapy, a section of the journal Frontiers in Immunology

RECEIVED 13 April 2022
ACCEPTED 04 July 2022
PUBLISHED 29 July 2022

CITATION
Yang M, Zheng H, Xu K, Yuan Q, Aihaiti Y, Cai Y and Xu P (2022) A novel signature to guide osteosarcoma prognosis and immune microenvironment: Cuproptosis-related lncRNA.
Front. Immunol. 13:919231.
doi: 10.3389/fimmu.2022.919231

A novel signature to guide osteosarcoma prognosis and immune microenvironment: Cuproptosis-related lncRNA

Mingyi Yang, Haishi Zheng, Ke Xu, Qiling Yuan, Yirixaiti Aihaiti, Yongsong Cai and Peng Xu*

Department of Joint Surgery, HongHui Hospital, Xi'an Jiaotong University, Xi'an, China

Objective: Osteosarcoma (OS) is a common bone malignancy with poor prognosis. We aimed to investigate the relationship between cuproptosis-related lncRNAs (CRLncs) and the survival outcomes of patients with OS.

Methods: Transcriptome and clinical data of 86 patients with OS were downloaded from The Cancer Genome Atlas (TCGA). The GSE16088 dataset was downloaded from the Gene Expression Omnibus (GEO) database. The 10 cuproptosis-related genes (CRGs) were obtained from a recently published article on cuproptosis in *Science*. Combined analysis of OS transcriptome data and the GSE16088 dataset identified differentially expressed CRGs related to OS. Next, pathway enrichment analysis was performed. Co-expression analysis obtained CRLncs related to OS. Univariate COX regression analysis and least absolute shrinkage and selection operator (LASSO) regression analysis were used to construct the risk prognostic model of CRLncs. The samples were divided evenly into training and test groups to verify the accuracy of the model. Risk curve, survival, receiver operating characteristic (ROC) curve, and independent prognostic analyses were performed. Next, principal component analysis (PCA) and t-distributed stochastic neighbor embedding (t-SNE) analysis were performed. Single-sample gene set enrichment analysis (ssGSEA) was used to explore the correlation between the risk prognostic models and OS immune microenvironment. Drug sensitivity analysis identified drugs with potential efficacy in OS. Real-time quantitative PCR, Western blotting, and immunohistochemistry analyses verified the expression of CRGs in OS. Real-time quantitative PCR was used to verify the expression of CRLncs in OS.

Results: Six CRLncs that can guide OS prognosis and immune microenvironment were obtained, including three high-risk CRLncs (AL645608.6, AL591767.1, and UNC5B-AS1) and three low-risk CRLncs (CARD8-AS1, AC098487.1, and AC005041.3). Immune cells such as B cells, macrophages, T-helper type 2 (Th2) cells, regulatory T cells (Treg), and immune functions such as APC co-inhibition, checkpoint, and T-cell co-inhibition were significantly downregulated in high-risk groups. In addition, we obtained four drugs with potential efficacy for OS: AUY922, bortezomib, lenalidomide, and Z.LLNle.CHO. The expression of LIPT1, DLAT, and

FDX1 at both mRNA and protein levels was significantly elevated in OS cell lines compared with normal osteoblast hFOB1.19. The mRNA expression level of AL591767.1 was decreased in OS, and that of AL645608.6, CARD8-AS1, AC005041.3, AC098487.1, and UNC5B-AS1 was upregulated in OS.

Conclusion: CRLncs that can guide OS prognosis and the immune microenvironment and drugs that may have a potential curative effect on OS obtained in this study provide a theoretical basis for OS survival research and clinical decision-making.

KEYWORDS

osteosarcoma, LncRNA, immunity, prognosis, cuproptosis

Introduction

Osteosarcoma (OS) is the most common primary bone tumor originating from primitive mesenchymal cells (1). OS primarily affects long bones, with sarcoma cells forming immature bone or osteoid tissues (2). OS is the most common primary bone cancer in children and adolescents and the third most common bone cancer in adults, after chondrosarcoma and chordoma (2). OS mainly affects children and adolescents aged 10–30 years and has a bimodal age distribution, with the first peak at 15–19 years (8 cases/million/year) and the second at 75–79 years (6 cases/million/year) (3, 4). OS is highly malignant, with lesions that can spread throughout the body and metastasize to distant sites, most often to the lungs (5). Chemotherapy and surgical resection are the standard treatments for OS (6). Metastatic OS frequently recurs and has a poor prognosis, and combined chemotherapy treatment slightly improves OS compared with surgical resection alone (7). The 5-year survival rate for patients with localized OS is 80%, and the 5-year survival rate for patients with metastatic OS is 15%–30% (8). Over the past 20 years, despite many chemotherapy regimens, the OS rate has not improved significantly (9). No successful OS-targeted therapies have been developed (2). Therefore, exploring new targets and features to improve the clinical efficacy and survival of patients with OS is necessary.

The top international academic journal *Science* announced the existence of cuproptosis and the 10 discovered cuproptosis-related genes (CRGs): ferredoxin 1 (FDX1), lipolytransferase1 (LIPT1), lipoyl synthase (LIAS), dihydrolipoamide dehydrogenase (DLD), dihydrolipoamide S-acetyltransferase (DLAT), pyruvate dehydrogenase E1 subunit alpha 1 (PDHA1), pyruvate dehydrogenase E1 subunit beta (PDHB), metal regulatory transcription factor 1 (MTF1), glutaminase (GLS), and cyclin-dependent kinase inhibitor 2A (CDKN2A) (10). Cuproptosis is a new form of cell death that depends on copper ions and is regulated by cells (10). The mechanism by which cuproptosis causes cell death is distinct from all other known regulatory mechanisms of cell death, including apoptosis, ferroptosis, pyroptosis, and necrosis (10).

Copper-induced cell death is closely related to mitochondrial metabolism and the tricarboxylic acid (TCA) cycle (10). After interfering with mitochondrial function, the sensitivity of cells to copper ions was significantly altered. Copper-induced cell death requires mitochondrial respiration rather than ATP from glycolysis. Furthermore, copper ions are not directly involved in the electron transport chain but only play a role in the TCA cycle. TCA-cycle-related metabolites are significantly increased in copper-sensitive cells (10). Copper ions directly bind to fatty acylated components in the TCA cycle, resulting in the abnormal aggregation of fatty acylated proteins and loss of iron–sulfur cluster proteins, leading to protein toxic stress responses and ultimately cell death (10). Copper-induced fatty acylation and iron–sulfur cluster proteins in human cancer cells are conserved from bacterial to human evolution, suggesting that copper ionophores are naturally synthesized and display antibacterial activity and that microbes may contribute to cuproptosis (11).

FDX1 and proteoacetylation are key regulators of copper-ionophore-induced cell death (10). Elesclomol and diethyldithiocarbamate are structurally different copper ionophores. FDX1 not only reduces Cu^{2+} to the more toxic Cu^{1+} but is also a direct target of the copper ionophore elesclomol (12). Knockdown of seven CRGs (FDX1, LIPT1, LIAS, DLD, DLAT, PDHA1, and PDHB) rescued the cytotoxic effects of elesclomol and diethyldithiocarbamate (10). These seven CRGs are positively regulated during cuproptosis, and MTF1, GLS, and CDKN2A are negatively regulated during cuproptosis (10). FDX1 deletion confers resistance to various copper ionophores (disulfiram, NSC319726, thiram, 8-HQ, and Zn-pyrithione). Deletion of FDX1 and LIAS resulted in copper-induced cell death. Protein fatty acylation is a highly conserved post-translational lysine modification that occurs in only four enzymes: dihydrolipoamide branched chain transacylase E2 (DBT), glycine cleavage system protein H (GCSH),

dihydrolipoamide S-succinyltransferase (DLST), and DLAT (13, 14). These enzymes are not only involved in regulating the metabolic complexes of carbon in the TCA cycle but also important components of the PDH complex (10). DLAT, PDHA1, and PDHB belong to the PDH complex, which is a protein target for fatty acylation. FDX1 is an upstream regulator of fatty acylation (10). FDX1 knockdown results in the accumulation of pyruvate and α-ketoglutarate and depletion of succinate, impairing protein fatty acylation by inhibiting the TCA cycle at PDH and α-ketoglutarate dehydrogenase (10). FDX1 knockout resulted not only in the loss of protein fatty acylation but also a marked decrease in cellular respiration at levels similar to those observed with LIAS deletion. DLAT and DLST can bind to copper ions, and when FDX1 deletion prevents protein fatty acylation, DLAT and DLST no longer bind to copper. Therefore, fatty acylation is necessary for copper ion binding (10). Copper ions directly bind to and induce oligomerization of fatty acylated DLAT, and the toxic production of fatty acylated proteins upon exposure to copper ionophores is partially mediated by abnormal oligomerization (10). Furthermore, depletion of the intracellular natural copper chaperone glutathione resulted in copper-dependent cell death, which was associated with decreased fatty acylation due to the attenuation of FDX1 and LIAS and increased DLAT oligomerization (10).

FDX1 and the abundance of fatty acylated proteins are highly correlated with various human tumors, and cell lines with high levels of fatty acylated proteins are sensitive to cuproptosis, suggesting that copper ionophore therapy could target tumors with this metabolic profile (10). A study found that OS was related to the TCA cycle (15). A meta-analysis study in an OS mouse model found that many key metabolites and most amino acids in glycolysis and TCA cycles were elevated during rapid tumor growth, possibly because of the high energy requirements and the conversion of anabolic processes during tumor proliferation (15). Serum metabolism studies in an OS mouse model of lung metastasis have shown reduced carbohydrate and amino acid metabolism but elevated lipid metabolism associated with tumor metastasis (15). Therefore, studying the correlation between OS and cuproptosis to explore the therapeutic targets of OS is necessary.

Studies have identified pyroptosis- and autophagy-related genes that can predict OS prognosis by using risk prognostic models (16, 17). In this study, a novel OS prognosis model was established to explore cuproptosis-related lncRNAs (CRLncs) that can guide OS prognosis and immune microenvironment. The model was effective in predicting the long-term prognosis of patients with OS.

Materials and methods

Data download and arrangement

The OS transcriptome data and clinical data of 86 cases were downloaded from The Cancer Genome Atlas (TCGA) database (https://portal.gdc.cancer.gov/) and included mRNAs and lncRNAs. The clinical data were sorted to include futime, fustat, sex, age at diagnosis in days, metastatic/non-metastatic, primary tumor site, and specific tumor site. The GSE16088 dataset, including 6 normal tissue samples and 14 OS tissue samples, was downloaded from the Gene Expression Omnibus (GEO) database (https://www.ncbi.nlm.nih.gov/geo/).

OS-related differentially CRGs

The 10 CRGs were intersected with genes in the OS transcriptome data to obtain OS-related CRGs. The limma package of R performed differential analysis on the GSE16088 dataset to obtain differentially expressed genes (DEGs). The screening criteria were $p < 0.05$ and $|\log FC| > 0.65$ (18). OS-related CRGs and DEGs were intersected to identify the differentially expressed OS-related CRGs.

Enrichment analysis

The clusterProfiler package of R was used to conduct the Kyoto Encyclopedia of Genes and Genomes (KEGG) enrichment analysis for OS-related differentially expressed CRGs, and the screening criterion was $p < 0.05$.

OS-related CRLncs

The limma package of R was used to perform co-expression analysis of OS-related differentially expressed CRGs and lncRNAs in OS transcriptome data to obtain OS-related CRLncs, and the screening criteria were |Pearson correlation coefficient| > 0.4 and $p < 0.001$ (19).

Construction of risk prognostic model

The survival package in R was used to obtain statistically significant ($p < 0.05$) CRLncs associated with OS prognosis through univariate COX regression analysis and calculate the hazard ratio (HR) value. The glmnet package in R was used to perform LASSO regression analysis to narrow the risk of overfitting and determine the optimal number of CRLncs involved in model building. The samples were divided into training and test groups to verify the accuracy of the model. A risk prognosis model was built for the total sample, training, and test groups.

$$\text{Risk} \quad \text{Score} = \sum_{i=1}^{n} (lncrnaexp_i \times coef_i)$$

where n represents the number of OS prognosis CRLncs, i is the ith CRLncs, coef is the regression coefficient, and the

expression of OS prognosis CRLncs is multiplied by the corresponding regression coefficient and accumulated to obtain the sample risk score (16). The samples in the total sample, training, and test groups were divided into high- and low-risk groups according to the median of the risk score.

Validation of risk prognostic model

Risk curve analysis, survival analysis, receiver operating characteristic (ROC) curve analysis, and independent prognosis analysis were performed on the risk prognostic models of the total sample, training, and test groups, respectively. R was used to draw the survival status map and risk heatmap of the risk prognosis model and observe the differences in patient survival time and OS prognosis CRLncs in high- and low-risk groups (17). The survival and survminer packages in R were used to construct survival curves, and the survival, survminer, and timeROC packages in R were used to plot ROC curves. The survival package in R was used to perform independent prognostic tests through univariate and multivariate COX regression analyses to test whether the risk score can be used as an independent prognostic factor (20).

Principal component analysis and t-distributed stochastic neighbor embedding analysis

Principal component analysis (PCA) and t-distributed stochastic neighbor embedding (t-SNE) analysis were performed on the risk prognostic model of the total sample group to observe whether the expression of the OS prognostic CRLncs involved in the model construction could distinguish patients in the high- and low-risk groups to test the accuracy of the model.

Tumor microenvironment analysis

The limma and estimate packages of R were used to perform tumor microenvironment analysis on OS transcriptome data to obtain immune scores, stromal scores, and total scores for each OS patient (21). The limma and ggpubr packages of R were used to analyze whether immune, stromal, and total scores differed in the risk prognostic model of the total sample group (16).

Single-sample gene set enrichment analysis

The GSVA, limma, and GSEABase packages in R were used to obtain enrichment scores for immune cells and immune function for OS transcriptome data. The limma, reshape2, and ggpubr packages in R were used to analyze the differences in immune cells and immune function in the risk prognosis model of the total sample group (16).

Drug sensitivity analysis

The limma, ggpubr, and pRRophetic packages of R were used to perform drug sensitivity analysis to determine which drugs had different sensitivities in the risk prognostic model of the total sample group and to screen potential therapeutic drugs for OS, with $p < 0.001$ as the screening criterion.

Cell culture

Human OS cell lines (HOS, 143B, and U2OS) and human normal osteoblast cell (hFOB1.19) were purchased from Wuhan Procell Life Science and Technology Co., Ltd. (Wuhan, China). Each cell line was cultured in its dedicated medium (Wuhan Procell Life Science and Technology Co. Ltd., Wuhan, China). Human OS cell lines were cultured at 37°C in an incubator with 5% CO_2. The hFOB1.19 cells were cultured in a 34°C incubator with 5% CO_2.

Real-time quantitative PCR

Total RNA was extracted from OS cell lines and hFOB1.19 using TRIzol Reagent (Cat. No. P118-05, GenStar, Beijing, China) according to the manufacturer's instructions. Total RNA was amplified by RT-PCR using SYBR Green Master Mix (Cat#: C0006, TOPSCIENCE, Shanghai, China) according to the manufacturer's instructions, and the mRNA levels of CRGs and CRLncs were detected. The primer pairs were synthesized by Accurate Biology (Changsha, China), and the primer pairs are listed in Table 1. All samples were normalized to β-actin, and the $2^{-\Delta\Delta Ct}$ method was used to evaluate relative expression levels.

Western blotting

OS cells and hFOB1.19 were harvested with radioimmuno precipitation assay (RIPA) buffer (Zhonghuihecai, Xi'an, China) and pelleted by centrifugation at 4°C for 15 min, and the supernatant was discarded. Next, 1/5 sodium dodecyl sulfate–polyacrylamide gel (SDS-PAGE) sample loading buffer, 5× (Beyotime, Shanghai, China) was added to the supernatant and heated in a 100°C metal bath for 10 min. The protein was separated on a 15% SDS-PAGE, transferred to a 0.22-μm polyvinylidene fluoride (PVDF) membrane (Millipore, USA), placed in 5%

TABLE 1 Primer sequences for RT-qPCR.

Genes	Forward	Reverse
β-actin	TGGCACCCAGCACAATGAA	CTAAGTCATAGTCCGCCTAGAAGCA
LIPT1	GCTCTGAATGCTGTCCAACCC	GCAATGGTGATAGGCAGTAGTCC
DLD	GCCGACGACCCTTTACTAAGAAT	GGACCAGCAACTACATCACCAAT
PDHA1	CAGACCATCTCATCACAGCCTACC	CCTCCTTTCCCTTTAGCACAACCT
DLAT	GTTCCCATCGGAGCGATCAT	GCTGCTGAGGAATCCAGTGT
FDX1	CCTGGCTTGTTCAACCTGTCA	CCAACCGTGATCTGTCTGTTAGTC
CDKN2A	AGCACTCACGCCCTAAGC	TGACTCAAGAGAAGCCAGTAACC
AL645608.6	AGGTCCCACCATCCTCACAA	CGGACCCGAACTCTCAGATG
CARD8-AS1	CCTCAGCTGGAATGCCTTCAT	GGGTTACACACATTCTCGGC
AL591767.1	TGAGCTTAAACAAGCTTAGGAGTTA	CGCCCAGCTGGTTATTTTTGA
AC098487.1	CTGTAGAGAAGAGGAACCGTAGC	TGGTTGACCTAGAAATGGAAGGAA
UNC5B-AS1	GGGCCGGAGTTCCAATCAA	GCATTTCCCTGAGGCAGGAT
AC005041.3	TATCTTGCACCCACACACCC	TTATTGAGCAGGCCTCCGTG

skimmed milk, blocked for approximately 2 h, and incubated with specific antibodies. Antibodies used were as follows: the DLAT (Cat. No. 13426-1-AP, 1:2,000), DLD (Cat. No. 16431-1-AP, 1:2,000), CDKN2A (Cat. No. 10883-1-AP, 1:1,000), and FDX1 (Cat. No. 12592-1-AP, 1:500) antibodies were purchased from Proteintech (Wuhan, China); PDHA1 (Cat. No. bs-4034R,1:500) and LIPT1 (Cat. No. bs-18298R,1:500) were purchased from Bioss (Beijing, China); and β-actin (Cat. No. AC026, 1:100,000, ABclonal). The protein bands were enhanced using a chemiluminescent kit (Vazyme, Nanjing, China).

Immunohistochemistry and hematoxylin–eosin staining

CRGs were experimentally verified by immunohistochemistry (IHC) staining. Three OS tissue samples and one normal osteogenic tissue sample were collected from patients at Honghui Hospital, affiliated with Xi'an Jiaotong University. None of the patients received anti-cancer treatment before tissue sample collection. All patients signed an informed consent form, and the study was approved by the hospital ethics committee.

Tissues were fixed and paraffinized before immunohisto chemistry (IHC) staining. Slides were cut to a width of 5 μm, dewaxed, and rehydrated. Endogenous peroxidase was inactivated by treatment with 3% H_2O_2 for 10 min, followed by incubation with a 5% bovine serum albumin (BSA) blocking solution for 1 h at room temperature. The cells were treated with hydrogen peroxide for 10 min to inactivate endogenous peroxidases. The sections were incubated with the corresponding protein antibodies overnight at 4° C. Antibodies used were as follows: the DLAT (Cat. No. 13426-1-AP, 1:500), DLD (Cat. No. 16431-1-AP, 1:500), and FDX1 (Cat. No. 12592-1-AP, 1:200) antibodies were purchased from Proteintech (Wuhan, China); PDHA1 (Cat. No. bs-4034R, 1:100) and LIPT1 (Cat No. bs-18298R, 1:100) were purchased from Bioss (Beijing, China); and CDKN2A (Cat. No. GB111143, 1:500, Servicebio). The sections were then incubated with biotinylated goat anti-rabbit secondary antibody for 30 min at 37°C. Color development was performed using freshly prepared 3,3′-diaminobenzidine (DAB) reagent (Boster, Wuhan, China). IHC staining of each tissue section was performed by two independent pathologists.

Statistical analysis

Statistical analysis and visualization were performed using R.4.1.2, GraphPad Prism v8.2.1 and SPSS 22.0. Experimental results were expressed as mean ± SD (standard deviation), and statistical significance was determined by one-way ANOVA. $p < 0.05$ was considered statistically significant. Each experiment was performed at least three times independently.

Results

OS-related differentially CRGs and enrichment analysis

Ten OS-related CRGs were identified. Difference analysis of the GSE16088 dataset obtained 6,291 DEGs: 2,936 upregulated DEGs and 3,355 downregulated DEGs. R was used to visualize volcano plots (Figure 1A) and heatmaps (Figure 1B). Finally, we identified six OS-related differentially expressed CRGs (Figure 2A). The six OS-related differentially expressed CRGs are highly expressed in OS. The six OS-related differentially CRGs were significantly enriched in the citrate cycle (TCA cycle); pyruvate metabolism; glycolysis/gluconeogenesis; carbon metabolism; biosynthesis of cofactors; glyoxylate and dicarboxylate metabolism; propanoate metabolism; glycine, serine, and threonine metabolism; bladder

cancer; tryptophan metabolism; valine, leucine, and isoleucine degradation; lysine degradation; central carbon metabolism in cancer; melanoma; non-small cell lung cancer; platinum drug resistance; p53 signaling pathway; glioma; pancreatic cancer; and chronic myeloid leukemia (Figure 2B).

Construction of risk prognostic model

A total of 118 OS-related CRLncs were identified by co-expression analysis (Figure 2C). Univariate COX regression analysis identified 14 CRLncs associated with OS prognosis, including 11 high-risk CRLncs (RPARP-AS1, AC012442.1, AL645608.6, AC006160.1, AP000251.1, SNHG1, VPS9D1-AS1, IRAIN, AL591767.1, LENG8-AS1, and UNC5B-AS1) and 3 low-risk CRLncs (CARD8-AS1, AC098487.1, and AC005041.3) (Figure 3A). According to the optimal penalty parameter (λ) value, the LASSO regression analysis determined that the optimal number of CRLncs participating in the model construction was 6 (Figures 3B, C). The risk score for each sample was obtained using the prognostic model formula. The total sample group was divided into a high-risk group (N = 47) and a low-risk group (N = 39). The training group was divided into high-risk (N = 21) and low-risk (N = 22) groups. The test group was divided into high-risk (N = 26) and low-risk (N = 17) groups.

Risk prognosis models predict the prognosis of patients with OS

The survival status map of the total sample, train, and test groups showed that the mortality rate of patients from the low-risk group to the high-risk group gradually increased (Figures 4A, 5A, 6A). The risk heatmaps of the total sample group, training group, and test group showed that from the low- to the high-risk group, the expression levels of AL645608.6, AL591767.1, and UNC5B-AS1 gradually increased, which are high-risk CRLncs, and the expression levels of CARD8-AS1, AC098487.1, and AC005041.3 gradually decreased, which are low-risk CRLncs (Figures 4B, 5B, 6B).

The survival curves of the total sample group ($p < 0.001$), training group ($p < 0.001$), and test group ($p = 0.027$) showed that the survival of patients in the high- and low-risk groups was significantly different (Figures 4C, 5C, 6C). The ROC curve of the total sample group had a higher area under curve (AUC) at 1 year (AUC = 0.795), 3 years (AUC = 0.817), and 5 years (AUC = 0.812) (Figure 4D). The ROC curve of the training group had a higher AUC at 1 year (AUC = 0.930), 3 years (AUC = 0.915), and 5 years (AUC = 0.947) (Figure 5D). The ROC curve of the test group had a higher AUC at 1 year (AUC = 0.658), 3 years (AUC = 0.691), and 5 years (AUC = 0.643) (Figure 6D).

Univariate independent prognostic analysis of the total sample group showed that the risk score ($p < 0.001$, HR = 1.000) and tumor metastasis ($p < 0.001$, HR = 4.770) can be used as independent prognostic factors, which are high-risk factors (Figure 4E). Multivariate independent prognostic analysis of the total sample group showed that the risk score ($p = 0.007$, HR = 1.000) and tumor metastasis ($p < 0.001$, HR = 3.970) can be used as independent prognostic factors, which are high-risk factors (Figure 4F). Univariate independent prognostic analysis of the training group showed that both risk score ($p = 0.003$, HR = 1.002), tumor metastasis ($p < 0.001$, HR = 9.264), and specific tumor site ($p = 0.040$, HR = 0.819) can be used as independent prognostic factors, among which risk score and tumor metastasis were high-risk factors

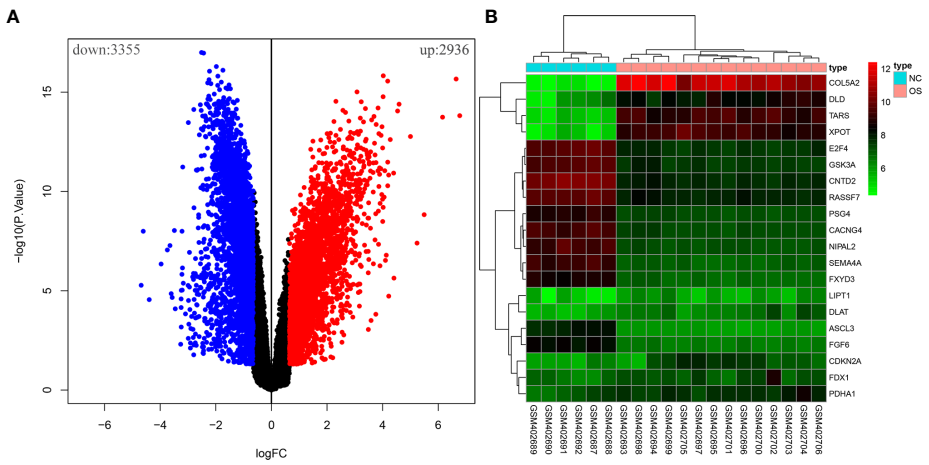

FIGURE 1
The differential analysis of the GSE16088 dataset. **(A)** Volcano plot of DEGs, red for high expression and blue for low expression. **(B)** Heatmap of DEGs, with high expression in red and low expression in green.

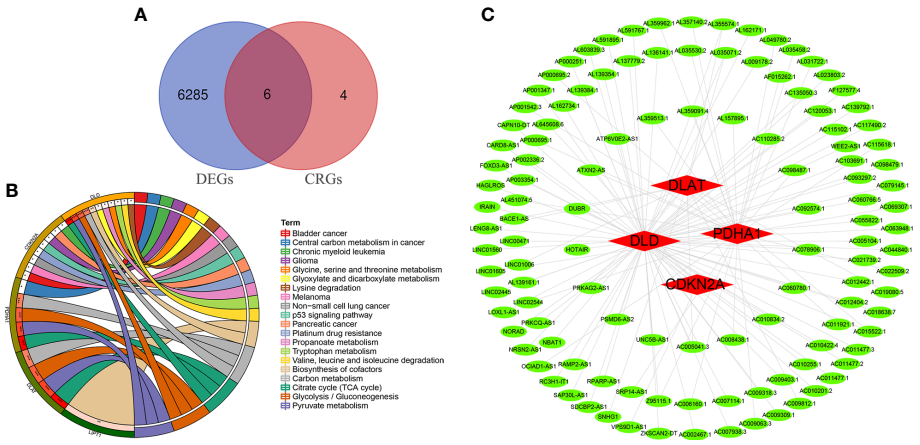

FIGURE 2
Differentially CRGs and CRLncs related to OS. **(A)** The intersection of DEGs and OS-related CRGs obtained OS-related differentially CRGs. **(B)** Pathway enrichment analysis of OS-related differentially CRGs. **(C)** By co-expression analysis, OS-related differentially CRGs yielded a total of 118 OS-related CRLncs.

and specific tumor sites were low-risk factors (Figure 5E). Multivariate independent prognostic analysis of the training group showed that the risk score (p = 0.034, HR = 1.001) and tumor metastasis (p = 0.002, HR = 9.017) can be used as independent prognostic factors, which are high-risk factors (Figure 5F). Univariate independent prognostic analysis of the test group showed that the risk score (p < 0.001, HR = 1.008) and tumor metastasis (p = 0.040, HR = 2.814) can be used as independent prognostic factors, which are high-risk factors (Figure 6E). Multivariate independent prognostic analysis of the test group showed that the risk score (p < 0.001, HR = 1.009) and tumor metastasis (p = 0.032, HR = 3.686) can be used as independent prognostic factors, which are high-risk factors (Figure 6F). Our risk prognostic model indicated that the risk score and tumor metastasis could be independent prognostic factors for patients with OS, and both were high-risk factors.

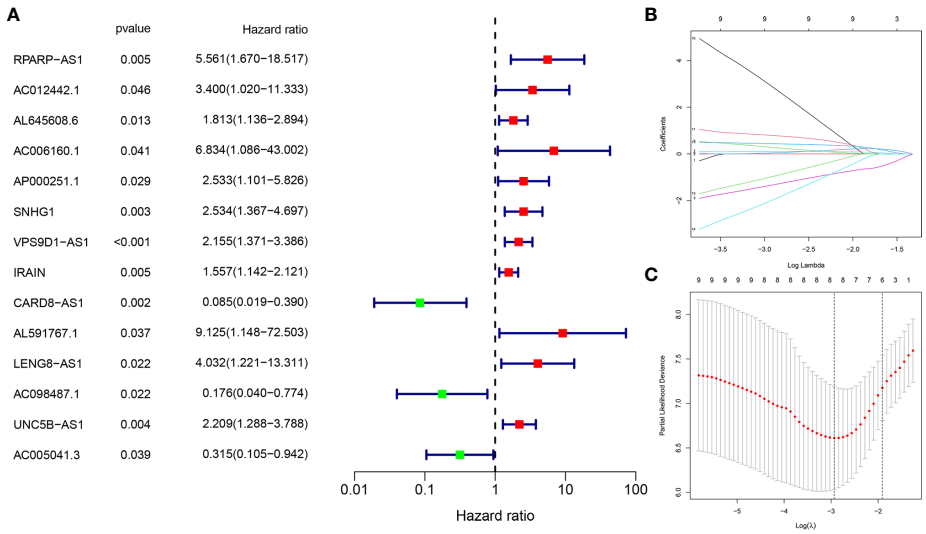

FIGURE 3
Construction of risk prognostic model. **(A)** Univariate Cox regression analysis obtained 14 candidate prognostic CRLncs for OS, including 11 high-risk CRLncs and three low-risk CRLncs. **(B)** LASSO regression analysis. **(C)** Selection of the optimal penalty parameter for LASSO regression.

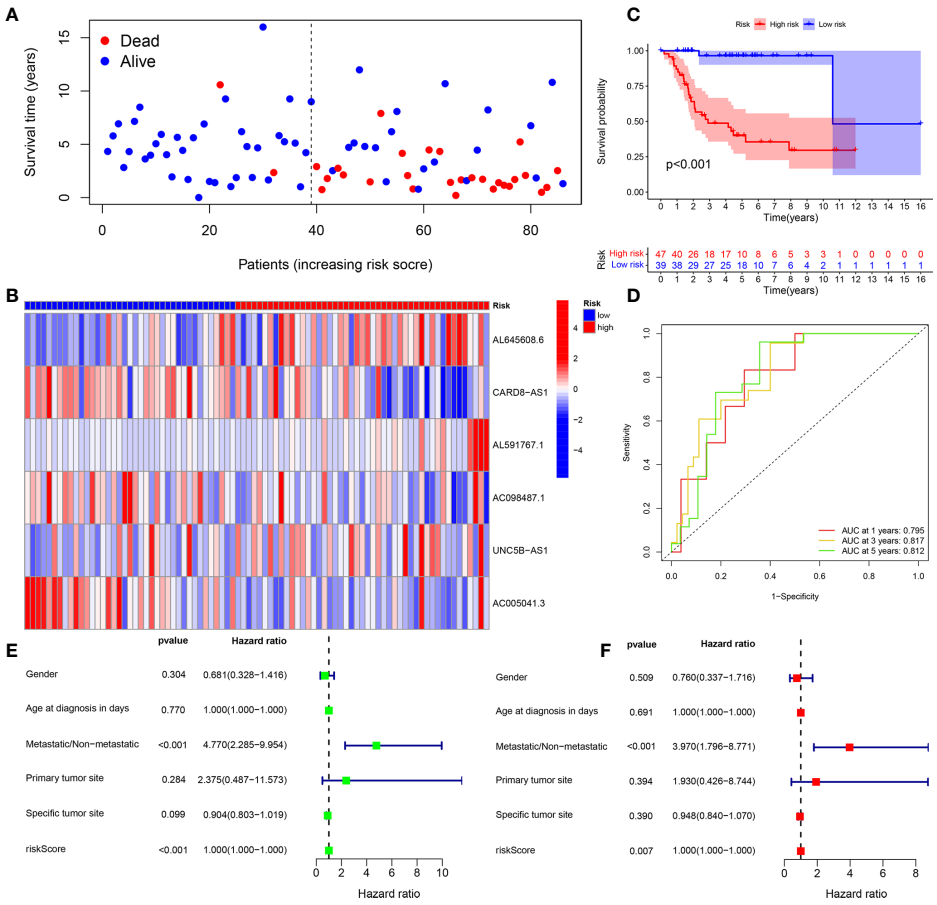

FIGURE 4
Total sample group. **(A)** Survival status map. **(B)** Risk heatmap. **(C)** Survival curve. **(D)** ROC curve. **(E)** Univariate COX regression analysis. **(F)** Multivariate COX regression analysis.

In addition, PCA and t-SNE analyses revealed that the expression levels of OS prognostic CRLncs involved in model construction could significantly distinguish patients in the high- and low-risk groups, illustrating the accuracy of the model (Figures 7A, B). Thus, our risk prognostic model can well predict the survival of patients with OS.

Risk prognostic models guide immune microenvironment of patients with OS

The tumor microenvironment difference analysis showed differences in the stromal cell scores ($p = 0.0044$), immune cell scores ($p = 0.022$), and total scores ($p = 0.0042$) in the high- and low-risk groups, and the scores in the low-risk group were higher than those in the high-risk group (Figure 7C). Differential analysis of immune cells showed that B cells, macrophages, T-helper type 2 (Th2) cells, and regulatory T cells (Tregs) were significantly downregulated in the high-risk group ($p < 0.001$) (Figure 8A). Differential analysis of immune function showed that APC co-inhibition, checkpoint, and T-cell co-inhibition were significantly downregulated in the high-risk group ($p < 0.001$) (Figure 8B).

Drugs with potential efficacy in OS

Drug sensitivity analysis revealed that AUY922 ($p = 0.00023$), bortezomib ($p = 0.00017$), lenalidomide ($p = 0.00028$), and Z.LLNle.CHO ($p = 0.00011$) showed significant sensitivity in the high- and low-risk groups. Patients in the low-risk group were more sensitive to AUY922, bortezomib, and Z.LLNle.CHO than patients in the high-risk group, and patients in the high-risk group were more sensitive to lenalidomide than patients in the low-risk group (Figure 8C).

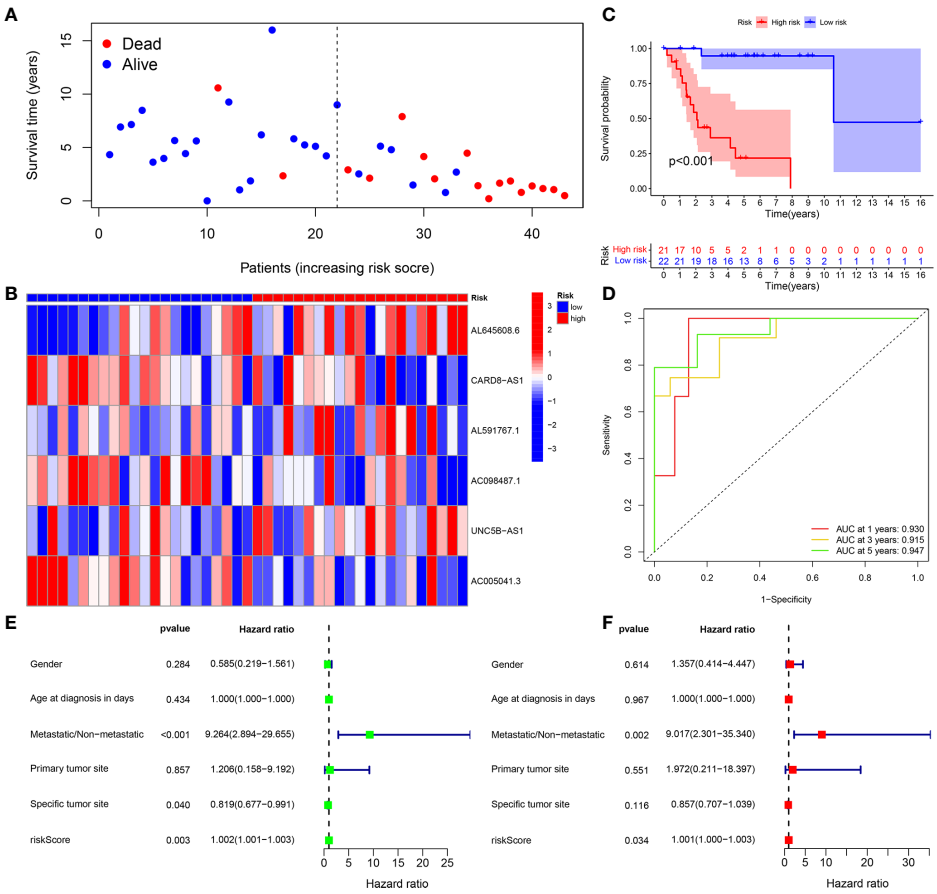

FIGURE 5
Training group. **(A)** Survival status map. **(B)** Risk heatmap. **(C)** Survival curve. **(D)** ROC curve. **(E)** Univariate COX regression analysis. **(F)** Multivariate COX regression analysis.

Validation of the expression of CRGs and CRLncs in OS

To further assess the expression of CRGs and CRLncs, we selected three OS cell lines to detect their mRNA and protein expression levels, and the control group was normal osteoblast hFOB1.19. Compared with normal osteoblast hFOB1.19, the mRNA expression level of DLD and FDX1 were significantly upregulated in 143B cell line, and DLAT was significantly highly expressed in U2OS cell line. In addition, the mRNA expression level of LIPT1 was significantly increased in three OS cell lines HOS, 143B, and U2OS compared to that in hFOB1.19 (Figure 9A). The mRNA expression level of AL591767.1 in the 143B cell line was decreased compared with the normal osteoblast hFOB1.19, and AL645608.6 was increased. The mRNA expression level of CARD8-AS1 and AC005041.3 were upregulated in three OS cell lines compared with normal osteoblast hFOB1.19. Besides, compared with normal osteoblast hFOB1.19, the mRNA expression level of AC098487.1 was upregulated in both HOS and U2OS cell lines, and the mRNA expression level of UNC5B-AS1 was upregulated in 143B and U2OS cell lines (Figure 9B).

Western blotting results showed that compared with normal osteoblast hFOB1.19, the protein expression level of DLAT was significantly highly expressed in HOS cell line, and the protein expression level of PDHA1 and CDKN2A were significantly upregulated in U2OS cell line. in addition, the protein expression level of LIPT1 was significantly elevated in both 143B and U2OS, and the protein expression level of FDX1 was significantly overexpressed in three osteosarcoma cell lines HOS, 143B, and U2OS (Figure 10).

The expression levels of DLAT, DLD, CDKN2A, FDX1, PDHA1, and LIPT1 proteins in OS and normal osteogenic tissues were detected by IHC using the corresponding antibodies and IgG (isotype). The results showed that the expression of DLAT, DLD, CDKN2A, FDX1, PDHA1, and LIPT1 was higher in OS tissues than in normal osteogenic tissues (Figure 11).

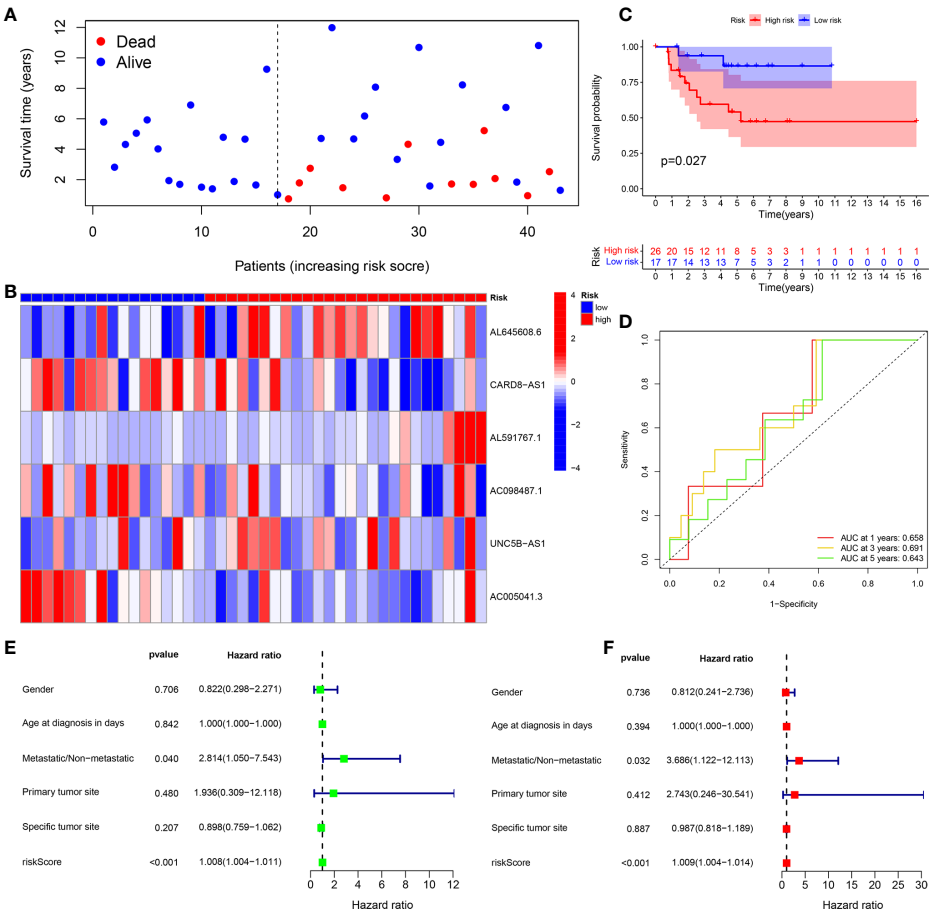

FIGURE 6
Test group. **(A)** Survival status map. **(B)** Risk heatmap. **(C)** Survival curve. **(D)** ROC curve. **(E)** Univariate COX regression analysis. **(F)** Multivariate COX regression analysis.

Overall, it was experimentally verified that the expression of LIPT1, DLAT, and FDX1 at both mRNA and protein levels was significantly elevated in OS cell lines compared with normal osteoblast hFOB1.19. This is consistent with the results of our bioinformatics analysis. LIPT1, DLAT, and FDX1 may be potential targets for the diagnosis and treatment of OS. Besides, the mRNA expression level of AL591767.1 was decreased in OS, and that of AL645608.6, CARD8-AS1, AC005041.3, AC098487.1, and UNC5B-AS1 was upregulated in OS.

Discussion

Similar to iron, copper is a basic element required for human activities (22). Copper plays an essential role as a cofactor for essential enzymes (22). Copper is a trace element in the human body, and the concentration of intracellular copper ions is maintained at very low levels by active homeostatic mechanisms. Once the threshold is exceeded, copper becomes toxic, leading to cell death (22, 23). Cells dependent on mitochondrial respiration are approximately 1,000 times more sensitive to copper ionophores than glycolytic cells, and mitochondrial antioxidants, fatty acids, and mitochondrial function inhibitors have a significant effect on copper ionophore sensitivity (10). An OS metabolomic study found that the TCA cycle was altered in OS, and both the TCA cycle and glutathione metabolism were downregulated in human OS cancer stem cells (24). When combined with a glutaminase inhibitor (CB-839) and metformin for the treatment of OS, CB-839 limits cell proliferation by forcing dependence on fatty-acid-derived carbons, which reduces aspartate biosynthesis and induces ketosis (25). The combination of CB-839 and metformin not only inhibits OS primary tumor growth but also reduces the risk of OS metastasis (25). In addition, OS cells treated with the combination showed decreased cellular mitochondrial respiration and an overall decrease in glycolysis and TCA cycle function (25). OS is related to the TCA cycle and

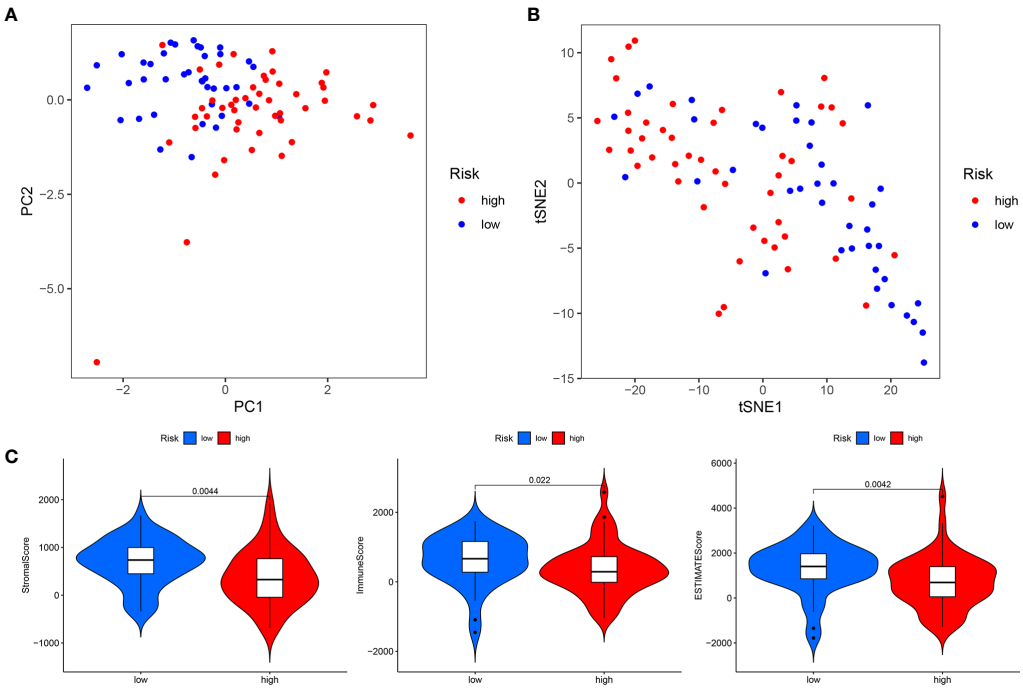

FIGURE 7
Total sample group. **(A)** Principal component analysis. **(B)** t-Distributed stochastic neighbor embedding analysis. **(C)** Differential analysis of tumor microenvironment.

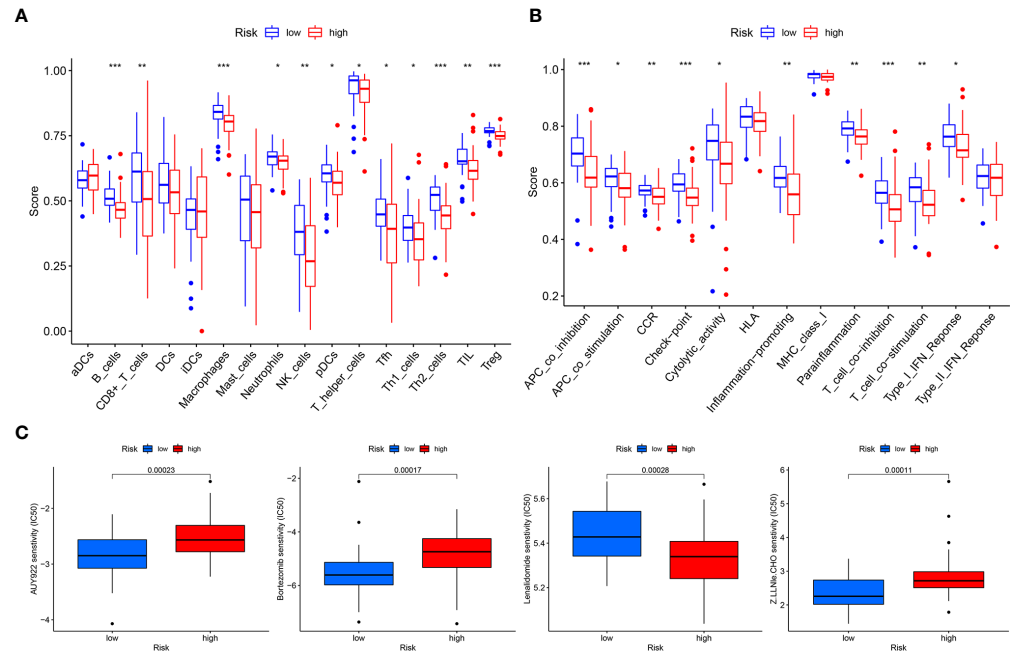

FIGURE 8
Total sample group. **(A)** Immune cell differential analysis for single sample gene set enrichment analysis. **(B)** Immune function differential analysis for single sample gene set enrichment analysis. **(C)** Drug sensitivity analysis.

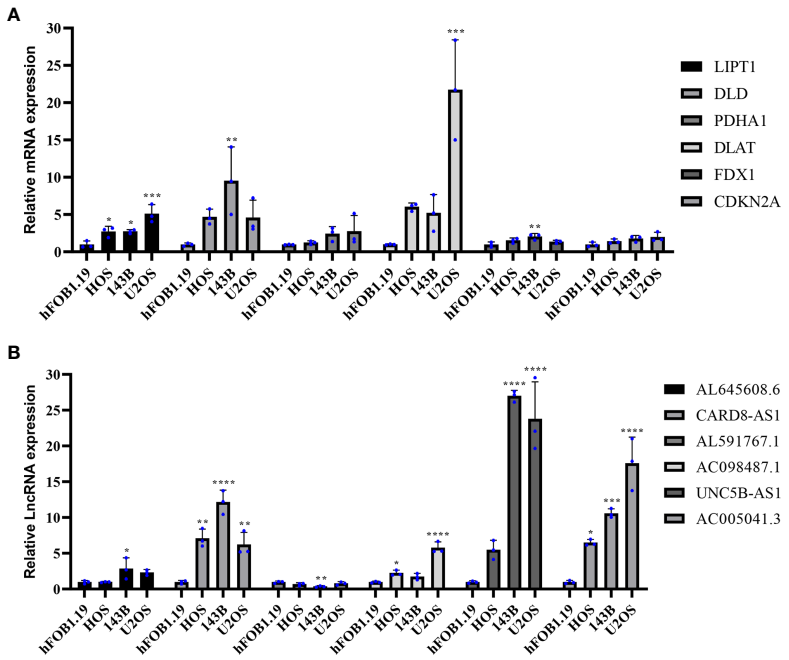

FIGURE 9
Validation of the mRNA expression level of CRGs and CRLncs in OS cell lines. **(A)** The mRNA expression level of CRGs. **(B)** The mRNA expression level of CRLncs. *$p < 0.05$, **$p < 0.01$, ***$p < 0.001$, ****$p < 0.0001$ each experiment was repeated three times.

mitochondrial metabolism. The specific mechanism of cuproptosis is that copper ions induce protein toxic stress responses by binding to fatty acid acylated components in the TCA cycle, inducing cell death (10). Therefore, research on CRLncs that can guide OS prognosis and the immune microenvironment would improve the clinical efficacy of OS.

In this study, a new OS prognosis model was established. Six CRLncs were involved in the construction of the model, including three high-risk CRLncs (AL645608.6, AL591767.1, and UNC5B-AS1) and three low-risk CRLncs (CARD8-AS1, AC098487.1, and AC005041.3). As the expression of high-risk CRLncs in OS increases, the patient risk increases. As the expression of low-risk CRLncs in OS increases, the patient risk decreases. The high- and low-risk groups of the prognostic model differed in their tumor microenvironment. We found that immune cells, such as B cells, macrophages, Th2 cells, and Treg, were significantly downregulated in the high-risk group. Immune functions such as APC co-inhibition, checkpoint, and T-cell co-inhibition were significantly downregulated in the high-risk group. In addition, we identified four drugs with significant sensitivity in the prognostic model (AUY922, bortezomib, lenalidomide, and Z.lle.CHO) that may improve the clinical efficacy of OS. Finally, it was experimentally verified that the expression of LIPT1, DLAT, and FDX1 at both mRNA

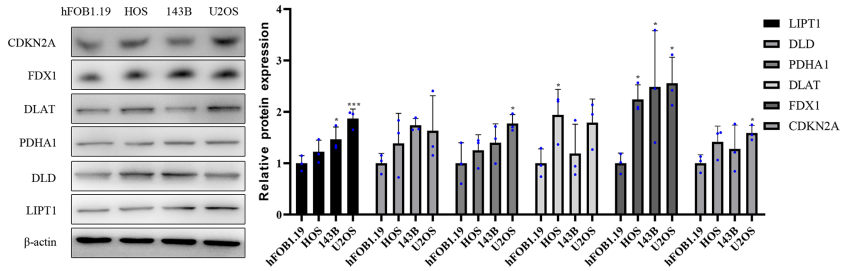

FIGURE 10
Validation of the protein expression levels of CRGs in OS cell lines. Representative protein grayscale bands. Statistical histogram of grayscale quantification of protein bands. *$p < 0.05$, ***$p < 0.001$, each experiment was repeated three times.

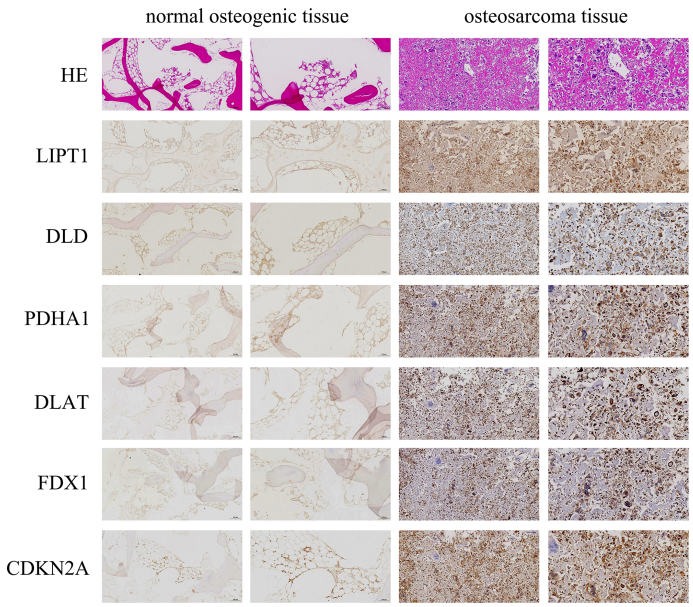

FIGURE 11
Immunohistochemistry (IHC) staining of OS and normal osteogenic tissue using anti-CRGs antibody and hematoxylin and eosin (HE) staining. Scale bar, 200 μm (left panel) and 100 μm (right panel).

and protein levels was significantly elevated in OS. Besides, the mRNA expression level of AL591767.1 was decreased in OS, and that of AL645608.6, CARD8-AS1, AC005041.3, AC098487.1, and UNC5B-AS1 was upregulated in OS.

We found that AL645608.6, UNC5B-AS1, and CARD8-AS1 were associated with tumor prognosis, which also reflected to a certain extent the reliability of the results of this study. AL645608.6 is highly correlated with clinical prognosis in patients with acute myeloid leukemia (26). UNC5B-AS1 not only promotes the malignant progression of prostate cancer by competitively binding to caspase-9 (27) but also promotes the proliferation, migration, and invasion of papillary thyroid cancer cell lines (28). CARD8-AS1 is not only a glioma-risk lncRNA (29) but is also significantly associated with overall survival in ovarian cancer (30). The results of studies related to AL591767.1, AC098487.1, and AC005041.3 remain unclear.

The immune environment of OS consists mainly of T lymphocytes and macrophages but also contains other subsets, such as B lymphocytes and mast cells (31). Downregulation of miR-138 expression in OS ameliorates CD4+CXCR5+ follicular helper T cell (Tfh) dysfunction and promotes B-cell differentiation (32). In OS, tumor-associated macrophages not only promote tumor growth and angiogenesis but also inhibit OS metastasis (33). M0 and M2 macrophages derived from the THP-1 human monocyte cell line promoted OS cell migration and invasion more significantly than M1 macrophages did (34). Th2 is also associated with OS metastasis, and the immune-related genes MSR1 and TLR7 associated with macrophages and Th2 can serve as anti-metastatic features of OS (35). Tregs have a potential role in the progression of OS, and the impetus of the antitumor efficacy of anti-PD-1 antibodies in OS mouse models may be decreased numbers of FOXP3+Tregs and increased tumor-infiltrating lymphocytes in the tumor microenvironment (36). A comprehensive analysis of zinc finger protein genes and OS prognosis and the tumor immune microenvironment revealed differences in APC co-inhibition and T-cell-co-inhibition between high- and low-risk groups (37). A study of hypoxic prognostic features associated with OS metastasis and immune infiltration found that immune checkpoints were downregulated in high-risk populations (38).

The combined use of the cyclin-dependent kinase inhibitor SCH727965 (SCH) and heat shock protein 90 inhibitor NVP-AUY922 (AUY922) can induce apoptosis in OS cells (39). SCH and AUY922 may be promising strategies for OS treatment. Bortezomib induces apoptosis and autophagy in OS cells *via* the mitogen-activated protein kinase pathway (40). Bortezomib inhibits OS cell growth and induces apoptosis by inhibiting proteasome (41). The association between lenalidomide and Z.LLNle.CHO and OS remains unclear. The results of this study show that lenalidomide and Z.LLNle.CHO may be potential therapeutic drugs for OS and provide a research direction for improving the clinical efficacy of OS.

However, this study has limitations. First, the sample size of tumors in this study was relatively small. Second, the CRLncs that can guide OS prognosis and the immune microenvironment obtained in this study require further research into the biological function.

Conclusion

In this study, a new OS prognosis model was established, and six CRLncs were involved in the construction of the model. Through tumor microenvironment and immune-related analyses, we found that these six CRLncs can guide the immune microenvironment of OS. Additionally, we identified four drugs that may have potential efficacy in OS treatment. The results of this study contribute to improving the clinical efficacy and overall survival of patients with OS.

Data availability statement

The data supporting the results of the study are available from the TCGA database(https://portal.gdc.cancer.gov/) and GEO database (https://www.ncbi.nlm.nih.gov/geo/). The accession number(s) can be found in the article/Supplementary Material.

Ethics statement

This study was reviewed and approved by the Biomedical Research Ethics Committee of HongHui Hospital, Xi'an Jiaotong University (No, 202206007). The patients/participants provided their written informed consent to participate in this study.

Author contributions

PX and MY designed the study. MY, HZ, and KX analyzed the datasets and interpreted the results. QY downloaded the data. YA and YC provided software support. MY wrote and edited the manuscript. PX provided the foundation and support. All authors contributed to the article and approved the submitted version.

Funding

This work was financially supported by the National Natural Science Foundation of China (No. 82072432).

Conflict of interest

The authors declare that the research was conducted in the absence of any commercial or financial relationships that could be construed as a potential conflict of interest.

Publisher's note

Supplementary material

The Supplementary Material for this article can be found online at: https://www.frontiersin.org/articles/10.3389/fimmu.2022.919231/full#supplementary-material

References

1. Cortini M, Avnet S, Baldini N. Mesenchymal stroma: Role in osteosarcoma progression. *Cancer Lett* (2017) 405:90–9. doi: 10.1016/j.canlet.2017.07.024

2. Czarnecka AM, Synoradzki K, Firlej W, Bartnik E, Sobczuk P, Fiedorowicz M, et al. Molecular biology of osteosarcoma. *Cancers (Basel)* (2020) 12(8):2130. doi: 10.3390/cancers12082130

3. Savage SA, Mirabello L. Using epidemiology and genomics to understand osteosarcoma etiology. *Sarcoma* (2011) 2011:548151. doi: 10.1155/2011/548151

4. Rickel K, Fang F, Tao J. Molecular genetics of osteosarcoma. *Bone* (2017) 102:69–79. doi: 10.1016/j.bone.2016.10.017

5. Zhang D, Cui G, Sun C, Lei L, Lei L, Williamson RA, et al. Hypoxia promotes osteosarcoma cell proliferation and migration through enhancing platelet-derived growth factor-bb/platelet-derived growth factor receptor-beta axis. *Biochem Biophys Res Commun* (2019) 512(2):360–6. doi: 10.1016/j.bbrc.2019.03.040

6. Bu X, Liu J, Ding R, Li Z. Prognostic value of a pyroptosis-related long noncoding rna signature associated with osteosarcoma microenvironment. *J Oncol* (2021) 2021:2182761. doi: 10.1155/2021/2182761

7. Wedekind MF, Wagner LM, Cripe TP. Immunotherapy for osteosarcoma: Where do we go from here? *Pediatr Blood Cancer* (2018) 65(9):e27227. doi: 10.1002/pbc.27227

8. Anderson ME. Update on survival in osteosarcoma. *Orthop Clin North Am* (2016) 47(1):283–92. doi: 10.1016/j.ocl.2015.08.022

9. Casali PG, Bielack S, Abecassis N, Aro HT, Bauer S, Biagini R, et al. Bone sarcomas: Esmo-paedcan-euracan clinical practice guidelines for diagnosis, treatment and follow-up. *Ann Oncol* (2018) 29(Suppl 4):iv79–95. doi: 10.1093/annonc/mdy310

10. Tsvetkov P, Coy S, Petrova B, Dreishpoon M, Verma A, Abdusamad M, et al. Copper induces cell death by targeting lipoylated tca cycle proteins. *Science* (2022) 375 (6586):1254–61. doi: 10.1126/science.abf0529

11. Raffa N, Won TH, Sukowaty A, Candor K, Cui C, Halder S, et al. Dual-purpose isocyanides produced by aspergillus fumigatus contribute to cellular copper sufficiency and exhibit antimicrobial activity. *Proc Natl Acad Sci U S A* (2021) 118(8):e2015224118. doi: 10.1073/pnas.2015224118

12. Tsvetkov P, Detappe A, Cai K, Keys HR, Brune Z, Ying W, et al. Mitochondrial metabolism promotes adaptation to proteotoxic stress. *Nat Chem Biol* (2019) 15(7):681–9. doi: 10.1038/s41589-019-0291-9

13. Solmonson A, DeBerardinis RJ. Lipoic acid metabolism and mitochondrial redox regulation. *J Biol Chem* (2018) 293(20):7522–30. doi: 10.1074/jbc.TM117.000259

14. Rowland EA, Snowden CK, Cristea IM. Protein lipoylation: An evolutionarily conserved metabolic regulator of health and disease. *Curr Opin Chem Biol* (2018) 42:76–85. doi: 10.1016/j.cbpa.2017.11.003

15. Hua Y, Qiu Y, Zhao A, Wang X, Chen T, Zhang Z, et al. Dynamic metabolic transformation in tumor invasion and metastasis in mice with lm-8 osteosarcoma cell transplantation. *J Proteome Res* (2011) 10(8):3513–21. doi: 10.1021/pr200147g

16. Zhang Y, He R, Lei X, Mao L, Jiang P, Ni C, et al. A novel pyroptosis-related signature for predicting prognosis and indicating immune microenvironment features in osteosarcoma. *Front Genet* (2021) 12:780780. doi: 10.3389/fgene.2021.780780

17. Li J, Tang X, Du Y, Dong J, Zhao Z, Hu H, et al. Establishment of an autophagy-related clinical prognosis model for predicting the overall survival of osteosarcoma. *BioMed Res Int* (2021) 2021:5428425. doi: 10.1155/2021/5428425

18. Cai W, Li H, Zhang Y, Han G. Identification of key biomarkers and immune infiltration in the synovial tissue of osteoarthritis by bioinformatics analysis. *PeerJ* (2020) 8:e8390. doi: 10.7717/peerj.8390

19. Fan Q, Liu B. Identification of a rna-seq based 8-long non-coding rna signature predicting survival in esophageal cancer. *Med Sci Monit* (2016) 22:5163–72. doi: 10.12659/msm.902615

20. Jiang F, Miao XL, Zhang XT, Yan F, Mao Y, Wu CY, et al. A hypoxia gene-based signature to predict the survival and affect the tumor immune microenvironment of osteosarcoma in children. *J Immunol Res* (2021) 2021:5523832. doi: 10.1155/2021/5523832

21. Qian H, Lei T, Hu Y, Lei P. Expression of lipid-metabolism genes is correlated with immune microenvironment and predicts prognosis in osteosarcoma. *Front Cell Dev Biol* (2021) 9:673827. doi: 10.3389/fcell.2021.673827

22. Kim BE, Nevitt T, Thiele DJ. Mechanisms for copper acquisition, distribution and regulation. *Nat Chem Biol* (2008) 4(3):176–85. doi: 10.1038/nchembio.72

23. Lutsenko S. Human copper homeostasis: A network of interconnected pathways. *Curr Opin Chem Biol* (2010) 14(2):211–7. doi: 10.1016/j.cbpa.2010.01.003

24. Zhong Z, Mao S, Lin H, Li H, Lin J, Lin JM. Alteration of intracellular metabolome in osteosarcoma stem cells revealed by liquid chromatography-tandem mass spectrometry. *Talanta* (2019) 204:6–12. doi: 10.1016/j.talanta.2019.05.088

25. Ren L, Ruiz-Rodado V, Dowdy T, Huang S, Issaq SH, Beck J, et al. Glutaminase-1 (Gls1) inhibition limits metastatic progression in osteosarcoma. *Cancer Metab* (2020) 8:4. doi: 10.1186/s40170-020-0209-8

26. Ding W, Ling Y, Shi Y, Zheng Z. Desa prognostic risk model of lncrnas in patients with acute myeloid leukaemia based on tcga data. *Front Bioeng Biotechnol* (2022) 10:818905. doi: 10.3389/fbioe.2022.818905

27. Tan S-F, Ni J-X, Xiong H. Lncrna unc5b-as1 promotes malignant progression of prostate cancer by competitive binding to caspase-9. *Eur Rev Med Pharmacol Sci* (2020) 24(5):2271–80. doi: 10.26355/eurrev_202003_20493

28. Wang Y, Bhandari A, Niu J, Yang F, Xia E, Yao Z, et al. The lncrna unc5b-as1 promotes proliferation, migration, and invasion in papillary thyroid cancer cell lines. *Hum Cell* (2019) 32(3):334–42. doi: 10.1007/s13577-019-00242-8

29. Lin X, Jiang T, Bai J, Li J, Wang T, Xiao J, et al. Characterization of transcriptome transition associates long noncoding rnas with glioma progression. *Mol Ther Nucleic Acids* (2018) 13:620–32. doi: 10.1016/j.omtn.2018.10.009

30. Li N, Zhan X. Identification of clinical trait-related lncrna and mrna biomarkers with weighted gene co-expression network analysis as useful tool for personalized medicine in ovarian cancer. *EPMA J* (2019) 10(3):273–90. doi: 10.1007/s13167-019-00175-0

31. Heymann MF, Lezot F, Heymann D. The contribution of immune infiltrates and the local microenvironment in the pathogenesis of osteosarcoma. *Cell Immunol* (2019) 343:103711. doi: 10.1016/j.cellimm.2017.10.011

32. Wang Z, Liang J, Jiang S, Zhao G, Lu J, Jiang B, et al. The effect of mir-138 on the function of follicular helper T cells and the differentiation of b cells in osteosarcoma. *Comput Math Methods Med* (2021) 2021:1–11. doi: 10.1155/2021/2057782

33. Zhao Y, Zhang B, Zhang Q, Ma X, Feng H. Tumor-associated macrophages in osteosarcoma. *J Zhejiang Univ Sci B* (2021) 22(11):885–92. doi: 10.1631/jzus.B2100029

34. Cascini C, Chiodoni C. The immune landscape of osteosarcoma: implications for prognosis and treatment response. *Cells* (2021) 10(7):1668. doi: 10.3390/cells10071668

35. Chen Z, Huang H, Wang Y, Zhan F, Quan Z. Identification of immune-related genes Msr1 and Tlr7 in relation to macrophage and type-2 T-helper cells in osteosarcoma tumor micro-environments as anti-metastasis signatures. *Front Mol Biosci* (2020) 7:576298. doi: 10.3389/fmolb.2020.576298

36. Yoshida K, Okamoto M, Sasaki J, Kuroda C, Ishida H, Ueda K, et al. Anti-Pd-1 antibody decreases tumour-infiltrating regulatory T cells. *BMC Cancer* (2020) 20(1):25. doi: 10.1186/s12885-019-6499-y

37. Sun X, Zheng D, Guo W. Comprehensive analysis of a zinc finger protein gene-based signature with regard to prognosis and tumor immune microenvironment in osteosarcoma. *Front Genet* (2022) 13:835014. doi: 10.1016/j.bbrc.2018.11.005

38. Fu Y, Bao Q, Liu Z, He G, Wen J, Liu Q, et al. Development and validation of a hypoxia-associated prognostic signature related to osteosarcoma metastasis and immune infiltration. *Front Cell Dev Biol* (2021) 9:633607. doi: 10.3389/fcell.2021.633607

39. Fu W, Sharma SS, Ma L, Chu B, Bui MM, Reed D, et al. Apoptosis of osteosarcoma cultures by the combination of the cyclin-dependent kinase inhibitor Sch727965 and a heat shock protein 90 inhibitor. *Cell Death Dis* (2013) 4:e566. doi: 10.1038/cddis.2013.101

40. Lou Z, Ren T, Peng X, Sun Y, Jiao G, Lu Q, et al. Bortezomib induces apoptosis and autophagy in osteosarcoma cells through mitogen-activated protein kinase pathway in vitro. *J Int Med Res* (2013) 41(5):1505–19. doi: 10.1177/0300060513490618

41. Shapovalov Y, Benavidez D, Zuch D, Eliseev RA. Proteasome inhibition with bortezomib suppresses growth and induces apoptosis in osteosarcoma. *Int J Cancer* (2010) 127(1):67–76. doi: 10.1002/ijc.25024

frontiers | Frontiers in Immunology

TYPE Original Research
PUBLISHED 19 August 2022
DOI 10.3389/fimmu.2022.986785

OPEN ACCESS

EDITED BY
Lin Qi,
Hunan Key Laboratory of Tumor Models and Individualized Medicine, Central South University, China

REVIEWED BY
Keywan Mortezaee,
Kurdistan University of Medical Sciences, Iran
Kevin Dzobo,
University of Cape Town, South Africa
Daniela Spano,
Department of Biomedical Sciences, (CNR), Italy
Shuko Harada,
University of Alabama at Birmingham, United States

*CORRESPONDENCE
Taiqiang Yan
yantqzh@163.com

SPECIALTY SECTION
This article was submitted to Cancer Immunity and Immunotherapy, a section of the journal Frontiers in Immunology

RECEIVED 05 July 2022
ACCEPTED 03 August 2022
PUBLISHED 19 August 2022

CITATION
Guo L, Yan T, Guo W, Niu J, Wang W, Ren T, Huang Y, Xu J and Wang B (2022) Molecular subtypes of osteosarcoma classified by cancer stem cell related genes define immunological cell infiltration and patient survival.
Front. Immunol. 13:986785.
doi: 10.3389/fimmu.2022.986785

Molecular subtypes of osteosarcoma classified by cancer stem cell related genes define immunological cell infiltration and patient survival

Lei Guo[1,2], Taiqiang Yan[1,2]*, Wei Guo[1,2], Jianfang Niu[1,2], Wei Wang[1,2], Tingting Ren[1,2], Yi Huang[1,2], Jiuhui Xu[1,2] and Boyang Wang[1,2]

[1]Musculoskeletal Tumor Center, Peking University People's Hospital, Beijing, China, [2]Beijing Key Laboratory of Musculoskeletal Tumor, Beijing, China

Recent studies have shown that tumor stemness has biological significance in tumorigenicity and tumor progression. However, the characteristics of TME immune infiltration in osteosarcoma mediated by the combined effects of multiple cancer stem cell-related genes remain unknown.

Methods: In this study, we identified different cancer stem cell-associated subtypes in osteosarcoma based on 25 cancer stem cell-associated genes by consensus clustering analysis, and we comprehensively evaluated the association between these subtypes and immunocytes infiltration in the TME. The cancer stem cell (CSC) score was constructed to quantify the stemness of individual tumors.

Results: We performed a comprehensive evaluation of 218 osteosarcoma patients based on 25 cancer stem cell-related genes. Three different cancer stem cells related subtypes were identified, which were related to different biological processes and clinical outcomes. The three subtypes have different TME cells infiltrating characteristics, and CSC Cluster A had a higher level of immunocyte infiltration compared to CSC Cluster B and C. We constructed a scoring system, called the CSC score, to assess the stemness of individual patients. Then we found that the prognosis of patients was predicted by CSC score, and patients with low CSC score had prolonged survival. Further analyses showed that low CSC score was correlated with enhanced immune infiltration. CSC score may predict the effect of immunotherapy, and patients with low CSC score may have better immune response and clinical prognosis.

Conclusions: This study demonstrates that there could be three cancer stem cell-associated subtypes in osteosarcoma and that they were associated with

different patient prognosis and TME immune infiltration characteristics. CSC score could be used to assess the stemness of individual patients, improve our comprehension of TME characteristics, and direct more effective immune therapy.

KEYWORDS

osteosarcoma, cancer stem cells, cancer stemness, molecular subtype, tumor microenvironment, drug

Introduction

Osteosarcoma (OS) originates from mesenchymal tissue and is one of the most common malignancies of bone tissue. OS is highly malignant, rapidly progressive, and highly susceptible to postoperative recurrence. In particular, OS that occurs in adolescence has a very high rate of disease progression. The 5-year survival rate for early OS patients is 40-60%, while only 5-20% for advanced OS patients (1). Currently, OS is mainly treated by surgery combined with neoadjuvant chemotherapy, but it does not completely solve the problem of distant metastasis and postoperative recurrence in OS patients. The root cause of the poor prognosis of OS is that the current treatment measures cannot remove the remaining tumor cells and eventually lead to the recurrence and metastasis of the tumor (2). Therefore, in order to improve patient survival, there is an urgent need to investigate the pathogenesis of osteosarcoma, to identify important targets that regulate the initiation and progression of osteosarcoma, and to assess their potential therapeutic value, which will bring new light to improve the overall prognosis of osteosarcoma.

Cancer stem cell (CSC) is commonly defined as tumor cell with stem cell-like characteristics. The presence of such cells will likely lead to heterogeneity within the tumor (3). Similar to normal stem cell, CSC has self-renewal potential and differentiation ability, and they can expand by symmetrical or asymmetrical divisions (4, 5). CSC expands in a symmetrical division. Excessive growth of CSC will eventually lead to tumor formation (6). Similarly, CSC plays significant roles in tumor metastasis (7–9) and chemotherapy resistance (10–14). CSC shows variability in different cancers, and CSC differs genetically and phenotypically (15). Since CSC has been shown to cause tumor initiation as well as recurrence, the search for specific markers of CSC is particularly important (16). Kevin et al. examined and compared the expression of various CSC markers such as ABCB1, ABCG2, ALDH1A1, CD24, and CD44 in tumors and adjacent normal tissues using publicly available databases and found that most CSC markers were more highly expressed in tumors (17). Kevin et al. found that the CSC marker CD44 plays an important role in tumor metastasis, drug resistance, immune evasion, and epithelial mesenchymal transition (18). However, since most of the markers specific to CSC are also present in adult tissue resident stem cell populations, human embryonic stem cells (hESC) or adult tissues, their clinical application is still very limited (16). The highly aggressive and chemotherapy resistance of CSC leads to more challenging tumor treatments (19–21). In recent years, an increasing number of studies have attempted to treat cancer by targeting CSC-associated drug resistance and metastasis (22, 23). Ramesh et al. summarized the role of different signaling pathways in breast CSC and proposed different therapeutic strategies to target CSC (24).

Immunotherapy to destroy tumor cells by identifying immune infiltration in the tumor has become an effective treatment for many advanced cancers (25). Immunotherapy can activate anti-tumor immunity and improve the condition of the TME. TME is a complex and diverse dynamic system composed of multiple immunocytes, cytokines and stromal cells, which is often considered to be immunosuppressive (26). TME serves as a physical environment that supports the development of cancer cells, so exploring its phenotypic and functional heterogeneity will have important implications for the treatment of cancer (27). Both immune evasion and CSC is thought to mediate tumor growth and metastasis, thus exploring the interaction between immunocytes and CSC in TME has a significant role in improving immunotherapy. Notably, Miranda et al. revealed that high stemness is associated with poor immune infiltration in 21 malignancies, demonstrating a potential interaction between CSC and immunocytes (28). Tumor-associated macrophages (TAMs) are tumor-infiltrating myeloid cells. These cells are capable of functional and morphological alterations when affected by the tumor microenvironment. Several studies have revealed the complexity of crosstalk between CSC and TAMs, confirming

Abbreviations: AUC, Area under the curve; CSC, Cancer stem cell; CSCRGs, cancer stem cells-associated genes; DCs, Dendritic cells; DEGs, Differentially expressed genes; OS, Osteosarcoma; PCA, Principal component analysis; ROC, Receiver operating characteristic; TAMs, Tumor-associated macrophages; TME, Tumor microenvironment.

that CSC is critical for recruitment with TAMs and that CSC may influence the polarization state of TAMs (29–32). Wei et al. discovered that CSC in malignant gliomas promote the survival of TAMs by secreting WISP1 (30). Similarly, Wen et al. demonstrated that CSC in glioblastoma multiforme can influence TAMs polarization and also recruit TAMs by secreting POSTN (31). Karina et al. found that CD44 could mediate the regulation of TAM for tumor stem cells *via* the PI3K-4EBP1-SOX2 pathway (32). CD8+ T cells have key roles in tumor immunity, and CSC interacts with CD8+ T cells in two main ways: CSC evades CD8+ T cell-mediated death (33) and CSC inhibits the antitumor immunity of CD8+ T cells (34, 35). Yu et al. found that CSC evaded cytotoxic T cell killing through TGFb-dependent upregulation of CD80 in murine epidermal squamous cell carcinoma (33). Jun et al. found that CSC in Glioblastoma multiforme inhibited T cells activation and proliferation, and triggered T cells apoptosis (35). Similarly, several studies have confirmed the correlation between CSC and tumorigenic dendritic cells (DCs) (36–38). Most studies have focused on individual CSC-associated genes and one type of immune cell, however CSC has the complexity of high synergistic effects of multiple genes. Therefore, exploring the infiltrative properties of TME cells mediated by the combined action of multiple CSC-related genes will help enhance our comprehension of osteosarcoma TME.

In this study, we included transcriptomic data and clinical information from a total of 218 osteosarcoma patients and identified three distinct CSC clusters in osteosarcoma. We evaluated the three CSC clusters comprehensively and systematically analyzed the association between different subtypes and TME. In addition, we constructed a CSC score system for quantifying CSC-related modalities in individual osteosarcoma patients, which was validated in multiple independent datasets. These results suggested the important roles of the combined action of multiple CSC-related genes in osteosarcoma TME.

Materials and methods

Data collection and preprocessing

RNA expression data and clinical information of osteosarcoma patients were downloaded from TARGET (https://ocg.cancer.gov/programs/target) and GEO (https://www.ncbi.nlm.nih.gov/geo/) databases. The following were the inclusion criteria: (a)osteosarcoma samples with gene expression matrix; (b)samples with clinical information such as age, gender, survival time, survival status, and whether metastasis occurred; (c)samples with expression values for more than half of the genes. Based on the above criteria, 4 eligible osteosarcoma cohorts (GSE21257, GSE39055, GSE16102, and TARGET-OS)were collected for further analysis. The batch effect of non-biotechnical bias was corrected using the "ComBat" package. The cohorts GSE21257, GSE39055 and GSE16102 were merged into the meta-cohort. 331 cancer stem cells-associated genes (CSCRGs) were obtained from the molecular marker database, of which 228 genes were expressed in the TARGET-OS cohort and meta-cohort. In the TARGET-OS cohort, we selected 25 CSCRGs for further studies using univariate COX analysis (P<0.05) (Supplementary Tables 1 and 2).

Identification of molecular subgroups and calculating DEGs

The consensus clustering was performed using the "ConsensusClusterPlus" package based on the expression matrix of the 25 CSCRGs (39). Differentially expressed genes (DEGs) between three clusters were analyzed using 'limma' package with the cutoff criteria of $P < 0.05$.

Functional analyses and TIME evaluation

The Gene Ontology (GO) enrichment was performed using the "clusterprofiler" package. The geneset "h.all.v7.5.1.symbols" was obtained from MSigDB. Mariathasan et al. had constructed a geneset in which genes related to certain biological processes were stored (40). Based on the above gene sets, we performed Gene set variation analysis (GSVA) by using the "GSVA" and "limma" packages to show alterations in signaling pathways among three clusters (41). Adjusted P value less than 0.05 was defined as statistically significant. The ESTIMATE algorithm was used to calculate the immune score, stromal score and tumor purity.

Estimation of TME cell infiltration

Cohorts of 23 immune infiltrating cells and 13 immune-related functions were obtained (42). And the score calculated with ssGSEA was used to express the relative abundance of different immunocytes and immune-related functions in every case (43). The abundance of six immunocytes were analyzed using the TIMER algorithm.

Construction of the CSC score

In order to quantify the stemness of individual tumors, we constructed a score system called CSC score, which was constructed in the following steps. We selected overlapping DEGs found in distinct CSC clusters and performed prognostic analyses of individual genes by using univariate Cox regression.

Extraction of genes with remarkable prognosis was used to construct the CSC score by principal component analysis (PCA). Principal component1 and Principal component2 were used in the construction of the CSC score. We also defined CSC score using a similar approach from previous studies (44, 45). CSC score =$\Sigma PC1_i + PC2_i$, i is the expression of genes associated with the CSC phenotype. We stratified the tumors into CSC score low and high subgroups using the surv-cutpoint function in the 'survival' package.

Drug sensitivity assessment

We used the 'pRRophetic' package to assess the sensitivity to different CSC clusters to small molecule drugs. In addition, the CellMiner database was utilized to assess the association between CSCRGs and different drugs (46).

Calculation of mRNAsi

Based on one-class logistic regression (OCLR) algorithm, the stemness index model trained from the Progenitor Cell Biology Consortium database was used to calculate tumor stemness (47, 48). The stemness index can be used to measure how similar tumor cells are to stem cells, with stemness index being a value between 0 (lowest) and 1 (highest). The closer the stemness index is to 1, the stronger the stem cell properties. We calculated transcriptome feature scores for the cohorts using the same Spearman correlation.

Clinical samples and immunohistochemistry

A total of 10 OS tissues were collected, all from Peking University People's Hospital. The samples were examined by three experienced pathologists. All patients provided informed consent, and the study protocol was approved by the Ethics Commttee of Peking University People' s Hospital (2019PHB198-01). Immunohistochemical examination was performed with *MEF2C* antibody (10056-1-AP, proteintech).

Cell culture and transfection

Human osteosarcoma cell line (143B) was purchased from the American Type Culture Collection (ATCC). 143B cells was cultured in DMEM (Gibco) containing 10% fetal bovine serum (FBS, Gibco) and 1% penicillin and streptomycin (Gibco). 143B cells were cultured in a humidified incubator with 5% CO2 at 37°C. Si-*MEF2C* (Suzhou, China, sequences: 5'GACAAGGAAUGGGAGGAUA3') and GP-transfect-Mate (Suzhou, China) were used for transfection.

Sphere formation assay

143B cells were inoculated at a density of 1000 cells/well in six-well ultra-low attachment plates (Corning). And the cells were cultured in DMEM/F12 medium (Gibco) containing N2 medium (Invitrogen), human EGF (20ng/ml, PeproTech) and human bFGF (20ng/ml, PeproTech) for 14 days. Spheres were observed in size and the number of spheres formed was calculated.

Cell adhesion assay

50 μl of vitronectin (PeproTech) or fibronectin (Biocoat) was added to each well of a 96-well plate and incubated overnight at 4°C. Unbound proteins were washed with PBS and closed with PBS containing 2% BSA for 2 hours at 37°C. 143B cells were inoculated at a density of 10000 cells/well in 96-well plate (Corning). And the cells were cultured in DMEM (Gibco) for 1 hour. Unbound cells were washed with PBS, fixed with 4% paraformaldehyde and stained with 0.1% crystal violet. Finally, the number of adherent cells was observed under the microscope.

Statistical analyses

Statistical analyses were performed *via* R (version 4.1.2), and survival analyses were performed using the Kaplan-Meier method. The Student's t test was used for normally distributed variables and the Wilcoxon rank sum test was used for non-normally distributed variables. The Kruskal-Wallis test and one-way ANOVA were used for the non-parametric and parametric methods, respectively (49). Correlations coefficients between the expression of CSCRGs and the TME infiltrating immunocytes were calculated by Spearman analysis. We used univariate Cox regression analysis to compute the hazard ratio (HR) of CSCRGs and CSC-related signature genes. To verify whether the constructed risk scores can be used as an independent prognostic factor independently of other clinical traits. Univariate and multivariate COX analyses of patients' age, gender, presence of metastasis, and CSC score were performed. The predictive performance of the CSC score was assessed by using receiver operating characteristic (ROC) curves, and the area under the curve (AUC) was calculated by the 'timeROC' package. P-value was bilateral and $P < 0.05$ was defined as statistically significant difference.

Results

Landscape of 25 cancer stem cells related genes in osteosarcoma

In this study, we finally selected 25 cancer stem cells related genes (CSCRGs) by univariate COX analysis in TARGET-OS cohort and later investigated the role of these genes in osteosarcoma. Metascape analysis and GO enrichment analysis were performed on 25 CSCRGs, which were seen to be enriched in multiple stemness-related regulatory pathways, and the results were shown in Figure 1A and Figure S1A. In addition, Spearman analysis was used to assess the relevance between 25 CSCRGs (Figure S1B). COX regression analysis was used to analyze the relationship of 25 CSCRGs with patient prognosis in osteosarcoma. The forestplot showed that *FOLR1, SEMA3B, SEMA4G, MYC, OVOL1 and MEF2C* were considered as risk factors (Figures S1C, D). The above analyses showed 25 CSCRGs

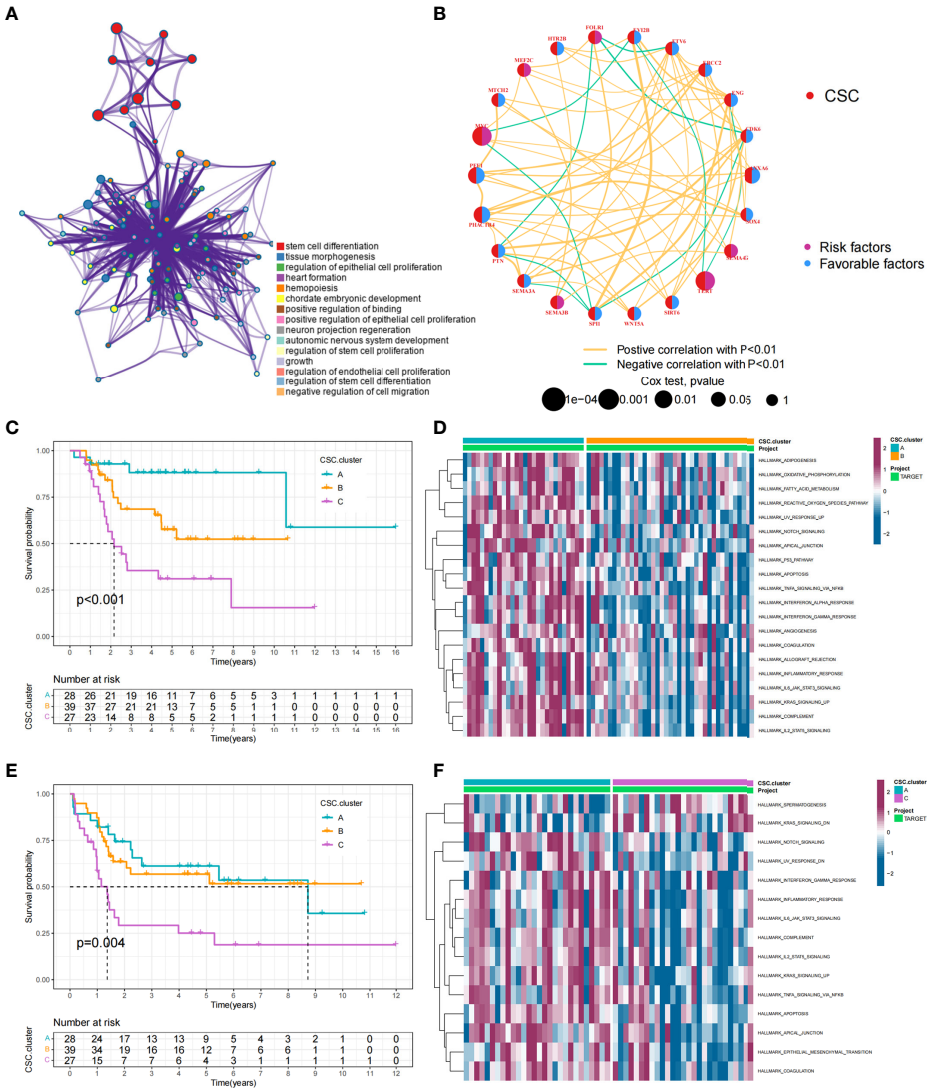

FIGURE 1
CSC-related subtypes and biological characteristics of each subtype. **(A)** Metascape enrichment network. Color codes indicate different clusters. **(B)** Interaction of 25 CSCRGs in osteosarcoma. The red color on the left half of the circle represented the type of gene. The blue color on the right half of the circle indicated favorable factors; the purple color on the right half of the circle indicated risk factors. The size of the circles was determined by the p-value, representing the impact of each gene on the prognosis of patients. The lines between genes indicated their interactions, positive correlations were shown in yellow and negative correlations were shown in green. **(C, D)** Kaplan-Meier curves of overall survival **(C)** and event-free survival **(D)** for 94 osteosarcoma patients in TARGET cohort with different CSC cluster, including 28 cases in CSC cluster A, 39 cases in CSC cluster B, and 27 cases in CSC cluster C (Log-rank test). **(E, F)** The heatmap visualized the results of the GSVA enrichment analysis in the TARGET cohort, and purple represents activated pathways and blue represents inhibited pathways.

played important roles in the development and progression of osteosarcoma.

Cancer stem cells related subtypes mediated by 25 CSCRGs

Data of 94 osteosarcoma patients in the TARGET-OS cohort were used for analysis. The network showed the interactions of the 25 CSCRGs and their prognostic significance for osteosarcoma patient (Figure 1B). The results indicated that these 25 CSCRGs were mutually regulated and played crucial roles in the development of osteosarcoma. We utilized consensus clustering algorithm to stratify samples into distinct CSC clusters based on the expression of the 25 CSCRGs. Consequently, we identified three distinct clusters, including 28 samples in cluster A, 39 samples in cluster B and 27 samples in cluster C (Figures S2A, B, Supplementary Tables 3, 4). Prognostic analysis for these three clusters indicated that CSC cluster A showed an excellent survival advantage, while CSC cluster C had the worst prognosis in TARGET-OS cohort (Figures 1C, D). We also noted that there were remarkable differences in expression levels of the 25 CSCRGs between distinct clusters (Figures S2C, D). *ANXA6, ENG, EVI2B, SEMA3E*, and *SPI1* were significantly elevated in CSC cluster A, *CDK6, ETV6, MYC, PHACTR4, PTN, SEMA3A*, and *SOX4* were evidently increased in CSC cluster B, and *SEMA4G* was evidently increased in CSC cluster C (Figures S2C, D).

TME cell infiltration characteristics in distinct cancer stem cells related subtypes

To explore the biological behaviors underlying these different CSC clusters, we performed GSVA enrichment analysis (Figures 1E, F). The results showed that CSC cluster A was markedly abundant in immune activation-related processes, such as complement, inflammatory and interferon gamma response, and the TNFA pathway, KARS pathway and apoptosis pathway were also enriched in CSC cluster A. Based on the above findings, we presumed that the better prognosis of CSC cluster A might be related to its high immune infiltration. Furthermore, we quantified the stromal score, immune score and tumor purity for the three clusters using ESTIMATE algorithm. The analysis showed that CSC cluster A had the highest immune score and stromal score, followed by CSC cluster B and C (Figures 2A, B). Conversely, CSC cluster B and C had higher tumor purity compared to CSC cluster A, suggesting that tumors in CSC cluster A were surrounded by more non-tumor components (immunocytes and stromal cells) (Figure 2C). In addition, a heat map was built by ssGSEA to visualize and compare the abundance of 23 immunocytes under different clusters (Figure 2D). The great majority of immunocytes such as anti-tumor lymphocyte cell subpopulations and NK T cells were mainly enriched in the CSC cluster A. We further described the immune infiltration profile using TIMER2.0 and observed consistent results (Figures 2E–H). The results showed that neutrophils, macrophages and myeloid dendritic cells were mainly enriched in the CSC cluster A, while CD8+ T cells were enriched in CSC cluster A and C. We also calculated 13 immune-related function scores using ssGSEA, and the results suggested that majority of immune-related functions were enriched in CSC cluster A (Figure 2I). Curiously, CSC cluster C also had a higher infiltration of immune cells but did not show the same survival advantage. DCs have been shown in previous studies to be responsible for antigen presentation and initial T cell activation, bridging innate and adaptive immunity, and their activation is dependent on high expression levels of MHC molecules, co-stimulatory factors and adhesion factors. Therefore, we compared the expression of MHC molecules, co-stimulatory molecules and adhesion molecules in the three CSC subtypes and found that most molecules including *CD40, CD80, CD86, HLA-C, HLA-DMC, HLA-DMB, HLA-DPB1, HLA-DRA, HLA-E*, and *ICAM1* were significantly elevated in CSC cluster A (Figure S2E). Thus, we hypothesize that although CSC cluster C had a higher immune infiltration, its antigen-presenting ability and ability to activate DCs were weaker compared to CSC cluster A. Therefore, CSC cluster C had a poorer survival prognosis compared to CSC cluster A. The results from GSVA analysis demonstrated that Pan-F-TBRS, antigen processing machinery, immune checkpoint, and CD8 T effector were enriched in CSC cluster A further corroborating our hypothesi (Figure S2F). Taking into account that PD-L1 is a proven biomarker to predict immunotherapy response (37), we identified a significant upregulation of PD-L1 expression levels in CSC cluster A (Figure S2G). Based on these findings, we identified three subtypes with distinct immune infiltration characteristics.

In addition, Spearman analysis was used to assess the specific relationship between the 25 CSCRGs and immunocyte infiltration or immune-related function (Figures 3A, B). High expression of *EVI2B, ENG* and *SPI1* was markedly associated with enhanced immunocyte infiltration and immune-related function, whereas *MEF2C, PHACTR4, MYC, PTN, SEMA3A* and *SEMA4G* high expression showed a negative correlation with the immunocyte infiltration and immune-related function level. Among the 25 CSCRGs, we focused on *MEF2C*, which was found to be markedly negatively correlated with substantial immune infiltration and immune-related function levels and the expression high of *MEF2C* was significantly negatively correlated with patient prognosis (Figure 3C). We firstly compared the overall level of immune cell infiltration in patients with high and low *MEF2C* expression. Patients with low *MEF2C* expression had higher immune scores, indicating that TME immune cell infiltration was markedly increased in patients with low *MEF2C* expression (Figure 3D). We then compared the differences in 23 immunocytes between the two subgroups with low and high *MEF2C* expression (Figure 3E).

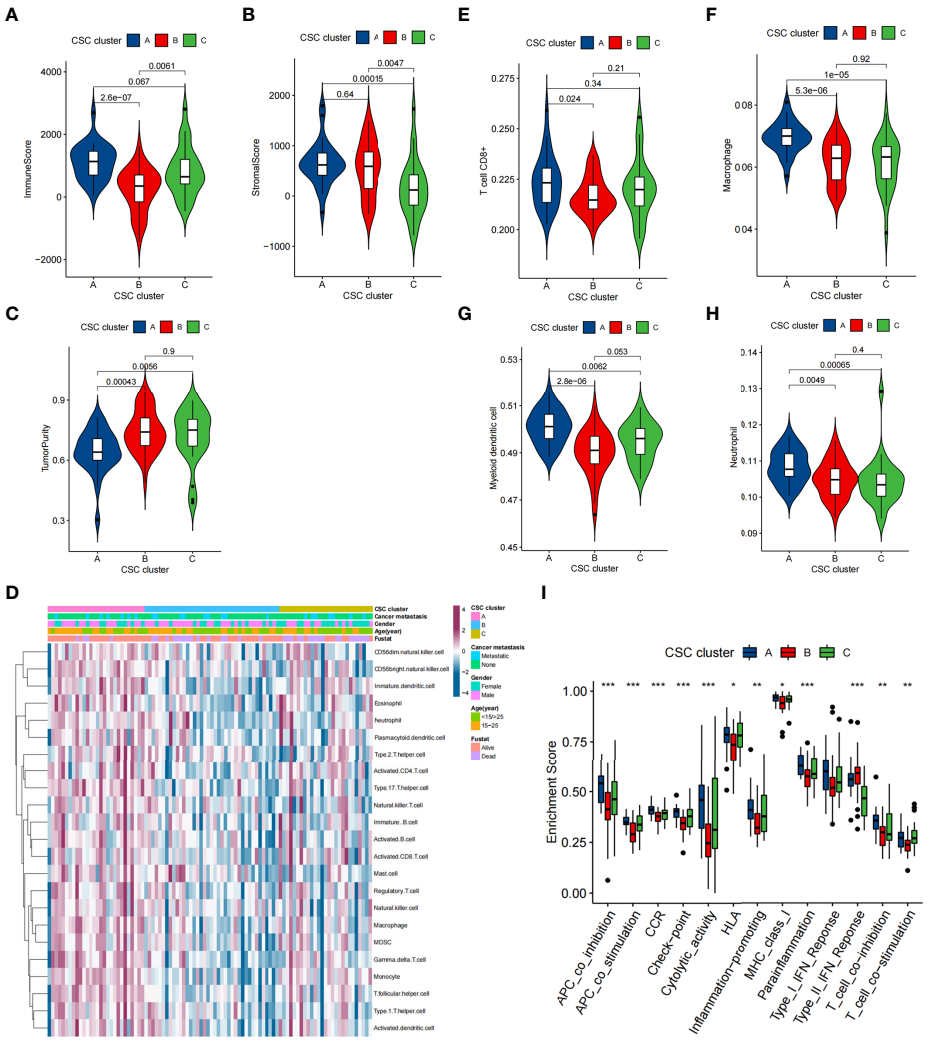

FIGURE 2
TME characteristics in distinct CSC clusters in the TARGET cohort. **(A–C)** Immune score **(A)**, stromal score **(B)** and tumor purity **(C)** of three CSC clusters were analyzed and plotted. The whisker contained 1.5 times the interquartile range. The bottom and top of the box indicate the 25th and 75th percentiles, and the thick line indicates the median value. **(D)** The heatmap used to visualize the infiltration of 23 immunocytes in three CSC clusters. CSC cluster, age, gender, patient survival status and tumor metastasis status were annotated. Purple represented high immune infiltration and blue represented low immune infiltration. **(E–H)** CD8+ T cells, neutrophils, macrophages and myeloid dendritic cells abundance in three CSC clusters was calculated using TIMER2.0. **(I)** Differences in the immune-related functions between three CSC Clusters. The bottom and top of the box indicate the 25th and 75th percentiles, and the thick line indicates the median value. (*P < 0.05; **P < 0.01; ***P < 0.001).

We found that high *MEF2C* expression was remarkably negatively associated with the levels of infiltration of multiple immune cells, including regulatory T cells, T follicular helper cells, type 1 T helper cells, macrophages, MDSCs, natural killer cells, activated DCs and CD8+ T cells (Figure 3E). DCs are responsible for antigen presentation and initial T cell activation, bridging the gap between innate and adaptive immunity [52]. According to these findings, we hypothesize that *MEF2C* may inhibit the cytotoxic T lymphocytes and activated DCs, thereby hindering the intratumoral anti-tumor immune response. Based on the above findings, we speculated that the expression of *MEF2C* could influence the prognosis of patients by affecting the infiltration of multiple immune cells.

Cancer stem cells related subtypes in GSE21257 cohort

To further confirm that the typing based on 25 CSCRGs was also applicable to other datasets, we performed validation with

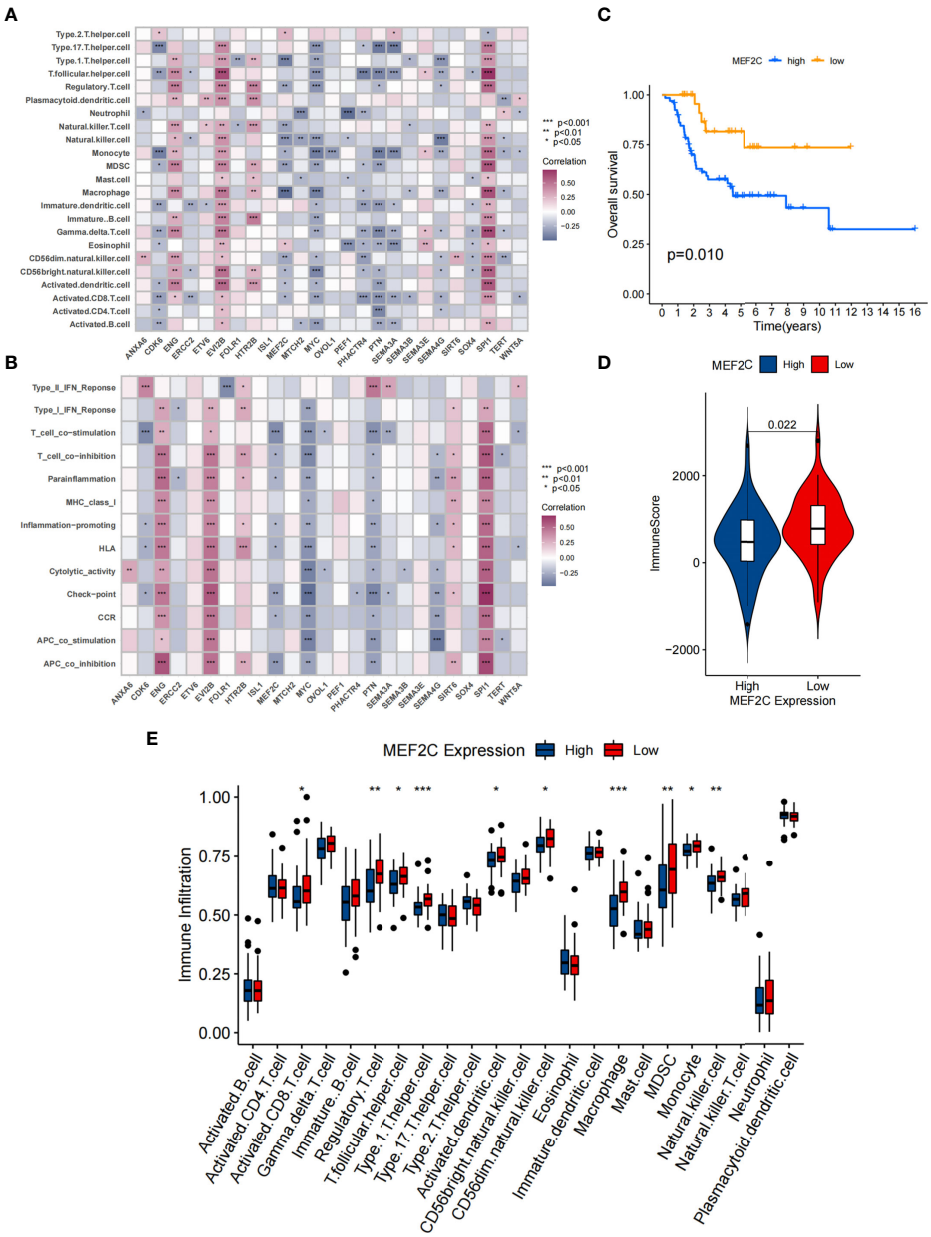

FIGURE 3
Correlation between TME infiltration and 25 CSCRGs and the relationship between MEF2C and immune infiltration. **(A)** The correlation between each immunocyte and each CSCRG by spearman analysis. Purple indicates positive correlation and blue indicates negative correlation. **(B)** The correlation between each immune-related function and each CSCRG using spearman analysis. Purple indicates positive correlation and blue indicates negative correlation. **(C)** Kaplan-Meier curves were used to analyze the survival of the high and low expressing MEF2C patient group. **(D)** Comparison of immune score between high and low MEF2C expressing subgroups. **(E)** Difference in the abundance of each immunocyte between MEF2C high expression and low expression subgroups. (*P < 0.05; **P < 0.01; ***P < 0.001).

the GSE21257 cohort. Similar to the clustering results of the TARGET-OS cohort, unsupervised clustering also revealed three completely different clusters of the 25 CSCRGs in the GSE21257 cohort (Supplementary Table 5, Figures S3A, B). The mRNA expression of 25 CSCRGs was significantly different in the three cluster (Figure 4A). Prognostic analysis indicated that the survival of CSC cluster A was better than that in CSC cluster B and C (Figure S3C). We also quantified the stromal score, immune score and tumor purity for the three clusters using ESTIMATE algorithm. The results showed that CSC cluster A

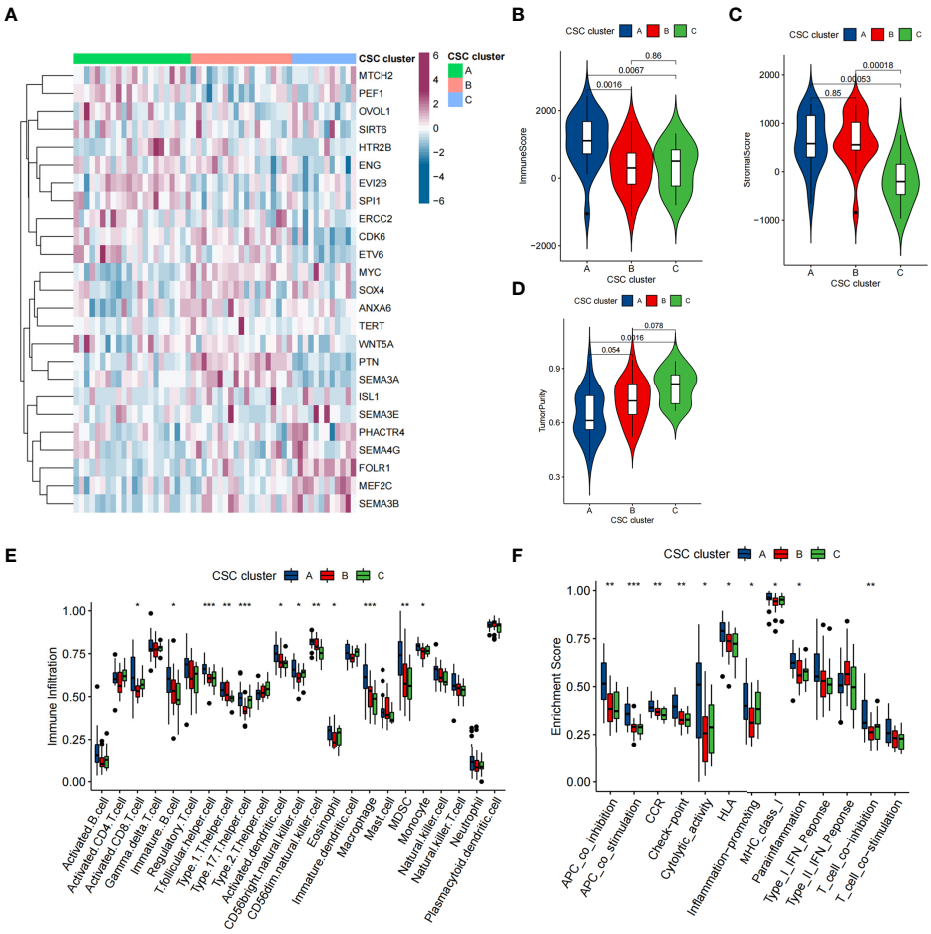

FIGURE 4
TME characteristics in distinct CSC clusters in GSE21257 cohort. **(A)** Unsupervised clustering of 25 CSCRGs in the GSE21257 cohort. CSC cluster, age and gender were annotated. Purple indicated high expression of the gene and blue indicated low expression of the gene. **(B–D)** Immune score **(B)**, stromal score **(C)** and tumor purity **(D)** of three CSC clusters were analyzed and plotted. **(E)** Difference in the abundance of each immunocyte between three CSC clusters. **(F)** Differences in the immune-related functions between three CSC Clusters. (*P < 0.05; **P < 0.01; ***P < 0.001).

had the highest immune score compared to CSC clusters B and C (Figure 4B), and CSC clusters A and B had a higher stromal score compared to CSC cluster C (Figure 4C). And consistent with the previous result, CSC cluster A had lower tumor purity (Figure 4D). We then analyzed the differences in immune infiltration between the three clusters, and we found the vast majority of immunocytes such as anti-tumor lymphocyte cell subpopulations and NK T cells were largely enriched in the CSC cluster A (Figure 4E). And consistent with previous results, most immune-related functions were enriched in CSC cluster A (Figure 4F). Similarly, the results of gsva analysis remained consistent with previous ones, showing enrichment of CD8 T-effects, immune checkpoints and Pan-F-TBRS in the CSC cluster A (Figure S3D).

Cancer stem cells phenotype-related DEGs in osteosarcoma

Previously, tumor samples were divided into three subtypes associated with CSC based on 25 CSCRGs, and to further explore the genetic alterations in these phenotypes, we determined 104 CSC-related DEGs using limma package in the TARGET-OS cohort (Figure 5A, Supplementary Table 6). We performed GO enrichment analysis on these DEGs, which were seen to be enriched in multiple stemness-related and immune regulation pathways (Figure 5B). Furthermore, the above analysis supported that DEGs were closely associated with tumor immunity and cancer stemness, and thus might be considered as CSCRGs. We performed consensus clustering

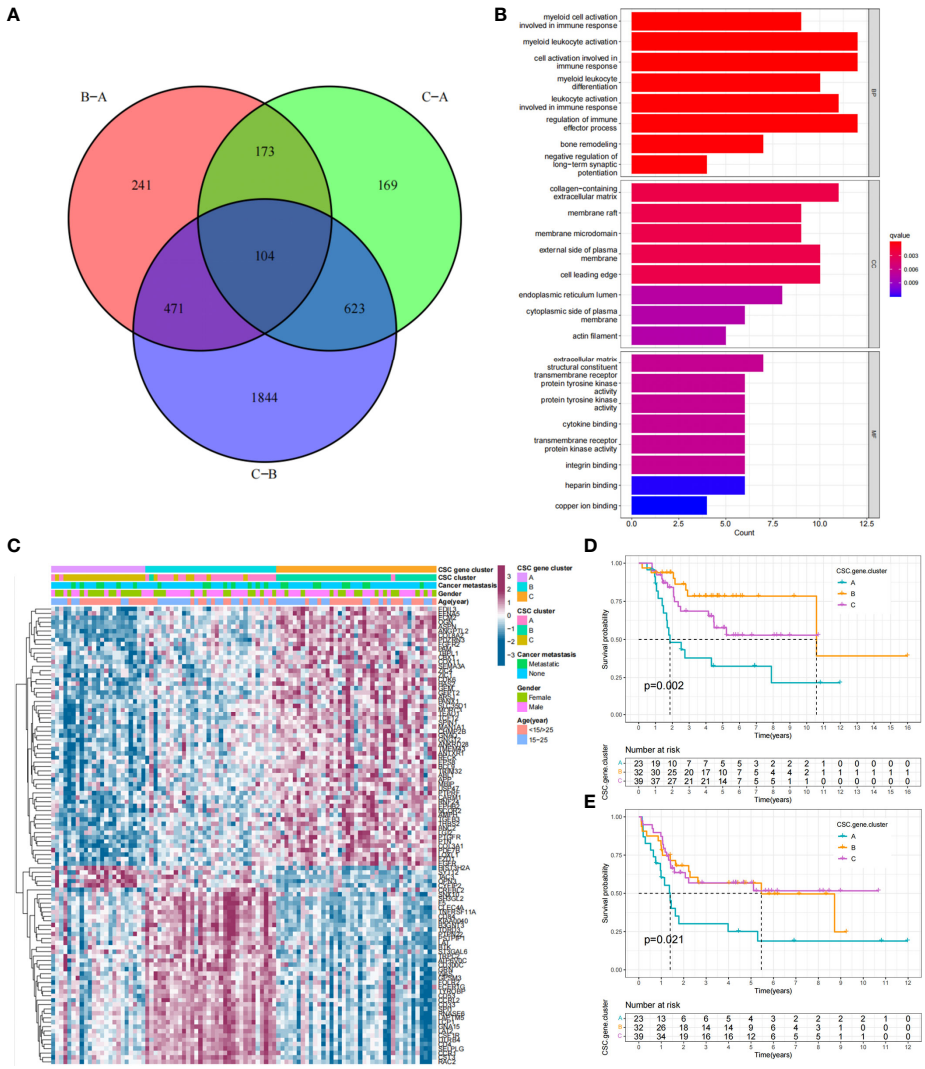

FIGURE 5
Functional annotation of DEGs and unsupervised clustering analysis based on DEGs. **(A)** Venn diagram showing the 104 CSC-related genes. B-A: DEGs between B and A; C-A: DEGs between C and A; C-B: DEGs between C and B, **(B)** GO enrichment analysis of the 104 CSC-related genes. The x-axis indicated the number of genes enriched. BP: biological process; CC: cellular component; MF: molecular function. **(C)** Unsupervised clustering of 104 CSC-related genes in the TARGET cohort. CSC gene cluster, CSC cluster, age, gender and tumor metastasis status were annotated. Purple indicated high expression of the gene and blue indicated low expression of the gene. **(D, E)** Kaplan-Meier curves of overall survival **(D)** and event-free survival **(E)** for 94 osteosarcoma patients in TARGET cohort with different CSC gene cluster, including 23 cases in CSC cluster A, 32 cases in CSC cluster B, and 39 cases in CSC cluster C (Log-rank test).

analysis on the 104 CSC phenotype-related genes obtained to further validate this regulatory mechanism and obtained three gene clusters (Figures S4A, B). We called these clusters as CSC gene cluster A-C. These results suggested that three distinct CSC subtypes indeed existed in osteosarcoma (Figure 5C). Among the three CSC gene clusters, 25 CSCRGs were found to be significantly differentially expressed, which was consistent with the expected results (Figure S4C). Survival analysis further showed prognostic differences between three CSC gene clusters. CSC gene cluster B was shown to be related to better prognosis, while CSC gene cluster A was proven to be related to worse prognosis (Figures 5D, E). To explore the roles of the 104 genes in immune infiltration, we examined the differences in 23 TME immune cells in the three clusters and showed that the most immunocytes increased in CSC gene cluster B (Figure S4D). Similarly, the result suggested that most immune-related functions were enriched in CSC gene cluster B (Figure S4E). Meanwhile, we found that PDL1 expression was significantly upregulated in CSC gene cluster B compared with CSC gene cluster A (Figure S4F). The above results once again suggested

that CSC-related genes played non-negligible regulatory roles in the formation of different TME landscapes.

Construction of the CSC score and exploration of its clinical significance

While previous studies have found important roles in prognosis and regulation of immune infiltration for CSC-related genes, these findings were only applicable to assess patient populations and could not be used to evaluate individual patients. Taking into account individual differences, we constructed a score system to quantitate CSC-related subtypes in single osteosarcoma patients based on the discovery of CSC-related signature genes, which we called CSC score. We constructed an alluvial diagram to illustrate the workflow of CSC score construction (Figure 6A). The result showed that CSC gene cluster A was related to higher CSC scores, and CSC gene cluster B was associated with lower CSC scores (Figure S5A). Notably, consistent with the expected results, CSC cluster B and C showed a higher CSC score than CSC cluster A (Figure S5B). We examined the relationship between CSC scores and certain biometric scores by Spearman analysis. The result showed that CSC score was negatively related to immune activation-related processes (Figure 6B). CSC score was also significantly negatively related to immune score (Figure S5C). Similarly, patients in the low CSC score subgroup had a higher degree of immune infiltration and were more enriched for immune-related functions compared to patients in the high CSC score subgroup (Figures S5D, E). The above analyses clearly indicated that low CSC score was remarkably correlated with immune infiltration. Based on the above findings, we concluded that the CSC score could better assess the CSC-related subtypes of individual tumors and further assess the tumor immune infiltration characteristics. Furthermore, we attempted to determine the value of CSC score in predicting patient prognosis. Patients were separated into low and high subgroups with a cutoff value of -0.3269, and patients with low CSC score had a better prognosis (Figures 6C, D). ROC curve analysis result verified the predictive advantage of the CSC score system (Figure S6A). We analyzed multiple clinical traits of patients using multivariate Cox regression and found that the CSC score system could potentially serve as an independent prognostic factor of osteosarcoma (Figure S6B). Futhermore, PD-L1 expression level was significantly higher in the group with low CSC score (Figure S6C). The constructed CSC scoring system was validated by meta-cohort, and patients with low CSC score indicated better prognosis (Figure 6E, Supplementary Table 7). To further validate the reliability of the CSC score system, we used a cohort (GSE21257) from the meta cohort to explore the association between CSC score and patient prognosis. Consistent with the results above, patients with low CSC score showed a significant survival advantage relative to patients with high score (Figure 6F). Similarly, ROC curve analysis result verified the predictive advantage of the CSC score system (Figure S6D). The above results strongly indicated that CSC scores could represent the CSC pattern of osteosarcoma patients and predict the prognosis of osteosarcoma patients.

CSC is associated with a variety of clinical traits such as tumor metastasis. We compared the differences of CSC score between different clinical subgroups in the TARGET cohort. Accordingly, we found that tumor metastasis was significantly related to higher CSC score, implying that these patients were characterized by poor immune infiltration, with a poorer clinical outcome (Figure 7A). And there were no differences in scores between age and gender subgroups (Figures S6E, F). In particular, we found that low CSC score subgroup showed a significant survival advantage both in patients who had developed tumor metastases and in those who did not (Figures 7B,C). Additional results showed that the predictive ability of the CSC score was not interfered by whether the tumor had metastasized, and the low CSC score group consistently showed a significant survival advantage in both patients with and without metastasis (Figures 7B, C). These results suggest that the CSC score can also be used to assess certain clinical symptoms such as tumor metastasis in osteosarcoma patients. Considering the strong correlation between CSC score and immune response in the above results, we investigated whether CSC score could predict treatment response to anti-PDL1 in patients in an independent immunotherapy cohort. We performed a systematic search that resulted in the inclusion of an immunotherapy cohort: uroepithelial carcinoma intervening with atezolizumab (IMvigor210 cohort). The result indicated that patients with low CSC score scores gained a survival advantage (Figure 7D). And there was a significant therapeutic advantage of anti-PDL1 treatment in patients with low CSC scores (Figure 7E). The above results suggested that the CSC score might be used to assess the therapeutic response and clinical prognosis of immunotherapy.

Exploring the correlation between CSC score and mRNAsi

Using the OCLR algorithm, the stemness index was computed for individual samples based on the gene expression profile of the patient. We compared the mRNAsi between different CSC clusters and showed that mRNAsi was significantly elevated in CSC cluster C (Figure 7F).Similarly, mRNAsi was significantly elevated in CSC gene cluster A (Figure 7G). We also found that patients with high *MEF2C* expression possessed higher mRNAsi (Figure 7H). Considering that mRNAsi represents the stemness of individual patients, we analyzed the correlation between CSC score and mRNAsi. The results revealed a significant positive relationship between CSC

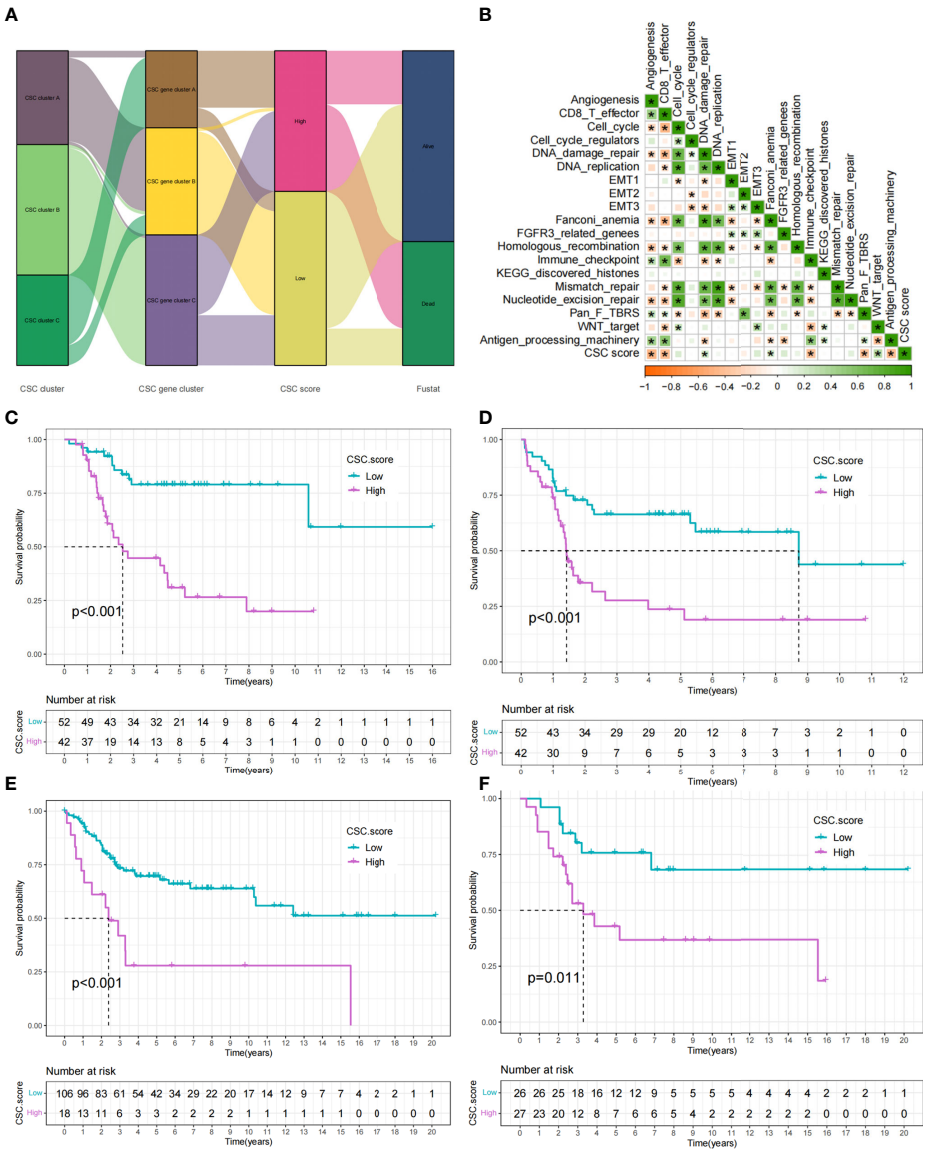

FIGURE 6
Construction of CSC score. **(A)** Alluvial diagram showing the changes of CSC cluster, CSC gene cluster, CSC score and patient survival status. **(B)** Correlations between CSC score and the certain gene signatures in TARGET cohort. Negative correlation was marked with yellow and positive correlation with green (*P < 0.05). **(C)** Survival analyses for high (42 cases) and low (52 cases) CSC score subgroups in TARGET cohort. **(D)** Event-free survival analyses for high (42 cases) and low (52 cases) CSC score subgroups in TARGET cohort. **(E)** Survival analyses for high (18 cases) and low (106 cases) CSC score subgroups in meta-cohort. **(F)** Survival analyses for high (27 cases) and low (26 cases) CSC score subgroups in GSE21257 cohort.

score and mRNAsi in the TARGET cohort (Figure 7I). However, the result showed a weak correlation between CSC score and mRNAsi (R=0.22). Therefore, unlike the previous result that the CSC score of CSC cluster A was significantly lower than cluster B, the mRNAsi of CSC cluster A was not significantly different from cluster B. Similarly, there was a significant positive correlation between CSC score and mRNAsi in both the meta cohort and the GSE21257 cohort (Figures 7J, K). The above results again demonstrated that the CSC score was a reliable scoring system that could represent the stemness of individual patients.

Drug sensitivity profiles of distinct cancer stem cells related subtypes

We performed a drug sensitivity analysis and identified 74 small molecule drugs that may be used in the treatment of

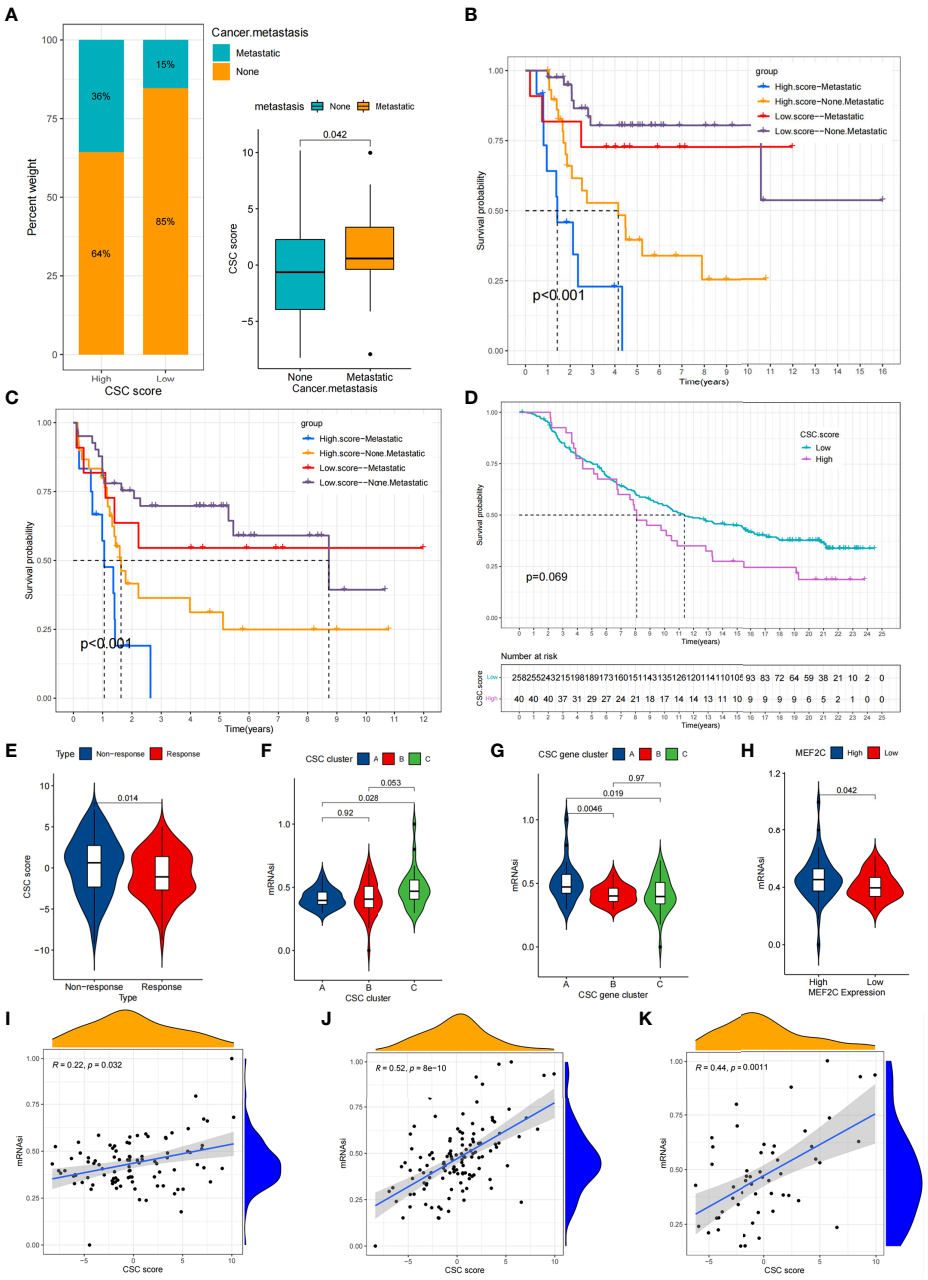

FIGURE 7
Comparison of CSC score between different clinical subgroups and relationship between mRNAsi and CSC score. **(A)** Comparison of CSC scores between tumor metastasis and tumor non-metastasis groups. **(B,C)** Kaplan-Meier curves of overall survival **(B)** and event-free survival **(C)** for 94 osteosarcoma patients in TARGET cohort with different tumor metastasis status. **(D)** Survival analyses for high (40 cases) and low (258 cases) CSC score subgroups in IMvigor210 cohort. **(E)** Comparison of CSC scores between patients who responded better to anti-PD-L1 therapy and those who responded less well. **(F)** Comparison of mRNAsi between three CSC clusters. **(G)** Comparison of mRNAsi between MEF2C high expression and low expression groups. **(H)** Comparison of mRNAsi between three CSC gene clusters. **(I–K)** CSC score and mRNAsi were significantly and positively correlated in the TARGET cohort **(I)**, meta cohort **(J)** and GSE21257 cohort **(K)**.

osteosarcoma (Supplementary Table 8). Sensitivity of 12 drugs in different CSC clusters was depicted in Figures 8A-L. The results showed that CSC cluster A was sensitive to BIRB.0796 and OSI.906, while CSC clutser B was sensitive to Methotrexate, Sorafenib, Sunitinib and Nilotinib, and CSC clutser C was more sensitive to Cisplatin, Doxorubicin, Imatinib, CHIR.99021, Pazopanib and Vinorelbine were more sensitive (Figures 8A-L). We then evaluated the relationship between 25 CSCRGs

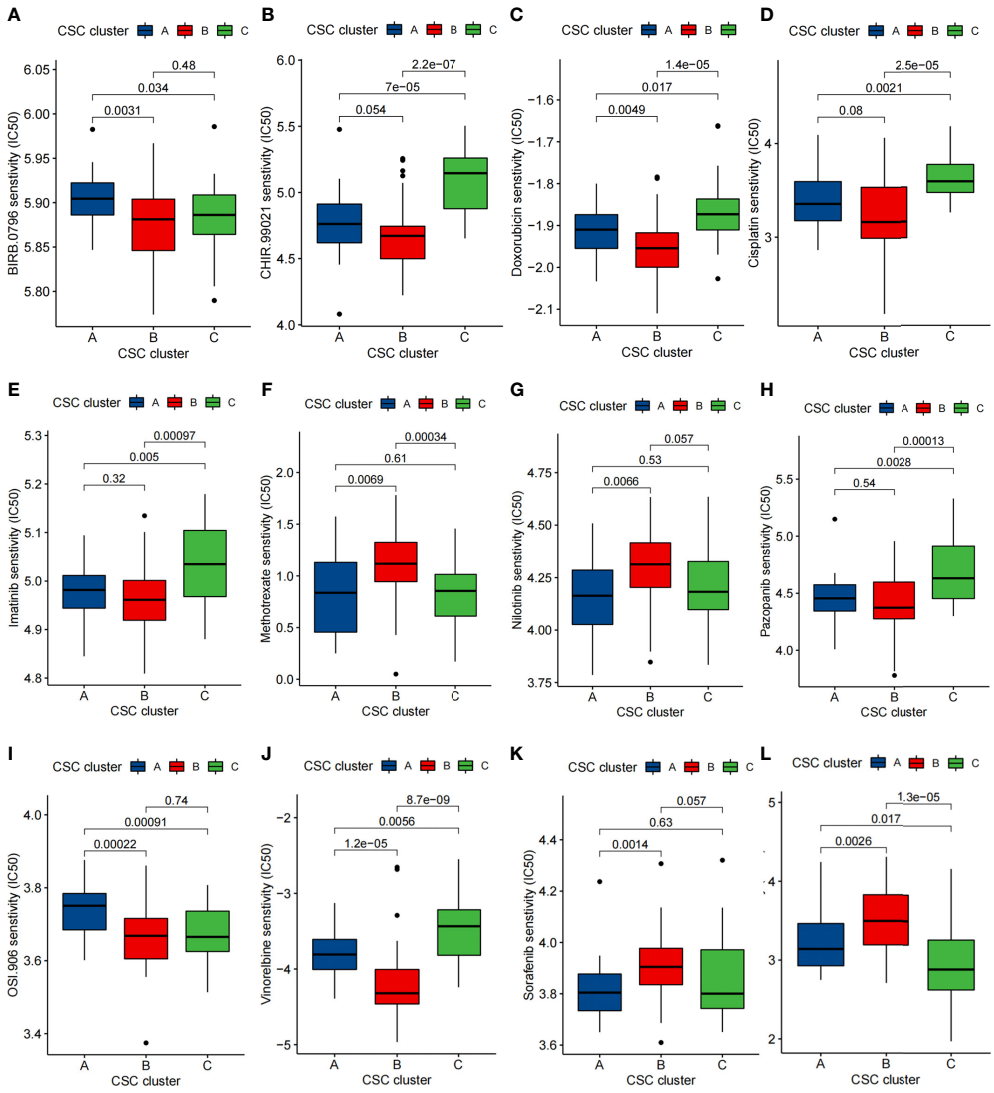

FIGURE 8
Comparison of drug sensitivity. **(A–L)** Comparison of IC50 of small molecule drugs between three CSC clusters.

expressions and drug sensitivity using the CellMiner database (Figure S7, Supplementary Table 9). The above findings indicated that exploring CSC subtypes in osteosarcoma patients could be used to guide the clinical use of drugs.

Immunohistochemical detection of *MEF2C* expression distribution

Given that *MEF2C* was found to affect prognosis, immune infiltration and stemness in osteosarcoma patients in our previous study, we verified the expression of *MEF2C* in clinical tissues of osteosarcoma patients by immunohistochemical experiments. The results showed that *MEF2C* was significantly expressed in clinical tissues of osteosarcoma patients (Figure 9A).

MEF2C affected the stemness of osteosarcoma cells

We used a sphere formation assay to examine the effect of *MEF2C* on tumor cell stemness (Figures 9B, C). The results showed that the si-*MEF2C* cells formed fewer sphere (Figure 9B) and the size of sphere was smaller (Figure 9C) compared to the control group. These results can tentatively demonstrate the effect of *MEF2C* on the maintenance of stemness of CSC in osteosarcoma. Our previous analysis

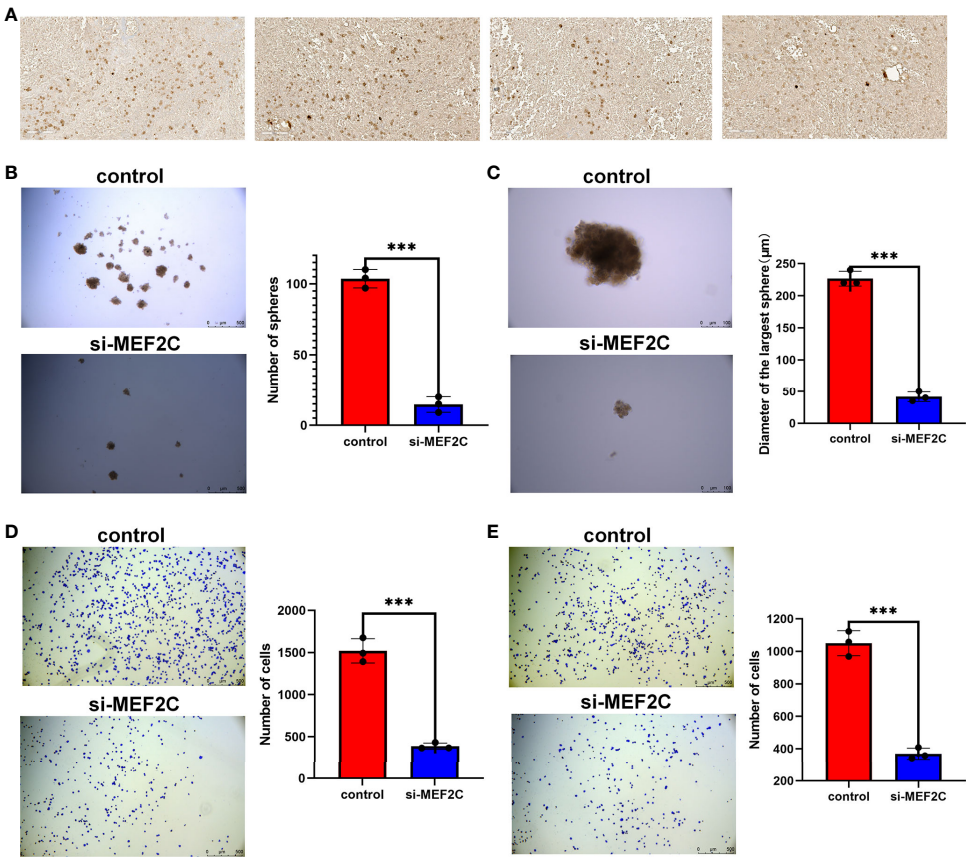

FIGURE 9
Immunohistochemical analysis of *MEF2C* expression in OS tissues and effect of *MEF2C* on the stemness of osteosarcoma cells. **(A)** Immunohistochemical analysis of *MEF2C* expression in OS tissues. **(B)** Comparison of the number of spheres between control and si-*MEF2C* groups. (***P < 0.001). **(C)** Comparison of the size of the largest of sphere between control and si-*MEF2C* groups. **(D)** Comparison of cell adhesion to vitronectin between control and si-*MEF2C* groups. **(E)** Comparison of cell adhesion to fibronectin between control and si-*MEF2C* groups.

showed that *MEF2C* affected immune infiltration in the TME. We also verified that *MEF2C* affects the adhesion of tumor cells to the extracellular matrix by cell adhesion assays (Figures 9D, E).The results showed that the adhesion of si-*MEF2C* cells to the extracellular matrix such as vitronectin (Figure 9D) and fibronectin (Figure 9E) was reduced compared with the control group.

Discussion

Recent studies have revealed that there is significant heterogeneity among tumor cells. Tumor heterogeneity is mainly manifested in several aspects such as gene expression profile, chemotherapy sensitivity, apoptosis resistance and tumorigenic ability (50). In tumor tissue, only a small proportion of tumor cells can initiate tumor formation, recurrence and metastasis, and the proportion of cells is cancer stem cells. Increasing evidence suggested that CSC plays significant roles in innate immunity, inflammation and antitumor effects (51). Nevertheless, most researches have focused on an individual cancer stem cell-associated gene or a single TME cell type, so the understanding of the overall TME infiltration characteristics mediated by the combination of multiple cancer stem cell-associated genes are not comprehensive. Exploring the combined role of multiple cancer stem cell-related genes in immune infiltration will help us further understand the role of CSC in tumor immunity and direct more effective immunotherapeutic strategies.

In this study, we identified three subtypes in osteosarcoma using the consensus clustering analysis based on 25 cancer stem cell-related genes. The three subtypes differed significantly in prognosis and had different immunophenotypes. Compared to CSC cluster B and C, CSC cluster A had more innate and adaptive immunity and stromal activation, and multiple immune-related activation pathways were also enriched in

CSC cluster A. However, curiously, CSC cluster C, which also had some immune cell infiltration, was not matched for the same survival advantage. Numerous studies have revealed that the immune excluded phenotype also exhibits a large immunoctyes infiltration, but the immune cells stayed in the interstitium surrounding the tumor cell nests rather than penetrating the parenchyma of the tumor cell nests (52, 53). We therefore speculated that CSC cluster C might be an immune excluded phenotype. We also found that PDL1 expression levels were significantly elevated in cluster A, suggesting that CSC-related clusters may have potential predictive value for immunotherapy. Previous researches have revealed that TME plays critical roles in tumor progression (54). Based on the above findings, we speculated that the better prognosis of CSC cluster A might be related to its high immune infiltration. Furthermore, differentially expressed genes between three different subtypes were shown to be correlated with immune activation and CSC. These DEGs were recognized as cancer stem cell-associated genes. Similarly, three molecular subtypes were identified based on the DEGs using the consensus clustering analysis, with significant prognostic differences between the three subtypes as well as a different immune infiltration landscape. The above results again demonstrated that three distinct cancer stem cell-associated subtypes were indeed present in osteosarcoma patients and that the combined effect of multiple cancer stem cell-associated genes played a significant role in immune infiltration.

Considering the heterogeneity among tumors, we constructed a score system called CSC score to quantify the individual and thus more precisely guide the treatment of individual patients. Cancer stem cell-associated subtype characterized by abundant immune infiltration had a lower CSC score. The result suggested that the CSC score was a valuable tool to evaluate the cancer stem cell-related phenotype of individual osteosarcoma patients and to evaluate their immune infiltration. CSC is closely associated with metastasis of tumors. Therefore, we compared the differences in CSC score of patients between different clinical subgroups. The results demonstrated that the CSC score can be used to assess the metastatic status of patients. Comprehensive analyses showed that CSC score could be an independent prognostic marker for osteosarcoma. Furthermore, we observed a correlation between CSC score and PD-L1, a predictor of immune response, implying that different cancer stem cell-associated subtypes may influence the efficacy of immunotherapy. In fact, we further validated in an independent immunotherapy cohort that the CSC score may be predictive of patient response to immunotherapy as well as survival. mRNAsi is thought to be correlated with patient stemness in various cancers. Therefore, we analyzed the correlation between CSC score and mRNAsi and found that CSC score also represented the stemness of the patients to some extent. The stemness of the tumor can affect the effectiveness of drug therapy. We found that different CSC clusters have distinct sensitivities to certain small molecule drugs, thus our CSC subtypes can provide some guidance for the drug treatment of osteosarcoma patients.

Along with exploring CSC-related phenotypes, we also explored the role of individual CSC-related genes in stemness as well as in the immune microenvironment. *MYC* is encoded by the proto-oncogene family and is an essential transcription factor for the bHLH superfamily of DNA-binding proteins (55). *MYC* regulates a wide range of stem cell processes such as self-renewal and differentiation through the regulation of numerous genes (56). *MYC* has been shown to maintain the stemness of CSC in a variety of tumors, and its role in osteosarcoma stem cells has also been revealed (57–60). Meanwhile, substantial studies have focused on the effect of *MYC* on the TME. Yi et al. revealed that *MYC* amplification was associated with low immune infiltration of triple-negative breast cancer and that *MYC* may be involved in immune escape of triple-negative breast cancer by Multi-Omics Profiling (61). Stephanie et al. revealed that MYC regulates the expression of PDL1 and CD47 on the surface of tumor cells, thus modulating the tumor immune response (62). Similarly, our results showed that high *MYC* expression was negatively associated with prognosis and multiple immune infiltrating cells in osteosarcoma patients. *MEF2C* is a transcription factor which is specifically expressed in muscle and neuronal lineages and is commonly upregulated in leukemia (63). Our analysis showed that *MEF2C* expression was upregulated in tumor tissues and was related to poor patient survival outcomes. Further analyses showed that high expression of *MEF2C* was significantly and negatively related to infiltration of most antitumor lymphocytes including CD8+ T cells, NK T cells and DCs. And notably, patients with high *MEF2C* expression had higher CSC score and mRNAsi compared to those with low expression. We further confirmed the expression of *MEF2C* in osteosarcoma tissues by immunohistochemical experiments. However, the specific mechanism of its regulation of osteosarcoma stem cells and its relationship with immune infiltration still need to be explored through further experiments. Similarly, we found that high expression of *SPI1* and *EVI2B* was highly positively related to immune infiltration. These results demonstrated the importance of exploring the combined effects of multiple CSC-related genes.

In this study, we included a total of 25 cancer stem cell-related genes, and further more cancer stem cell-related genes can be included subsequently to optimize the accuracy of CSC-related subtypes. As well as the specific mechanism of the effect of some of these 25 CSCRGs on the phenotype of CSC has not been clarified, so further studies can be conducted on them

subsequently. Since we used limited public datasets in this study, our findings need to be further validated in additional datasets. In this study, we initially verified the effect of *MEF2C* on the malignant phenotype of osteosarcoma by bioinformatics analysis, and verified the expression of *MEF2C* in osteosarcoma tissues by IHC. Our subsequent study will further explore the effect of *MEF2C* on the stemness of osteosarcoma through experiments. In addition, because of the relatively limited number of osteosarcoma patients currently receiving immunotherapy, this study explored the efficacy of CSC score to predict immunotherapy based on a cohort of urothelial carcinoma, and a cohort of osteosarcoma patients receiving immunotherapy would still be needed to further validate our hypothesis.

In conclusion, in this study we classified patients into three distinct subtypes based on cancer stem cell-related genes and systematically described the association between the different subtypes and the TME immunocyte infiltration characteristics. We further determined that the CSC score could be used to assess the clinical characteristics and the immune infiltration of individual osteosarcoma patients. This study provided novel ideas in identifying new tumor subtypes of osteosarcoma, guiding individualized specific therapy, and improving patient response to immunotherapy in the future.

Data availability statement

The original contributions presented in the study are included in the article/Supplementary Material. Further inquiries can be directed to the corresponding author.

Ethics statement

The studies involving human participants were reviewed and approved by Ethics Commttee of Peking University People's Hospital. The patients/participants provided their written informed consent to participate in this study.

Author contributions

LG and TY designed the study and wrote and revised the manuscript. WG, JN, WW, and TR acquired and analyzed the data. BW, YH, and JX wrote the manuscript. All authors read and approved the final manuscript.

Funding

This work was supported by a grant from the National Natural Science Foundation of China (#81972513).

Conflict of interest

The authors declare that the research was conducted in the absence of any commercial or financial relationships that could be construed as a potential conflict of interest.

Publisher's note

Supplementary material

The Supplementary Material for this article can be found online at: https://www.frontiersin.org/articles/10.3389/fimmu.2022.986785/full#supplementary-material

References

1. Meltzer PS, Helman LJ. New horizons in the treatment of osteosarcoma. *N Engl J Med* (2021) 385(22):2066–76. doi: 10.1056/NEJMra2103423

2. Gill J, Gorlick R. Advancing therapy for osteosarcoma. *Nat Rev Clin Oncol* (2021) 18(10):609–24. doi: 10.1038/s41571-021-00519-8

3. Kusoglu A, Biray Avci C. Cancer stem cells: A brief review of the current status. *Gene* (2019) 681:80–5. doi: 10.1016/j.gene.2018.09.052

4. Bjerkvig R, Tysnes BB, Aboody KS, Najbauer J, Terzis AJ. Opinion: The origin of the cancer stem cell: Current controversies and new insights. *Nat Rev Cancer* (2005) 5(11):899–904. doi: 10.1038/nrc1740

5. Matsui W, Huff CA, Wang Q, Malehorn MT, Barber J, Tanhehco Y, et al. Characterization of clonogenic multiple myeloma cells. *Blood* (2004) 103(6):2332–6. doi: 10.1182/blood-2003-09-3064

6. Hill RP. Identifying cancer stem cells in solid tumors: Case not proven. *Cancer Res* (2006) 66(4):1891–5; discussion 0. doi: 10.1158/0008-5472.CAN-05-3450

7. Al-Hajj M, Wicha MS, Benito-Hernandez A, Morrison SJ, Clarke MF. Prospective identification of tumorigenic breast cancer cells. *Proc Natl Acad Sci U.S.A.* (2003) 100(7):3983–8. doi: 10.1073/pnas.0530291100

8. Hermann PC, Huber SL, Herrler T, Aicher A, Ellwart JW, Guba M, et al. Distinct populations of cancer stem cells determine tumor growth and metastatic activity in human pancreatic cancer. *Cell Stem Cell* (2007) 1(3):313–23. doi: 10.1016/j.stem.2007.06.002

9. Collins AT, Berry PA, Hyde C, Stower MJ, Maitland NJ. Prospective identification of tumorigenic prostate cancer stem cells. *Cancer Res* (2005) 65 (23):10946–51. doi: 10.1158/0008-5472.CAN-05-2018

10. Garcia-Mayea Y, Mir C, Masson F, Paciucci R, ME LL. Insights into new mechanisms and models of cancer stem cell multidrug resistance. *Semin Cancer Biol* (2020) 60:166–80. doi: 10.1016/j.semcancer.2019.07.022

11. Gottesman MM, Fojo T, Bates SE. Multidrug resistance in cancer: Role of atp-dependent transporters. *Nat Rev Cancer* (2002) 2(1):48–58. doi: 10.1038/nrc706

12. Ginestier C, Hur MH, Charafe-Jauffret E, Monville F, Dutcher J, Brown M, et al. Aldh1 is a marker of normal and malignant human mammary stem cells and a predictor of poor clinical outcome. *Cell Stem Cell* (2007) 1(5):555–67. doi: 10.1016/j.stem.2007.08.014

13. Singh S, Brocker C, Koppaka V, Chen Y, Jackson BC, Matsumoto A, et al. Aldehyde dehydrogenases in cellular responses to Oxidative/Electrophilic stress. *Free Radic Biol Med* (2013) 56:89–101. doi: 10.1016/j.freeradbiomed.2012.11.010

14. Najafi M, Farhood B, Mortezaee K. Cancer stem cells (CSCs) in cancer progression and therapy. *J Cell Physiol* (2019) 234(6):8381–95. doi: 10.1002/jcp.27740

15. Dzobo K, Senthebane DA, Rowe A, Thomford NE, Mwapagha LM, Al-Awwad N, et al. Cancer stem cell hypothesis for therapeutic innovation in clinical oncology? taking the root out, not chopping the leaf. *OMICS* (2016) 20(12):681–91. doi: 10.1089/omi.2016.0152

16. Walcher L, Kistenmacher AK, Suo H, Kitte R, Dluczek S, Strauss A, et al. Cancer stem cells-origins and biomarkers: Perspectives for targeted personalized therapies. *Front Immunol* (2020) 11:1280. doi: 10.3389/fimmu.2020.01280

17. Dzobo K, Ganz C, Thomford NE, Senthebane DA. Cancer stem cell markers in relation to patient survival outcomes: Lessons for integrative diagnostics and next-generation anticancer drug development. *OMICS* (2021) 25(2):81–92. doi: 10.1089/omi.2020.0185

18. Dzobo K, Sinkala M. Cancer stem cell marker CD44 plays multiple key roles in human cancers: Immune Suppression/Evasion, drug resistance, epithelial-mesenchymal transition, and metastasis. *OMICS* (2021) 25(5):313–32. doi: 10.1089/omi.2021.0025

19. Batlle E, Clevers H. Cancer stem cells revisited. *Nat Med* (2017) 23 (10):1124–34. doi: 10.1038/nm.4409

20. Dawood S, Austin L, Cristofanilli M. Cancer stem cells: implications for cancer therapy. *Oncol (Williston Park)* (2014) 28(12):1101–7, 10.

21. Dzobo K, Senthebane DA, Ganz C, Thomford NE, Wonkam A, Dandara C. Advances in Therapeutic Targeting of Cancer Stem Cells within the Tumor Microenvironment: An updated review. *Cells* (2020) 9(8). doi: 10.3390/cells9081896

22. Dzobo K. Taking a full snapshot of cancer biology: Deciphering the tumor microenvironment for effective cancer therapy in the oncology clinic. *OMICS* (2020) 24(4):175–9. doi: 10.1089/omi.2020.0019

23. Vlashi E, Pajonk F. Cancer stem cells, cancer cell plasticity and radiation therapy. *Semin Cancer Biol* (2015) 31:28–35. doi: 10.1016/j.semcancer.2014.07.001

24. Butti R, Gunasekaran VP, Kumar TVS, Banerjee P, Kundu GC. Breast cancer stem cells: Biology and therapeutic implications. *Int J Biochem Cell Biol* (2019) 107:38–52. doi: 10.1016/j.biocel.2018.12.001

25. Galluzzi L, Chan TA, Kroemer G, Wolchok JD, Lopez-Soto A. The Hallmarks of Successful Anticancer Immunotherapy. *Sci Transl Med* (2018) 10 (459). doi: 10.1126/scitranslmed.aat7807

26. Hinshaw DC, Shevde LA. The tumor microenvironment innately modulates cancer progression. *Cancer Res* (2019) 79(18):4557–66. doi: 10.1158/0008-5472.CAN-18-3962

27. Miranda A, Hamilton PT, Zhang AW, Pattnaik S, Becht E, Mezheyeuski A, et al. Cancer stemness, intratumoral heterogeneity, and immune response across cancers. *Proc Natl Acad Sci U.S.A.* (2019) 116(18):9020–9. doi: 10.1073/pnas.1818210116

28. Huang YK, Wang M, Sun Y, Di Costanzo N, Mitchell C, Achuthan A, et al. Macrophage spatial heterogeneity in gastric cancer defined by multiplex immunohistochemistry. *Nat Commun* (2019) 10(1):3928. doi: 10.1038/s41467-019-11788-4

29. Tao W, Chu C, Zhou W, Huang Z, Zhai K, Fang X, et al. Dual role of Wisp1 in maintaining glioma stem cells and tumor-supportive macrophages in glioblastoma. *Nat Commun* (2020) 11(1):3015. doi: 10.1038/s41467-020-16827-z

30. Zhou W, Ke SQ, Huang Z, Flavahan W, Fang X, Paul J, et al. Periostin secreted by glioblastoma stem cells recruits M2 tumour-associated macrophages and promotes malignant growth. *Nat Cell Biol* (2015) 17(2):170–82. doi: 10.1038/ncb3090

31. Wu A, Wei J, Kong LY, Wang Y, Priebe W, Qiao W, et al. Glioma cancer stem cells induce immunosuppressive Macrophages/Microglia. *Neuro Oncol* (2010) 12(11):1113–25. doi: 10.1093/neuonc/noq082

32. Gomez KE, Wu F, Keysar SB, Morton JJ, Miller B, Chimed TS, et al. Cancer cell CD44 mediates Macrophage/Monocyte-driven regulation of head and neck cancer stem cells. *Cancer Res* (2020) 80(19):4185–98. doi: 10.1158/0008-5472.CAN-20-1079

33. Miao Y, Yang H, Levorse J, Yuan S, Polak L, Sribour M, et al. Adaptive immune resistance emerges from tumor-initiating stem cells. *Cell* (2019) 177 (5):1172–86.e14. doi: 10.1016/j.cell.2019.03.025

34. Lee Y, Shin JH, Longmire M, Wang H, Kohrt HE, Chang HY, et al. Cd44+ cells in head and neck squamous cell carcinoma suppress T-Cell-Mediated immunity by selective constitutive and inducible expression of pd-L1. *Clin Cancer Res* (2016) 22(14):3571–81. doi: 10.1158/1078-0432.CCR-15-2665

35. Wei J, Barr J, Kong LY, Wang Y, Wu A, Sharma AK, et al. Glioblastoma cancer-initiating cells inhibit T-cell proliferation and effector responses by the signal transducers and activators of transcription 3 pathway. *Mol Cancer Ther* (2010) 9(1):67–78. doi: 10.1158/1535-7163.MCT-09-0734

36. Grange C, Tapparo M, Tritta S, Deregibus MC, Battaglia A, Gontero P, et al. Role of hla-G and extracellular vesicles in renal cancer stem cell-induced inhibition of dendritic cell differentiation. *BMC Cancer* (2015) 15:1009. doi: 10.1186/s12885-015-2025-z

37. Hsu YL, Chen YJ, Chang WA, Jian SF, Fan HL, Wang JY, et al. Interaction between Tumor-Associated Dendritic cells and Colon Cancer Cells Contributes to Tumor Progression *Via* Cxcl1. *Int J Mol Sci* (2018) 19(8). doi: 10.3390/ijms19082427

38. Pellegatta S, Poliani PL, Corno D, Menghi F, Ghielmetti F, Suarez-Merino B, et al. Neurospheres enriched in cancer stem-like cells are highly effective in eliciting a dendritic cell-mediated immune response against malignant gliomas. *Cancer Res* (2006) 66(21):10247–52. doi: 10.1158/0008-5472.CAN-06-2048

39. Mlecnik B, Tosolini M, Kirilovsky A, Berger A, Bindea G, Meatchi T, et al. Histopathologic-based prognostic factors of colorectal cancers are associated with the state of the local immune reaction. *J Clin Oncol* (2011) 29(6):610–8. doi: 10.1200/JCO.2010.30.5425

40. Mariathasan S, Turley SJ, Nickles D, Castiglioni A, Yuen K, Wang Y, et al. Tgfbeta attenuates tumour response to pd-L1 blockade by contributing to exclusion of T cells. *Nature* (2018) 554(7693):544–8. doi: 10.1038/nature25501

41. Hanzelmann S, Castelo R, Guinney J. Gsva: Gene set variation analysis for microarray and rna-seq data. *BMC Bioinf* (2013) 14:7. doi: 10.1186/1471-2105-14-7

42. Charoentong P, Finotello F, Angelova M, Mayer C, Efremova M, Rieder D, et al. Pan-cancer immunogenomic analyses reveal genotype-immunophenotype relationships and predictors of response to checkpoint blockade. *Cell Rep* (2017) 18 (1):248–62. doi: 10.1016/j.celrep.2016.12.019

43. Newman AM, Liu CL, Green MR, Gentles AJ, Feng W, Xu Y, et al. Robust enumeration of cell subsets from tissue expression profiles. *Nat Methods* (2015) 12 (5):453–7. doi: 10.1038/nmeth.3337

44. Sotiriou C, Wirapati P, Loi S, Harris A, Fox S, Smeds J, et al. Gene expression profiling in breast cancer: Understanding the molecular basis of histologic grade to improve prognosis. *J Natl Cancer Inst* (2006) 98(4):262–72. doi: 10.1093/jnci/djj052

45. Zeng D, Li M, Zhou R, Zhang J, Sun H, Shi M, et al. Tumor microenvironment characterization in gastric cancer identifies prognostic and immunotherapeutically relevant gene signatures. *Cancer Immunol Res* (2019) 7 (5):737–50. doi: 10.1158/2326-6066.CIR-18-0436

46. Reinhold WC, Sunshine M, Liu H, Varma S, Kohn KW, Morris J, et al. Cellminer: A web-based suite of genomic and pharmacologic tools to explore transcript and drug patterns in the nci-60 cell line set. *Cancer Res* (2012) 72 (14):3499–511. doi: 10.1158/0008-5472.CAN-12-1370

47. Malta TM, Sokolov A, Gentles AJ, Burzykowski T, Poisson L, Weinstein JN, et al. Machine learning identifies stemness features associated with oncogenic dedifferentiation. *Cell* (2018) 173(2):338–54.e15. doi: 10.1016/j.cell.2018.03.034

48. Wang Z, Wang Y, Yang T, Xing H, Wang Y, Gao L, et al. Machine Learning Revealed Stemness Features and a Novel Stemness-Based Classification with Appealing Implications in Discriminating the Prognosis, Immunotherapy and Temozolomide Responses of 906 Glioblastoma Patients. *Brief Bioinform* (2021) 22 (5). doi: 10.1093/bib/bbab032

49. Hazra A, Gogtay N. Biostatistics series module 3: Comparing groups: Numerical variables. *Indian J Dermatol* (2016) 61(3):251–60. doi: 10.4103/0019-5154.182416

50. Nassar D, Blanpain C. Cancer stem cells: Basic concepts and therapeutic implications. *Annu Rev Pathol* (2016) 11:47–76. doi: 10.1146/annurev-pathol-012615-044438

51. Clarke MF. Clinical and therapeutic implications of cancer stem cells. *N Engl J Med* (2019) 380(23):2237–45. doi: 10.1056/NEJMra1804280

52. Gajewski TF. The next hurdle in cancer immunotherapy: Overcoming the non-T-Cell-Inflamed tumor microenvironment. *Semin Oncol* (2015) 42(4):663–71. doi: 10.1053/j.seminoncol.2015.05.011

53. Salmon H, Franciszkiewicz K, Damotte D, Dieu-Nosjean MC, Validire P, Trautmann A, et al. Matrix architecture defines the preferential localization and migration of T cells into the stroma of human lung tumors. *J Clin Invest* (2012) 122 (3):899–910. doi: 10.1172/JCI45817

54. Galon J, Bruni D. Approaches to treat immune hot, altered and cold tumours with combination immunotherapies. *Nat Rev Drug Discovery* (2019) 18 (3):197–218. doi: 10.1038/s41573-018-0007-y

55. Yang L, Shi P, Zhao G, Xu J, Peng W, Zhang J, et al. Targeting cancer stem cell pathways for cancer therapy. *Signal Transduct Tar Ther* (2020) 5(1):8. doi: 10.1038/s41392-020-0110-5

56. Dang CV. Myc, Metabolism, Cell Growth, and Tumorigenesis. *Cold Spring Harb Perspect Med* (2013) 3(8). doi: 10.1101/cshperspect.a014217

57. Galardi S, Savino M, Scagnoli F, Pellegatta S, Pisati F, Zambelli F, et al. Resetting cancer stem cell regulatory nodes upon myc inhibition. *EMBO Rep* (2016) 17(12):1872–89. doi: 10.15252/embr.201541489

58. Lee KM, Giltnane JM, Balko JM, Schwarz LJ, Guerrero-Zotano AL, Hutchinson KE, et al. Myc and Mcl1 cooperatively promote chemotherapy-resistant breast cancer stem cells *Via* regulation of mitochondrial oxidative phosphorylation. *Cell Metab* (2017) 26(4):633–47.e7. doi: 10.1016/j.cmet.2017.09.009

59. Sancho P, Burgos-Ramos E, Tavera A, Bou Kheir T, Jagust P, Schoenhals M, et al. Myc/Pgc-1alpha balance determines the metabolic phenotype and plasticity of pancreatic cancer stem cells. *Cell Metab* (2015) 22(4):590–605. doi: 10.1016/j.cmet.2015.08.015

60. Wang JY, Wu PK, Chen PC, Lee CW, Chen WM, Hung SC. Generation of osteosarcomas from a combination of Rb silencing and c-myc overexpression in human mesenchymal stem cells. *Stem Cells Transl Med* (2017) 6(2):512–26. doi: 10.5966/sctm.2015-0226

61. Xiao Y, Ma D, Zhao S, Suo C, Shi J, Xue MZ, et al. Multi-omics profiling reveals distinct microenvironment characterization and suggests immune escape mechanisms of triple-negative breast cancer. *Clin Cancer Res* (2019) 25(16):5002–14. doi: 10.1158/1078-0432.CCR-18-3524

62. Casey SC, Tong L, Li Y, Do R, Walz S, Fitzgerald KN, et al. Myc regulates the antitumor immune response through Cd47 and pd-L1. *Science* (2016) 352 (6282):227–31. doi: 10.1126/science.aac9935

63. Cante-Barrett K, Pieters R, Meijerink JP. Myocyte enhancer factor 2c in hematopoiesis and leukemia. *Oncogene* (2014) 33(4):403–10. doi: 10.1038/onc.2013.56

frontiers | Frontiers in Immunology

TYPE Original Research
PUBLISHED 29 August 2022
DOI 10.3389/fimmu.2022.908436

OPEN ACCESS

EDITED BY
Peter Brossart,
University of Bonn, Germany

REVIEWED BY
Rong Jin,
Peking University, China
Melina Elpi Marmarelis,
University of Pennsylvania,
United States
Roberto Ferrara,
National Cancer Institute Foundation
(IRCCS), Italy

*CORRESPONDENCE
Yan Wang
wangyanyifu@163.com
Hai-Yan Xu
xuhaiyan7609@sina.com

†These authors have contributed
equally to this work

SPECIALTY SECTION
This article was submitted to
Cancer Immunity
and Immunotherapy,
a section of the journal
Frontiers in Immunology

RECEIVED 30 March 2022
ACCEPTED 05 August 2022
PUBLISHED 29 August 2022

CITATION
Li H-S, Lei S-Y, Li J-L, Xing P-Y,
Hao X-Z, Xu F, Xu H-Y and Wang Y
(2022) Efficacy and safety of
concomitant immunotherapy and
denosumab in patients with advanced
non-small cell lung cancer carrying
bone metastases: A retrospective
chart review.
Front. Immunol. 13:908436.
doi: 10.3389/fimmu.2022.908436

Efficacy and safety of concomitant immunotherapy and denosumab in patients with advanced non-small cell lung cancer carrying bone metastases: A retrospective chart review

Hong-Shuai Li[1†], Si-Yu Lei[1†], Jun-Ling Li[1], Pu-Yuan Xing[1], Xue-Zhi Hao[1], Fei Xu[1], Hai-Yan Xu[2*] and Yan Wang[1*]

[1]Department of Medical Oncology, National Cancer Center/National Clinical Research Center for Cancer/Cancer Hospital, Chinese Academy of Medical Sciences and Peking Union Medical College, Beijing, China, [2]Department of Comprehensive Oncology, National Cancer Center/National Clinical Research Center for Cancer/Cancer Hospital, Chinese Academy of Medical Sciences and Peking Union Medical College, Beijing, China

Background: Synergistic anti-tumor effects were observed *in vivo* and *in vitro* when immune checkpoint inhibitors (ICIs) were combined with denosumab. However, the clinical benefit and safety of this synergy have not been adequately evaluated in non-small cell lung cancer (NSCLC).

Methods: Consecutive charts of NSCLC patients with bone metastases between December 2020 and December 2021 in the Chinese National Cancer Center were reviewed. The entire cohort was divided into one experimental group (denosumab + ICIs [DI]) and three control groups (denosumab + non-ICIs [DnI], phosphates + ICIs [PI], phosphates + non-ICIs [PnI]). Real-world objective response rates (ORRs), median progression-free survival (mPFS), skeletal-related events (SREs), and adverse events (AEs) were compared between groups.

Results: A total of 171/410 (41.7%) patients with advanced or recurrent NSCLC carrying bone metastases who received bone-targeted therapy were eligible for analysis. Although the DI group showed a better benefit trend, differences were not statistically significant concerning the therapeutic efficacy among the DI group (n = 40), PI group (n = 74), DnI group (n = 15), and PnI group (n = 42) (ORRs: 47.5%, 43.2%, 33.3%, and 40.5%, respectively, $p = 0.799$; and mPFS: 378, 190, 170, and 172 days, respectively, $p = 0.115$; SREs: 5%, 10.8%, 13.3%, and 11.9%, respectively, $p = 0.733$). Nevertheless, further analysis in the NON-DRIVER cohort revealed a greater benefit for the DI group ($p = 0.045$). Additionally, the AEs of the DI group were not significantly different from those of the PI, DnI, and PnI groups (AEs: 27.5%, 39.2%, 26.7%, and 28.6%,

respectively, p = 0.742). Furthermore, the multivariate analysis revealed the independent prognostic role of DI treatment for PFS in the overall cohort. Within the DI group, we did not observe differences in benefit among different mutational subgroups (p = 0.814), but patients with single-site bone metastasis (p = 0.319) and high PD-L1 expression (p = 0.100) appeared to benefit more, though no significant differences were observed.

Conclusions: Denosumab exhibited synergistic antitumor efficacy without increasing toxicity when used concomitantly with ICIs in patients with advanced non-small cell lung cancer carrying bone metastases.

KEYWORDS

immunotherapy, non-small cell lung cancer, bone metastases, efficacy, safety, denosumab, synergistic efficacy

1. Introduction

In recent years, lung cancer incidence and mortality rates have remained high as the aging population has intensified, along with the effects of industrialization and air pollution (1). As the main body of lung cancer, the 5-year overall survival (OS) rate of metastatic non-small cell lung cancer (NSCLC) patients is only 5% (2). In the past 20 years, the treatment of lung cancer has undergone radical changes, especially with the in-depth development of the molecular pathology of lung cancer and the rise of immunotherapy, including monoclonal antibodies (mAbs) blocking programmed cell death 1 (PD-1)/PD1 ligand 1 (PD-L1) and the cytotoxic T-lymphocyte-associated antigen 4 (CTLA-4), known as immune checkpoint inhibitors (ICIs). In the renowned KEYNOTE-024 trial, pembrolizumab obtained a 5-year OS rate of 31.9%, which is granted as an effective first-line treatment option for NSCLC patients with PD-L1 TPS ≥50% by the FDA (3). However, ICI resistance is a challenge that we must embrace. To overcome the resistance and expand the population benefiting from ICIs, non-redundant mechanisms of tumor-induced immunosuppression need to be explored, and combinatory therapy is expected to be more effective (4).

Receptor activator of nuclear factorκB ligand (RANKL, also called TNFSF11) is a member of the tumor necrosis factor (TNF) superfamily and a ligand both for RANK (also called TNFRSF11A) and osteoprotegerin (OPG, also called TNFRSF11B) (5). The RANK–RANKL–OPG axis is essential for physiological bone resorption and destruction, and it also plays an important role in pathological states such as osteoporosis and bone destruction at the foci of bone metastases (2, 5–7). As the first fully human anti-RANKL mAb, denosumab was demonstrated to be non-inferior to zoledronic acid (ZA) in delaying time to the first on-study skeletal-related events (SREs) in a randomized, double-blind study enrolling multiple advanced cancer types (including lung cancer) (8) and has been approved by the FDA for preventing SREs in solid tumors. Unexpectedly, the exploratory analysis also revealed an OS benefit of denosumab over ZA in NSCLC patients with bone metastases (hazard ratio [HR] = 0.78, 9.5 vs. 8.0 months; p = 0.01) (9).

Increasing evidence indicates that the survival benefit may stem from the synergistic anti-tumor effects of the combination of ICIs and denosumab (10–14). Series studies conducted by Ahern et al. revealed *via* a mouse model, that the combination of RANKL inhibitor and ICIs significantly increased the number of infiltrating T cells and expression of anti-tumor cytokines (IFN-γ, etc.) in the tumor microenvironment (TME) compared to a single agent, and the combination therapy significantly reduced mouse tumor burden (11, 12).

Recently, several retrospective studies have suggested the feasibility of this combination regimen in advanced NSCLC patients with bone metastases (14–18). However, the findings of these studies need further confirmation due to the lack of suitable control groups and the presence of confounding factors. This study evaluated the efficacy and safety of the combination of ICIs and denosumab for advanced NSCLC patients with bone metastases in a real-world setting.

2. Methods

2.1. Study design and rationale

A retrospective, observational chart review was conducted on NSCLC patients with bone metastases who were enrolled in the Chinese National Cancer Center between December 2020

and December 2021. To fully assess the synergistic effects of denosumab and ICIs, based on the therapeutic pattern of systematic therapy and bone-targeted therapy (BTT), the entire cohort was divided into one experimental group (denosumab + ICIs [DI]) and three control groups (denosumab + non-ICIs [DnI], phosphates + ICIs [PI], phosphates + non-ICIs [PnI]). Real-world objective response rates (ORRs), median progression-free survival (mPFS), adverse events (AEs), and SREs were planned to be compared between groups. The DnI and PnI groups were set up to verify whether a difference in efficacy existed between denosumab and phosphates in the absence of ICIs (in the context of no synergistic condition existing), thus establishing a baseline for comparison between the DI and PI groups. On this basis, a synergistic effect of DI treatment would be confirmed if the efficacy of the DI group was better than that of the PI group (Figure 1).

2.2. Patient eligibility, grouping, and data collection

Patients diagnosed with NSCLC who have received chemotherapy either alone or along with ICI (pembrolizumab, nivolumab, atezolizumab, sintilimab, or camrelizumab) as well as concomitant BTT (phosphates [including zoledronic acid, pamidronate disodium, or ibandronate monosodium] or denosumab) were identified. Concomitant therapy was defined as receipt of BTT at any point before systematic therapy (chemotherapy combined with ICI or not) initiation, or no later than 30 days following systematic therapy initiated at least 4 months before the data cutoff (31 December 2021). Demographics, clinicopathological information, molecular features, and detailed treatment history data were extracted from electronic medical records. Patients with too much key clinical information missing were excluded.

Sub-cohorts were defined during the data analysis. The NON-DRIVER cohort included cases without *EGFR*, *HER-2*, *ALK*, *ROS1*, *MET*, *RET*, and *BRAF* mutations, except for *KRAS* mutations. The WILD-TYPE cohort included cases without *EGFR*, *HER-2*, *ALK*, *ROS1*, *MET*, *RET*, *BRAF*, or *KRAS* mutations.

All charts were reviewed by the primary author, the confidentiality of all patients was maintained by assigning each patient a study number, and all data were securely stored in the hospital. The study was conducted in accordance with the Declaration of Helsinki (as revised in 2013). Institutional Review Board approval of the study protocol was obtained (No.: NCC-008296) before study conduct and informed patient consent was waived as this was a retrospective study.

2.3. Treatment and efficacy/toxicity evaluation

In this real-world study, denosumab was administered subcutaneously at 120 mg approximately every 28 days, while phosphates were administered intravenously approximately every 21 days. The PD-1 or PD-L1 inhibitor was administered by intravenous injection approximately every 3 weeks, and the specific dosage was determined according to the specific drug instructions. Phosphates were generally administered within three days of the administration of ICIs. Patient compliance was confirmed from the electronic medical records.

Real-world tumor response was analyzed and produced by trained extractors following a pre-defined process, including an integrated assessment of radiologist reports and clinical

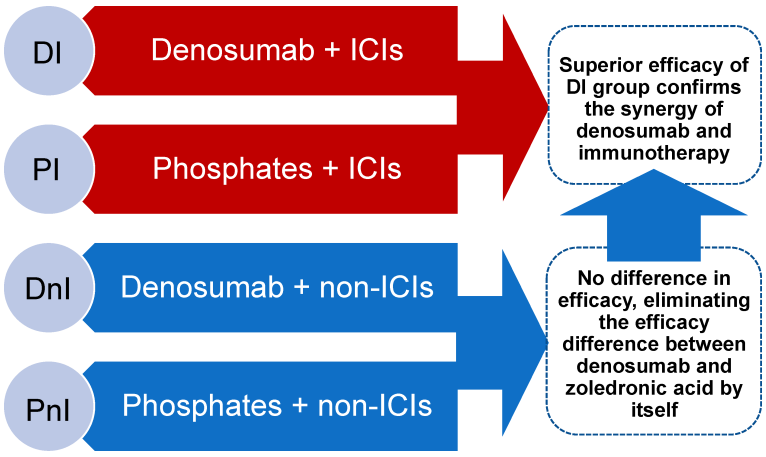

FIGURE 1
Study design and rationale.

documentation data. The frequency of imaging review to assess response was every 6–8 weeks in a real-world setting. The objective tumor response was determined according to the Response Evaluation Criteria in Solid Tumors (RECIST 1.1) guidelines (19). The objective response was divided into two categories: the objective response was divided into complete response (CR) and partial response (PR), while the disease control was divided into CR, PR, or stable disease (SD).

Toxicity was assessed according to the Common Terminology Criteria for Adverse Events (version 5.0). Acute phase AEs such as flu-like reactions, including fever, myalgia, and chills, were counted only as treatment-related if they occurred within 24 h of phosphate infusion; otherwise, they were not counted as AEs to BTT.

2.4. Statistical analysis

Categorical variables were reported as absolute numbers and percentages. The chi-square test was used for comparisons between different groups. The data cut-off date was 28 February 2022, when the disease status of the patients was confirmed. PFS was defined as the time from concomitant administration to disease progression or death from any cause. Patients who were lost to follow-up were judged to be censored and the last determinable time of survival was used as the time of termination of follow-up. The relationship between various variables and survival was evaluated using the Kaplan–Meier method. Differences between survival curves were tested for statistical significance using the Log-rank test. Significant prognostic predictors for patients identified by univariate analyses were further assessed by multivariate analyses using the Cox proportional hazards regression model. Statistical analyses were performed, and analytic graphs were created using GraphPad Prism 8 software (GraphPad Software, San Diego, CA, USA). An α value of 0.05 was used as the examination standard.

3. Results

3.1 Baseline characteristics

In total, 171/410 (41.7%) patients with NSCLC carrying bone metastases who were treated with BTT were enrolled at the Chinese National Cancer Center between December 2020 and December 2021 (Figure 2). Based on different treatment combinations of systematic therapy and BTT, the overall cohort was divided into 4 groups: DI (n = 40), PI (n = 74), DnI (n = 15), and PnI (n = 42). The baseline characteristics of the four groups are displayed in

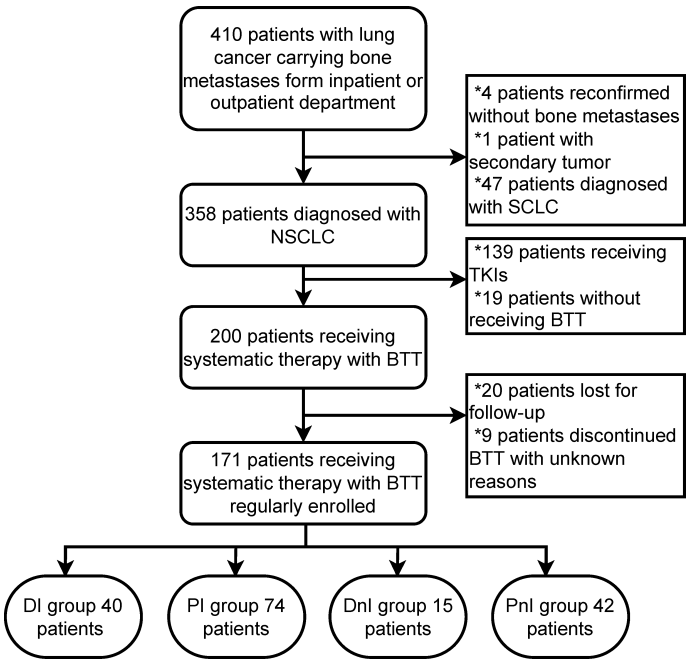

FIGURE 2
Flow chart of patient selection. NSCLC, non-small cell lung cancer; SCLC, small-cell lung cancer; BTT, bone-targeted therapy; TKIs, tyrosine-kinase inhibitors; DI, denosumab + ICIs; DnI, denosumab + non-ICIs; PI, phosphates + ICIs; PnI, phosphates + non-ICIs.

TABLE 1 Baseline characteristics between four treatment subgroups (n = 171).

Characteristics	Treatment modality/n (%)				p[&]
	DI group (n = 40)	PI group (n = 74)	DnI group (n = 15)	PnI group (n = 42)	
Age					0.444
<60	21 (52.5)	33 (44.6)	10 (66.7)	20 (47.6)	
≥60	19 (47.5)	41 (55.4)	5 (33.3)	22 (52.4)	
Gender					0.217
Female	5 (12.5)	15 (20.3)	5 (33.3)	12 (28.6)	
Male	35 (87.5)	59 (79.7)	10 (66.7)	30 (71.4)	
Smoking history[#]					0.614
Never smoker	10 (25)	18 (24.3)	7 (46.7)	14 (33.3)	
Ever smoker	5 (12.5)	9 (12.2)	1 (6.7)	3 (7.1)	
Current smoker	24 (60)	44 (59.5)	6 (40)	21 (50)	
Unknown	1 (2.5)	3 (4.1)	1 (6.7)	4 (9.5)	
DM/HT history					0.485
No	26 (65)	44 (59.5)	10 (66.7)	31 (73.8)	
Yes	14 (35)	30 (40.5)	5 (33.3)	11 (26.2)	
Histology					**0.038**
AC	31 (77.5)	51 (68.9)	14 (93.3)	37 (88.1)	
SCC	5 (12.5)	18 (24.3)	1 (6.7)	1 (2.4)	
Others*	4 (10)	5 (6.8)	0	4 (9.5)	
Grade					0.211
Well differentiated	2 (5)	0	0	0	
Moderately differentiated	2 (5)	11 (14.9)	1 (6.7)	3 (7.1)	
Poorly differentiated	15 (37.5)	34 (45.9)	4 (26.7)	19 (45.2)	
Undifferentiated	2 (5)	1 (1.4)	0	1 (2.4)	
Unknown	19 (47.5)	28 (37.8)	10 (66.7)	19 (45.2)	
Mutation status					0.145
ALK	0	0	0	1 (2.4)	
ROS1	0	0	0	1 (2.4)	
MET	0	1 (1.4)	0	0	
RET	1 (2.5)	0	0	1 (2.4)	
BRAF	2 (5)	3 (4.1)	0	3 (7.1)	
HER2	2 (5)	2 (2.7)	2 (13.3)	3 (7.1)	
EGFR	7 (17.5)	8 (10.8)	5 (33.3)	10 (23.8)	
KRAS	16 (40)	21 (28.4)	4 (26.7)	11 (26.2)	
Wild-type	12 (30)	39 (52.7)	4 (26.7)	12 (28.6)	
***TP53* co-mutation**					0.200
No	24 (60)	57 (77)	12 (80)	32 (76.2)	
Yes	16 (40)	17 (23)	3 (20)	10 (23.8)	
PD-L1 level					**0.010**
<1%	6 (15)	20 (27)	9 (70)	12 (28.6)	
1%-49%	10 (25)	10 (13.5)	1 (6.7)	10 (23.8)	
≥50%	12 (30)	16 (21.6)	0	3 (7.1)	
Unknown	12 (30)	28 (37.8)	5 (33.3)	17 (40.5)	
Brain metastases					0.338
No	30 (75)	64 (86.5)	12 (80)	37 (88.1)	
Yes	10 (25)	10 (13.5)	3 (20)	5 (11.9)	
Bone metastases					0.457
Single	6 (15)	19 (25.7)	4 (26.7)	7 (16.7)	

(Continued)

TABLE 1 Continued

Characteristics	Treatment modality/n (%)				p[&]
	DI group (n = 40)	PI group (n = 74)	DnI group (n = 15)	PnI group (n = 42)	
Multiple	34 (85)	55 (74.3)	11 (73.3)	35 (83.3)	
Visceral metastases					0.543
No	27 (67.5)	49 (66.2)	10 (66.7)	33 (78.6)	
Yes	13 (32.5)	25 (33.8)	5 (33.3)	9 (21.4)	
Application line					0.255
1	27 (67.5)	57 (77)	11 (73.3)	36 (85.7)	
2	8 (20)	14 (18.9)	3 (20)	4 (9.5)	
3	4 (10)	3 (4.1)	0	2 (4.8)	
4	1 (2.5)	0	1 (6.7)	0	
ECOG PS					0.294
0	11 (27.5)	10 (13.5)	4 (26.7)	9 (21.4)	
1	27 (67.5)	55 (74.3)	10 (66.7)	32 (76.2)	
2	2 (5)	9 (12.2)	1 (6.7)	1 (2.4)	

DI, denosumab + ICIs; DnI, denosumab + non-ICIs; PI, phosphates + ICIs; PnI, phosphates + non-ICIs; DM, diabetes mellitus; HT, hypertension; AC, adenocarcinoma; SCC, squamous cell carcinoma; ALK, anaplastic lymphoma receptor tyrosine kinase; ROS1, ROS proto-oncogene 1, receptor tyrosine kinase; MET, MET proto-oncogene, receptor tyrosine kinase; RET, ret proto-oncogene; BRAF, B-Raf proto-oncogene, serine/threonine kinase; HER2, erb-b2 receptor tyrosine kinase 2; EGFR, epidermal growth factor receptor; KRAS, Kirsten Rat Sarcoma Viral Oncogene Homolog; PD-L1, programmed death-ligand 1; ECOG PS, Eastern Cooperative Oncology Group performance status. *Current smoker refers to someone who has smoked more than 100 cigarettes (including hand-rolled cigarettes, cigars, cigarillos, etc.) in their lifetime and has smoked in the last 28 days. Ever smoker refers to someone who has smoked more than 100 cigarettes in their lifetime but has not smoked in the last 28 days. Never smoker is someone who has not smoked more than 100 cigarettes in their lifetime and does not currently smoke. [&]The chi-square test was employed for the comparative analysis. [#]Including large cell neuroendocrine carcinoma, sarcomatoid carcinoma, and adenosquamous carcinoma.
Bold values indicate that the differences are statistically significant.

Table 1. **A** higher proportion of adenocarcinoma histology was observed in the DnI and PnI groups (p = 0.038), while a higher proportion of PD-L1 expression in the DI and PI groups (p = 0.010) was observed, and the highest proportion of *KRAS* mutation in the DI group (p = 0.145) was revealed, despite a significant difference being unreached. No statistically significant differences were observed for other baseline characteristics.

For the DI group, a predominant proportion of males (87.5%) was observed. More than half (60%) of patients were current smokers, and the majority of patients (77.5%) had adenocarcinoma histology. Non-driver patients (including *KRAS*-mutated and wild-type ones) account for most of the DI group. Nearly 70% of patients initiated BTT along with the first-line systematic therapy. Most patients had multiple bone metastases (85%) and a PS status of 1 (67.5%) (Table 1).

3.2 Efficacy evaluation

Among the 40 evaluable patients in the DI group, 19 (47.5%), 19 (47.5%), and two (5%) had PR, SD, and *de novo* resistance to DI treatment, respectively. The ORR was 47.5% and the disease control rate (DCR) was 95% (Figure 3). At the data cut-off date, the mPFS was 378 days (95% CI, 118.5–636.5 days), and the median follow-up duration was 198 days (95% CI, 181.6–214.4 days) in the DI group. The PFS was mature in 14 (35%) patients, and the tumors of 26 patients were still under control (Figure 4).

By contrast, the DI group showed a trend for better ORR (Figure 3) and mPFS (Figure 5A) than those of the PI, DnI, and PnI groups (ORRs: 47.5%, 43.2%, 33.3%, and 40.5%, respectively, p = 0.799; and mPFS: 378, 190, 170, and 172 days, respectively, p = 0.115), though the differences were not statistically significant. To exclude the confounding effect of driver genes on efficacy, we extracted the NON-DRIVER (including *KRAS*-mutated and wild-type cases) cohort, WILD-TYPE cohort, and *KRAS* cohort from the overall cohort. Kaplan–Meier analysis in the NON-DRIVER cohort confirmed a statistically significant benefit for the DI group over the control groups (mPFS: NR, 225, 170, and 133 days, respectively, p = 0.045) (Figure 5B). In the WILD-TYPE cohort, a more pronounced benefit for the DI group appeared to be observed, but due to the reduced cohort scale, there was insufficient statistical power to demonstrate a statistically significant difference (p = 0.125) (Figure 5C). In the *KRAS* cohort, the DI group also showed a trend for better therapeutic efficacy than that of the control groups (mPFS: 230, 148, 170, and 133 days, respectively). Nevertheless, the advantage of the mPFS of the DI group was less obvious (p = 0.452) (Figure 5D).

With regards to SRE prevention, the DI group demonstrated a trend for a lower SRE rate than that of the PI, DnI, and PnI

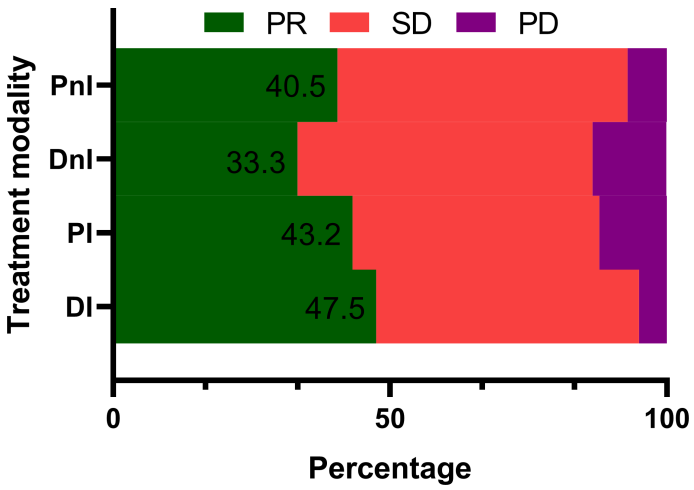

FIGURE 3
Treatment responses of different treatment modalities (n = 171). PR, partial response; SD, stable disease; PD, progressive disease; DI, denosumab + ICIs; DnI, denosumab + non-ICIs; PI, phosphates + ICIs; PnI, phosphates + non-ICIs.

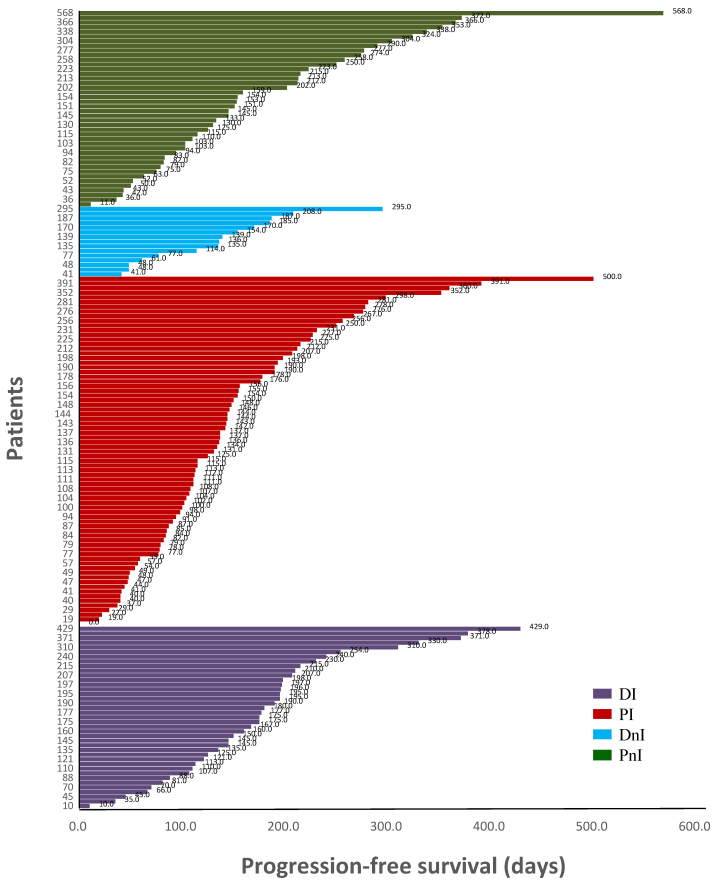

FIGURE 4
Swimming plot of different treatment modalities (n = 171). DI, denosumab + ICIs; DnI, denosumab + non-ICIs; PI, phosphates + ICIs; PnI, phosphates + non-ICIs.

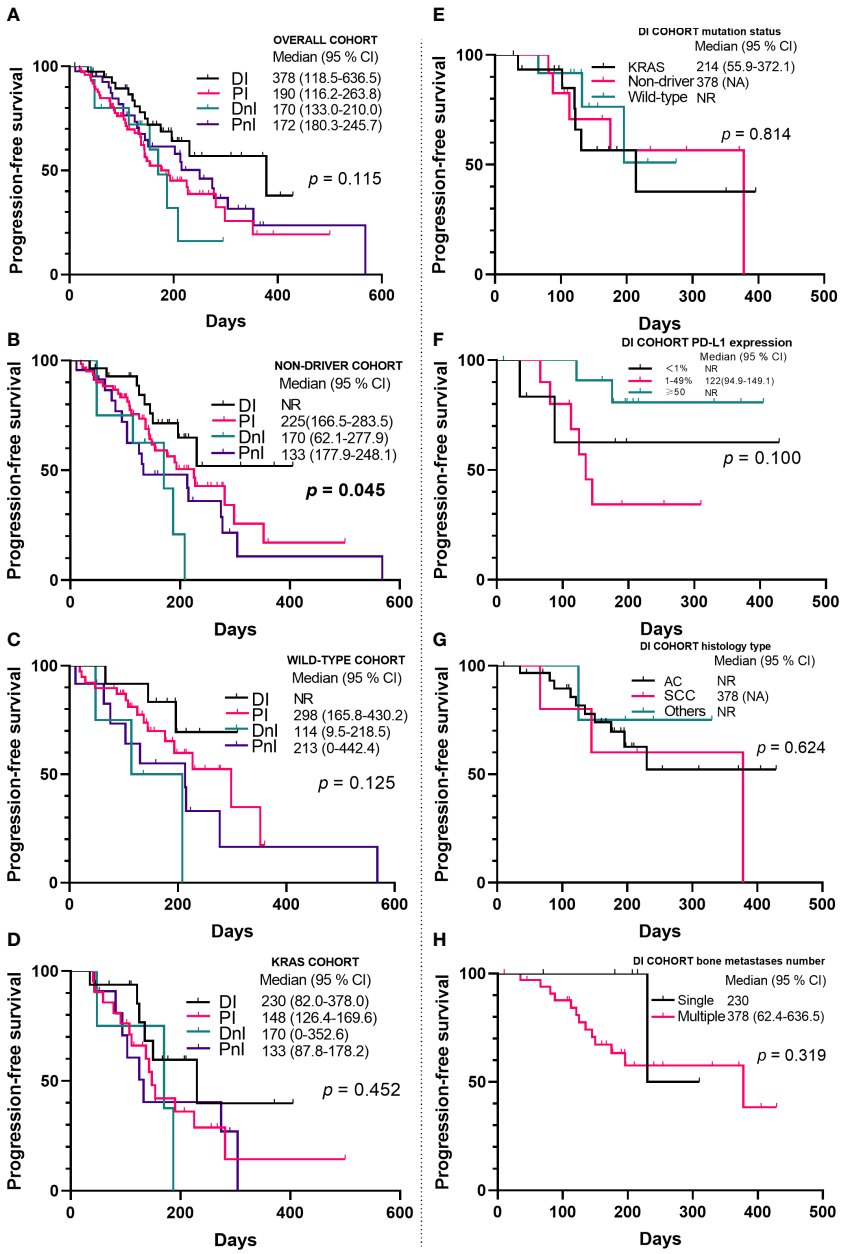

FIGURE 5
Kaplan–Meier analyses of progression-free survival in the overall cohort **(A–D)** (n = 171) and the DI cohort **(E–H)** (n = 40). NR, not reached; PD-L1, programmed death ligand-1; AC, adenocarcinoma; SCC, squamous cell carcinoma; DI, denosumab + ICIs; DnI, denosumab + non-ICIs; PI, phosphates + ICIs; PnI, phosphates + non-ICIs.

groups (5%, 10.8%, 13.3%, and 11.9%, respectively), though a significant difference was not reached ($p = 0.733$) (Table 2).

3.3 Survival analysis

To determine the influence of different variates on prognosis, we conducted univariate and multivariate analyses (Table 3) for the whole cohort. In the univariate analysis, visceral metastases ($p = 0.021$), application line ($p = 0.006$), and Eastern Cooperative Oncology Group performance status (ECOG PS) ($p = 0.001$) were all statistically significant prognostic factors for PFS. In the multivariate analysis, mutation status ($p = 0.043$), PD-L1 expression level ($p = 0.036$), application line ($p = 0.011$), ECOG PS ($p = 0.021$), and treatment modality ($p = 0.042$) were independent predictors of PFS (Table 3). Specifically, we also

TABLE 2 Skeletal-related events between four treatment subgroups (n = 171).

SREs	Treatment modality/n (%)				Total/n (%)*
	DI group (n = 40)	PI group (n = 74)	DnI group (n = 15)	PnI group (n = 42)	
Pathologic fractures	1 (2.5)	1 (1.4)	0	1 (2.4)	3 (1.8)
Bone surgery	0	1 (1.4)	0	0	1 (0.6)
Bone radiotherapy	1 (2.5)	5 (6.8)	2 (13.3)	4 (9.5)	12 (7.0)
Spinal cord compression	0	1 (1.4)	0	0	1 (0.6)
Malignant hypercalcemia	0	0	0	0	0
Total/n (%)	2 (5)	8 (10.8)	2 (13.3)	5 (11.9)	17 (9.9)

DI, denosumab + ICIs; DnI, denosumab + non-ICIs; PI, phosphates + ICIs; PnI, phosphates + non-ICIs; SREs, skeletal-related events. *Calculated as the percentage of the overall cohort.

examined the effect of different variables on the efficacy within the DI group (Figures 5E–H). We did not observe differences in benefit among different mutational subgroups (p = 0.814), but patients with single-site bone metastasis (p = 0.319) and high PD-L1 expression (p = 0.100) appeared to benefit more, though no significant differences were observed.

3.4 Toxicity evaluation

The most frequent AEs were pyrexia (12.3%) in the overall cohort, followed by fatigue (4.1%), arthralgia (3.5%), myalgia (3.5%), and renal failure (3.5%) (Table 4). The PI group showed a trend for higher overall AEs than those of the DI, DnI, and PnI groups (39.2%, 27.5%, 26.7%, and 28.6%, respectively), though a significant difference was not reached (p = 0.742). The DI group demonstrated relatively comparable levels of AEs to the PnI group but fewer AEs than the PI group regarding pyrexia, arthralgia, myalgia, and renal failure.

4. Discussion

Based on previous studies, we further explored and confirmed the synergistic effects and safety of ICIs and denosumab. Through setting three parallel comparative subgroups, we found that concomitant therapy in the DI group was associated with better PFS and with a good safety profile.

The RANK–RANKL pathway is best known for its essential role in the biological and pathological processes of bone. RANKL produced by osteoblasts and bone marrow mesenchymal cells can attract aggregation of RANK-expressing cancer cells and induce migration of cancer cells through specific signaling cascade activation (especially the MAPK pathway), thus leading to bone metastasis formation and bone destruction (2). In addition to its bone-derived role, evidence has shown that it plays an important role in promoting tumor growth in a variety of malignancies and is confirmed as a worse prognostic factor (2, 4–7). In a *KRAS*^{G12D}-driven lung cancer model, Rao et al. (20) found that RANK expression appeared in the early stages of highly plastic tumor development, suggesting that RANK was a driver of early tumor progression. Further studies revealed that the complex interaction of the RANK/RANKL pathway and mitochondrial respiratory metabolism ultimately directly stimulated the proliferation of *KRAS*^{G12D} mutant stem-like lung cancer cells through activation of the p38 and NF-κB pathways (20). Targeting RANKL seems to be a promising anti-tumor approach, but unfortunately, the randomized open-label phase III SPLENDOUR trial, which was designed to evaluate whether the addition of denosumab to standard first-line platinum-based doublet chemotherapy improved OS in advanced NSCLC, failed to demonstrate a clinical benefit (21).

However, besides cancer cells, RANK and RANKL are also expressed extensively in the TME, with RANK mainly on immature dendritic cells, immunosuppressive m2-type macrophages, and myeloid-derived suppressor cells, whereas RANKL mainly on CD8+ T cells (including regulatory T cells) (4). As a cytokine expressed on T cells, RANKL stimulates the survival of RANK-expressing dendritic cells (DCs) and enhances the ability of DCs to trigger the proliferation of naïve T cells (22). In the TME, RANKL interacts with RANK to coordinate various immunosuppressive processes through a variety of mechanisms (4). The 3LL lung adenocarcinoma mouse model constructed by Liede et al. showed that RANKL inhibitor combined with PD-1 mAb had a better therapeutic effect than RANKL inhibitor and PD-1 mAb alone (14). The study of Ahern et al. found that the combination of RANKL inhibitor and PD-1 mAb in a mouse model could further increase the number of infiltrating $CD4^+$ and $CD8^+$ T cells that can produce both IFN-γ and TNF in the TME, thus verifying the antitumor synergy effect of PD-1 mAb and RANKL inhibitor (12). However, in the early days, the immunomodulatory role of the RANK–RANKL pathway did not receive much attention or application until the development and application of denosumab.

Currently, as the first fully human anti-RANKL mAb, denosumab has been approved by the FDA for the prevention of SRE in solid tumors, including melanoma and lung cancer.

TABLE 3 Univariate and multivariate analyses of PFS in the whole cohort (n = 171).

Variables	n	Univariate analysis*		Multivariate analysis#		
		Median	*p*	HR	95% CI	*p*
Age			0.279			
<60/≥60	84/87	230/193				
Gender			0.457			
Female/Male	37/134	353/208				
Smoking history			0.200			
Never smoker	49	213				
Ever smoker	18	154				
Current smoker + Unknown	104	225				
DM/HT history			0.577			
No/Yes	111/60	225/213				
Histology			0.757			
AC	133	208				
SCC	25	227				
Others#	13	250				
Grade			0.914			
Well + Moderately differentiated	7	202				
Poor + Undifferentiated differentiated	37	187				
Unknown	39	227				
Mutation status						**0.043**
KRAS	52	250		–	–	–
Driver gene	52	154		0.518	0.282–0.951	0.034
Wild-type	67	227		0.543	0.316–0.931	0.026
***TP53* co-mutation**			0.489			
No/Yes	125/46	227/187				
PD-L1 expression level				0.814	0.671–0.986	**0.036**
<1%	47	154				
1%-49%	31	215				
≥50%	31	NR				
Unknown	62	225				
Brain metastases			0.981			
No/Yes	143/28	215/176				
Bone metastases			0.866			
Single/Multiple	36/135	215/213				

(Continued)

10.3389/fimmu.2022.908436

TABLE 3 Continued

Variables	n	Univariate analysis*		Multivariate analysis#		
		Median	*p*	HR	95% CI	*p*
Visceral metastases			**0.021**			
No/Yes	119/52	230/154				
Treatment modality			0.115			**0.042**
DI group	40	378		-	-	-
PI group	74	190		2.223	1.173–4.215	0.014
DnI group	15	170		2.785	1.113–6.971	0.029
PnI group	42	250		1.989	0.984–4.021	0.056
Application line			**0.006**	1.621	1.118–2.351	**0.011**
1	131	227				
2	29	125				
≥3	11	133				
ECOG PS			**0.001**	1.814	1.095–3.008	**0.021**
0	34	298				
1	124	225				
2	13	77				

DI, denosumab + ICIs; DnI, denosumab + non-ICIs; PI, phosphates + ICIs; PnI, phosphates + non-ICIs; DM, diabetes mellitus; HT, hypertension; AC, adenocarcinoma; SCC, squamous cell carcinoma; KRAS, Kirsten Rat Sarcoma Viral Oncogene Homolog; PD-L1, programmed death-ligand 1; ECOG PS, Eastern Cooperative Oncology Group performance status. *Current smoker refers to someone who has smoked more than 100 cigarettes (including hand-rolled cigarettes, cigars, cigarillos, etc.) in their lifetime and has smoked in the last 28 days. Ever smoker refers to someone who has smoked more than 100 cigarettes in their lifetime but has not smoked in the last 28 days. Never smoker is someone who has not smoked more than 100 cigarettes in their lifetime and does not currently smoke. *The log-rank test was employed for the comparative analysis. #The Cox's proportional hazards regression model was used to analyze the influencing factors of PFS. Set the first subgroup for each variable as reference. [#]Including large cell neuroendocrine carcinoma, sarcomatoid carcinoma, and adenosquamous carcinoma.
Bold values indicate that the differences are statistically significant.

10.3389/fimmu.2022.908436

TABLE 4 Treatment-emergent AEs between four treatment subgroups (n = 171).

AEs	Treatment modality/n (%)				Total/n (%)*
	DI group (n = 40)	PI group (n = 74)	DnI group (n = 15)	PnI group (n = 42)	
Pyrexia	4 (10)	11 (14.9)	1 (6.7)	5 (11.9)	21 (12.3)
Bone pain	1 (2.5)	0	0	1 (2.3)	2 (1.2)
Arthralgia	1 (2.5)	4 (5.4)	0	1 (2.3)	6 (3.5)
Chills	0	0	0	0	0
Myalgia	1 (2.5)	4 (5.4)	0	1 (2.3)	6 (3.5)
Renal failure	1 (2.5)	3 (4.1)	1 (6.7)	1 (2.3)	6 (3.5)
Hypocalcemia	1 (2.5)	1 (1.4)	1 (6.7)	0	3 (1.8)
Toothache	0	2 (2.7)	0	1 (2.3)	3 (1.8)
Fatigue	1 (2.5)	3 (4.1)	1 (6.7)	2 (9.5)	7 (4.1)
Osteonecrosis of jaw	0	1 (1.4)	0	0	1 (0.6)
Feet numbness	1 (2.5)	0	0	0	1 (0.6)
Total/n (%)	11 (27.5)	29 (39.2)	4 (26.7)	12 (28.6)	56 (32.7)

DI, denosumab + ICIs; DnI, denosumab + non-ICIs; PI, phosphates + ICIs; PnI, phosphates + non-ICIs; AEs, adverse events. There were no fatal AEs. *Calculated as the percentage of the overall cohort.

For melanoma, in a retrospective study, Afzal and Shirai evaluated the synergistic effect of immune checkpoint inhibitors combined with denosumab in patients with metastatic melanoma, and the results showed that the PFS and OS of the group receiving the combination therapy were 11.6 months and 57 months, respectively, compared with 4.15 months and 22.8 months in the ICIs monotherapy group (10). For NSCLC, a retrospective clinical study that included 166 patients with advanced NSCLC by Liede et al. showed that continuous use of denosumab with ICIs significantly increased ORR (p <0.0001) and prolonged OS (p <0.0001) (14). Although the study of Liede et al. is very enlightening, due to the lack of an external control group, only patients with longer and shorter combination therapy within the study cohort were compared. This may lead to a reversal in deriving causality and consequent unfirm conclusion, because patients who were able to receive a longer duration of combination therapy (with better ORR and longer OS) may themselves be sensitive to immunotherapy, rather than as a result of the combination of denosumab. The same concern is also present in the study by Cao et al. (16). Bongiovanni et al. circumvented this by setting both the control group (immunotherapy monotherapy) and the experimental group (denosumab/ZA + immunotherapy). However, treatment with ZA was confounded in the study arm, so the synergistic effect of denosumab and immunotherapy could not be accurately assessed. Furthermore, it is possible that the additional prolongation of survival in the experimental group shown by the study results was due to the survival benefit of BTT by reducing SREs rather than synergy with immunotherapy (15). A summary of published data on the combination of denosumab and ICIs is demonstrated in Table 5.

Therefore, to exclude the effect of confounding factors and to enhance the persuasiveness of the study, we set up one experimental group and three control groups. Besides, we also explored the effect of mutation status on the efficacy of combination therapy. The results of the study suggested an improved PFS for the DI group compared with the PI group in the overall cohort (p = 0.115), which was more pronounced in the WILD-TYPE cohort (p = 0.125) and the NON-DRIVER cohort (p = 0.045). Meanwhile, we did not observe significant differences in PFS between the DnI and PnI groups. Hence, it is feasible to assume that the improved efficacy of denosumab over ZA originated from a synergistic effect with ICIs rather than from a difference in the ability to reduce SREs between denosumab and ZA. Our study results were partly supported by previous data from Bongiovanni et al. (15), whose work indicated a better mPFS (15.9 months; 95%CI, 5.1–not estimable) of patients receiving denosumab (n = 6) than those treated with ICIs alone or with ZA (p = 0.068).

Two prospective studies concerning the DI treatment of lung cancer are currently underway. The DENIVOS (NCT03669523) study aims to evaluate the combination of denosumab and nivolumab in the second line of NSCLC with bone metastases. The POPCORN study (ACTRN12618001121257) is designed to provide information about the activity and safety of the combination of denosumab and nivolumab compared with nivolumab alone in the preoperative treatment of resectable NSCLC (23). Hopefully, these studies will shed light on the future exploration and application of the combination of denosumab and ICIs in NSCLC.

This study has some inherent limitations. First, as this study was a single-center study, and the included patients were mainly from urban areas, there was a selection bias. Second, the number of patients in individual groups in the study cohort was too small, which may affect the statistical test validity. Third, there were confounding factors in the study, such as different brands of PD-

TABLE 5 Previously published data on combination of denosumab and ICIs.

Author	Region	Year	Study Design	Comparison arms	Study Scale (n)	Histology (n/%)	First Line (n/%)	PD-1/PD-L1	BTT (n/%)	≥50% PD-L1 Expression (n/%)	ORR* (%)	PFS	OS
Bongiovanni (15)	Italy	2021	Retrospective	ICIs vs. ICIs + D/ZA	46	44 (95.7) AC	10 (21.7)	Nivolumab, Pembrolizumab, Atezolizumab	6 (20.0) with D; 24 (80.0) with ZA	NA	7.6 vs. 64.6#	4.0 vs. 7.1 months	15.8 vs. 21.8 months
Cao (16)	USA	2021	Retrospective	Duration of ICIs and D overlap (<3 vs. >3 months)	69	69 (100) AC	32 (46.4)	Pembrolizumab, Atezolizumab, Ipilimumab +Nivolumab	69 with D	16 (23.2)	3.88 vs. 14.92, overall 18.8	1.9 vs.6.0 months	3.6 vs. 11.5 months
Liede (14)	USA	2018	Retrospective	Duration of ICIs and D overlap (0–6 vs. 6–14 vs. >14 weeks)	166	105 (63.3) Non-squamous	37 (22.3)	Nivolumab Pembrolizumab Ipilimumab	166 with D	NA	No comparison data available, overall 33.1	NA	8.3 vs. 16.6 vs. 19.9 weeks
Ferrara (17)^	Italy	2021	Retrospective	ICIs vs. ICIs + D	49	NA	NA	NA	16 with D	NA	NA	1.8 vs. 2.6 months	3.5 vs. 15.1 months
				ICIs vs. ICIs + ZA	62	NA	NA	NA	29 with ZA	NA	NA	NA	3.8 vs. 3.5 months
Tsuchiya (18)	Japan	2022	Retrospective	ICIs vs. ICIs + D/ZA	29	22 (75.9) AC	8 (27.6)	Nivolumab, Pembrolizumab, Atezolizumab	20 (95.2) with D; 1 (3.4) with ZA	9 (36.0)	0 vs. 15; 0 vs. 35#	NA	2.5 vs. 16.0 months
Present study	China	2022	Retrospective	DI vs. PI vs. DnI vs. PnI	171	133 (77.8) AC	131 (76.6)	Pembrolizumab, Nivolumab, Atezolizumab, Sintilimab, Camrelizumab	55 (32.2) with D; 116 (67.8) with P	31 (18.1)	47.5 vs. 43.2 vs. 33.3 vs. 40.5	378 vs. 190 vs. 170 vs. 172 days	NA

ICIs, immune checkpoint inhibitors; AC, adenocarcinoma; BTT, bone targeted agents; PD-1, programmed death 1; PD-L1, programmed death ligand 1; D, denosumab; P, phosphates; ZA, zoledronic acid; DI, denosumab + ICIs; DnI, denosumab + non-ICIs; PI, phosphates + ICIs; PnI, phosphates + non-ICIs; ORR, objective response rate; PFS, progression-free survival; OS, overall survival; NA, not available. * Per RECIST 1.1. # Per MDA criteria. ^ Analyses were performed on patients with high bone tumor burden ≥3 bone metastases at ICIs baseline.
N/A, Not available.

10.3389/fimmu.2022.908436

1/PD-L1 inhibitors and phosphates. In addition, patients receiving denosumab may not have been randomly selected because some physicians may prefer denosumab to phosphates, and the relatively higher cost of denosumab may also be an important factor in deciding whether a patient will receive denosumab or not. Although these influencing factors were not assessed in this study, they may still have influenced the outcomes. Finally, potential efficacy biomarkers, including RANKL and RANK, were not investigated. All of these have the potential to affect the reliability of the study results. Therefore, the results of the study should be interpreted with caution.

In conclusion, our findings suggest a synergistic effect of denosumab in combination with ICIs in the treatment of NSCLC patients carrying bone metastases, and this combination has a good safety profile.

Data availability statement

The original data presented in the study are included in the article/supplementary material. Further inquiries can be directed to the corresponding authors.

Ethics statement

The studies involving human participants were reviewed and approved by the Ethics Committee of National Cancer Center/ Cancer Hospital, Chinese Academy of Medical Sciences and Peking Union Medical College. The patients/participants provided their written informed consent to participate in this study.

Author contributions

Conception and design: H-SL, S-YL, H-YX, and YW. Administrative support: H-SL, JLL, PYX, XZH, HYX, and YW Provision of study materials or patients: J-LL, P-YX, X-ZH, HYX, and YW. Collection and assembly of data: H-SL and S-YL. Data analysis and interpretation: H-SL, S-YL, JLL, PYX, XZH, FX, and HYX Manuscript writing: All authors. Final approval of manuscript: All authors. All authors contributed to the article and approved the submitted version.

Funding

This work was supported by the National Natural Science Foundation of China (Grant No. 82072590) and the Beijing Health Promotion Association (Grant No. 2021-053-ZZ).

Acknowledgments

We would like to thank the support of all enrolled patients and their relatives, and we would also like to thank Editage (www.editage.cn) for English language editing.

Conflict of interest

The authors declare that the research was conducted in the absence of any commercial or financial relationships that could be construed as a potential conflict of interest.

Publisher's note

All claims expressed in this article are solely those of the authors and do not necessarily represent those of their affiliated organizations, or those of the publisher, the editors and the reviewers. Any product that may be evaluated in this article, or claim that may be made by its manufacturer, is not guaranteed or endorsed by the publisher.

References

1. Barta JA, Powell CA, Wisnivesky JP. Global epidemiology of lung cancer. *Ann Glob Health* (2019) 85:1–16. doi: 10.5334/aogh.2419

2. Deligiorgi MV, Trafalis DT. Repurposing denosumab in lung cancer beyond counteracting the skeletal related events: an intriguing perspective. *Expert Opin Biol Ther* (2020) 20:1331–46. doi: 10.1080/14712598.2020.1790522

3. Reck M, Rodríguez-Abreu D, Robinson AG, Hui R, Csőszi T, Fülöp A, et al. Pembrolizumab versus chemotherapy for PD-L1-Positive non-Small-Cell lung cancer. *N Engl J Med* (2016) 375:1823–33. doi: 10.1056/NEJMoa1606774

4. Ahern E, Smyth MJ, Dougall WC, Teng MWL. Roles of the RANKL-RANK axis in antitumour immunity - implications for therapy. *Nat Rev Clin Oncol* (2018) 15:676–93. doi: 10.1038/s41571-018-0095-y

5. Peters S, Clézardin P, Márquez-Rodas I, Niepel D, Gedye C. The RANK-RANKL axis: an opportunity for drug repurposing in cancer? *Clin Transl Oncol* (2019) 21:977–91. doi: 10.1007/s12094-018-02023-5

6. Ming J, Cronin SJF, Penninger JM. Targeting the RANKL/RANK/OPG axis for cancer therapy. *Front Oncol* (2020) 10:1283. doi: 10.3389/fonc.2020.01283

7. Casimiro S, Vilhais G, Gomes I, Costa L. The roadmap of RANKL/RANK pathway in cancer. *Cells* (2021) 10(8):1978. doi: 10.3390/cells10081978

8. Henry DH, Costa L, Goldwasser F, Hirsh V, Hungria V, Prausova J, et al. Randomized, double-blind study of denosumab versus zoledronic acid in the treatment of bone metastases in patients with advanced cancer (excluding breast and prostate cancer) or multiple myeloma. *J Clin Oncol Off J Am Soc Clin Oncol* (2011) 29:1125–32. doi: 10.1200/jco.2010.31.3304

9. Scagliotti GV, Hirsh V, Siena S, Henry DH, Woll PJ, Manegold C, et al. Overall survival improvement in patients with lung cancer and bone metastases treated with denosumab versus zoledronic acid: subgroup analysis from a randomized phase 3 study. *J Thorac Oncol* (2012) 7:1823–9. doi: 10.1097/JTO.0b013e31826aec2b

10. Afzal MZ, Shirai K. Immune checkpoint inhibitor (anti-CTLA-4, anti-PD-1) therapy alone versus immune checkpoint inhibitor (anti-CTLA-4, anti-PD-1) therapy in combination with anti-RANKL denosumuab in malignant melanoma: a retrospective analysis at a tertiary care center. *Melanoma Res* (2018) 28:341–7. doi: 10.1097/cmr.0000000000000459

11. Ahern E, Harjunpää H, Barkauskas D, Allen S, Takeda K, Yagita H, et al. Co-Administration of RANKL and CTLA4 antibodies enhances lymphocyte-mediated antitumor immunity in mice. *Clin Cancer Res Off J Am Assoc Cancer Res* (2017) 23:5789–801. doi: 10.1158/1078-0432.Ccr-17-0606

12. Ahern E, Harjunpää H, O'Donnell JS, Allen S, Dougall WC, Teng MWL, et al. RANKL blockade improves efficacy of PD1-PD-L1 blockade or dual PD1-PD-L1 and CTLA4 blockade in mouse models of cancer. *Oncoimmunology* (2018) 7: e1431088. doi: 10.1080/2162402x.2018.1431088

13. Faget J, Contat C, Zangger N, Peters S, Meylan E. RANKL signaling sustains primary tumor growth in genetically engineered mouse models of lung adenocarcinoma. *J Thorac Oncol* (2018) 13:387–98. doi: 10.1016/j.jtho.2017.11.121

14. Liede A, Hernandez RK, Wade SW, Bo R, Nussbaum NC, Ahern E, et al. An observational study of concomitant immunotherapies and denosumab in patients with advanced melanoma or lung cancer. *Oncoimmunology* (2018) 7:e1480301. doi: 10.1080/2162402x.2018.1480301

15. Bongiovanni A, Foca F, Menis J, Stucci SL, Artioli F, Guadalupi V, et al. Immune checkpoint inhibitors with or without bone-targeted therapy in NSCLC patients with bone metastases and prognostic significance of neutrophil-to-Lymphocyte ratio. *Front Immunol* (2021) 12:697298. doi: 10.3389/fimmu.2021.697298

16. Cao Y, Afzal MZ, Shirai K. Does denosumab offer survival benefits? -our experience with denosumab in metastatic non-small cell lung cancer patients treated with immune-checkpoint inhibitors. *J Thorac Dis* (2021) 13:4668–77. doi: 10.21037/jtd-21-150

17. Manglaviti S, Galli G, Bini M, Labianca A, Zecca E, Brambilla M, et al. 184P bone-targeted agents (BTA) improve survival in advanced non-small cell lung cancer (aNSCLC) patients (pts) with high bone tumor burden (HBTB) treated with PD-(L)-1 inhibitors (ICIs). *J Thorac Oncol* (2021) 16:S797. doi: 10.1016/S1556-0864(21)02026-8

18. Asano Y, Yamamoto N, Demura S, Hayashi K, Takeuchi A, Kato S, et al. The therapeutic effect and clinical outcome of immune checkpoint inhibitors on bone metastasis in advanced non-Small-Cell lung cancer. *Front Oncol* (2022) 12:871675. doi: 10.3389/fonc.2022.871675

19. Therasse P, Arbuck SG, Eisenhauer A. New guidelines to evaluate the response to treatment in solid tumors (RECIST guidelines). *J Natl Cancer Inst* (2000) 92:201–16. doi: 10.1093/jnci/92.3.205

20. Rao S, Sigl V, Wimmer RA, Novatchkova M, Jais A, Wagner G, et al. RANK rewires energy homeostasis in lung cancer cells and drives primary lung cancer. *Genes Dev* (2017) 31:2099–112. doi: 10.1101/gad.304162.117

21. Peters S, Danson S, Hasan B, Dafni U, Reinmuth N, Majem M, et al. A randomized open-label phase III trial evaluating the addition of denosumab to standard first-line treatment in advanced NSCLC: The European thoracic oncology platform (ETOP) and European organisation for research and treatment of cancer (EORTC) SPLENDOUR trial. *J Thorac Oncol* (2020) 15:1647–56. doi: 10.1016/j.jtho.2020.06.011

22. Anderson DM, Maraskovsky E, Billingsley WL, Dougall WC, Tometsko ME, Roux ER, et al. A homologue of the TNF receptor and its ligand enhance T-cell growth and dendritic-cell function. *Nature* (1997) 390:175–9. doi: 10.1038/36593

23. Ahern E, Cubitt A, Ballard E, Teng MWL, Dougall WC, Smyth MJ, et al. Pharmacodynamics of pre-operative PD1 checkpoint blockade and receptor activator of NFkB ligand (RANKL) inhibition in non-small cell lung cancer (NSCLC): study protocol for a multicentre, open-label, phase 1B/2, translational trial (POPCORN). *Trials* (2019) 20:753. doi: 10.1186/s13063-019-3951-x

frontiers | Frontiers in Oncology

TYPE Review
PUBLISHED 27 September 2022
DOI 10.3389/fonc.2022.951167

OPEN ACCESS

EDITED BY
Jawed Akhtar Siddiqui,
University of Nebraska Medical Center,
United States

REVIEWED BY
Costantino Errani,
Rizzoli Orthopedic Institute
(IRCCS), Italy
Said Elshafae,
Benha University, Egypt

*CORRESPONDENCE
Min Mao
maomin0708@163.com

†These authors have contributed
equally to this work and share
first authorship

SPECIALTY SECTION
This article was submitted to
Cancer Immunity
and Immunotherapy,
a section of the journal
Frontiers in Oncology

RECEIVED 23 May 2022
ACCEPTED 12 September 2022
PUBLISHED 27 September 2022

CITATION
Tong Y, Cao Y, Jin T, Huang Z, He Q
and Mao M (2022) Role of Interleukin-
1 family in bone metastasis of
prostate cancer.
Front. Oncol. 12:951167.
doi: 10.3389/fonc.2022.951167

Role of Interleukin-1 family in bone metastasis of prostate cancer

Yuanhao Tong[1†], Yinghao Cao[2†], Tianzhe Jin[3†], Zhengwei Huang[1], Qinyuan He[4] and Min Mao[2*]

[1]School of Medicine, Zhejiang University, Hangzhou, China, [2]Department of Orthopedics, Shanghai General Hospital, Shanghai Jiao Tong University School of Medicine, Shanghai, China, [3]Department of Gynecologic Oncology, Women's Hospital, School of Medicine, Zhejiang University, Hangzhou, China, [4]Organization Department, Suzhou Traditional Chinese Medicine Hospital, Suzhou, China

Prostate cancer (PCa) is one of the most fatal diseases in male patients with high bone metastatic potential. Bone metastasis severely shortens overall survival and brings skeletal-related events (SREs) which reduces the life quality of patients, and this situation is currently regarded as irreversible and incurable. The progression and metastasis of PCa are found to be closely associated with inflammatory cytokines and chemokines. As pivotal members of inflammatory cytokines, Interleukin-1 (IL-1) family plays a crucial role in this process. Elevated expression of IL-1 family was detected in PCa patients with bone metastasis, and accumulating evidences proved that IL-1 family could exert vital effects on the progression and bone metastasis of many cancers, while some members have dual effects. In this review, we discuss the role of IL-1 family in the bone metastasis of PCa. Furthermore, we demonstrate that many members of IL-1 family could act as pivotal biomarkers to predict the clinical stage and prognosis of PCa patients. More importantly, we have elucidated the role of IL-1 family in the bone metastasis of PCa, which could provide potential targets for the treatment of PCa bone metastasis and probable directions for future research.

KEYWORDS

interleukin-1 family, inflammation, cancer immunity, prostate cancer, bone metastasis

Introduction

In 2020, PCa is the fifth leading cause of cancer death among men, with an estimated 1.4 million new cases and 375,000 deaths worldwide. The age-standardized incidence and mortality rate of PCa is 30.7% and 7.7% respectively (1). Generally, patients with early-stage and low-risk PCa can be treated with prostatectomy or radiation, while patients

with advanced stages of PCa could be treated with androgen deprivation therapy (ADT), as androgen and androgen receptor (AR) were found to play an important role in the progression of PCa (2). However, ADT is only effective in the early course of tumors. The majority of advanced cancer patients, which are called castration-resistant prostate cancer (CRPC) or neuroendocrine prostate cancer (NEPC), still have no response to currently available ADT (3) (4). As reported, the mean survival time of the patients with the metastasis of CRPC is approximately 14 months (range 9-30) (5).

As reported, 65-75% of advanced PCa patients have bone metastasis (6), furthermore, the rate of metastasis to bone even reaches 90% in CRPC patients (7). The 5-year survival rate of PCa without metastasis is nearly 100%, however, once metastasis, as reported, the 5-year survival rate is merely 28.2%, and the mean survival time of patients with bone metastasis is only 19 months in PCa (8). Bone metastasis often cause SREs, including debilitating bone pain, nerve root or spine cord compression, vertebral fractures, hypercalcemia, and bone marrow infiltration that leads to cytopenia (9), resulting in a severe decline of patients' life quality. PCa bone metastasis are predominantly present in the axial bones including the spine (90%), sacrum and pelvis (10). The spine is the major metastatic site of bone in PCa.

Currently, bone metastasis targeting agents include bisphosphonates and denosumab. They are usually applied to reduce SREs, such as pain and fracture, through modeling the bone microenvironment. However, the current palliative treatments could not be applied to prevent bone metastasis and improve the prognosis of metastasis PCa. Immune therapy, which is considered a potential treatment option for metastatic PCa, recently has received increasing attention. For example, Sipuleucel-T, a cellular immunotherapy which has already been approved by the US Food and Drug Administration (FDA), could improve the overall survival of PCa, while it has no effect to suppress the progression of PCa (11). In addition, as reported, immune checkpoint inhibitors, including anti-PD-1 and anti-CTLA4, also do not function well in metastatic PCa (12). Although single CTLA4 blockade and anti-PD-1 therapy are not effective, they show a curative effect when combined with radiotherapy or chemotherapy (13). This could be explained by the "Cancer Immunoediting" theory that tumor cells that can avoid immune recognition will survive and escape from immune therapy (14). Additionally, validated predictive biomarkers are urgently needed to assess patients' responses to treatment.

Considering the poor prognosis of bone metastatic PCa, further research should be performed to elucidate the potential mechanism of the immune environment in PCa to detect more curative and effective immunotherapy.

Mechanism of PCa metastasis

Inflammation and PCa bone metastasis

Several types of research have evidenced that inflammation is significantly correlated with cancer (15–17). It is widely acknowledged that inflammation exerts a vital role in maintaining homeostasis as a defense mechanism against infection and injury. However, when the homeostasis is broken, exaggerated inflammation can also promote tumorigenesis, and progression and metastasis (18). In most occasions, systemic inflammation characterizes the early stages of the metastatic cascade.

Accumulated evidence has proven that inflammation promotes bone metastasis through various mechanisms. Pro-inflammatory cytokines and other immune agents including chemokines and selectins, as the key components of tumor microenvironment, exert a vital role in the survival, proliferation and metastasis of tumor (19, 20). The microenvironment determines the metastatic place by supporting the formation of a pre-metastatic niche and bone colonization, metastatic dormancy and reactivation (21). The process of metastasis begins with cancer cells invading adjacent tissue and the formation of EMT. Previous research found that MMPS induced by Myeloid-derived suppressor cells (MDSCs) can remodel the extracellular matrix and promote tumor migration (22), and MDSCs can also mediate suppression of anti-tumor response (23). It was evidenced that cancer stem cells(CSCs) activated by inflammatory signaling can promote bone metastasis and induce resistance to treatment (24). Tumor-associated macrophages (TAM) are also reported to be closely involved in PCa bone metastasis by promoting angiogenesis and immune evasion (18). Furthermore, bone marrow adipocytes, which are closely associated with inflammation, are found to favor bone metastasis by attracting invading tumor cells and by activating the NF-κB pathway and producing inflammatory cytokines and chemokines (18, 25). Another significant component of the inflammatory environment, cancer-associated factors (CAFs), also exert a crucial role in bone metastasis directly or indirectly. For example, stromal-derived factor 1 (SDF-1/CXCL12) secreted by CAFs promotes bone metastasis by interacting with cancer cells through CXCR4, while CAFs-secreted epidermal growth factor receptor (EGFR) can promote bone metastasis by directly interacting with tumor cells (26).

Inflammatory mediators also play vital roles in the progression and metastasis of PCa, with some of them promoting tumor growth while others exerting antitumor function. For example, TNF-α, IL-6, IL-8, and IL-23 mediate inflammation resulting in tumor growth, and TGF-β and CXCL12/CXCR4 mainly promote metastasis. Inversely, IL-10 and IL-12 suppress tumor growth by inducing IFN-γ and activating T and NK cells (27).

IL-6, a significant proinflammatory cytokine, was proved by accumulating evidences that it exerts a crucial role in tumor cell proliferation, colonization, angiogenesis, and bone metastasis (Figure 1). The expression of IL-6 can be upregulated by inflammation in the bone, and two main pathways play vital roles in the process. Prostaglandin E2(PGE2) and TGF-β directly upregulate IL-6, while IL-1β and lipopolysaccharides stimulate IL-6 production *via* NF-κB activation (28). It was demonstrated that IL-6 has an important role on PCa cell growth, metastasis, and bone remodeling mainly through JAK-STAT3, MAPK and PI3K–AKT pathways (29). IL-6 can promote the progression and metastasis of PCa through stimulating STAT3 expression and upregulating the paracrine insulin-like growth factor(IGF) axis (30). It was also reported that IL-6 can induce the expression of RANKL after activating STAT3, causing a direct stimulation of osteoclast activity, and finally resulting in bone destruction (31). IL-6 and oncostatin-M (OSM) are found to promote PCa cell invasion through the PI3K/AKT pathway (32). In addition, a recent study demonstrated that IL-6 and IL-6R expression was positively correlated with the level of plasma PSA in PCa. Therefore, these studies collectively elucidated that IL-6 could act as a potential inflammatory biomarker in the progression and metastasis of PCa (33).

Increasing evidence demonstrated that TGF-β probably exerts a dual function, promoting or suppressing the progression and metastasis of PCa, depending on the tumor stage. TGF-β suppresses tumor growth in the early stage of PCa development by inhibiting cell proliferation and inducing apoptosis. TGF-β not only exerts its growth inhibitory effect on target cells but also functions on stromal fibroblasts and inflammatory cells. Meanwhile, TGF-β was regarded as the key suppressor of tumor infiltrating macrophages, NK cells, and effector T cells thus promoting immune tolerance (34). While it exerts an inverse effect in the later stages, including epithelial-to-mesenchymal transition (EMT), immunosuppression, extracellular matrix degradation and angiogenesis (35). Accumulating evidence proved that high expression of TGF-β is associated with tumor metastasis and worse prognosis in PCa patients (36). TGF-β was found to induce extracellular matrix proteins, cell adhesion proteins, and proteases in PCa mainly through Smad signaling (37). It was demonstrated that TGF-β exerts the function of bone modeling by regulating the differentiation, proliferation, and function of osteoblast and osteoclast (38). Research has also reported that TGF-β can regulate the expression of connective tissue growth factor (CTGF), IL-11, CXCR4, and MMP-1 to promote bone metastasis by inducing angiogenesis, invasion, and homing to bone (39, 40). Furthermore, TGF-β can promote bone metastasis by regulating the expression of genes involved in bone metastasis (41). Interestingly, prostate transmembrane protein androgen-induced 1 (PMEPA1), one of the genes induced by TGF-β, inhibits TGF-β signaling and bone metastasis in negative feedback (42).

Immune evasion in prostate cancer

Immune evasion plays a crucial role in PCa progression and metastasis, which involves many factors. For example, prostate cancer cells express few tumor antigens, which results in a low immune response. Absence of human leukocyte antigen (HLA) class I also leads to impaired cytotoxic T lymphocyte and tumor survival. Additionally, the expression of immune checkpoint

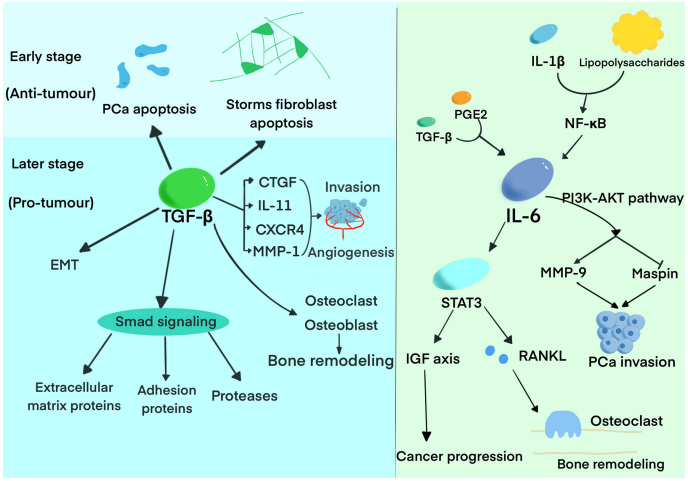

FIGURE 1
The roles of TGF-β and IL-6 in the progression and bone metastasis of PCa. The diagram summarized the pivotal functions of TGF-β and IL-6 has in the progression of bone metastasis.

ligands on cancer cells, such as PD-L1, which binds to PD-1, causes metastasis and a low response to immune checkpoint inhibitors (43).

Several factors function in the process of immune evasion. For example, EMT was found to be associated with upregulated indoleamine 2,3-dioxygenase-1(IDO1) and an increased number of regulatory T cells, which promotes immune evasion (44). IFN-γ can induce the expression of PD-L1 by activating NF-κB and RelB nuclear translocation. And PD-L1 can inhibit NK cells and cytotoxic T lymphocytes, suppressing the effect of immune therapy (45). Androgen receptor plays a vital role in immune evasion by regulating PVR, an immunological checkpoint gene (also named CD55), through its enhancer (46). Dickkop-1 (DKK1) plays a vital role in immune evasion in double-negative prostate cancer(DNPC), While ET1 induced by IL-1 can suppress DKK1 (47, 48).

MDSCs also play a crucial role in immune evasion. MDSC is mainly regulated by factors secreted by tumor cells, such as stem cell factor(SCF) and vascular endothelial growth factor(VEGF) which increase the number of MDSCs and inflammatory cytokines and chemokines such as IL-4, IL-6, IFN-γ, and IL-1β which suppress MDSC. IDO can mediate the recruitment of MDSCs relying on Treg (49). The mechanisms of MDSCs inducing immune evasion include decreased expression of l-selectin by T cells, upregulation of oxidative stress, induction of immunosuppressive cells such as regulatory T(Treg) and T helper(Th)17 cells which inhibit the normal tumor-suppressing function of T cells (50). MDSCs can also regulate tumor angiogenesis and remodel the microenvironment through VEGF, bFGF, Bv8, and MMP-9 to promote tumor progression (51). Research has shown that bisphosphonates can inhibit the mobilization of MDSCs (50).

Moreover, IL-33, a member of the IL-1 family, was reported to be involved in immune surveillance, and its absence can lead to immune evasion through “Cancer Immunoediting” (52).

As the IL-1 family are involved widely in inflammation and are associated with a large number of proinflammatory cytokines, they are found to be closely associated with PCa progression, and many further kinds of research on the role of IL-1 in PCa and bone metastasis have been carried out.

IL-1 family and PCa progression

The IL-1 family currently comprises of nine proinflammatory cytokines (IL-1α, IL-1β, IL-18, IL-33, IL-36α, IL-36β, IL-36γ) as well as two anti-inflammatory cytokines (IL-1RA, IL-36RA, IL-37, IL-38). Based on IL-1 consensus sequence and the signaling receptor chain, IL-1 family can be divided into 3 subgroups: secreted molecules with agonistic activity (IL-1α, IL-1β, IL-18, IL-33, IL-36Ra, IL-36α, IL-36β, IL-36γ), receptor antagonists (IL-1RA, IL-36Ra, IL-38), and an anti-inflammatory cytokine (IL-37). They can also be categorized into 3 subfamilies according to the length of the precursor and the length of the pro piece for this precursor: IL1 subfamily (IL-1α, IL-1β, IL-33), IL-18 subfamily (IL-18 and IL-37), and IL-36 subfamily (IL-36RA, IL-36α, IL-36β, IL-36γ, IL-38), while IL-1RA is not concluded in the subfamilies (53, 54). IL-1 family was found to promote cancer progression through interacting with inflammatory cytokines and downstream pathways, while some members of it exert anti-tumorigenic functions (55) (Figure 2).

There are two major agonistic IL-1 ligands, IL-1α and IL-1β, and one antagonistic ligand IL-1RA, and all of them can be activated by NF-κB. Both IL-1α and IL-1β were shown to exert a dual functions in promoting and suppressing tumor progression. It was noticed that overexpression of IL-1α may have anti-tumor effects (56). IL-1α could also suppress the progression of the tumor by inducing G0-G1 phase cell cycle arrest in PCa (56). IL-1β was reported to induce Th1 and Th17 to strengthen the anti-tumor effect. IL-1β also exerts anti-tumor effects, which can prevent metastatic cells from colonization in the metastatic place, thus inhibiting metastasis (55). Studies also found that IL-1α and IL-1β play a role in cancer eradication mediated by tumor-specific Th1 (57). As to the pro-tumor ability, both IL-1β and IL-1α are found to contribute to tumor angiogenesis and invasiveness in the process of PCa progression (58). Additionally, IL-1α and IL-1β are found to be able to reprogram AR+ PCa cells to AR- PCa cells, resulting in CRPC and treatment resistance (59). It was reported that IL-1α can interact with IL-6 to generate PSMA/PSA prostate clones (60). Two ETS family members associated with PCa malignancy and poor prognosis for patients, epithelium-specific ETS (E26 transformation-specific) and ESE1 (or E74-like factor (ELF3), can be activated by IL-1β through NF-κB pathway (61). IL-1β can also induce the expression of endothelin 1 (ET-1) and matrilysin 1, which are implicated in PCa progression (62, 63). IL-1β was also reported to induce IL-8 through the MAPK pathway to promote PCa proliferation (64). IL-1RA is a specific receptor antagonist, and its expression is negatively related to Gleason score. Studies demonstrated that IL-1RA can inhibit the activity of IL-1α and IL-1β (65). Many studies have reported that IL-1RA can reduce tumor-mediated inflammation and invasion (65, 66).

IL-18, which is a proinflammatory cytokine structurally similar to IL-1β, is significantly associated with poor prognosis in PCa (67). IL-18 also exerts a dual function of promoting or suppressing tumor progression. Similar to IL-1β, IL-18 could also promote tumor progression by regulating the myeloid differentiation factor 88 (MyD88)/NF-κB signaling pathway (68). Various evidence firstly demonstrated that IL-18 is closely associated with tumor growth. This conclusion came from that elevated expression of IL-18 by tumor cells were

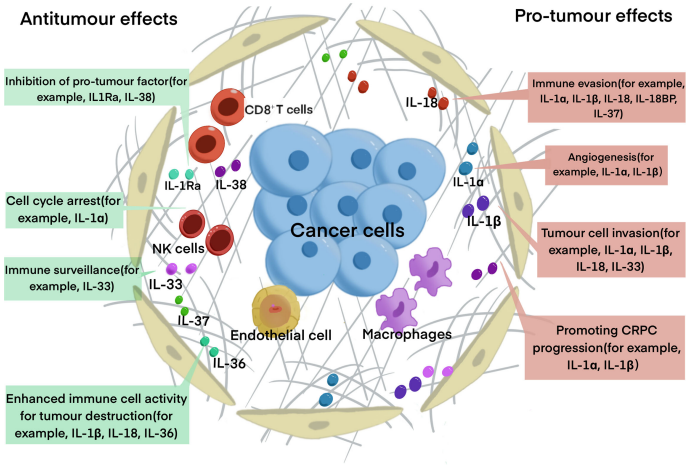

FIGURE 2
The roles of IL-1 family in PCa progression. The diagram summarized the major function of IL-1 family has in PCa progression. Some of the cytokines, for example, IL-1Ra, IL-33 and IL-37 have anti-tumor function, IL-1α and IL-1β have pro-tumor function, while IL-18 and IL-33 have dual functions.

observed in the serum of PCa patients (69). A high level of IL-18 was found to be associated with angiogenesis, tumor cell migration, and metastasis (67). It was reported that IL-18 can also mediate evasion of anti-tumor immune response (55). While IL-18 also has a tumor-suppressive effect that it was shown to activate CD4+T cells and NK cells and suppress the progression of tumor metastasis. Multiple shreds of evidence show that IL-18 can activate macrophages to release IFN-γ and neutrophils to produce TNF. However, elevated expression of IL-18 binding protein (IL-18BP), an inhibitory IL-18 receptor, was found to be associated with resistance to anti-tumor immune responses and correlates with poor prognosis in patients with PCa (70).

Previous studies widely acknowledged that IL-33 functions as immune surveillance in the immune system, which was found to regulate homeostasis, and works as an alarmin in response to infection or stress (71). And the loss of IL-33 expression was found to be associated with recurrence and metastatic immune evasion (52). Apart from its anti-tumor effect, accumulative studies have demonstrated its crucial role in malignancy (72). It is involved in many processes of tumor progression, such as oncogenesis, tumor growth, angiogenesis, metastasis and immune evasion (72). The IL-33/ST2 axis is emerging as a potent modulator of the TME. It was found to remodel the TME to promote malignancy or induce tumor regression by recruiting a cohort of immune cells (73).

Research on IL-36 mainly focuses on IL-36γ. IL-36γ was shown to strengthen the effector functions of CD8+T cells, NK cells, and γδ T cells, making the tumor microenvironment favor tumor destruction, and ultimately to have profound anti-tumor effects, suppressing both tumor growth and metastasis (74). It was also reported that IL-36γ has the potential to decrease MDSCs and increase IFN-positive CD4+ and CD8+ T cells (75).

IL-37 exerts a negative effect on cancer cell proliferation and invasion through STAT3 signaling (76, 77). IL-37 was reported to suppress the activation of NF-κB and MAPK, and negatively regulate proinflammatory cytokines and pro-tumor signaling pathways (78). However, high levels of IL-37 in the serum of patients with certain cancers such as ovarian cancer were found to be associated with poor prognosis, poor overall survival and progression-free survival (79), while the connection of IL-37 with PCa is unclear yet. IL-37 was also found to downregulate the expression of TIM3 on canonical NK cells, which plays a vital role in the anti-tumor immune response by inhibiting the immune suppression mediated by Treg. Blocking IL-37 was proved to eliminate Treg suppression of canonical NK cells (80). Similar to the molecular structures of IL-1RA and IL36Ra, IL-38 is considered as the antagonist of the IL-1 receptor. IL-38 mainly exerts its function by inhibiting Th17 (75).

IL-1 family and bone metastasis of PCa

Bone metastasis of PCa goes through a series of processes, including EMT, formation of a pre-metastatic niche, bone colonization, metastatic dormancy, reactivation, and reconstruction in the bone niche (21). Many pieces of research have demonstrated that IL-1 families are closely involved in this process (Figure 3).

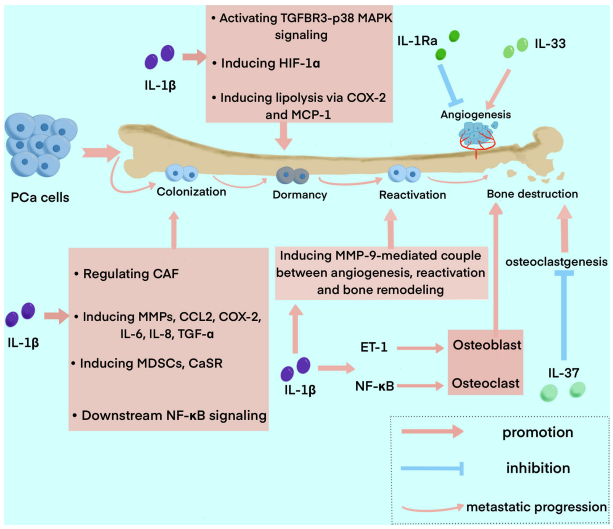

FIGURE 3
The roles of IL-1 family in the process of bone metastasis in PCa. The diagram summarized the major functions of IL-1 family exert in the process of bone metastasis, including colonization, dormancy, reactivation, and bone destruction. IL1β is widely involved in the whole process, while IL-1Ra, IL-33, and IL-37 mainly play a role in angiogenesis and bone destruction.

Recent research on the role IL-1 family plays in PCa bone metastasis mainly focus on IL-1β. IL-1β was found to be able to transform the bone stroma into a niche favorable for metastasis, and promote bone colonization of metastatic tumor cells (81). It was reported that IL-1β secreted by metastatic PCa cells promotes colonization and progression to the bone with neuroendocrine features (82). Previous studies elucidated that the formation of CAF and bone stromal alterations, as the key drivers of early colonization in IL-1β-mediated bone metastasis, can be regulated by many factors. For instance, COX-2, S100A4 and TNF13 expressed in human bone mesenchymal could be upregulated by IL-1β secreted by metastatic PCa cells (81). And the elevation of CAF can be blocked by anakinra, an IL-1R antagonist (83). IL-1β was also found to regulate the expression of tumor-related genes in the bone stroma (81). Studies also reported that IL-1β can induce the expression of many other factors related to bone metastasis and inflammation, such as matrix MMPs, CCL2, COX-2, IL-6, IL-8 and TGF-α (84, 85). MMPs induced by IL-1β can also promote the development of a metastasis niche to other factors such as integrin αvβ3, an adhesion molecule (86). IL-1β can also induce MDSCs, which is one of the major suppressors of antitumor immunity and a crucial element in cancer progression and metastasis (87). A study also showed that IL-1β stimulates CaSR expression, which may impact calcium homeostasis, thus influencing the progression and bone metastasis of PCa (88). It has been shown that a direct relationship between bone marrow-derived IL-1β and NF-κB, one of its main downstream transcription factors, favors PCa stem cell colonization and outgrowth within the bone (89, 90). Furthermore, the significant interaction of NF-κB/STAT3 with downstream inflammatory pathways assures a constant positive feedback, resulting in signal amplification of PCa cells (91).

After cancer cell colonization, TGF-β2 induced by IL-1β promotes PCa cell dormancy *via* activation of TGFBR3–p38 MAPK signaling (92). Additionally, IL-1β can upregulate hypoxia-inducible transcription factor-1α(HIF-1α), which transcripts VEGF and COX-2 and promotes angiogenic activity, thus providing a microenvironment favorable for tumor growth in bone metastatic sites (93, 94). Furthermore, it was demonstrated that metastatic PCa cells interact with bone marrow adipocytes to promote IL-1β expression, and in turn, IL-1β upregulates COX-2 and MCP-1 to induce lipolysis and an inflammatory phenotype. This could explain the mechanism of the insensitivity of PCa to Docetaxel (84). In addition, paracrine factors from bone marrow stromal cells (BMSC) can also cause apoptosis of metastatic PCa cells in the bone marrow, while IL-1β-induced p62/SQSTM1 is a fundamental factor for cell survival in this process as an apoptosis protector (95, 96).

Beyond the process of bone colonization and metastatic dormancy, metastatic tumor cells are reactivated and result in bone reconstruction. The role the IL-1 family plays in the reactivation of metastatic dormant cells in bone is unclear, yet, while the MMP-9-mediated couple between angiogenesis and bone resorption may have an implication for reactivation, and the process is closely associated with IL-1β (97). Furthermore, it was found that increased osteoclast activity is also related to the reactivation of dormant cells (97). Bone metastasis of PCa is usually osteoblastic. On the contrary, previous research have shown that IL-1, RANKL and TNF-α are implicated in the osteolytic phenotype of PCa reported in some cases (98, 99). ET-

1 induced by IL-1β is associated with the osteosclerotic lesion, which suppresses DKK-1, the inhibitor of Wnt (48, 100). And NF-κB activated by IL-1β promotes osteolytic lesions by inducing osteoclast cells through pathways such as GM-CSF and RANKL (101). In one study, IL-1β was reported to have the potential to inhibit metastasis by decreasing the chemotaxis of PCa bone metastasis and can inhibit PCa cell growth and bone metastasis with other cytokines such as TNF-α (102).

Microenvironmental IL-1β has also been shown in studies to enhance breast cancer metastatic colonization in the bone by activating Wnt signaling (103, 104). However, the role of IL-1 in the Wnt signaling pathway in PCa is unclear, yet, which could be a possible target to inhibit IL-1 signal transduction.

IL-1RA mainly exerts anti-tumor function, which was reported to inhibit bone metastasis by reducing tumor inflammation, angiogenesis, and immune suppression (65, 66). IL-1RA was found to be associated with a clinical pathological feature, so that IL-1RA is inversely correlated with Gleason score and pathological stage (105). The tumor burden was significantly reduced in animals treated with IL-1RA (81). A study demonstrated that inhibition of IL-6 expression by IL-1RA increases progression-free survival (75).

There is no concrete evidence of the role IL-18 plays in bone metastasis up to now, while considering its association with angiogenesis, tumor cell migration, and metastasis, the following studies should focus on the function this cytokine has in bone metastasis (55).

IL-33 was found to play a role in immune surveillance, and its absence can lead to immune evasion, which is a key process in bone metastasis (52). IL-33 was also reported as a key driver of treatment resistance in PCa, which could be a possible target for upregulating sensitivity to cancer treatment (106). Research reported that reduced IL-33 expression in PCa is connected with metastasis (52). As accumulative evidence proved that IL-33 plays a role in malignancy, such as angiogenesis, metastasis, and immune evasion, its dual role in bone metastasis is necessary to be discovered (72).

IL-37 shows a negative effect on cancer cell proliferation and invasion through the STAT3 signaling pathway (76). A study demonstrated that IL-37 inhibits osteoclastogenesis and bone resorption mediated by RANKL or LPS and relieves inflammatory bone destruction and bone resorption (107). In the study, IL-37 was reported to affect the activation of NF-κB and IκBα in response to RANKL, thus inhibiting osteoclast formation. Furthermore, IL-37 can also decrease the phosphorylation of inhibitors of IκBα and NF-κB(p65) and the expression of nuclear factor of activated T cells c1 (107).

Possible treatment therapies targeted at IL-1 family

The majority of patients with bone metastasis cannot be diagnosed until they suffer from SREs, which is usually the late stage of metastasis, thus missing the optimal time for treatment. Therefore, valid early biomarkers are urgently needed. IL-1α is reported to show a negative correlation with biochemical advancement, IL1β is linked to clinical T stage, and IL-1RA has an inverse correlation with Gleason score (83). IL-18 is also associated with poor prognosis and decreased survival (67). Furthermore, as the reduced expression of IL-33 in PCa is connected with metastasis, it could be a possible biomarker to detect the metastasis and prognosis of PCa patients. Thus, the IL-1 family can be possible biomarkers for early diagnosis to carry out the timely treatment.

Even though a number of current bone therapeutic agents can successfully prevent PCa from spreading to the bones, only a small percentage of PCa patients have long-lasting benefits from them. Consequently, there is an urgent need for the development of innovative therapeutic approaches to inhibit the bone metastasis of PCa. According to the findings that IL-1 plays a vital role in tumorigenesis, including proliferation, angiogenesis, and metastasis, it could be an effective target of chemotherapy. Table 1 summarized the major functions and the mechanism of the IL-1 family.

Anakinra, the approved IL-1RA medicine, was proved to reduce tumor growth and metastasis in preclinical PCa models. Treatment with anakinra creates an immunological-friendly milieu, making CRPC more susceptible to immune checkpoint blockade (108). At the same time, IL-1RA upregulation induced by a combination of immune checkpoint inhibition and MDSC-targeted treatment is essential for reducing MDSC infiltration, which is another key factor in metastasis. Additionally, the IL1β-neutralizing human antibody, Canakinumab, the human antibody targeting IL-1α, MABp1, and Rilonacept, a dimeric fusion protein made up of the ligand-binding domain of human IL-1R and IL-1RAcP are all under preclinical experiment and show effectiveness to different degrees (109). However, their effects on inhibiting bone metastasis are unclear now.

As IL-1β is widely involved in the process of bone metastasis, including the establishment of a pre-metastatic niche, bone colonization, metastatic dormancy, reactivation, and bone reconstruction, it could be an ideal target to prevent bone metastasis. Research reported that the knockdown of IL-1β significantly inhibited the bone progression of highly metastatic PCa cells (82). Inhibiting IL-1β was reported to promote cell apoptosis induced by BMSC paracrine factors (82). As Increased reactive oxygen species (ROS) along with inflammation are involved in PCa, the antioxidant arbutin was found to decrease the expression of IL-1β (110). Given that IL-1β mediates the insensitivity of PCa to docetaxel, inhibiting IL-1β could make PCa cells sensitive to chemotherapy again (84). However, IL-1α and IL1β show inverse effects in each stage of the malignant process, so which and when to target should be precisely answered (109). Similarly, IL-18 and IL-33 also exert dual functions in the process of bone metastasis in different stages, thus having a deep insight into the specific function these

TABLE 1 Role of IL-1 family in bone metastasis and possible therapy which is currently known.

Cytokines	Function	Mechanism	Treatment
IL-1α	Unknown		
IL-1β	Pro-tumour	Establishing a pre-metastatic niche (81) Dormancy (82) Reactivation (93) Angiogenesis (93) Bone remodeling (97)	Knockdown: Significantly inhibited bone metastasis (82) Make PCa cells sensitive to chemotherapy (84)
	Anti-tumour	Decrease the chemotaxis of PCa (102)	N/A
IL-1RA	Anti-tumour	Reduce tumour inflammation (65) Angiogenesis (65) Immune recruitment (66)	Anakinra (approved) (108) Rilonacept (under experiment) (109)
IL-18	Unknown		
IL-33	Pro-tumour	Treatment resistance (106) Angiogenesis (72) Metastasis (72) Immune evasion (72)	N/A
	Anti-tumour	Immune surveillance (52)	N/A
IL-36	Unknown		
IL-37	Anti-tumour	Inhibition of osteoclastogenesis and bone resorption (107)	N/A
IL-38	Unknown		

N/A - not applicable

cytokines play in different phases is fundamental to subsequent treatment. Given that IL-37 shows the feature of inhibiting osteoclastogenesis, activation of IL-37 could be another possible therapy. In addition, combining IL-1 blockade with immune checkpoint inhibitors, such as anti-PD-1 and anti-CTLA4, has shown effectiveness in breast cancer, and their combination in PCa is also worth researching as the IL-1 family exert a vital role in immune response and immune microenvironment (111).

Conclusions

As we reviewed above, PCa progression and metastasis have a close relationship with inflammatory cytokines. It is well known that the IL-1 family plays a crucial role in regulating the progression and bone metastasis of PCa. IL-1 family always exerts the unique functions in the bone metastasis of PCa. IL-1β could promote bone colonization of metastatic tumor cells through transforming the bone stroma into a niche. Furthermore, IL-1β could promote osteolytic activity and induce the dormancy, angiogenesis, and reactivation of tumor cells in PCa. IL-1RA could probably suppress bone metastasis through regulating inflammation, angiogenesis and immune response in PCa. To date, the role of IL-18 in bone metastasis of PCa is still debated. Recent studies have revealed that IL-33 could play a dual role in bone metastasis of PCa through regulating the immune surveillance and the progression of tumor. On the contrary, IL-37 could significantly inhibit the proliferation and invasion of tumor cells in PCa. Meanwhile, IL-37 could reduce bone resorption through inhibiting osteoclastogenesis. Considering the pivotal roles of IL-1 family in bone metastasis of PCa, the development of the novel reliable molecular targeted agents to provide individualized clinical treatments for PCa is urgently needed. For instance, Canakinumab, IL-1β-neutralizing human antibody, and MABp1, the IL-1α inhibitor, have demonstrated clinical benefits for PCa patients with bone metastasis. The inhibition of IL-1β has proven considerable efficacy in suppressing tumor progression through inhibiting angiogenesis and osteolytic activity of PCa cells. In addition, Anakinra, as the approved IL-1RA medicine, is widely applied to reduce tumor growth and bone metastasis in PCa.

In conclusion, despite prior research studies have validated the efficacy of IL-1 family-directed agents in bone metastasis of PCa, the exact mechanisms of IL-1 family, such as IL-1α, IL-18, IL-33, IL-38, are urgently needed to be fully elucidated. It is still unknown whether the combination of immune checkpoint inhibitor therapy and IL-1 family-directed agents would

probably demonstrates superiority over immune checkpoint inhibitors monotherapy in bone metastasis of PCa.

Author contributions

YT and MM contributed to the design and conception of the review, YC, TJ, ZH, and QH wrote sections of the manuscript. All authors contributed to manuscript revision, read, and approved the submitted version.

Funding

This study was supported by grants from the National Natural Science Foundation of China (NSFC) (82103532).

Conflict of interest

The authors declare that the research was conducted in the absence of any commercial or financial relationships that could be construed as a potential conflict of interest.

Publisher's note

References

1. Sung H, Ferlay J, Siegel RL, Laversanne M, Soerjomataram I, Jemal A, et al. Global cancer statistics 2020: Globocan estimates of incidence and mortality worldwide for 36 cancers in 185 countries. *Ca-a Cancer J Clin* (2021) 71(3):209–49. doi: 10.3322/caac.21660

2. Culig Z. Response to androgens and androgen receptor antagonists in the presence of cytokines in prostate cancer. *Cancers* (2021) 13(12):145–90. doi: 10.3390/cancers13122944

3. Ge R, Wang Z, Montironi R, Jiang Z, Cheng M, Santoni M, et al. Epigenetic modulations and lineage plasticity in advanced prostate cancer. *Ann OF Oncol* (2020) 31(4):470–9. doi: 10.1016/j.annonc.2020.02.002

4. Tsuzuki S, Park SH, Eber MR, Peters CM, Shiozawa Y. Skeletal complications in cancer patients with bone metastases. *Int J Urol* (2016) 23(10):825–32. doi: 10.1111/iju.13170

5. Kirby M, Hirst C, Crawford ED. Characterising the castration-resistant prostate cancer population: A systematic review. *Int J Clin Pract* (2011) 65 (11):1180–92. doi: 10.1111/j.1742-1241.2011.02799.x

6. Selvaggi G, Scagliotti GV. Management of bone metastases in cancer: A review. *Crit Rev Oncol Hematol* (2005) 56(3):365–78. doi: 10.1016/j.critrevonc.2005.03.011

7. Gartrell BA, Coleman R, Efstathiou E, Fizazi K, Logothetis CJ, Smith MR, et al. Metastatic prostate cancer and the bone: Significance and therapeutic options. *Eur Urol* (2015) 68(5):850–8. doi: 10.1016/j.eururo.2015.06.039

8. Pond GR, Sonpavde G, de Wit R, Eisenberger MA, Tannock IF, Armstrong AJ. The prognostic importance of metastatic site in men with metastatic castration-resistant prostate cancer. *Eur Urol* (2014) 65(1):3–6. doi: 10.1016/j.eururo.2013.09.024

9. Riquelme MA, Cardenas ER, Jiang JX. Osteocytes and bone metastasis. *Front IN Endocrinol* (2020) 11:13–58. doi: 10.3389/fendo.2020.567844

10. Gdowski AS, Ranjan A, Vishwanatha JK. Current concepts in bone metastasis, contemporary therapeutic strategies and ongoing clinical trials. *J OF Exp Clin Cancer Res* (2017) 36:178–92. doi: 10.1186/s13046-017-0578-1

11. Handy CE, Antonarakis ES. Sipuleucel-T for the treatment of prostate cancer: Novel insights and future directions. *Future Oncol* (2018) 14(10):907–17. doi: 10.2217/fon-2017-0531

12. Taneja SS. Re: Safety, activity, and immune correlates of anti-Pd-1 antibody in cancer. *J Urol* (2012) 188(6):2149–. doi: 10.1016/j.juro.2012.08.169

13. Sena LA, Denmeade SR, Antonarakis ES. Targeting the spectrum of immune checkpoints in prostate cancer. *Expert Rev Clin Pharmacol* (2021) 14(10):1253–66. doi: 10.1080/17512433.2021.1949287

14. Claps M, Mennitto A, Guadalupi V, Sepe P, Stellato M, Zattarin E, et al. Immune-checkpoint inhibitors and metastatic prostate cancer therapy: Learning by making mistakes. *Cancer Treat Rev* (2020) 88:258–72. doi: 10.1016/j.ctrv.2020.102057

15. de Bono JS, Guo C, Gurel B, De Marzo AM, Sfanos KS, Mani RS, et al. Prostate carcinogenesis: Inflammatory storms. *Nat Rev Cancer* (2020) 20(8):455–69. doi: 10.1038/s41568-020-0267-9

16. Taniguchi K, Karin M. Nf-kappa b, inflammation, immunity and cancer: Coming of age. *Nat Rev Immunol* (2018) 18(5):309–24. doi: 10.1038/nri.2017.142

17. Sfanos KS, De Marzo AM. Prostate cancer and inflammation: The evidence. *Histopathology* (2012) 60(1):199–215. doi: 10.1111/j.1365-2559.2011.04033.x

18. Goebel A, Dell'Endice S, Jaschke N, Paehlig S, Shahid A, Hofbauer LC, et al. The role of inflammation in breast and prostate cancer metastasis to bone. *Int J OF Mol Sci* (2021) 22(10):183–98. doi: 10.3390/ijms22105078

19. Sfanos KS, Yegnasubramanian S, Nelson WG, De Marzo AM. The inflammatory microenvironment and microbiome in prostate cancer development. *Nat Rev Urol* (2018) 15(1):11–24. doi: 10.1038/nrurol.2017.167

20. Platz EA, Kulac I, Barber JR, Drake CG, Joshu CE, Nelson WG, et al. A prospective study of chronic inflammation in benign prostate tissue and risk of prostate cancer: Linked pcpt and select cohorts. *Cancer Epidemiol Biomarkers Prev* (2017) 26(10):1549–57. doi: 10.1158/1055-9965.EPI-17-0503

21. Ban J, Fock V, Aryee DNT, Kovar H. Mechanisms, diagnosis and treatment of bone metastases. *Cells* (2021) 10(11):312–43. doi: 10.3390/cells10112944

22. Akkari L, Gocheva V, Kester JC, Hunter KE, Quick ML, Sevenich L, et al. Distinct functions of macrophage-derived and cancer cell-derived cathepsin z combine to promote tumor malignancy *Via* interactions with the extracellular matrix. *Genes Dev* (2014) 28(19):2134–50. doi: 10.1101/gad.249599.114

23. Veglia F, Perego M, Gabrilovich D. Myeloid-derived suppressor cells coming of age. *Nat Immunol* (2018) 19(2):108–19. doi: 10.1038/s41590-017-0022-x

24. Greten FR, Grivennikov SI. Inflammation and cancer: Triggers, mechanisms, and consequences. *Immunity* (2019) 51(1):27–41. doi: 10.1016/j.immuni.2019.06.025

25. Herroon MK, Rajagurubandara E, Hardaway AL, Powell K, Turchick A, Feldmann D, et al. Bone marrow adipocytes promote tumor growth in bone *Via* Fabp4-dependent mechanisms. *Oncotarget* (2013) 4(11):2108–23. doi: 10.18632/oncotarget.1482

26. Prajapati P, Lambert DW. Cancer-associated fibroblasts not-So-Innocent bystanders in metastasis to bone? *J Bone Oncol* (2016) 5(3):128–31. doi: 10.1016/j.jbo.2016.03.008

27. Suva LJ, Nicholas RW, Gaddy D. Inflammatory cytokines and their role in bone metastasis and osteolysis. *Bone And Cancer* (2009) 2009:141–55. doi: 10.1007/978-1-84882-019-7_9

28. Tawara K, Oxford JT, Jorcyk CL. Clinical significance of interleukin (Il)-6 in cancer metastasis to bone: Potential of anti-Il-6 therapies. *Cancer Manage Res* (2011) 3:177–89. doi: 10.2147/CMR.S18101

29. Ara T, DeClerck YA. Interleukin-6 in bone metastasis and cancer progression. *Eur J Cancer* (2010) 46(7):1223–31. doi: 10.1016/j.ejca.2010.02.026

30. Lou W, Ni ZY, Dyer K, Tweardy DJ, Gao AC. Interleukin-6 induces prostate cancer cell growth accompanied by activation of Stat3 signaling pathway. *Prostate* (2000) 42(3):239–42. doi: 10.1002/(SICI)1097-0045(20000215)42:3<239::AID-PROS10>3.0.CO;2-G

31. Hashizume M, Hayakawa N, Mihara M. Il-6 trans-signalling directly induces rankl on fibroblast-like synovial cells and is involved in rankl induction by tnf-alpha and il-17. *Rheumatology* (2008) 47(11):1635–40. doi: 10.1093/rheumatology/ken363

32. Smith DA, Kiba A, Zong Y, Witte ON. Interleukin-6 and oncostatin-m synergize with the Pi3k/Akt pathway to promote aggressive prostate malignancy in mouse and human tissues. *Mol Cancer Res* (2013) 11(10):1159–65. doi: 10.1158/1541-7786.MCR-13-0238

33. Katongole P, Sande OJ, Nabweyambo S, Joloba M, Kajumbula H, Kalungi S, et al. Il-6 and il-8 cytokines are associated with elevated prostate-specific antigen levels among patients with adenocarcinoma of the prostate at the Uganda cancer institute. *Future Oncol* (2022) 18(6):661–7. doi: 10.2217/fon-2021-0683

34. Massague J. Tgf beta in cancer. *Cell* (2008) 134(2):215–30. doi: 10.1016/j.cell.2008.07.001

35. Ahel J, Hudorovic N, Vicic-Hudorovic V, Nikles H. Tgf-beta in the natural history of prostate cancer. *Acta Clinica Croatica* (2019) 58(1):128–38. doi: 10.20471/acc.2019.58.01.17

36. Trivedi T, Pagnotti GM, Guise TA, Mohammad KS. The role of tgf-beta in bone metastases. *Biomolecules* (2021) 11(11):21. doi: 10.3390/biom11111643

37. Bello-DeOcampo D, Tindall DJ. Tgf-Beta/Smad signaling in prostate cancer. *Curr Drug Targets* (2003) 4(3):197–207. doi: 10.2174/1389450033491118

38. Bonewald LF, Mundy GR. Role of transforming growth factor-beta in bone remodeling. *Clin Orthopaedica and Related Res* (1990) 250):261–76. doi: 10.1097/00003086-199001000-00036

39. Juarez P, Guise TA. Tgf-beta in cancer and bone: Implications for treatment of bone metastases. *Bone* (2011) 48(1):23–9. doi: 10.1016/j.bone.2010.08.004

40. Cao Z, Kyprianou N. Mechanisms navigating the tgf-beta pathway in prostate cancer. *Asian J Urol* (2015) 2(1):11–8. doi: 10.1016/j.ajur.2015.04.011

41. Sterling JA, Edwards JR, Martin TJ, Mundy GR. Advances in the biology of bone metastasis: How the skeleton affects tumor behavior. *Bone* (2011) 48(1):6–15. doi: 10.1016/j.bone.2010.07.015

42. Fournier PGJ, Juarez P, Jiang G, Clines GA, Niewolna M, Kim HS, et al. The tgf-beta signaling regulator Pmepa1 suppresses prostate cancer metastases to bone. *Cancer Cell* (2015) 27(6):809–21. doi: 10.1016/j.ccell.2015.04.009

43. Ollivier L, Labbe M, Fradin D, Potiron V, Supiot S. Interaction between modern radiotherapy and immunotherapy for metastatic prostate cancer. *Front Oncol* (2021) 11:57–73. doi: 10.3389/fonc.2021.744679

44. Kolijn K, Verhoef EI, Smid M, Boettcher R, Jenster GW, Debets R, et al. Epithelial-mesenchymal transition in human prostate cancer demonstrates enhanced immune evasion marked by Ido1 expression. *Cancer Res* (2018) 78 (16):4671–9. doi: 10.1158/0008-5472.CAN-17-3752

45. Philippou Y, Sjoberg HT, Murphy E, Alyacoubi S, Jones KI, Gordon-Weeks AN, et al. Impacts of combining anti-Pd-L1 immunotherapy and radiotherapy on the tumour immune microenvironment in a murine prostate cancer model. *Br J Cancer* (2020) 123(7):1089–100. doi: 10.1038/s41416-020-0956-x

46. Wang Y, Li J, Li J, Li P, Wang L, Di L. An enhancer-based analysis revealed a new function of androgen receptor in tumor cell immune evasion. *Front IN Genet* (2020) 11:72–81. doi: 10.3389/fgene.2020.595550

47. Wise DR, Schneider JA, Armenia J, Febles VA, McLaughlin B, Brennan R, et al. Dickkopf-1 can lead to immune evasion in metastatic castration-resistant prostate cancer. *JCO Precis Oncol* (2020) 4:1167–79. doi: 10.1200/PO.20.00097

48. Clines GA, Mohammad KS, Bao Y, Stephens OW, Suva LJ, Shaughnessy JDJr., et al. Dickkopf homolog 1 mediates endothelin-1-Stimulated new bone formation. *Mol Endocrinol* (2007) 21(2):486–98. doi: 10.1210/me.2006-0346

49. Holmgaard RB, Zamarin D, Li Y, Gasmi B, Munn DH, Allison JP, et al. Tumor-expressed ido recruits and activates mdscs in a treg-dependent manner. *Cell Rep* (2015) 13(2):412–24. doi: 10.1016/j.celrep.2015.08.077

50. Groth C, Hu X, Weber R, Fleming V, Altevogt P, Utikal J, et al. Immunosuppression mediated by myeloid-derived suppressor cells (Mdscs) during tumour progression. *Br J OF Cancer* (2019) 120(1):16–25. doi: 10.1038/s41416-018-0333-1

51. De Cicco P, Ercolano G, Ianaro A. The new era of cancer immunotherapy: Targeting myeloid-derived suppressor cells to overcome immune evasion. *Front IN Immunol* (2020) 11:112–33. doi: 10.3389/fimmu.2020.01680

52. Saranchova I, Han J, Huang H, Fenninger F, Choi KB, Munro L, et al. Discovery of a metastatic immune escape mechanism initiated by the loss of expression of the tumour biomarker interleukin-33. *Sci Rep* (2016) 6:145–72. doi: 10.1038/srep30555

53. Mantovani A, Dinarello CA, Molgora M, Garlanda C. Interleukin-1 and related cytokines in the regulation of inflammation and immunity. *Immunity* (2019) 50(4):778–95. doi: 10.1016/j.immuni.2019.03.012

54. Zhang W, Borcherding N, Kolb R. Il-1 signaling in tumor microenvironment. In: Birbrair A, editor. *Tumor microenvironment: The role of interleukins, pt a*, Gewerbestrasse 11, CHAM CH-6330, Switzerland: Springer International Publishing AG (2020). 1240:1–23.

55. Baker KJ, Houston A, Brint E. Il-1 family members in cancer; two sides to every story. *Front Immunol* (2019) 10:34–51. doi: 10.3389/fimmu.2019.01197

56. Maund SL, Barclay WW, Hover LD, Axanova LS, Sui G, Hipp JD, et al. Interleukin-1 alpha mediates the antiproliferative effects of 1,25-dihydroxyvitamin d-3 in prostate Progenitor/Stem cells. *Cancer Res* (2011) 71(15):5276–86. doi: 10.1158/0008-5472.CAN-10-2160

57. Haabeth OAW, Lorvik KB, Yagita H, Bogen B, Corthay A. Interleukin-1 is required for cancer eradication mediated by tumor-specific Th1 cells. *Oncoimmunology* (2016) 5(1):23–54. doi: 10.1080/2162402X.2015.1039763

58. Ferrer FA, Miller LJ, Andrawis RI, Kurtzman SH, Albertsen PC, Laudone VP, et al. Vascular endothelial growth factor (Vegf) expression in human prostate cancer: *In situ* and *in vitro* expression of vegf by human prostate cancer cells. *J Urol* (1997) 157(6):2329–33. doi: 10.1016/S0022-5347(01)64775-X

59. Thomas-Jardin SE, Kanchwala MS, Jacob J, Merchant S, Meade RK, Gahnim NM, et al. Identification of an il-1-Induced gene expression pattern in ar(+) pca cells that mimics the molecular phenotype of ar(-) pca cells. *Prostate* (2018) 78 (8):595–606. doi: 10.1002/pros.23504

60. Ben Jemaa A, Bouraoui Y, Ben Rais N, Nouira Y, Oueslati R. Cytokine profiling identifies an interaction of il-6 and il-1 alpha to drive psma-psa prostate clones. *Immunobiology* (2016) 221(12):1424–31. doi: 10.1016/j.imbio.2016.07.002

61. Longoni N, Sarti M, Albino D, Civenni G, Malek A, Ortelli E, et al. Ets transcription factor Ese1/Elf3 orchestrates a positive feedback loop that constitutively activates nf-kappa b and drives prostate cancer progression. *Cancer Res* (2013) 73(14):4533–47. doi: 10.1158/0008-5472.CAN-12-4537

62. Le Brun G, Aubin P, Soliman H, Ropiquet F, Villette JM, Berthon P, et al. Upregulation of endothelin 1 and its precursor by il-1 beta, tnf-alpha, and tgf-beta in the Pc3 human prostate cancer cell line. *Cytokine* (1999) 11(2):157–62. doi: 10.1006/cyto.1998.0407

63. Klein RD, Borchers AH, Sundareshan P, Bougelet C, Berkman MR, Nagle RB, et al. Interleukin-1 beta secreted from monocytic cells induces the expression of matrilysin in the prostatic cell line lncap. *J Biol Chem* (1997) 272(22):14188–92. doi: 10.1074/jbc.272.22.14188

64. Tsai C-Y, Lee T-S, Kou YR, Wu Y-L. Glucosamine inhibits il-1 beta-mediated il-8 production in prostate cancer cells by mapk attenuation. *J Cell Biochem* (2009) 108(2):489–98. doi: 10.1002/jcb.22278

65. Ricote M, Garcia-Tunon I, Bethencourt FR, Fraile B, Paniagua R, Royuela M. Interleukin-1 (Il-1 alpha and il-1 beta) and its receptors (Il-1ri, il-1rii, and il-1ra) in prostate carcinoma. *Cancer* (2004) 100(7):1388–96. doi: 10.1002/cncr.20142

66. Apte RN, Voronov E. *The inflammatory milieu of tumors cytokines and chemokines that affect tumor growth and metastasis*. (2012) 2012: 57–80

67. Okamoto M, Azuma K, Hoshino T, Imaoka H, Ikeda J, Kinoshita T, et al. Correlation of decreased survival and il-18 in bone metastasis. *Internal Med* (2009) 48(10):763–73. doi: 10.2169/internalmedicine.48.1851

68. Hirooka Y, Nozaki Y. Interleukin-18 in inflammatory kidney disease. *Front Med* (2021) 8:111–32. doi: 10.3389/fmed.2021.639103

69. Dwivedi S, Goel A, Natu SM, Mandhani A, Khattri S, Pant KK. Diagnostic and prognostic significance of prostate specific antigen and serum interleukin 18 and 10 in patients with locally advanced prostate cancer: A prospective study. *Asian Pacific J Cancer Prev* (2011) 12(7):1843–8.

70. Wang X, Breeze A, Kulka M. N-3 polyunsaturated fatty acids inhibit ifn-Gamma-Induced il-18 binding protein production by prostate cancer cells. *Cancer Immunol Immunother* (2015) 64(2):249–58. doi: 10.1007/s00262-014-1630-z

71. Afferni C, Buccione C, Andreone S, Galdiero MR, Varricchi G, Marone G, et al. The pleiotropic immunomodulatory functions of il-33 and its implications in tumor immunity. *Front Immunol* (2018) 9:123–43. doi: 10.3389/fimmu.2018.02601

72. Shen J-X, Liu J, Zhang G-J. Interleukin-33 in malignancies: Friends or foes? *Front Immunol* (2018) 9:234–86. doi: 10.3389/fimmu.2018.03051

73. Larsen KM, Minaya MK, Vaish V, Pena MMO. The role of il-33/St2 pathway in tumorigenesis. *Int J Mol Sci* (2018) 19(9):249–98. doi: 10.3390/ijms19092676

74. Wang X, Zhao X, Feng C, Weinstein A, Xia R, Wen W, et al. Il-36 gamma transforms the tumor microenvironment and promotes type 1 lymphocyte-mediated antitumor immune responses. *Cancer Cell* (2015) 28(3):296–306. doi: 10.1016/j.ccell.2015.07.014

75. Boersma B, Jiskoot W, Lowe P, Bourquin C. The interleukin-1 cytokine family members: Role in cancer pathogenesis and potential therapeutic applications in cancer immunotherapy. *Cytokine Growth Factor Rev* (2021) 62:1–14. doi: 10.1016/j.cytogfr.2021.09.004

76. Luo C, Shu Y, Luo J, Liu D, Huang DS, Han Y, et al. Intracellular il-37b interacts with Smad3 to suppress multiple signaling pathways and the metastatic phenotype of tumor cells. *Oncogene* (2017) 36(20):2889–99. doi: 10.1038/onc.2016.444

77. Yuan ZL, Guan YJ, Wang LJ, Wei WY, Kane AB, Chin YE. Central role of the threonine residue within the P+1 loop of receptor tyrosine kinase in Stat3 constitutive phosphorylation in metastatic cancer cells. *Mol and Cell Biol* (2004) 24 (21):9390–400. doi: 10.1128/MCB.24.21.9390-9400.2004

78. Abulkhir A, Samarani S, Amre D, Duval M, Haddad E, Sinnett D, et al. A protective role of il-37 in cancer: A new hope for cancer patients. *J Leukocyte Biol* (2017) 101(2):395–406. doi: 10.1189/jlb.5RU0816-341R

79. Huo J, Hu J, Liu G, Cui Y, Ju Y. Elevated serum interleukin-37 level is a predictive biomarker of poor prognosis in epithelial ovarian cancer patients. *Arch Gynecol and Obstetri* (2017) 295(2):459–65. doi: 10.1007/s00404-016-4258-8

80. Sarhan D, Hippen KL, Lemire A, Hying S, Luo X, Lenvik T, et al. Adaptive nk cells resist regulatory T-cell suppression driven by Il37. *Cancer Immunol Res* (2018) 6(7):766–75. doi: 10.1158/2326-6066.CIR-17-0498

81. Shahriari K, Shen F, Worrede-Mahdi A, Liu Q, Gong Y, Garcia FU, et al. Cooperation among heterogeneous prostate cancer cells in the bone metastatic niche. *Oncogene* (2017) 36(20):2846–56. doi: 10.1038/onc.2016.436

82. Liu Q, Russell MR, Shahriari K, Jernigan DL, Lioni MI, Garcia FU, et al. Interleukin-1 beta promotes skeletal colonization and progression of metastatic prostate cancer cells with neuroendocrine features. *Cancer Res* (2013) 73(11):3297–305. doi: 10.1158/0008-5472.CAN-12-3970

83. D'Oronzo S, Brown J, Coleman R. The role of biomarkers in the management of bone-homing malignancies. *J Bone Oncol* (2017) 9:1–9. doi: 10.1016/j.jbo.2017.09.001

84. Herroon MK, Diedrich JD, Rajagurubandara E, Martin C, Maddipati KR, Kim S, et al. Prostate tumor cell-derived Il1 beta induces an inflammatory phenotype in bone marrow adipocytes and reduces sensitivity to docetaxel *Via* lipolysis-dependent mechanisms. *Mol Cancer Res* (2019) 17(12):2508–21. doi: 10.1158/1541-7786.MCR-19-0540

85. Qu X, Tang Y, Hua S. Immunological approaches towards cancer and inflammation: A cross talk. *Front Immunol* (2018) 9:73–89. doi: 10.3389/fimmu.2018.00563

86. McCabe NP, De S, Vasanji A, Brainard J, Byzova TV. Prostate cancer specific integrin alpha V beta 3 modulates bone metastatic growth and tissue remodeling. *Oncogene* (2007) 26(42):6238–43. doi: 10.1038/sj.onc.1210429

87. Bunt SK, Yang L, Sinha P, Clements VK, Leips J, Ostrand-Rosenberg S. Reduced inflammation in the tumor microenvironment delays the accumulation of myeloid-derived suppressor cells and limits tumor progression. *Cancer Res* (2007) 67(20):10019–26. doi: 10.1158/0008-5472.CAN-07-2354

88. Canaff L, Hendy GN. Calcium-sensing receptor gene transcription is up-regulated by the proinflammatory cytokine, interleukin-1 beta - role of the nf-kappa b pathway and kappa b elements. *J Biol Chem* (2005) 280(14):14177–88. doi: 10.1074/jbc.M408587200

89. Thomas-Jardin SE, Dahl H, Nawas AF, Bautista M, Delk NA. Nf-kappa b signaling promotes castration-resistant prostate cancer initiation and progression. *Pharmacol Ther* (2020) 211:93–112. doi: 10.1016/j.pharmthera.2020.107538

90. Wang X, Fang Y, Sun W, Xu Z, Zhang Y, Wei X, et al. Endocrinotherapy resistance of prostate and breast cancer: Importance of the nf-kappa b pathway (Review). *Int J Oncol* (2020) 56(5):1064–74. doi: 10.3892/ijo.2020.4990

91. Roca H, McCauley LK. Inflammation and skeletal metastasis. *BoneKEy Rep* (2015) 4:706–. doi: 10.1038/bonekey.2015.75

92. Yu-Lee L-Y, Yu G, Lee Y-C, Lin S-C, Pan J, Pan T, et al. Osteoblast-secreted factors mediate dormancy of metastatic prostate cancer in the bone *Via* activation of the tgf beta riii-P38mapk-Ps249/T252rb pathway. *Cancer Res* (2018) 78 (11):2911–24. doi: 10.1158/0008-5472.CAN-17-1051

93. Voronov E, Shouval DS, Krelin Y, Cagnano E, Benharroch D, Iwakura Y, et al. Il-1 is required for tumor invasiveness and angiogenesis. *Proc Natl Acad Sci of the U.S.A.* (2003) 100(5):2645–50. doi: 10.1073/pnas.0437939100

94. Kuwano T, Nakao S, Yamamoto H, Tsuneyoshi M, Yamamoto T, Kuwano M, et al. Cyclooxygenase 2 is a key enzyme for inflammatory cytokine-induced angiogenesis. *FASEB J* (2004) 18(2):300–10. doi: 10.1096/fj.03-0473com

95. Chang MA, Morgado M, Warren CR, Hinton CV, Farach-Carson MC, Delk NA. P62/Sqstm1 is required for cell survival of apoptosis-resistant bone metastatic prostate cancer cell lines. *Prostate* (2014) 74(2):149–63. doi: 10.1002/pros.22737

96. Chang MA, Patel V, Gwede M, Morgado M, Tomasevich K, Fong EL, et al. Il-1 beta induces P62/Sqstm1 and represses androgen receptor expression in prostate cancer cells. *J Cell Biochem* (2014) 115(12):2188–97. doi: 10.1002/jcb.24897

97. Byrne NM, Summers MA, McDonald MM. Tumor cell dormancy and reactivation in bone: Skeletal biology and therapeutic opportunities. *JBMR PLUS* (2019) 3(3):123–43. doi: 10.1002/jbm4.10125

98. Body J-J, Casimiro S, Costa L. Targeting bone metastases in prostate cancer: Improving clinical outcome. *Nat Rev Urol* (2015) 12(6):340–56. doi: 10.1038/nrurol.2015.90

99. Lee Y, Schwarz E, Davies M, Jo M, Gates J, Wu J, et al. Differences in the cytokine profiles associated with prostate cancer cell induced osteoblastic and osteolytic lesions in bone. *J Orthopeadic Res* (2003) 21(1):62–72. doi: 10.1016/S0736-0266(02)00095-5

100. Hall CL, Kang SN, MacDougald OA, Keller ET. Role of wnts in prostate cancer bone metastases. *J Cell Biochem* (2006) 97(4):661–72. doi: 10.1002/jcb.20735

101. Xu J, Wu HF, Ang ESM, Yip K, Woloszyn M, Zheng MH, et al. Nf-kappa b modulators in osteolytic bone diseases. *Cytokine Growth Factor Rev* (2009) 20 (1):7–17. doi: 10.1016/j.cytogfr.2008.11.007

102. Ritchie CK, Andrews LR, Thomas KG, Tindall DJ, Fitzpatrick LA. The effects of growth factors associated with osteoblasts on prostate carcinoma proliferation and chemotaxis: Implications for the development of metastatic disease. *Endocrinology* (1997) 138(3):1145–50. doi: 10.1210/en.138.3.1145

103. Eyre R, Alferez DG, Santiago-Gomez A, Spence K, McConnell JC, Hart C, et al. Microenvironmental Il1 beta promotes breast cancer metastatic colonisation in the bone *Via* activation of wnt signalling. *Nat Commun* (2019) 10:156–243. doi: 10.1038/s41467-019-12807-0

104. Eyre R, Spence K, Alferez D, Santiago-Gomez A, Hart C, Simoes B, et al. The bone metastatic niche promotes breast cancer stem cell activity *Via* il-1 beta-wnt signalling. *Eur J Cancer* (2016) 61:S65–S. doi: 10.1016/S0959-8049(16)61224-8

105. Torrealba N, Rodriguez-Berriguete G, Fraile B, Olmedilla G, Martinez-Onsurbe P, Guil-Cid M, et al. Expression of several cytokines in prostate cancer: Correlation with clinical variables of patients. *Relationship Biochem Progres Malignance Cytokine* (2017) 89:105–15. doi: 10.1016/j.cyto.2016.08.008

106. Kudo-Saito C, Miyamoto T, Imazeki H, Shoji H, Aoki K, Boku N. Il33 is a key driver of treatment resistance of cancer. *Cancer Res* (2020) 80(10):1981–90. doi: 10.1158/0008-5472.CAN-19-2235

107. Tang R, Yi J, Yang J, Chen Y, Luo W, Dong S, et al. Interleukin-37 inhibits osteoclastogenesis and alleviates inflammatory bone destruction. *J OF Cell Physiol* (2019) 234(5):7645–58. doi: 10.1002/jcp.27526

108. Lu X, Horner JW, Paul E, Shang X, Troncoso P, Deng P, et al. Effective combinatorial immunotherapy for castration-resistant prostate cancer. *Nature* (2017) 543(7647):728–+. doi: 10.1038/nature21676

109. Apte RN, Voronov E. Immunotherapeutic approaches of il-1 neutralization in the tumor microenvironment. *J Leukocyte Biol* (2017) 102 (2):293–306. doi: 10.1189/jlb.3MR1216-523R

110. Safari H, Zabihi E, Pouramir M, Morakabati P, Abedian Z, Karkhah A, et al. Decrease of intracellular ros by arbutin is associated with apoptosis induction and downregulation of il-1 beta and tnf-alpha in lncap; prostate cancer. *J Food Biochem* (2020) 44(9):218–98. doi: 10.1111/jfbc.13360

111. Zhou J, Tulotta C, Ottewell PD. Il-1 beta in breast cancer bone metastasis. *Expert Rev Mol Med* (2022) 24:133–76. doi: 10.1017/erm.2022.4

frontiers | Frontiers in Immunology

TYPE Case Report
PUBLISHED 27 September 2022
DOI 10.3389/fimmu.2022.980456

OPEN ACCESS

EDITED BY
Marco Ponzetti,
University of L'Aquila, Italy

REVIEWED BY
Xun Lin,
Pfizer, United States
Marco Maruzzo,
Veneto Institute of Oncology (IRCCS), Italy

*CORRESPONDENCE
Norio Yamamoto
norinori@med.kanazawa-u.ac.jp

SPECIALTY SECTION
This article was submitted to Cancer Immunity and Immunotherapy, a section of the journal Frontiers in Immunology

RECEIVED 28 June 2022
ACCEPTED 12 September 2022
PUBLISHED 27 September 2022

CITATION
Asano Y, Yamamoto N, Hayashi K, Takeuchi A, Miwa S, Igarashi K, Higuchi T, Taniguchi Y, Morinaga S, Horimoto T, Nakai M, Kadono Y, Nojima T and Tsuchiya H (2022) Case report: Complete remission of bone metastasis from renal cell carcinoma in histopathological examination after treatment with immune checkpoint inhibitors.
Front. Immunol. 13:980456.
doi: 10.3389/fimmu.2022.980456

Case report: Complete remission of bone metastasis from renal cell carcinoma in histopathological examination after treatment with immune checkpoint inhibitors

Yohei Asano[1], Norio Yamamoto[1]*, Katsuhiro Hayashi[1], Akihiko Takeuchi[1], Shinji Miwa[1], Kentaro Igarashi[1], Takashi Higuchi[1], Yuta Taniguchi[1], Sei Morinaga[1], Takashi Horimoto[2], Masaharu Nakai[3], Yoshifumi Kadono[4], Takayuki Nojima[1] and Hiroyuki Tsuchiya[1]

[1]Department of Orthopaedic Surgery, Kanazawa University Graduate School of Medical Sciences, Kanazawa, Japan, [2]Department of Orthopaedic Surgery, Kaga Medical Center, Kaga, Japan, [3]Department of Urology, Kaga Medical Center, Kaga, Japan, [4]Department of Integrative Cancer Therapy and Urology, Kanazawa University Graduate School of Medical Sciences, Kanazawa, Japan

Recently, the prognosis of metastatic renal cell carcinoma (mRCC) has improved owing to the development of immunotherapy using immune checkpoint inhibitors (ICIs). However, there have been few studies on the therapeutic effect of ICIs in bone metastases from renal cell carcinoma (RCC). We report a case in which pulmonary and humeral metastases from RCC were significantly ameliorated using ICIs, while surgery for a pathological fracture of the humerus significantly improved the patient's quality of life (QoL). A 70-year-old man who underwent a left nephrectomy for RCC developed multiple pulmonary metastases and humeral metastasis with a pathological fracture one year after surgery, and combined treatment with nivolumab and ipilimumab was initiated. After four courses of ICI treatment, multiple pulmonary metastases had almost disappeared, and the tumor at the fracture site had shrunk remarkably. However, the shoulder joint function had decreased due to the fracture, worsening his QoL. Therefore, he underwent surgery and returned to normal daily life one month after. Postoperative histopathological examination of bone and soft tissue at the fracture site revealed no malignancy. To our knowledge, this is the first case report of complete remission of bone metastasis of RCC based on histopathological examination with ICI treatment.

KEYWORDS

renal cell carcinoma (RCC), immune checkpoint inhibitor (ICI), nivolumab, bone metastasis (BM), pathological fracture

Introduction

Among patients with renal cell carcinoma (RCC), 25–30% already have distant metastasis at the time of diagnosis (1, 2), and 30% of patients with metastatic RCC (mRCC) have bone metastasis (3). The 5-year overall survival (OS) rate for mRCC, including patients with bone metastasis, has been reported to be 12% (1, 2), and the prognosis is very poor. Bone metastatic lesions from RCC are osteolytic changes, and skeletal-related events (SRE), such as severe bone pain, pathological fractures, and spinal compression, occur in > 70% of patients with mRCC (4). The quality of life (QoL) and prognosis of patients with mRCC are worsened by SRE (4, 5), and bone metastasis is a poor prognostic factor (6–8). However, in recent years, the development of immune checkpoint inhibitors (ICIs) has improved the prognosis of mRCC in some clinical trials (9, 10), and ICIs have become the standard treatment (11). In mRCC patients with intermediate-risk/poor-risk by the International Metastatic RCC Database Consortium (IMDC) risk classification (12), the 5-year OS rate was dramatically improved to 43% with ICI treatment (13). Similarly, although improvement in median survival time of mRCC with bone metastases has been reported (14), there are few reports regarding the therapeutic effect of ICIs on bone metastases in RCC. We report the first case of multiple pulmonary and humeral metastases in a patient with RCC that was dramatically ameliorated by ICI treatment, and complete remission was observed on histopathological examination.

Case presentation

A 70-year-old man diagnosed with RCC underwent a left nephrectomy because preoperative radiological examinations showed no distant metastasis and was followed up without drug treatment after the surgery. One year after the surgery, radiological examination revealed two lung metastases (Figure 1A), for which drug treatment was recommended, but the patient refused this. Eight months later, left upper arm pain appeared during his sleep, and X-ray radiographs revealed a fracture in the diaphysis of the humerus with osteolytic changes. Magnetic resonance imaging (MRI) showed a mass lesion extending to the outside of the fracture site, which was considered a pathological fracture due to bone metastasis (Figure 1B). He was clinically diagnosed with multiple metastases of RCC, and the IMDC risk classification (12) was evaluated as poor based on Karnofsky performance status < 80%, anemia, and high serum-corrected calcium. Since the pulmonary metastases had not been treated, ICI treatment using nivolumab and ipilimumab was immediately initiated to prioritize systemic treatment. The pathological fracture was treated conservatively with denosumab and concomitant functional brace fixation. After four courses of ICI treatment, the pulmonary metastases had almost disappeared (Figure 2A), and the therapeutic effect was evaluated as a partial response (PR) based on the Response Evaluation Criteria in Solid Tumors (RECIST) version 1.1 (15). Furthermore, the tumor at the pathological fracture site showed remarkable shrinkage (Figure 2B). However, the left shoulder joint function was significantly decreased due to the pathological fracture, and the active range of motion could not be evaluated. Since there was no metastasis to other sites, the pulmonary metastases had almost disappeared, and a long-term prognosis was expected, surgical treatment for pathological fracture was planned to improve shoulder joint function. Seven months after the diagnosis of pathological fracture, surgery was performed under general anesthesia. The soft tissue suspected that the tumor at the fracture site was resected, and curettage in the medullary cavity was performed to refresh the fracture site. The medullary cavity was then filled with cement, and an intramedullary nail was inserted. Finally, cement was added to the defect at the fracture site, and screw fixation of the nail was

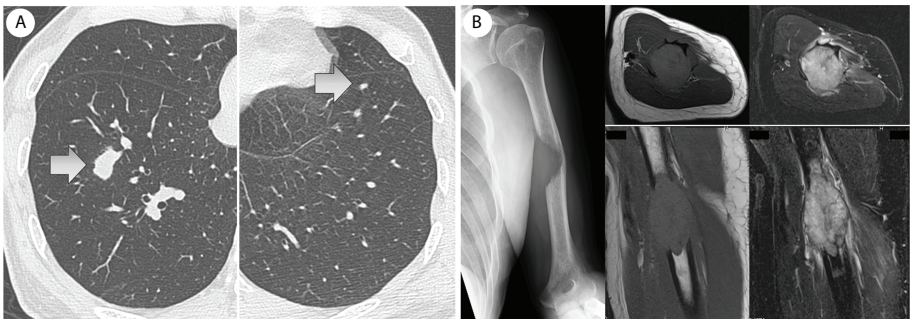

FIGURE 1
(A) One year after the left nephrectomy, two lung metastases were revealed by computed tomography. **(B)** Eight months later, a left humerus fracture with osteolytic change was revealed by X-ray. Magnetic resonance imaging (MRI) showed an extraskeletal mass at the fracture site (left: T1-weighted image, right: fat-suppressed T2-weighted image), and it was considered to be a pathological fracture due to bone metastasis.

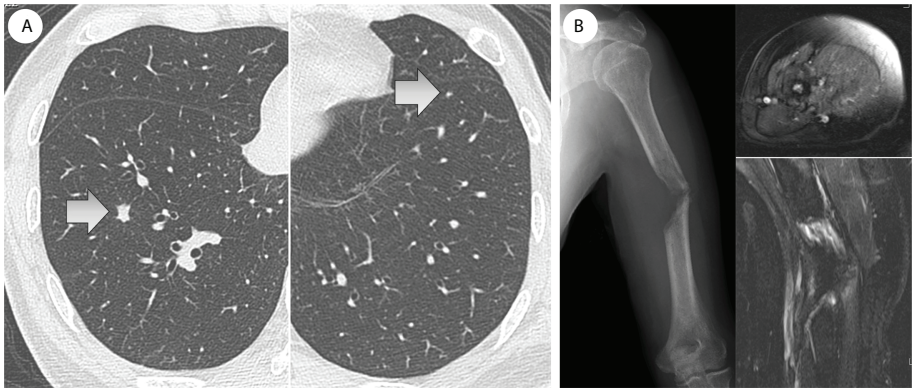

FIGURE 2
(A) After four courses of ICI treatment, the pulmonary metastases had almost disappeared. **(B)** Furthermore, the tumor at the fracture site had shrunk remarkably and almost disappeared (MRI: gadolinium-enhancement).

performed (Figure 3). Postoperatively, histopathological examination of the soft tissue at the fracture site and medullary cavity showed no evidence of malignancy, and bone healing after the fracture was observed (Figure 4). Based on the histopathological findings, humerus metastasis of RCC was evaluated as complete remission after ICI treatment. One month after the surgery, the pain of motion disappeared, and auto-flexion and abduction improved to 160° and 170°, respectively. To assess his postoperative QoL, the patient-reported outcomes using the disability of the arm, shoulder and hand (DASH) score (16) was performed and showed significant improvement (from 66.7 preoperatively to 20.0 postoperatively). The shoulder joint function and his QoL were greatly improved by the surgery for the pathological fracture. Seventeen months after the surgery, nivolumab monotherapy was continued without immune-related adverse events, and no recurrence or metastasis was observed. The patient has returned to his normal daily life and continues to be followed up with radiological examinations every six months.

Discussion

Multiple pulmonary and humeral metastases from RCC were dramatically ameliorated by ICI treatment, and surgical treatment for the pathological fracture of the humerus remarkably improved shoulder joint function and QoL. To our knowledge, this is the first case report in which a bone metastatic lesion of RCC treated with ICIs was evaluated as complete remission based on histopathological examination.

Strategies for the treatment of mRCC have generally been considered based on the IMDC risk classification (12). Currently, in pharmacological therapy of mRCC, the ICI treatment using nivolumab and ipilimumab is approved as the first-line treatment for the patient evaluated as intermediate or poor in IMDC risk classification. The combined treatment with these ICIs significantly improved the 12-month overall survival rate (80% vs. 72%, $p<0.001$) and response rate (42% vs. 27%, $p<0.001$) for mRCC compared to the conventional standard treatment group treated with sunitinib in a phase III study (CheckMate 214) (9). The development of ICI treatment has brought a paradigm shift in the treatment strategy for patients with untreated advanced clear cell RCC who had insufficient therapeutic effects from conventional drug treatment and had poor prognoses (6, 7, 11).

Two case reports have shown that bone metastases from RCC were significantly improved by ICI treatment (17, 18). In both cases, nivolumab, which was introduced as a second-line treatment after the molecular-targeted drug, improved bone metastases. Vuyyala et al. (17) reported that a solitary scapular metastasis with osteolytic change was remodeled with osteosclerotic change by nivolumab treatment without the concomitant use of a bone-modifying agent (BMA). Marsh et al. (18) reported that the accumulation of a solitary thoracic vertebral body on positron emission tomography (PET) disappeared after nivolumab treatment. In both cases, although the therapeutic effect of nivolumab on bone metastasis was CR on radiological evaluation, no histopathological evaluation was performed. In our case, as in previous reports, remarkable amelioration of bone metastasis by ICI treatment was revealed on radiological examination. Furthermore, complete remission at the bone metastatic lesion was observed on histopathological examination, which is the first case report to evaluate the therapeutic effect of ICI on bone metastasis.

Bone metastasis in the long bones of the extremities is associated with a risk of pathological fracture, which is an SRE (19). In most cases, although non-surgical treatment including

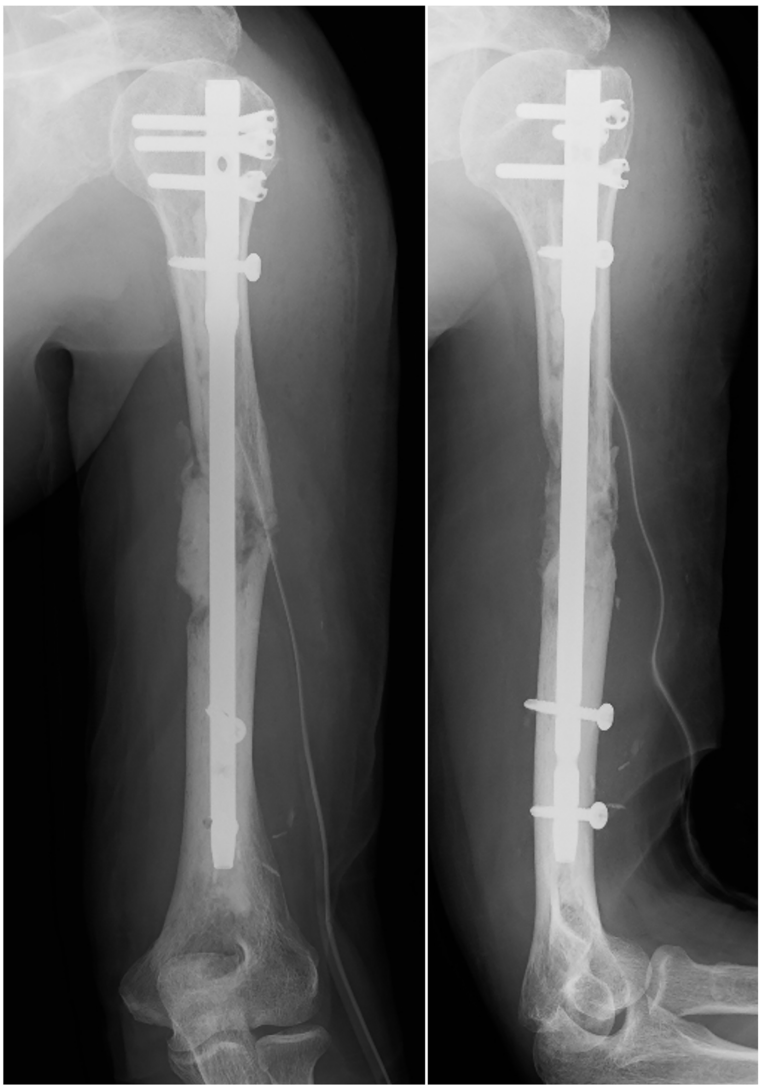

FIGURE 3
Postoperative X-ray.

drug therapy with BMA and radiation therapy are considered (20, 21), surgical treatment may be performed for impending fractures based on the Mirels' score (22) and for pathological fractures to improve function. In our case, ICI treatment significantly ameliorated multiple pulmonary and humeral metastases, and a long-term prognosis could be expected. However, a pathological fracture of the humerus significantly reduced the shoulder joint function and interfered with his daily life. Therefore, surgical treatment was performed to improve joint function and QoL. Postoperative histopathological examination revealed complete remission of bone metastasis with ICI treatment; thus, it was suggested that multidisciplinary therapy including ICIs may improve metastasis to the long bones in the extremities without surgery if pathological fracture can be prevented. For optimal management of long bone metastases to prevent SREs, including pathological fractures, early diagnosis of those metastases by radiological examinations is very important. After the diagnosis, careful conservative follow-up should be performed, such as fixation with functional bracing in the upper extremity and non-weight-bearing in the lower extremity. In addition, initiation of bone modifying agents such as denosumab may be recommended.

In our case, denosumab was used concomitantly, which might have affected its therapeutic effect on bone metastases. The effectiveness of combined treatment with ICIs and denosumab in bone metastases has been reported in melanoma and non-small cell lung cancer (23–27). Although there have been no reports on the combined treatment for bone

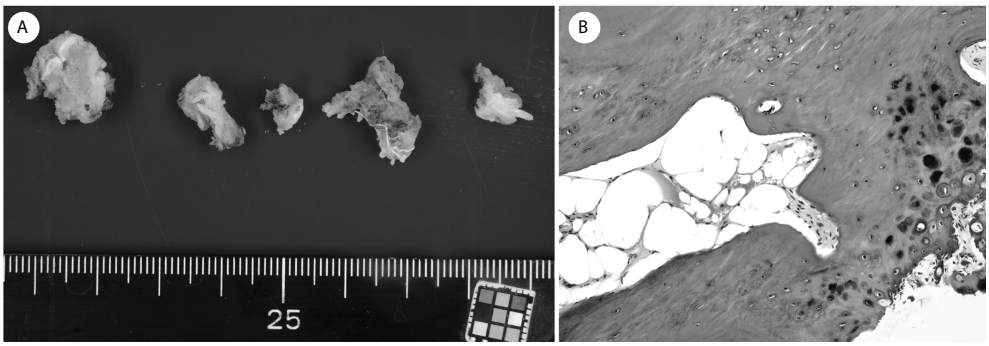

FIGURE 4
(A) The soft tissue at the fracture site. **(B)** Histopathological examination showed no evidence of malignancy, and the bone healing process after the fracture was observed.

metastases from RCC, denosumab has been licensed in treatment for mRCC and may be recommended the combined use.

Conclusion

Multiple pulmonary and humeral metastases from RCC were dramatically ameliorated by ICI treatment with nivolumab and ipilimumab. Furthermore, surgical treatment for pathological fractures of the humerus remarkably improved shoulder joint function and QoL. To our knowledge, this is the first case report of complete remission of bone metastasis from RCC based on histopathological examination with ICI treatment. Multidisciplinary therapy with ICIs may influence the therapeutic strategies for mRCC with bone metastases.

Data availability statement

The original contributions presented in the study are included in the article/supplementary material. Further inquiries can be directed to the corresponding author.

Ethics statement

Written informed consent was obtained from the individual(s) for the publication of any potentially identifiable images or data included in this article.

Author contributions

The manuscript was drafted by YA and NY. YA, NY, KH, AT, SMi, KI, TH, YT, SMo, TH, MN, YK and HT examined and treated the patient. TN performed the histopathological assessment. YA and NY analyzed data, and YA wrote the manuscript. NY and HT supervised this study. All authors contributed to the article and approved the submitted version.

Acknowledgments

We would like to thank Editage (www.editage.com) for English language editing.

Conflict of interest

The authors declare that the research was conducted in the absence of any commercial or financial relationships that could be construed as a potential conflict of interest.

Publisher's note

All claims expressed in this article are solely those of the authors and do not necessarily represent those of their affiliated organizations, or those of the publisher, the editors and the reviewers. Any product that may be evaluated in this article, or claim that may be made by its manufacturer, is not guaranteed or endorsed by the publisher.

References

1. Ljungberg B, Campbell SC, Choi HY, Jacqmin D, Lee JE, Weikert S, et al. The epidemiology of renal cell carcinoma. *Eur Urol* (2011) 60(4):615–21. doi: 10.1016/j.eururo.2011.06.049

2. Gupta K, Miller JD, Li JZ, Russell MW, Charbonneau C. Epidemiologic and socioeconomic burden of metastatic renal cell carcinoma (mRCC): A literature review. *Cancer Treat Rev* (2008) 34:193–205. doi: 10.1016/j.ctrv.2007.12.001

3. Bianchi M, Sun M, Jeldres C, Shariat SF, Trinh QD, Briganti A, et al. Distribution of metastatic sites in renal cell carcinoma: A population-based analysis. *Ann Oncol* (2012) 23:973–80. doi: 10.1093/annonc/mdr362

4. Santini D, Procopio G, Porta C, Ibrahim T, Barni S, Mazzara C, et al. Natural history of malignant bone disease in renal cancer: Final results of an Italian bone metastasis survey. *PloS One* (2013) 8:e83026. doi: 10.1371/journal.pone.0083026

5. Kinnane N. Burden of bone disease. *Eur J Oncol Nurs* (2007) 11 Suppl 2):S28–31. doi: 10.1016/j.ejon.2007.07.002

6. Motzer RJ, Escudier B, Bukowski R, Rini BI, Hutson TE, Barrios CH, et al. Prognostic factors for survival in 1059 patients treated with sunitinib for metastatic renal cell carcinoma. *Br J Cancer* (2013) 108:2470–7. doi: 10.1038/bjc.2013.236

7. Motzer RJ, Escudier B, Oudard S, Hutson TE, Porta C, Bracarda S, et al. Phase 3 trial of everolimus for metastatic renal cell carcinoma: Final results and analysis of prognostic factors. *Cancer* (2010) 116:4256–65. doi: 10.1002/cncr.25219

8. Patil S, Figlin RA, Hutson TE, Michaelson MD, Négrier S, Kim ST, et al. Prognostic factors for progression free survival and overall survival with sunitinib targeted therapy and with cytokine as first-line therapy in patients with metastatic renal cell carcinoma. *Ann Oncol* (2011) 22:295–300. doi: 10.1093/annonc/mdq342

9. Motzer RJ, Tannir NM, McDermott DF, Arén Frontera O, Melichar B, Choueiri TK, et al. Nivolumab plus ipilimumab versus sunitinib in advanced renal-cell carcinoma. *N Engl J Med* (2018) 378(14):1277–90. doi: 10.1056/NEJMoa1712126

10. Negishi T, Furubayashi N, Takamatsu D, Ieiri K, Nishiyama N, Kitamura H, et al. Radiographical efficacy of systemic treatment for bone metastasis from renal cell carcinoma. *Oncol Lett* (2020) 20(5):267. doi: 10.3892/ol.2020.12130

11. Tung I, Sahu A. Immune checkpoint inhibitor in first-line treatment of metastatic renal cell carcinoma: A review of current evidence and future directions. *Front Oncol* (2021) 11:707214. doi: 10.3389/fonc.2021.707214

12. Heng DY, Xie W, Regan MM, Warren MA, Golshayan AR, Sahi C, et al. Prognostic factors for overall survival in patients with metastatic renal cell carcinoma treated with vascular endothelial growth factor-targeted agents: results from a large, multicenter study. *J Clin Oncol* (2009) 27(34):5794–9. doi: 10.1200/JCO.2008.21.4809

13. Motzer RJ, McDermott DF, Escudier B, Burotto M, Choueiri TK, Hammers HJ, et al. Conditional survival and long-term efficacy with nivolumab plus ipilimumab versus sunitinib in patients with advanced renal cell carcinoma. *Cancer* (2022) 128(11):2085–97. doi: 10.1002/cncr.34180

14. Escudier B, Sharma P, McDermott DF, George S, Hammers HJ, Srinivas S, et al. CheckMate 025 randomized phase 3 study: outcomes by key baseline factors and prior therapy for nivolumab versus everolimus in advanced renal cell carcinoma. *Eur Urol* (2017) 72:962–71. doi: 10.1016/j.eururo.2017.02.010

15. Eisenhauer EA, Therasse P, Bogaerts J, Schwartz LH, Sargent D, Ford R, et al. New response evaluation criteria in solid tumours: revised RECIST guideline (version 1.1). *Eur J Cancer* (2009) 45(2):228–47. doi: 10.1016/j.ejca.2008.10.026

16. Hudak PL, Amadio PC, Bombardier C. Development of an upper extremity outcome measure: the DASH (disabilities of the arm, shoulder and hand). *Am J Ind Med* (1996) 29(6):602–8. doi: 10.1002/(SICI)1097-0274(199606)29:6<602::AID-AJIM4>3.0.CO;2-L

17. Vuyyala S, Gandhi S, Kuechle JB, George S. Complete remission of bone metastases in renal cell carcinoma with nivolumab. *Cureus* (2019) 11(8):e5531. doi: 10.7759/cureus.5531

18. Marsh S, Wang J. Complete remission of liver and bone metastases after nivolumab treatment in a patient with renal cell carcinoma: The potential implication of MLH1 mutations. *Oncol Cancer Case Rep* (2017) 3:125.

19. Saad F, Lipton A, Cook R, Chen YM, Smith M, Coleman R. Pathologic fractures correlate with reduced survival in patients with malignant bone disease. *Cancer* (2007) 110(8):1860–7. doi: 10.1002/cncr.22991

20. Jehn CF, Diel IJ, Overkamp F, Kurth A, Schaefer R, Miller K, et al. Management of metastatic bone disease algorithms for diagnostics and treatment. *Anticancer Res* (2016) 36(6):2631–7.

21. Taunk NK, Spratt DE, Bilsky M, Yamada Y. Spine radiosurgery in the management of renal cell carcinoma metastases. *J Natl Compr Cancer Netw* (2015) 13:801–9. doi: 10.6004/jnccn.2015.0093

22. Mirels H. Metastatic disease in long bones. a proposed scoring system for diagnosing impending pathologic fractures. *Clin Orthop Relat Res* (1989) 249):256–64.

23. Angela Y, Haferkamp S, Weishaupt C, Ugurel S, Becker JC, Oberndörfer F, et al. Combination of denosumab and immune checkpoint inhibition: Experience in 29 patients with metastatic melanoma and bone metastases. *Cancer Immunol Immunother* (2019) 68:1187–94. doi: 10.1007/s00262-019-02353-5

24. Liede A, Hernandez RK, Wade SW, Bo R, Nussbaum NC, Ahern E, et al. An observational study of concomitant immunotherapies and denosumab in patients with advanced melanoma or lung cancer. *Oncoimmunology* (2018) 7:e1480301. doi: 10.1080/2162402X.2018.1480301

25. Ahern E, Harjunpää H, O'Donnell JS, Allen S, Dougall WC, Teng MWL, et al. RANKL blockade improves efficacy of PD1-PD-L1 blockade or dual PD1-PD-L1 and CTLA4 blockade in mouse models of cancer. *Oncoimmunology* (2018) 7:e1431088. doi: 10.1080/2162402X.2018.1431088

26. Asano Y, Yamamoto N, Hayashi K, Takeuchi A, Miwa S, Igarashi K, et al. Complete response of bone metastasis in non-small cell lung cancer with pembrolizumab: Two case reports. *Anticancer Res* (2021) 41(3):1693–9. doi: 10.21873/anticanres.14933

27. Asano Y, Yamamoto N, Demura S, Hayashi K, Takeuchi A, Kato S, et al. The therapeutic effect and clinical outcome of immune checkpoint inhibitors on bone metastasis in advanced non-Small-Cell lung cancer. *Front Oncol* (2022) 12:871675. doi: 10.3389/fonc.2022.871675

frontiers | Frontiers in Immunology

TYPE Review
PUBLISHED 13 October 2022
DOI 10.3389/fimmu.2022.871076

OPEN ACCESS

EDITED BY
Alejandro López-Soto,
University of Oviedo, Spain

REVIEWED BY
Dominique Heymann,
Université de Nantes,
Institut de Cancérologie de l'Ouest,
France
Binghao Li,
Zhejiang University, China

*CORRESPONDENCE
Yunfeng Li
410985380@qq.com

SPECIALTY SECTION
This article was submitted to
Cancer Immunity
and Immunotherapy,
a section of the journal
Frontiers in Immunology

RECEIVED 07 February 2022
ACCEPTED 28 September 2022
PUBLISHED 13 October 2022

CITATION
Yu L, Zhang J and Li Y (2022) Effects
of microenvironment in osteosarcoma
on chemoresistance and the promise
of immunotherapy as an
osteosarcoma therapeutic modality.
Front. Immunol. 13:871076.
doi: 10.3389/fimmu.2022.871076

Effects of microenvironment in osteosarcoma on chemoresistance and the promise of immunotherapy as an osteosarcoma therapeutic modality

Lei Yu, Jian Zhang and Yunfeng Li*

Department of Radiation Oncology, The Second Affiliated Hospital of Jilin University, Changchun, China

Osteosarcoma (OS) is one of the most common primary malignant tumors originating in bones. Its high malignancy typically manifests in lung metastasis leading to high mortality. Although remarkable advances in surgical resection and neoadjuvant chemotherapy have lengthened life expectancy and greatly improved the survival rate among OS patients, no further breakthroughs have been achieved. It is challenging to treat patients with chemoresistant tumors and distant metastases. Recent studies have identified a compelling set of links between hypoxia and chemotherapy failure. Here, we review the evidence supporting the positive effects of hypoxia in the tumor microenvironment (TME). In addition, certain anticancer effects of immune checkpoint inhibitors have been demonstrated in OS preclinical models. Continued long-term observation in clinical trials is required. In the present review, we discuss the mutualistic effects of the TME in OS treatment and summarize the mechanisms of immunotherapy and their interaction with TME when used to treat OS. We also suggest that immunotherapy, a new comprehensive and potential antitumor approach that stimulates an immune response to eliminate tumor cells, may represent an innovative approach for the development of a novel treatment regimen for OS patients.

KEYWORDS

Osteosarcoma, tumor microenvironment, chemoresistance, immunotherapy, immune checkpoint inhibitors

1 Introduction

Osteosarcoma (OS) is an osteoid-producing malignancy of mesenchymal origin. Worldwide incidence is 3.4 cases per million people per year (1). OS (accounting for 56%) is much more common than Ewing sarcoma, chondrosarcoma, and chordoma (2). Primary OS affects children, teenagers, and elders, with age-specific incidence varying according to histological subtype (Table 1). OS typically affects patients aged 10–30 years. In the group aged 25–59 years, the male to female incidence ratio of OS is 1.28:1 and the number is elevated (1.43:1) in the group aged 0–24 years. In addition, the ratio varies in diverse populations (3). OS frequently arises in the long bones (particularly the distal femur or the epiphysis of the proximal tibia) (3, 4). OS carcinogenesis is a complex process involving genetic mutations and dysregulation of epigenetic pathways (5). However, through whole-genome and exome sequencing, transcriptome assessment of gene expression, and epigenetic modifications, it was revealed that there was remarkable genomic complexity and significant inter-patient heterogeneity of genes in OS samples (6).

Currently, the standard treatment protocol for patients with OS comprises extensive surgical resection, radiotherapy, and administration of chemotherapeutic agents. The current curative regimen combines surgery with multiple modes of chemotherapy using several cytotoxic agents, such as cis-platinum, doxorubicin, high-dose methotrexate, and ifosfamide during preoperative and postoperative periods (7). Surgical excision is preferred over systemic therapy for recurrent disease while unresectable cases would be treated by systemic therapy or comprehensive therapy (8). *Via* radiotherapy, we can take advantage of ionizing radiation to help eliminate microscopic or minimal residual disease in situations where substantial surgical resection is not feasible (9). However, in the majority of OS cases, the efficacy of radiotherapy is limited, and the indications for this approach are finite (10). Despite aggressive interventions, patient outcomes have not significantly improved over the last 20 years. During this period, the well-known phenomenon of chemotherapeutic resistance has prevented improvements in prognosis (7).Furthermore, OS prognosis has not improved over the past several decades. Facing these hindrances to current curative regimens, identifying novel therapeutics is critical to promote the management of OS.

Multidrug resistance is a difficult problem that results in unsatisfactory clinical outcomes (11). In recent years, many studies have demonstrated that the tumor microenvironment (TME) appears to influence clinical outcome and therapeutic response by regulating tumor chemoresistance (12, 13). Managing TME-related drug resistance may profoundly affect cancer therapeutic strategies. TME-related multidrug resistance can be mediated by hypoxic conditions and soluble factors secreted by tumors or stromal cells. Inhibiting extracellular ligand–receptor interactions and downstream pathways are among the TME-targeted treatment methods (13). We propose that focusing on the primary mechanism of TME-related multidrug resistance would yield substantially greater benefits. A combination of drugs that can simultaneously attack tumor cells and the TME may help reduce chemoresistance. Herein, we review the effects and mechanisms of chemoresistance regulated by the OS TME through hypoxia and immune cells. This review also suggests the novel and therapeutic potential of immunotherapy for the management of OS treatment.

There is a pressing need to investigate novel therapies that could impact OS because of its resistance to chemotherapy. Immunotherapy has gained considerable attention since it has demonstrated efficacy in the treatment of cancers. For instance, the combination of nab-paclitaxel and atezolizumab was recently approved by the Food and Drug Administration (FDA) for patients with unresectable locally advanced or metastatic TNBC whose tumors express PD-L1 based on a PFS benefit over chemotherapy in the Impassion130 trial (14). Interactions between TME modulation and the immune system may enhance therapeutic efficacy. Immunotherapy is a promising therapeutic strategy for improving the curative efficacy of existing OS treatments despite chemoresistance. In the current review, we present the mechanism of TME-related chemoresistance and describe the modulatory effects of the TME in OS treatment. Subsequently, we discuss new technologies and strategies— immunotherapy that can be adapted to explore the roles of the TME in improving the curative effects of drug treatment by modifying TME-associated factors. A better understanding of the molecular mechanisms of immunological

Abbreviations: ACT, adoptive T cell transfer; BIM, BH3-only protein, a mediator of apoptosis; CAR, chimeric antigen receptor; CSCs, cancer stem cells; CSF1R, colony-stimulating factor 1 receptor; CTL, cytotoxic T cells; CTLA4, cytotoxic T lymphocyte associated protein 4; EMA, European Medical Agency; EMT, epithelial-mesenchymal transition; HIFs, hypoxia-inducible factors; HRE, hypoxia response element; ICIs, immune checkpoint inhibitors; IDO, indoleamine 2,3-dioxygenase; IFNγ, interferon-gamma; iNOS, inducible nitric oxide synthase; JNK, Jun N-terminal kinase; LAG-3, lymphocyte-activation gene 3; MDSCs, myeloid-derived suppressor cells; Met, metformin; NF-κB, nuclear factor-kappa B; ORR, objective response rate; OS, osteosarcoma; OXPHOS, decreased oxidative phosphorylation; PD-1, programmed death-1 and; PD-L1, programmed death-ligand 1; PFS, progression-free survival; PGE2, prostaglandin E2; PMN-MDSCs, polymorphonuclear MDSCs; ROS, reactive oxygen species; SDF-1, stromal cell-derived factor-1; SIRPα, signal regulatory protein α; STAT3, signal transducer and activator of transcription 3; TAMs, tumor-associated macrophages; TCR, T cell receptor,; TCRs, T cell receptors; TIC, tumor-initiating cell; TIGIT, anti-T cell immunoreceptor with Ig and ITIM domains; TILs, tumor-infiltrating lymphocytes; TME, tumor microenvironment; Tregs, regulatory T cells; TSA, tumor-specific antigens; VCAM-1, vascular cell adhesion molecule 1; VEGF, vascular endothelial growth factor.

TABLE 1 Categories and treatment options for OS.

Subtype of OS	Incidence	Common anatomical distribution	Chemosensitivity	Radiosensitivity
Conventional OS (3 subtypes: osteoblastic, chondroblastic, fibroblastic)	75.0%	Metaphysis of long bone around knee and shoulder joint, axial skeleton	Sensitive	Radiotherapy can be useful
Parosteal OS	3.5–4%	Posterior cortex of distal femur	Hyposensitivity	Hyposensitivity
Telangiectatic OS	3–4%	Similar to conventional OS	Sensitive	Hyposensitivity
Periosteal OS	1.5–2%	Tibia or femur	Hyposensitivity	Hyposensitivity
Small cell OS	1.5%	—	Sensitive	Sensitive
Low grade central OS	1–2%	Intramedullary distal femur, proximal tibia, pelvis	—	—
High-grade surface OS	<1%	Long bone, distal femur	Sensitive	Radiotherapy can be useful

therapy is required, as current research suggests that this may be a more promising method to develop and implement optimal preventive and curative approaches to treating patients with OS. Our review of the active mechanisms of immune-cell regulation within the TME and the impressive clinical results achieved by stimulating antitumor immune responses supports the implementation of immunotherapy together with anticancer therapies for the treatment of OS.

2 Mechanisms of TME-mediated chemotherapy resistance in OS

The TME is composed of multiple cell types (fibroblasts, endothelial cells, and immune cells), extracellular components that surround tumor cells and are nourished by the vasculature (chemokines, cytokines, hormones, and ECM), and various physical and chemical factors surrounding tumor cells (hypoxia and acidic environment) (15). The TME plays a pivotal role in carcinogenesis, tumor development, and metastasis. For example, the TME makes a remarkable contribution to the acquisition and maintenance of cancer hallmarks, such as inducing angiogenesis, sustaining proliferative signaling, resisting cell death, and activating invasion and metastasis (15). The TME also exerts profound effects on therapeutic efficacy. TME-reduced multidrug resistance results from sustained crosstalk between tumor cells and their surrounding matrix. Owing to genomic instability, tumor cells are prone to chemoresistance, whereas non-tumor cells in the TME are more genetically stable and susceptible to stimulation. Hence, the insight that cancer progression and therapeutic resistance are closely related to the TME raises the possibility that efforts devoted to targeting TME elements or their signaling pathways could achieve therapeutic advances for cancer patients.

2.1 Hypoxic TME and chemoresistance in OS

Tumor cells typically live in a state of hypoxia because of hypermetabolism, abnormal proliferation, and high oxygen consumption (16). A compelling set of links between drug resistance and hypoxia-inducible factors (HIFs) has emerged (17). Following hypoxia, HIFs secreted for hypoxic adaptation are capable of triggering the expression of a variety of genes related to erythropoiesis, glycolysis, and angiogenesis, as well as restore oxygen homeostasis at the epigenetic and transcriptional levels (18, 19). Undoubtedly, hypoxia may result in an acidic environment and the Warburg effect is the typical example: tumor cells tend to obtain energy through glycolysis. Through H +-ATPases, Na+-H+ exchangers, and HCO3- transporters, the acidoid can be transported from an intracellular area to an extracellular one (20, 21). In addition, the rapid tumor proliferation and abnormal vascular structures accelerate further accumulation of acid, eventually leading to an extracellular pH of 6.7–7.1 for tumor cells and an intracellular pH > 7.4. In comparison, the extracellular and intracellular pH of normal cells is approximately 7.4 and 7.2, respectively (12).

2.1.1 Hypoxic TME induces chemoresistance by regulating signaling pathways

Accumulating evidence suggests that hypoxia plays a vital role in the molecular mechanisms underlying drug-resistant cancers by regulating gene expression (Table 2). For instance, overexpression of efflux transporters (primarily the ATP-binding cassette [ABC] superfamily of pump proteins, including P-glycoprotein [P-gp] encoded by the multidrug resistance gene 1 [MDR-1]) may amplify the efflux of certain drugs from tumor cells, thereby resulting in resistance to anticancer drug (37–39). Roncuzzi et al. (35) showed that hypoxia-inducible factor 1-alpha (HIF-1α), the most influential regulator of cell adaptation to hypoxia, promotes export of intracellular doxorubicin by increasing the level of P-gp in OS. Furthermore, by modulating the expression of c-Myc and p21, HIF-1α can prevent doxorubicin-induced OS apoptosis, indicating that HIF-1α could be a valuable therapeutic target. Ma et al. (40) determined that overexpression of spindle-and kinetochore-associated complex subunit 1 (SKA1) can reduce expression of some multidrug resistance genes, such as *ABCB1 (MDR1)*, *ABCC2 (MRP2)*, and *GSTP1*, as well as enhance sensitivity to the drugs

TABLE 2 A schematic diagram of the expression of hypoxic and drug resistance factors.

Study. (year). Ref	Source	Mechanism	Target gene	Expression change	Clinic characters relatedness
Wang et al.(2019) (22)	MG-63 and U2-os cells	Visfatin was involved in cisplatin resistance of OS cells by upregulating expression of Snail via HIF-1α induced transcription	Snail and its mRNA	↑	cisplatin resistance
Keremu et al.(2019) (23)	20 osteosarcoma patient samples and human OS cell lines (MG-63, U-2OS and SaoS-2)	Overexpression of miR-199a resensitizes cisplatin resistant cells to cisplatin through inhibition of HIF-1α	miR-199a	↑	cisplatin resistance
Zheng et al.(2017) (24)	U-2OS (derived from bone tissues of a 15-year-old OS patient) and MG-63 (derived from bone tissues of a 14-year-old OS patient) cells	HIF-1α-induced Mxd1 up-regulation suppresses the expression of PTEN under hypoxia, which leads to the activation of PI3K/AKT antiapoptotic and survival pathway	Mxd1	↑	hypoxia-induced cisplatin resistance
Guo et al.(2017) (25)	MG63, U2OS and 143B cells	MiR-335 targets CSCs and regulates OS stem cell-like properties via downregulated POU5F1 to synergize with chemotherapeutic drugs	miR-335	↓	stem cell-like properties
Ma et al.(2017) (26)	Human OS cells (SOSP-9607, MG-63, SaOS-2)	Hypoxia increased the expression of MRG and enhanced the sensitivity of EPI and IFO in OS patients	SKA1	↓	chemotherapy resistance
Zhao et al.(2016) (27)	MG-63 and U2-os cells	Hypoxia reduced sensitivity to Dox by promoting the AMPK signaling and has no association with HIF-1α	AMPK	↑	Dox resistance and Dox-induced apoptosis
Zhou et al.(2016) (28)	human OS cell lines (MG-63, U-2OS and SaoS-2)	Hypoxia induced microRNA-488 expression to promote proliferation, reduce apoptosis and decrease the Dox sensitivity of OS cells	microRNA-488	↑	tumor proliferation, apoptosis and Dox resistance
Wang et al.(2016) (29)	human OS cell lines MG-63, U2OS, Saos-2 and normal os-teoblastic cell line HOB	miR-367 suppressed the increase of KLF4 induced by ADR in OS cells, as well as Bax and cleaved caspase-3	MiR-367	↑	ADR-induced apoptosis
Lin et al.(2016) (30)	U2OS and G293 cell lines	miR-202 promotes chemotherapy resistance by targeting PDCD4	miR-202	↑	Dox resistance and Dox-induced apoptosis
Xu et al.(2016) (31)	MG-63 cell line and Dox-resistant cell line (Mg-63/Dox)	miR-30a downregulated in Mg-63/Dox and miR-30a reduced chemoresistance via suppressing Beclin-1-mediated autophagy	miR-30a	↓	chemoresistance and autophagy
Li et al.(2016) (32)	human MG-63 OS cells	Notch signaling is up-regulated in human OS cells under hypoxia and Notch1 may represent a viable target to overcome chemoresistant OS cells in a hypoxic niche by regulating MRP1 gene expression.	Notch1 and MRP1	↑	chemoresistant
Guo et al.(2015) (33)	human MG-63 OS cells	HIF-1α inhibitor combined with paxilitaxel blocked autophagy and augmented the anti-tumor effects.	—	—	paxilitaxel-induced apoptosis
Zhang et al.(2015) (34)	human OS cell lines (MG-63 and U-2OS)	miR-301a and HMGCR were up-regulated in chemotherapy-resistant OS, subsequently reduced Dox-induced cell apoptosis and contributed to chemoresistance of OS cells	miR-301a	↑	Dox resistance and Dox-induced apoptosis
Roncuzzi et al.(2014) (35)	human MG-63 OS cells	HIF-1α hindered Dox-induced apoptosis and promoted the outward transport of intracellular Dox by activating P-gp expression in OS in normoxic conditions	c-Myc	↓	Dox-induced apoptosis
			p21	↑	Dox-induced apoptosis
			MDR-1/P-gp	↑	Dox resistance

(Continued)

TABLE 2 Continued

Study. (year). Ref	Source	Mechanism	Target gene	Expression change	Clinic characters relatedness
Scholten et al.(2014) (36)	Human OS cells (143B, MNNG/HOS, MG-63)	Hypoxic OS cells can be sensitized to Dox treatment by inhibition of the Wnt/β-catenin signaling pathway	Wnt/β-catenin signaling pathway	↓	Dox-mediated toxicity

*CSCs, cancer stem cells; ADR, adriamycin; Dox, Dox;↑, upregulated; ↓, downregulated.

epirubicin and ifosfamide, which have been used in OS patients. Downregulation of SKA1 expression is mediated by hypoxia, which increases chemoresistance in human OS cells. Li et al. (32) concluded that hypoxia and the Notch signaling pathway display crosstalk. Specifically, hypoxia upregulates the Notch signaling pathway in human OS cells, contributing to OS cell proliferation and G0/G1-S-G2/M phase transition and consequently promoting multidrug resistance. Western blot analysis showed hypoxia elevated secretion of HIF-1α and Notch1, resulting in the upregulation of *MRP1* (which encodes a homolog of the multidrug resistance protein).

Another mechanism of hypoxic TME function was reported by Zhao et al. (27). Hypoxia visibly impaired the sensitivity of U2-OS cells to doxorubicin by upregulating the AMPK signaling pathway. This impaired sensitivity was independent of HIF-1α but was promoted by hypoxia in U2-OS cells. Further research (27) has confirmed that the primary mechanism is associated with a distinct upregulation of phosphorylated AMPK and phosphorylated acetyl-CoA carboxylase (ACC). Both were modulated by the AMPK activator AICAR and the AMPK inhibitor Compound C. AICAR and Compound C decreased or increased the sensitivity of U2-OS cells to doxorubicin by promoting or downregulating AMPK activity, respectively. Therefore, the prevalent application of HIF inhibitors in clinical settings remains controversial, despite progress made in the research of many types of tumors (41).

2.1.2 Hypoxic TME induces chemoresistance by regulating autophagy

Autophagy, also known as type II programmed cell death, is a self-digestion process by which cells form double-membraned autophagic vesicles that sequester damaged, denatured, or senescent organelles, and target them for degradation in lysosomes (42). The complicated relationship between autophagy and carcinoma indicates that it plays a dual role in tumorigenesis and tumor development (43). In the early stages of tumorigenesis, the inhibition of autophagy promotes cell proliferation, indicating that this process plays an inhibiting role in the earliest stages of tumor development. Later in tumor development, autophagy inhibits tumor cell apoptosis and promotes metastasis, allowing tumor cells to continue proliferating. Increasing evidence supports that autophagy can cope with intracellular and environmental stresses, such as hypoxia or nutrient shortage, thereby favoring tumor progression (42, 44). For instance, the ATG4B chemical inhibitor (a cysteine proteinase that activates LC3 which is crucial for OS development) may result in autophagy deficiency and a decreased proliferation *in vitro* and tumor growth *in vivo* (45). This indicates that autophagy is capable in promoting proliferation and resistance to anti-cancer therapy in OS tumor cells (46, 47). As a result, tumor cells can survive under conditions of hypoxia or nutrient deficiency *via* autophagy in advanced stages of tumor development. A recent study by Moscowitz et al. (48) suggests that hypoxia could promote resistance to irradiation by activating autophagy to accelerate the clearing of reactive oxygen species (ROS) in MG-63 human OS cells. These hypoxia-exposed OS cells displayed compartmental recruitment of GFP-tagged LC3 and restored the radiation sensitivity on autophagy inhibition, showing the possible causative link between hypoxia and autophagy. The regulating function does not just apply to radiotherapy-resistance. Zhang et al. (49) showed that CD271+ OS cells showed a higher autophagy activity than CD271- OS cells under hypoxia while autophagy deficiency in the CD271+ cells restored chemotherapeutic sensitivity and restricted the advantage of CD271+ OS cells in terms of tumorigenesis *in vivo*. Additionally, autophagy can promote tumor cell growth by inducing angiogenesis (50).

In contrast, autophagy can protect tumor cells from the damage of chemotherapy and/or radiotherapy; however, it can induce programmed apoptosis of tumor cells in response to antineoplastic drugs. Therefore, the complicated role of autophagy in tumor treatment is bidirectional and has been examined by a growing number of scholars. The results of a recent study (33) suggested that paxilitaxel and a HIF-1α inhibitor can be used to effectively improve OS chemotherapy in the future. This study illustrates that PTX induces autophagy through the HIF-1α pathway. Moreover, in rescue studies, co-treatment with the HIF-1α inhibitor YC-1 and autophagy inhibitor 3-methyladenine markedly blocked autophagy and blunted PTX resistance (33).

2.1.3 Hypoxic TME induces chemoresistance by modulating microRNAs

There is evidence that microRNA (miRNA) dysregulation is predictive of tumor progression and prognosis and contributes to tumorigenic processes (Table 2). HIF-1α has been identified as a direct target of miRNAs in multiple tumor types. For instance, the overexpression of miR-199a re-sensitizes cisplatin-resistant cells by inhibiting the HIF-1α pathway *in vitro* and *in vivo* (23). Furthermore, exogenous overexpression of miR-488 induced proliferation and suppressed sensitivity to doxorubicin in OS cells by targeting the tumor suppressor BIM (BH3-only protein, a mediator of apoptosis). Hypoxia can induce expression of miR-488, which is present in high concentrations in primary OS tissues and OS-derived cells, by binding to the hypoxia response element (HRE) in its promoter (28).

2.2 Immune cells within the TME modulate chemoresistance in OS

At the onset of carcinogenesis, immune cells infiltrate the TME. Intriguingly, the dynamic tumor immune landscape has a profound impact on tumor development and dissemination, and the activation state of immune cells within the TME can fluctuate.

2.2.1 Tumor-associated macrophages modulate chemoresistance in OS

Tumor-associated macrophages (TAMs) are key components of the TME and in most cases display tumor-suppressive properties and therapeutic response regulations. In solid tumors, TAMs are rooted in circulating monocytes rather than in proliferating resident macrophages within tumors. Monocytes in the bone marrow can enter neoplasms *via* the bloodstream and subsequently differentiate into macrophages. Based on their polarization condition, macrophages are classified as type M1 or M2. M1 macrophages differentiate in response to the Th1 cytokine interferon-gamma (IFNγ), whereas M2 macrophages are activated by Th2 cytokines, such as interleukin (IL)-4, IL-10, and IL-13 (51, 52). Similarly, M1 macrophages are generally considered to be cancer-fighting, while M2 macrophages promote carcinogenesis (53, 54). In fact, the TME plays a major regulatory role in the functional polarization of TAMs (54).

Chemotherapeutic agents may induce misdirected repair responses orchestrated by TAMs, contributing to limiting tumoricidal efficacy in drug applications (55). Compelling evidence has revealed that TAMs can mediate resistance to certain chemotherapeutics (5-fluorouracil, doxorubicin, paclitaxel, and platinum salts) and anti-VEGF (vascular endothelial growth factor) treatment *in vitro* and *in vivo* (56–59). Multiple mechanisms underlie the contribution of TAMs to chemoresistance: (i) several chemokines secreted by tumor cells increase the recruitment of immunosuppressive TAMs and suppress $CD8^+$ T cell responses during chemotherapy (60); (ii) TAMs develop the capacity to create a number of inhibitory cytokines, such as IL-1β, IL-6, IL-10, and TGF-β, consequently blocking the activation of an effective adaptive response and leading to T cell suppression in the TME (51, 61); (iii) TAM-derived cathepsins may mediate the activation of the nuclear factor-kappa B (NF-κB) signaling pathway and the signal transducer and activator of transcription 3 (STAT3) to facilitate therapeutic resistance (62–64); (iv) TAMs increase the tumor initiating potency of cancer stem cells (CSCs) and preserve CSCs from chemotherapy damages, thereby blunting chemotherapeutic responses (64); (v) by upregulating the enzyme cytidine deaminase that metabolizes the drug following its transport into cancer cells, TAMs can produce acquired resistance to chemotherapy (65).

Specifically, TAMs can activate STAT3, promote epithelial-mesenchymal transition (EMT), and upregulate matrix metallopeptidase 9 (MMP-9) in OS cells to facilitate chemoresistance. Evidence verified in animal models and OS patients demonstrated that TAMs possess the ability to induce OS cell migration and invasion by upregulating cyclooxygenase-2 (COX-2) and MMP9, phosphorylating STAT3, and promoting EMT (66). Shao et al. discovered that M2 TAMs enhanced the tumor initiation and stem-like capacity of CSCs by upregulating the number of CD117(+)Stro-1(+) cells accompanied by an increase in CSC markers (CD133, CXCR4, and Oct4) (67). This indicates that M2 TAMs induce OS cells to acquire stem cell characteristics and subsequently enhance the drug resistance of OS. Furthermore, evidence from this study suggest that the ratio of M1 to M2 macrophages could transform the OS chemoresistance by regulating the TME. Taken together, there is a growing interest in TAM-centered treatment regimens, which involve converting TAM-polarization from an M2 to M1 phenotype in the TME, transporting anticancer drugs into the TME *via* TAMs, suppressing the recruitment of monocytes and TAMs, and neutralizing the original tumor products of TAMs (68).

Based on the crucial role that TAMs play in OS growth and metastasis, many clinical trials were moved forward (Table 3). For instance, the use of mifamurtide (the liposome-encapsulated muramyl and macrophage-activating agent) as an effective immunomodulatory can greatly improve the event-free survival rate, suppress tumor proliferation, and induce cell differentiation by switching TAM-polarization from an M2 phenotype to M1 in patients with OS (69–72). Induced by IFN-γ, mifamurtide can activate macrophages to exert antitumor activities (73). In a phase II clinical trial, mifamurtide combined with chemotherapeutics (cisplatin, doxorubicin, methotrexate, and ifosfamide) promoted the elevation of the overall survival rate and progression-free survival (PFS) rate through the infiltration of activated

TABLE 3 Schematic diagram of progressive clinical trials on OS TAM-centered treatments.

Clinical trial	Phase	Combined drug	Interventions	Therapeutic target
NCT02441309	II	Ifosfamide + Mifamurtide	Group 1: mifamurtide alone; Group 2: ifosfamide alone for 6 weeks then ifosfamide + Mifamurtide for 6 weeks, then mifamurtide alone for 30 weeks; Group 3: ifosfamide + mifamurtide for 12 weeks then mifamurtide alone for 24 weeks. All participants will receive 36 weeks or more of mifamurtide.	Macrophage
NCT00631631	—	—	Mifamurtide (L-MTP-PE), intravenous, at a dose of 2 mg/m^2 twice weekly (at least 3 days apart) for 12 weeks, and then weekly for an additional 24 weeks, for a total of 48 doses in 36 weeks.	Macrophage
NCT03811886	I	Natalizumab	Traditional 3 + 3 escalation of natalizumab at a weight-based dosing 2 mg/kg not exceeding 300 mg. If no subjects experience a dose limiting toxicity (DLT), 3 more subjects are enrolled at the next dose of 3 mg/kg, not to exceed 300 mg. If no subjects experience a DLT, 3 more subjects will be enrolled at the next and final dose of 4 mg/kg, not exceeding 300mg.	TAMs
NCT01459484	II	Methotrexate, Cisplatinum, Doxorubicine, Ifosfamide + Mifamurtide	Group1: Chemotherapy for patients who over express ABCB1/P-glycoprotein:PRE-SUGERY TREATMENT: methotrexate:12 g/m2 (3cycles) + cisplatinum:120 mg/m2 (3 cycles), doxorubicin + ADM 75 mg/m2 (3 cycles); POST-SURGERY TREATMENT for good responder patients with positive PGLYCOPROTEIN:methotrexate 12 g/m2 (10 Cycles) cisplatinum 120 mg/m2; Doxorubicin 90 mg/m2 MEPACT 2 mg/m2 twice a week for the first 3 months the weekly for the next 6 months (total length of treatment: 44 weeks); POST-SURGERY TREATMENT for poor responder patients with positive P-GLYCOPROTEIN: methotrexate 12 g/m2; cisplatinum 120 mg/m2; doxorubicin 90 mg/m2, ifosfamide 15 g/m2 MEPACT 2 mg/m2 twice a week for the first 3 months the weekly for the next 6 months (total length of treatment 44 weeks);Group 2: high-grade osteosarcoma treatment for patients who do not over express ABCB1/P-glycoprotein: high-grade osteosarcoma that does not over express ABCB1/P-glycoprotein will be treated with a standard 3-drug regimen PRE-SUGERY TREATMENT: methotrexate: 12 g/m2 (3 cycles), cisplatinum: 120 mg/m2 (3 cycles) doxorubicin: ADM 75 mg/m2 (3 cycles) POST-SURGERY TREATMENT: methotrexate 12 g/m2 (10 cycles), cisplatinum 120 mg/m2; doxorubicin 90 mg/m2 (total length 34 weeks)	TAMs
NCT02584647	I	Sirolimus + PLX3397	Subjects with unresectable or metastatic sarcoma will take orally PLX3397 (600 - 1000mg) in combination with Sirolimus (2-6 mg) daily	TAMs
NCT02502786	II	GM-CSF + humanized anti-GD2 antibody: hu3F8	One cycle consists of treatment with hu3F8 at a dose of 2.4 mg/kg/dose for 3 days (day 1, 3, and 5) in the presence of subcutaneous (sc) GM-CSF (day 4 through 5). These 3 doses of hu3F8 and 10 days of GM-CSF constitute a treatment cycle. Cycles are repeated at ~2–4-week intervals between first days of hu3F8, through 5 cycles.	GM-CSF

macrophages in the adolescent OS group (71). To remodel the immune response, mifamurtide has been ratified by the European Medical Agency for the adjuvant chemotherapy of nonmetastatic OS (74). Additionally, the specific blocking of receptor-ligand binding between macrophages and OS cells may improve phagocytosis and antitumor effects of macrophages, and appears to be a promising strategy for cancer therapy. Colony-stimulating factor 1 receptor (CSF1R), which is capable of controlling the differentiation and survival of macrophages and is related to the prognosis of OS, can be selectively suppressed by pexidartinib (a novel small molecule tyrosine kinase inhibitor) (75, 76). Pexidartinib depletes TAMs and boost antitumor immune responses by blocking CSF1R and has been identified to be safe and well-tolerated in anti-cancer therapy (77, 78). It is currently being recruited for unresectable OS patients who are treated with pexidartinib combined with sirolimus (NCT02584647). In addition, the α4-integrin located on the surface of TAMs is able to bind to vascular cell adhesion molecule 1 (VCAM-1) that is expressed in the OS cytomembrane, resulting in the significant protection of OS cells from pro-apoptotic cytokines (79). Therefore, it would be effective to prevent tumor proliferation and metastasis in OS by using antibodies that are directed against α4-integrin, such as natalizumab (NCT03811886) (80).

Owing to the antitumor effects of macrophages in tumorigenesis, the application of immunomodulatory therapy is gaining increased attention. A variety of macrophage-related immune checkpoint inhibitors (ICIs) have been found to inhibit the proliferation and metastasis of OS through TAMs (Table 3). For instance, the transmembrane protein CD47, which is overexpressed in human OS samples, is an innate immune checkpoint and binds to the inhibitory receptor signal regulatory protein α (SIRPα) on the surface of TAMs, playing roles in the evasion of phagocytosis and cell mortality (81–84). Preclinical studies have indicated that CD47 may be a potential therapeutic target in OS treatment. The anti-CD47 monoclonal antibody may enhance the phagocytic effects of macrophages by restraining the interaction between CD47 and SIRPα in OS mouse models (84, 85). The efficacy of CD47 mAb + doxorubicin therapy demonstrates visibly increased TAM levels and their further phagocytic capabilities in mouse models of OS, resulting in an additive therapeutic effect (86). It was also confirmed that SIRPα knockout macrophages boost phagocytosis in an OS-bearing mice model (87). Although

clinical trials are performed with CD47/SIRPα blocking on multiple malignancies, such as B-cell lymphomas (NCT02953509), acute myeloid leukemia (NCT05266274), non-small cell lung cancer (NCT04881045), there are currently no ongoing registered clinical trials in OS using this concept. However, even without CD47 targeting drugs in OS therapy, these suggested strategies targeting CD47/SIRPα may still be an efficient treatment strategy in patients with OS (88).

2.2.2 Myeloid-derived suppressor cells modulate chemoresistance in OS

Myeloid-derived suppressor cells (MDSCs) are consisting of myeloid progenitor cells, immature macrophages, immature granulocytes, and immature dendritic cells. These cells expand during carcinogenesis and significantly suppress T cell responses (89). The regulatory mechanisms of MDSCs are related to multiple immunosuppressive factors in suppressing T cell-mediated antitumor immunity, including the production of ROS, inducible nitric oxide synthase (iNOS), COX-2, TGF-β, and arginase (90–92). In return, tumor cells secrete COX-2 and prostaglandin E2 (PGE2) to provoke MDSCs expressing arginase and iNOS (93). Due to the novel focus of MDSCs as the target in OS immunotherapy, several studies have been highlighted (Table 4).

For instance, Uehara et al. (98) found that metformin (Met) reduced the number of MDSCs in tumors, particularly polymorphonuclear MDSCs (PMN-MDSCs), which is independent of T cells. The molecular mechanism underlying this phenomenon involves decreased oxidative phosphorylation (OXPHOS) and increased glycolysis in the metabolism of MDSCs regulated by Met, suggesting that we should regard the regulation of metabolism of MDSCs as a potential therapeutic strategy. Additionally, the reduced reactive oxygen species (ROS) concentration and proton leakage in MDSCs and TAMs could be confirmed in the OS tumor model (98). Furthermore, to suppress T cell function, MDSCs not only remove the key nutrients for T cell proliferation and metabolism by freeing ROS, but also inhibiting the trafficking of CTLs into the tumor (101). A recent study (96) showed that OS tissues were infiltrated by MDSCs with the ability to inhibit CTL expansion. Moreover, MDSCs were CXCR4+, and migrated toward the stromal cell-derived factor-1 (SDF-1) gradient in the OS TME. The axis of CXCR4/SDF-1 may mediate reduced apoptosis of MDSCs by activating the downstream AKT pathway. The authors also note that the anti-PD-1 anti-body immunotherapy effect was strengthened by targeting CXCR4 in an OS murine model. Moreover, IL-18 induced MDSCs to infiltrate into the tumor parenchyma in an OS model, suggesting an IL-18 inhibitor as a potential strategy in MDSC-targeted immunotherapy in patients with OS (99). MDSCs play a crucial role in refractoriness to several chemotherapeutic agents, such as doxorubicin, cisplatin, and ifosfamide, which are standard treatments for OS (95, 102, 103).

A localized disease approach cure rate of nearly 70% is achieved, while a metastatic disease approach cure rate of less than 25% can be achieved. Hence, therapies that prevent OS metastasis are crucial to patients with OS. Using MDSC-targeted therapy for blocking OS metastasis may also be a possible

TABLE 4 A schematic diagram of promising therapeutic roles of MDSCs in OS.

Study. (year). Ref	Source	Mechanism	Promising therapeutic target
Ligon et al.(2021) (94)	tissue from OS patients	Targeting MDSCs suppressing T-cell infiltration into the PM of OS to block OS metastasis	Gene regulation
Deng et al.(2020) (95)	80 OS patients from database and 27 OS patients	Neoadjuvant chemotherapy reduce the MDSCs number and convert OS into an immune “hot” tumor.	MDSCs’ reduction
Jiang et al.(2019) (96)	K7M2 mouse OS model	OS-infiltrating MDSCs were CXCR4 positive and would migrate toward an SDF-1 gradient. The axis of CXCR4/SDF-1 could reduce the apoptosis of MDSCs.	MDSCs’ apoptosis induction
Shi et al.(2019) (97)	K7M2 mouse OS model	Combining SNA with anti-PD1 regulated innate immune cells, slowed OS tumor growth and prolonged survival time of tumor-bearing mice *via* inhibiting the function of MDSCs with a selective PI3Kδ/γ inhibitor to enhance responses to immune checkpoint blockade.	Supplement classical immunotherapy
Uehara et al.(2019) (98)	K7M2neo OS model	Met regulated the metabolism of MDSCs to decrease OXPHOS and enhance glycolysis to inhibit OS growth.	MDSCs’ metabolism
Guan et al.(2017) (99)	Mouse tumor model	IL-18 inducing MDSC to infiltrate into the OS parenchyma	MDSCs’ migration
Long et al.(2016) (100)	NSG mice	ATRA treatment enhances efficacy of GD2-CAR T cells against OS by eradicating monocytic MDSCs and diminishing the suppressive capacity of granulocytic MDSCs.	MDSCs’ reduction

treatment as MDSCs inhibit the infiltration of T-cells into the PMN, especially pulmonary metastasis.

Overall, both hypoxia and immune cells within the TME serve as basic modulators of OS chemoresistance. However, there is more involving the correlation between hypoxia and the immune landscape. Many scholars would like to further explore the impact and interplay of hypoxia and immunity within the TME.

2.3 Angiogenesis-mediated drug resistance in OS

The process of angiogenesis is complex, highly adaptive, and a hallmark of cancer, which is crucial for tumor growth, metastasis, and drug resistance. A variety of processes accompany angiogenesis, including endothelial cell proliferation, differentiation, migration, recruitment of smooth muscle cells, and maturation of blood vessels (104). An imbalance between pro- and anti-angiogenic signals in tumors can form an abnormal vascular network that typically displays dilated, convoluted, and hyperpermeable vessels, resulting in spatiotemporal heterogeneity in either tumor blood flow and oxygenation or increased tumor interstitial fluid pressure (105). Moreover, dysregulation of angiogenic and angiocrine activities can trigger altered bone homeostasis (106). The physiological consequences of these vascular abnormalities and the resultant microenvironment fuel tumor progression are conspicuous in the impaired efficacy of chemotherapy, radiotherapy, and immunotherapy (105). Apart from the influence of angiogenesis in hypoxia, acidity, and increased interstitial fluid pressure toward drug resistance, the abnormal vascular structure of OS also limits delivery of anticancer drugs (107). As chemotherapeutics must cross blood vessel walls and penetrate tumor tissues to kill cancer cells, anticancer drug distribution is asymmetrical. Therefore, a proportion of target tumor cells located proximal to tumor blood vessels receive a potentially lethal concentration of the cytotoxic agent (108). Consequently, the killing effect of the drug is limited.

Preclinical studies (109–112) of OS have shown that anti-angiogenic inhibitors transform the abnormal tumor vasculature into normal vasculature, characterized by attenuation of hyperpermeability, a normal basement membrane, increased vascular pericyte coverage, and a resultant decline in tumor hypoxia and interstitial fluid pressure. In return, the ameliorative vascular phenotype could favor the metabolic profile of the TME, delivery of chemotherapy agents, efficacy of radiotherapy and immunotherapy, and a diminution in metastatic cells shed by tumors into circulation in mice. Clinical trials (113–116) of targeted anti-angiogenic drugs have demonstrated that OS patients with a low OS vascularization phenotype have higher overall and relapse-free survival rates. Furthermore, patients with a low OS vascularization phenotype showed a better response to neoadjuvant chemotherapy than that of other patient groups.

Although combinatorial regimens of anti-angiogenic drugs and chemotherapeutic agents have been widely accepted, several clinical studies (117, 118) found that these combinations yielded unsatisfactory results. For instance, the observed histological response and event-free survival rate in a phase II trial did not support further evaluation of the combination of chemotherapy and bevacizumab in OS (119). This may be due to the anti-angiogenic therapy itself. Although the abnormal structure and function of cancerous vasculature leads to an anoxic microenvironment and increases the difficulty of drug delivery, it is one of the main routes for immune cells as well as chemotherapy agents to travel through the blood vessels. Hence, the inhibition of vascular production affects the delivery and final efficacy of anticancer drugs.

Notably, cells and structures integrated within the TME strongly shape the functions of one another, modulating antitumor therapy. For instance, pre-existing blood vessels fail to perfuse the tumor sufficiently during tumor growth; thus, a microenvironment deficient in oxygen and nutrients is formed where metabolites and immunosuppressive modulators accumulate (120). The resultant anoxic microenvironment stabilizes HIF-1α or HIF-2α, subsequently activating PDK1 and LDH-A, promoting an acidic extracellular environment (121, 122). Furthermore, HIF-regulated vascular endothelial growth factors can induce angiogenesis (121). In addition, hypoxia alters cellular metabolism and regulates expression of several immunomodulatory molecules, thereby influencing the infiltration and phenotype of immune cells (122–124). Other hypoxia-driven signals affect immune cells as well, such as acidic environments, cytokines, and nutrient fluctuations. Thus, it seems that there is a complex and powerful relationship among anoxic and acidic environments, the tumor vascular system, and immune cells, orchestrating cellular progression and metastasis, ultimately leading to drug resistance (125).

All TME components mentioned above play important roles in drug resistance in OS therapy. Given the barriers involved in chemoresistance, novel therapeutic approaches to treat OS is urgently needed. In the present review, we summarize the effects and mechanisms of the TME in terms of chemoresistance in OS. Moreover, we pay considerable attention to immune cells, a key component of the TME, as a valid strategy to address drug resistance due to the clinical success of emerging ICIs in immunotherapy. A detailed analysis of other popular treatment regimens is beyond the scope of this manuscript. Thus, suggest that those interested in reading other comprehensive reviews to find them elsewhere (126, 127). The current review highlights the therapeutic potential of immunotherapy in the management of OS. Herein, we review recent advances in promising new immune checkpoint targets

for their use in the improvement of chemoresistance and treatment effects in OS therapy.

3 Immunotherapy: A promising therapeutic option for OS

Efficacious cancer treatment remains challenging due to chemoresistance and toxicity. Therefore, limited success can be achieved with traditional chemotherapy. Tumor cells induce TME to suppress antitumor immunity, and immunosuppressive cells and cytokines constitute the extrinsic factors of tumor drug resistance. Today, immunotherapy is regarded as a promising and revolutionary therapeutic option for multiple cancers and has received considerable attention. The discovery of cancer therapy through inhibition of negative immune regulation was recognized with the 2018 Nobel Prize. Detailed classification of the main tumor-infiltrating immune cell lineages is shown in Figure 1.

Human antibodies targeting immune checkpoint proteins are used to break immune tolerance and activate T cell responses. These antibodies are called ICIs and include cytotoxic T lymphocyte associated protein 4 (CTLA4), programmed death-1 (PD-1), and programmed death-ligand 1 (PD-L1) (128–130). A variety of methods such as adoptive T cell transfer (ACT), STING agonists, and cancer vaccines leverage the immune system to assis in recognizing and rejecting tumors. However, recent studies have highlighted that the TME can inhibit the functions of immune cells to favor immunological resistance and suppress antitumor effector functions, indicating the interwoven relationship between the TME and immunotherapy (131–133).

In addition, diverse strategies have been proposed to either enhance the function of antitumor effector cells or to dampen the protumor activities of immunosuppressive cells (134). In the following section, we will present a general review of current state-of-the-art immunotherapies as well as the obstacles that must be addressed to increase their efficacy.

3.1 Application of ICIs

To reactivate the immunological response of T cells and restore immune activity in the TME, a single or combined dose of ICIs inhibits the transmission of immunosuppressive signals, eventually contributing to the antitumor effect. Two types of ICIs have been approved by the FDA thus far: CTLA4 (ipilimumab) as well as PD-1 (nivolumab and pembrolizumab) or PD-L1 (atezolizumab) (135). Owing to the high response rates of prolonged duration among certain subsets of melanoma, non-small-cell lung cancer, and renal-cell carcinoma, the desire to establish new clinical trials for OS has increased (136–139). Of note, this enthusiasm should be moderated because of the hysteretic anti-OS drug testing meditated by ICIs. The insensitive effect for OS treatment has been revealed according to the preclinical studies showed in anti-PD-1 monotherapy (140). It is of great value to evaluate the role of chemoresistance to therapeutic ICIs in OS and to enhance the sensitivity of OS tissue to anti-PD-1 monoclonal antibodies. Therefore, more research is required to design successful endogenous antitumor activity and a prospective application to improve tumor immunogenicity. Significantly, the factors determining the remarkable efficacy of ICIs may include but are not limited to T cell intratumoral distribution, expression of PD-1/PD-L1, tumor antigenicity, and fitness of tumor-infiltrating T cells (127).

3.1.1 PD-1/PD-L1 in OS

PD-1 (CD279) is expressed on the surface of activated CD8+ T cells, B cells, and NK cells (141). The ligands of PD-1 are PD-L1 (CD274 or B7-H1) and PD-L2 (CD273 or B7-DC), which are typically expressed on the surface of APCs, tumor cells, and tumor-infiltrating lymphocytes (TILs) within the TME (141). The engagement of PD-1 and PD-L1/PD-L2 results in a negative signal for the inhibition of cytokine secretion and lymphocyte proliferation, interferes with the formation of immunological synapses, and inhibits T cell receptors (TCRs) (142, 143), resulting in an attenuated antitumor immune response (Figure 2).

Studies involving PD-1, PD-L1, and TIL expression in OS cell lines and tumor tissues are listed in Table 5 (139, 144–151). According to a series of studies, in 15 patients with OS, biopsy samples demonstrated PD-1 and PD-L1 expression (47 and 53%, respectively) and metastases samples showed 40 and 47%, respectively, whereas resection samples showed no expression at all, indicating that biopsy or metastatic samples are most useful in determining whether PD-1 and PD-L1 are active (152). Using flow cytometry, PD-1 expression was measured in 56 OS patients and 42 healthy donors, revealing that PD-1 expression was significantly upregulated in both peripheral CD4+ and CD8+ T cells in OS patients (150). Furthermore, cases with metastasis had a higher proportion of PD-1 expression in CD4+ T cells (150), particularly within the lung (153). Moreover, researchers have suggested that in the stage III cases, the expression quantity of PD-1 on CD4+ T cells was significantly increased. PD-1 expression on CD8+ T cells varied with tumor stage, as it began to increase from stage II onward. These results (150) showing dysregulated PD-1 expression in patients with OS suggests its critical role in the development of this disease. Additionally, although PD-L1 expression in OS cell lines varies widely from low to high, doxorubicin-resistant OS cells seem to express higher PD-1 than that of non-resistant wild-type cells (154).

There have been promising results in preclinical OS mouse models where the PD-1 and PD-L1 pathways have been blocked. In a mouse model of metastatic OS, the function of T cells can be

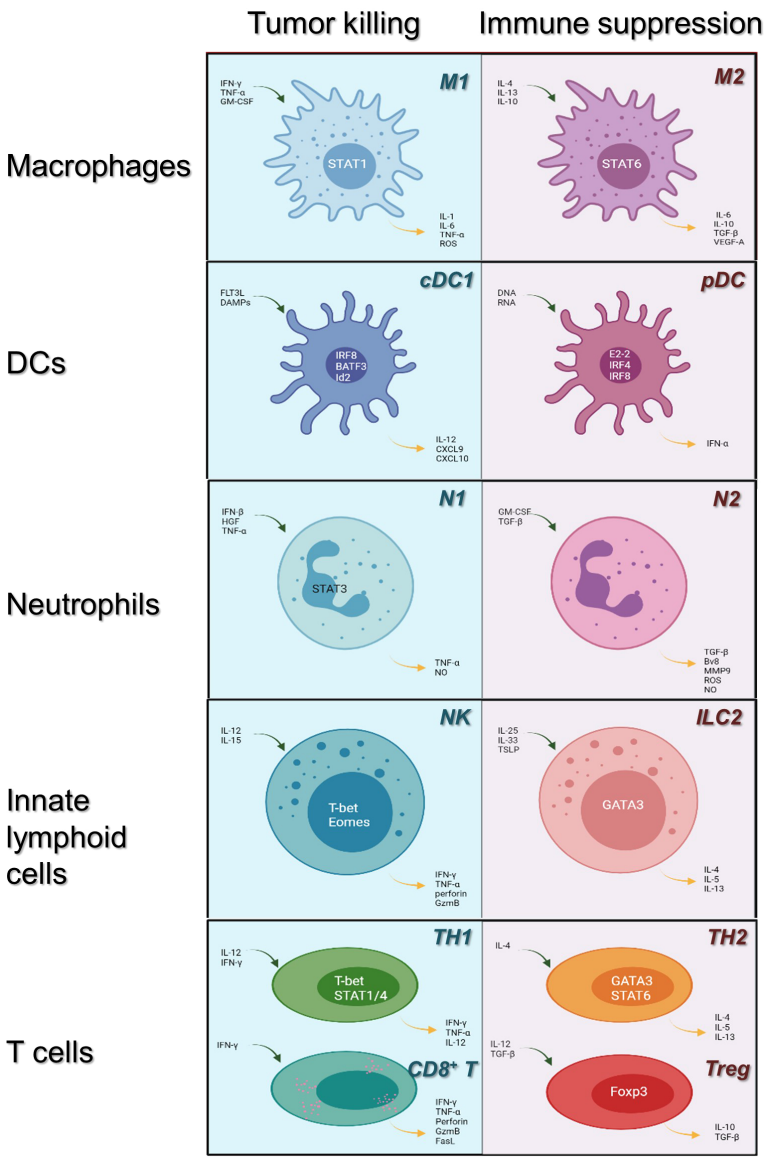

FIGURE 1
Immune cells in the tumor microenvironment: roles in tumor killing and immune suppression. Immune cells may evolve into antitumor or pro-tumor phenotypes in response to their microenvironment. Here, we review the category of the major innate immune cell lineages (in rows) based on their roles in tumor killing and immune suppression (light blue, left; pale red, right, respectively). Main transcription factors occupy the center of each cell; blue arrows indicate cytokines upstream of each phenotype, whereas yellow arrows indicate downstream cytokines. cDC1, conventional dendritic cells 1; pDC, plasmacytoid dendritic cells; NK, natural killer cells; ILC 2, innate lymphoid cell type 2; TH1/2, $CD4^+$ T helper cell types 1 or 2; CD8+ T: CD8+ T cells; Tregs: CD4+ regulatory T cells.

significantly activated by interactions with the PD-1/PD-L1 antibody *in vitro* and *in vivo*, consequently resulting in an increased survival rate (155). In a humanized mouse model, Zheng et al. (156) confirmed that nivolumab restrained OS metastasis by boosting CD4+ and CD8+ lymphocytes as well as the cytolytic activity of CD8+ T cells in the lung. This indicates that the PD-1 blockade effectively controlled OS pulmonary metastasis but did not affect primary lesions *in vivo*. When given sequentially and continuously, anti–PD–L1 combinatorial treatment (atezolizumab) with GD2– or HER2 –BsAb enhanced T cell function *in vivo* and improved tumor control and survival time in the OS mouse model (157).

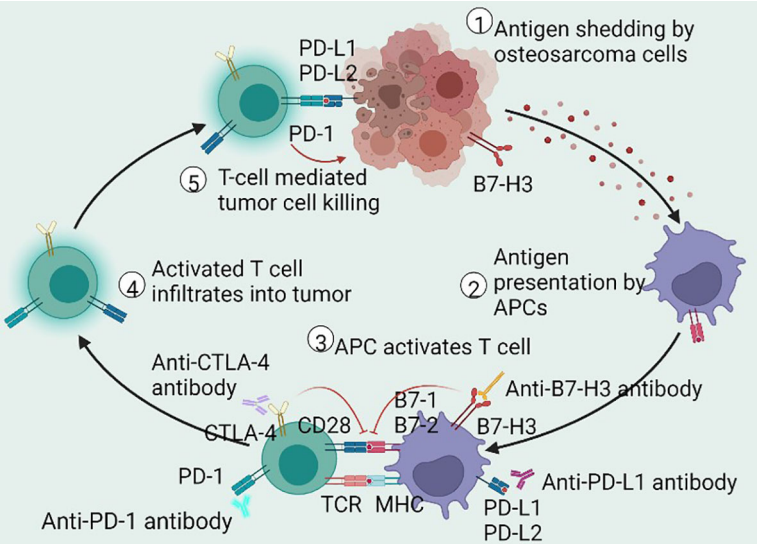

FIGURE 2
Schematic of antitumor immune cycle. The immune cycle starts from the production of neoantigens in dying or dead OS cells, endocytosed by APCs for presentation or cross-presentation on MHC. Then, the antigen-loading APCs migrate to the draining lymph nodes to activate antigen-specific T cells. Activated T cells then infiltrate the tumor cells to drive adaptive immune response and to restrain tumor growth. These antitumor immune responses are modified by immune checkpoint mechanisms. The interaction of PD-1 and PD-L1 inhibits intracellular signaling pathways on T cell activation, whereas CTLA-4 prompts inhibitory effects by competitively depriving CD28 ligand and mechanistically binding B7 molecules. Antibodies that affect ICIs may sustainably stimulate the antitumor immune response in patients with OS. OS, osteosarcoma; APCs, antigen-presenting cells; MHC, major histocompatibility complex; PD-1, programmed cell death receptor-1; CTLA-4, cytotoxic T lymphocyte-associated protein 4; B7-H3, B7 homolog 3; PD-L1/PD-L2, programmed cell death receptor-1/2 ligand; ICIs, immune checkpoint inhibitors.

Furthermore, Liu et al. (158) revealed that atezolizumab suppressed tumor proliferation and induced immune-independent apoptosis of OS by impairing intracellular mitochondria, resulting in increased ROS and cytochrome-c leakage, subsequently activating the Jun N-terminal kinase (JNK) pathway to give rise to apoptosis.

As for clinical trials, compared to the objective response rate (ORR) (18%) of the advanced soft tissue cohort, the ORR in the bone sarcoma cohort was 5% with 1PR/22 in OS within the open-label multicenter phase II trial of pembrolizumab (SARC028) (159). This study showed that the activity of the anti-PD-1 immunotherapy in bone sarcomas was limited because of the ineffective ORR. In another phase II trial in advanced OS (Norway/Rizzoli collaboration trial, NCT03013127), pembrolizumab was well-tolerated but only demonstrated minor clinically significant antitumor activity (160). We summarized the clinical trials using ICIs for patients with OS in Table 6.

3.1.2 CTLA-4 in OS

CTLA-4 (CD152) is a transmembrane glycoprotein primarily expressed by T cells (161). In the immune cycle, T cells can be activated when antigens are presented to TCRs by MHC-I or MHC-II, which is amplified by a costimulatory signal in the form of the co-activating receptor CD28 binding to CD80 (B7–1) and CD86 (B7–2) expressed on antigen-presenting cells (APCs) (162). CTLA-4 can bind to CD80/CD86. Due to the greater affinity of CTLA4 to B7 proteins than to CD28, CTLA4 delivers inhibitory signals of T cell proliferation to downregulate immune responses by preventing the binding of CD28 with CD80/CD86 in the priming phase (135), as shown in Figure 2. CTLA4-mediated inhibitory signaling is complex and occurs within the lymph nodes, whereas it is generally in the peripheral tissue where PD-1-mediated inhibitory signaling takes place. Although CTLA4 and PD-1 signals inhibit the activity of AKT signaling pathways, the targeted signaling molecules are disparate. CTLA4 signaling dampens T cell activation pathways by interacting with IL-2, serine/threonine phosphatase PP2A, and SHP2, which directly dephosphorylates CD3ζ (163). In addition, recent studies have revealed a significant association between CTLA4 genetic polymorphisms and susceptibility to OS (164, 165).

In another notable study, scientists tested combinatorial anti-CTLA-4 and anti-PD1/PD-L1 therapy in an animal model of metastatic OS, showing that this regimen resulted in the complete control of tumors and immunity to further tumor inoculation (166), suggesting that such therapy may be more beneficial than stand-alone monotherapy. In addition, the CTLA-4 antibody, which combines with dendritic cells, can decrease the level of

TABLE 5 Studies of PD-1/PD-L1 expression in OS.

Study	Samples	Detection techniques	Positive Expression of PD-1/PD-L1	Clinical guide
Chen et al. (2020) (139)	15 OS patients	IHC	Biopsy samples (PD-1 47% and PD-L1 53%); none in resections; metastases samples (PD-1 40% and PD-L1 47%)	Assessment of PD-1/PD-L1 in biopsy or metastatic specimens have clinical value in predicting therapeutic response.
Torabi et al. (2017) (144)	OS samples	Western blot	Positive PD-L1 expression	—
		qRT-PCR	More content of PD-1 mRNA	—
	26 OS samples	IHC	PD-1 detected in all tissue samples	—
Costa Arantes et al. (2017) (145)	9 oral OS patients of 13	IHC	High positive expression of PD-L1	No significant correlation of PD-L1 gene expression with clinicopathologic features.
Sundara et al. (2017) (146)	85 samples	IHC	Positive rate of PD-L1 is 27.8%	Higher expression of PD-L1 was detected in metastatic lesions (48%)
Koirala et al. (2016) (147)	Cell lines	Western blot	Positive rate of PD-L1 is 40%	Primary OS tumor expressing PD-L1 were more likely to contain cells that express PD-1.
		qRT-PCR	Positive rate of PD-L1 mRNA is 75% within 21 cell lines	—
	107 tissue samples	IHC, flow cytometry	Positive rate of PD-L1 mRNA is 67% within tumor specimens	Expression level of PD-L1 is connected with the presence of T cells, DCs and NK cells.
		Western blot	Positive rate of PD-L1 is 30% within patient samples	—
Lussier et al. (2015) (148)	16 patients	IHC	Positive rate of PD-L1 is 75% within the metastatic OS	Metastatic tumors can tolerize infiltrating T cells within TME by PD-L1 interactions
Chowdhury et al. (2015) (149)	15 OS patients of 115 pediatric tumors	IHC	Positive rate of PD-L1 expression is 47% among OS patients	Patients expressing PD-L1 showed distinctly better survival
Zheng et al. (2015) (150)	56 OS patients	IHC, flow cytometry	High expression level of PD-1 is detected in peripheral CD4+ and CD8+ T cell within OS patients	PD-1 is involved in tumor progression.
Shen et al. (2014) (151)	OS cell lines	qRT-PCR, IHC, flow cytometry	There is slightly higher PD-L1 expression of drug-resistant variants OS cell lines in comparison with that in parental cell lines	—
	38 patients with OS	qRT-PCR, IHC, flow cytometry	High PD-L1 expression level (23.7%)	—
			Intermediate PD-L1 expression level (50%)	Median survival time is 89 months at low levels of PD-L1 but is only 28 months at high levels of PD-L1.
			Low PD-L1 expression level (10.5%)	PD-L1 expression is distinctly related to TIL expression.
			Negative PD-L1 expression level	Pulmonary metastatic cases showed higher PD-L1 expression than that of the non-pulmonary metastatic lesions.

*OS, osteosarcoma; PD-1, programmed cell death receptor-1; PD-L1, Programmed cell death receptor-1 ligand-1; IHC, immunohistochemistry; qRT-PCR, quantitative real time polymerase chain reaction; DCs, dendritic cells; NK cells, natural killer cells; TME, tumor microenvironment; TILs, Tumor-infiltrating lymphocytes.

CD4+ regulatory T cells (Tregs) and increase the concentration of cytotoxic T cells in metastatic OS mice for tumor suppression (167, 168). In a phase I trial with ipilimumab, four of 33 patients with advanced pediatric solid tumors (including eight OS patients) confirmed stable disease and two patients had unconfirmed stable disease by standard RECIST criteria, indicating that there is no objective tumor regression under the treatment with ipilimumab (169). Recent meta-analysis showed that CTLA-4 is significantly associated with OS risk and may play a crucial role in carcinogenesis of OS (164, 170). A full description of the clinical trials is provided in Table 6.

In summary, although the application of PD-1 or PD-L1 antibodies showed promising outcomes in suppressing tumor growth in an OS mouse model, the effects of ICIs had limited therapeutic benefit for patients with OS in clinic trials. Unfortunately, there have been no current breakthroughs in clinical trials involving new drugs developed for this dilemma. However, mifamurtide was shown to improve overall survival in a phase III trial (70). Moreover, mifamurtide would promote immune cell to infiltrate into OS metastases, consequently improving the efficacy of anti-PD-1 antibodies (171).

TABLE 6 Clinical trials of immune checkpoints inhibitors for patients with osteosarcoma.

Clinical trial	Phase	Treatment	Intervention	Immunotherapy targets
NCT02301039 (SARC028)	II	Pembrolizumab	Pembrolizumab will be administered i.v. at 200 mg every 3 weeks	PD-1
NCT03013127	II	Pembrolizumab	Pembrolizumab 200 mg i.v. every 3 weeks for up to 35 cycles	PD-1
NCT05182164 (PEMBROCABOSARC)	II	Pembrolizumab + Cabozantinib	Pembrolizumab will be administered i.v on day 1 every 3 weeks (200 mg). Cabozantinib will be administered per OS once daily (40 mg)	PD-1
NCT02500797	II	Nivolumab	Patients receive nivolumab i.v over 30 minutes once every 2 weeks. Cycles repeat every 42 days for up to 108 weeks in the absence of disease progression or unacceptable toxicity. Patients who progress after 10 weeks on single agent nivolumab may elect to cross over to Arm II.	PD-1
NCT03628209	I/II	Nivolumab + Zacitidine	Participants will be treated with nivolumab i.v., 3 mg/kg on days 1 and 15 of each cycle. Phase I Dose Escalation - Dose level 1: NA. Dose level 2: 60 mg/m^2. Dose level 3: 75 mg/m^2. Phase II Expansion - Treated at recommended Phase II dose (RP2D).	PD-1
NCT04803877	II	Regorafenib + Nivolumab	Regorafenib 40 mg + 480 mg i.v. over 30 min every 28 days for patients aged 18 and older; regorafenib 20 mg + nivolumab 3 mg/kg (maximum dose 240 mg) will be administered i.v. over 30 minutes on day 1 and 15 of each 28-day cycle for subjects younger than 18 years;	PD-1
NCT02304458	I/II	Nivolumab + Ipilimumab	—	PD-1 + CTLA-4
NCT05302921	II	Nivolumab + Ipilimumab	Nivolumab and ipilimumab will be given on day 1 of 21-day cycles for cycles 1-4, followed by nivolumab alone on days 1 and 15 of 28-day cycles for cycles 5+. Patients will receive up to 13 cycles of therapy unless unacceptable toxicity or progression of disease.	PD-1 + CTLA-4
NCT05019703 (TACOS study)	II	Atezolizumab + Cabozantinib	Patients receive atezolizumab IV over 60 minutes on day 1 and cabozantinib PO QD on days 1-21.	PD-L1
NCT01445379	I	Ipilimumab	Ipilumumab given on day 1 of a 21-day cycle for 4 cycles, from cycle 5+	CTLA-4

*IV, Intravenous; OS, osteosarcoma.

3.1.3 T cell immunoreceptor with Ig and ITIM domains in OS

T cell immune checkpoint molecules may be prospective immunotherapeutic targets for tumor therapy. Currently, anti-T cell immunoreceptor with Ig and ITIM domains (TIGIT) therapies are considered curative checkpoint markers because of their potential to treat hepatocellular carcinoma and breast cancer by modulating CD8+ T cells, Tregs, and NK cells (172, 173). Wang et al. showed that macrophage M1 types, which are highly infiltrated in metastatic cases, could predict the overall survival and disease-free survival of OS, which would be positively connected to immune checkpoints PD-L1, CTLA4, and TIGIT (174). Zhou et al. (175) revealed that TIGIT was widely expressed in CD8+ T, CD4+ T, and NK cells, and that Tregs showed high immunoinhibitory molecules involving TIGIT in OS through bioinformatics analysis, indicating that TIGIT blocking may be a promising avenue for OS treatment. In addition, peripheral blood CD3+ T cells were isolated from OS tissues with high and low infiltrated TIGIT+CD3+ T cells respectively for the detection of cytotoxic activities of the CD3 + T cells. These results (175) suggest that the TIGIT-blocking antibody substantially reinforced the cytotoxicity of CD3+ T cells to promote the death of OS cells, demonstrating the possibility of TIGIT inhibition for future OS therapies.

3.1.4 Indoleamine 2,3-dioxygenase in OS

The beginning and rate-limiting stages of the kynurenine pathway in the metabolism of the essential amino acid tryptophan are catalyzed by the intracellular enzyme indoleamine 2,3-dioxygenase (IDO) (176). The biological function of IDO involves the protection of tumor cells by inhibiting attacks from T cells (177). High expression of IDO was observed in multiple tumors, such as pulmonary, colorectal, and melanoma (178–180), indicating a clinical adverse prognostic factor (179). Liebau et al. (181) demonstrated for the first time that IDO was activated by IFN-γ in four human OS cell lines and concluded that IDO was highly expressed in human OS cells. Urakawa et al. also confirmed these findings (182). Furthermore, the authors revealed that elevated IDO expression in OS was associated with metastasis and a poor clinical outcome in patients by univariate analysis.

However, the multivariate analysis has been particularly disappointing, showing that there was no discernible link between IDO expression and metastasis-free survival or overall survival. Taken together, IDO may be a reliable and promising prognostic predictor and has the potential to become a novel molecular target in the therapy for OS. At present, more research is required to undertake the challenges of improving immunotherapy efficacy.

3.2 Adoptive T cell transfer in OS

ACT refers to collecting innate T cells from cancer patients, expanding or genetically engineered them *ex vivo*, and retransferring them back into the patient with the intent to specifically kill cancer cells. There are currently three major modalities of ACT: TILs, engineered T cell receptor (TCR) T cells, and chimeric antigen receptor (CAR) T cells. Among these three categories, CAR T cell therapy has facilitated transformational advancements in the management of cancer treatments. For instance, the impressive results of CAR-T therapy trials prompted its usage by the FDA in refractory large B cell lymphoma and acute lymphoblastic leukemia (183, 184). For OS, clinical trials have been performed with several promising target antigens. For instance, HER2-CAR T cells proved to be therapeutic for OS through xenograft *in vitro* and *in vivo* models. Phase I/II clinical trials were conducted by applying CAR-T therapy in patients with relapsed/refractory HER2-positive sarcoma, with 16 enrolled OS patients (84%) (185). Out of these 16 patients, none (100%) had an objective response. Three patients (19%) had stable disease for 12–15 weeks while 11 patients (69%) had progressive disease. The value of this study is that it confirms that dose-limiting toxicity is not observed in HER2-CAR T cell reception, which prepares for additional studies that combine ACT with other anticancer treatments to enhance their expansion and persistence. Presently, breakthrough successes have been achieved in the clinic for hematological malignancies and have gained interest in developing ongoing trials to extend CAR-T therapy application to solid tumors as well as its usage beyond cancer. Additionally, T lymphocytes expressing CAR or TCR can recognize a wide range of antigens and are not restricted to tumor-specific antigens due to retaining their endogenous TCR expression (127). Therefore, autoimmune diseases or other immune-mediated hyper-responses may be triggered in patients undergoing ACT.

3.3 Targeting NK cells in OS

A strategy that incorporates NK cells into OS treatment represents a promising immunotherapeutic approach to boost tumoricidal properties. Although activated NK cells can express PD-1 (186) and CTLA4 (187), more research is required to determine whether ICIs directly affect NK cells. It has been reported that anti-PD-1 treatment can re-engage NK cell antitumor responses in multiple myeloma (188). Furthermore, blockade of CTLA4 or release of cytokines can overcome the stagnancy in NK cell antitumor responses (161). Clinical trials (189) have shown that NK cells may have the potential to attack and eliminate cancer cells for OS prevention and treatment response. Compared to normal controls, the quantitative observation of lower-level NK cell defects in peripheral blood of patients with OS indicated the regulatory role of NK cells in human autoimmunity and OS tumor development. NK cell antitumor activity is determined by reactivity and inhibition of NK cells and their engagement by cognate ligands toward target tumor cells (190). Metastatic and primary OS cells are susceptible to activated/expanded NK cell lysis both *in vivo* and *in vitro*, which relies on heterogeneous interactions between the NK group-2 member D (NKG2D) receptor and NKG2D ligands (NKG2DL) (191). In other words, NK cells can kill OS cells, including the tumor-initiating cell (TIC) compartment, in an NKG2D–NKG2DL dependent manner. In addition, the NK cell-derived NK-92 cell line has been genetically modified to express CARs that target both hematological malignancies and solid tumor antigens in preclinical and clinical trials (192), such as GD2 on neuroblastomas (193) or HER2 on neoplasms (194).

However, despite these conflicting results, several hindrances need to be overcome to maximize the curative effects of NK cell-based immunotherapies. Such obstacles include patients needing to be injected with a large number of cells, the lack of cellular memory, poor NK cell infiltration of solid tumors, limited expansion *in vivo*, and systemic toxicity of cytokines such as IL-2 (195, 196). Hence, to optimize NK cell infiltration and performance in solid tumors, it is imperative that strategies be developed to address these issues.

4 Discussion

OS is the most common malignant bone tumor. Although OS is sensitive to some chemotherapeutic drugs, cancer cells may develop chemoresistance. Although advances in neoadjuvant chemotherapy and their rapid and wide applications have a crucial impact on the overall survival rate of patients with OS, their overall survival rate has not significantly improved over the last 30 years. Similarly, the prognosis of patients with metastatic or recurrent OS remains poor, with an overall five-year survival rate of 20% (197). Current standard treatment for OS therapy is the delivery of chemotherapeutic agents such as high-dose methotrexate, doxorubicin, and platinum salts. However, clinical outcomes from chemotherapy have been reported to be unsatisfactory in recent studies. To date, there have been no obvious breakthroughs in clinical trials of new drugs developed for this dilemma. Furthermore, many clinical trials have found that the efficacy of most promising targeted therapies is very poor and far below expectations (198–202).

The main reasons for the lack of development of OS therapy include tumor heterogeneity, chemoresistance, and the lack of discovery of tumor-specific antigens (TSA) in OS. Some studies have emphasized that the TME is involved in the proliferation and migration of cancer cells (199, 203). Despite vital improvements made in preclinical trials, many clinical trials

targeting the TME to suppress tumor growth or improve drug resistance have failed to show promising efficacy in multiple cancers. The only exception is immunotherapy, including the usage of ICIs (15). In fact, most anticancer therapies act on immune regulatory factors that comprise part of the TME. The immune microenvironment should also be regarded as a clinical treatment option. Furthermore, these cells and molecules that constitute the OS microenvironment may improve the chemoresistance and enrich potential therapeutic targets for OS therapy, such as blood vessels, T cells, and macrophages (198, 204–206). Given the barriers of OS treatment involved in chemoresistance, novel therapeutic approaches to treat OS is urgently needed. The immune system is a significant part of the OS microenvironment, in which cytokines are closely related to the development and dynamic balance of bone cells. As a novel antitumor model, immunotherapy benefits from the immune system in a subtle way to improve anticancer treatment efficacy. Finding biomarkers that can be used to predict responses is a leading difficulty in immunotherapy but would help determine the best possible treatment options. Multiple tumor immune phenotypes (PD-1 or PD-L1 expression), somatic genomic characteristics (mutational burden and microsatellite instability), the gut microbiome (207), and the HLA class I genotype (208) have all been proposed as predictors of responses to checkpoint inhibitors.

4.1 Mechanisms of unsatisfactory effects of ICIs against OS

Though ICIs such as PD-1 or PD-L1 showed promising results in preclinical research, OS showed minor tumor regression with the usage of ICIs based on the current clinical trial results listed in Table 6. The main reason for the unsatisfactory effects of PD-1 antibodies can be summarized into four points: 1) insufficient immunogenicity of TSA: the lack of highly immunogenic TSA resulting in the inability of T cells to recognize tumor cells. A higher burden of nonsynonymous mutations with durable clinical benefit displayed in patients with non-small cell lung cancer treated by anti-PD-1 through exome sequencing (209). Therefore, we hypothesized that tumors with high mutational burden have a higher probability of producing more neoantigens with sufficient immunogenicity to induce antigen-specific T cell responses; 2) dysfunction of MHC: variable PD-L1 expression and frequent loss of MHC I facilitates immune evasion of OS cells. The mutation of beta 2-microglobulin (β2-GM) led to dysfunctional antigen presentation of HLA I complexes, which were active in the MHC I pathway, resulting in the weakening cytotoxicity of T cells (210); 3) paucity of CD8+ T cells: shortage of CD8+ T cells upregulated multiple inhibitory receptors, such as CTLA-4, PD-1, T cell immunoglobulin, mucin domain 3 (TIM-3), T cell immunoglobulin, TIGIT, and lymphocyte-activation gene 3 (LAG-3), as well as by producing immunosuppressive cytokines or other soluble factors (211, 212); 4) inhibition of the TME: immunosuppressive mechanisms in the TME involve the suppressive action of Tregs, MDSCs, TAMs, or other undefined cells, and the specific mechanism of these cells as mentioned above. Furthermore, cytokines and tumor-derived chemokines would also meditate drug resistance by recruiting immunosuppressive cells into the TME (213).

4.2 Future perspectives

Targeting components of the TME, such as immune cells, immunosuppressive cytokines, and inhibitory receptors of T cells may be a novel therapeutic approach to improve the dilemma of drug-resistance and the unconspicuous OS tumor recession. Although the significant breakthroughs toward improving outcomes of TME target therapies have been made *in vitro* and *in vivo*, promising efficacy in human OS patients remains to be seen. In multiple malignancy, immunotherapy is the jewel in the crown because of its the unique exception of feeble TME targeting therapy (15). Therefore, immunotherapy involving ICIs could be an effective and alternative tact to avoid the hindrance faced in OS treatments. For the success of OS immunotherapy, it is necessary to expound the mechanism of immunosurveillance, confirm TSA for OS, and conduct collaborative multicenter research.

Several biological features of OS imply that modulation of the immune response regulation may be beneficial. However, nuances within the specific TME and the complexity of the immune system make it an extremely challenging work. As seen with conventional chemotherapy drugs, tumors utilize multiple pathways to resist immunotherapy, suggesting that combinatorial approaches targeting multiple pathways will be explored to achieve robust responses. Chemotherapy, radiotherapy, tumor-vaccines, and ICIs, or compatibility with ACT, may yield meaningful clinical benefits. Additionally, in the OS microenvironment, Tregs, TAMs, and MDSCs could play crucial roles in immunoreaction with overactivated inhibitory receptors including PD-1, CTLA-4, and TIGIT. In order to develop targeted immunotherapies through utilizing those immunologic markers in intratumoral microenvirenments, we must better understand and characterize the OS immune system. Other adults strategies explored, including the combination of PD-1 agents and IDO since IDO has been shown to inhibit T-cell proliferation and induce Tregs, among other immunosuppressive properties. The ubiquitous expression of IDO in primary OS may make the combinatorial strategy more attractive for OS treatments.

A more comprehensive understanding of the mechanisms of resistance is likely to be required for the development of effective

therapies for patients with OS, identifying predictive biomarkers to help guide the appropriate usage of these treatments, as well as developing rational combinatorial treatments to overcome such resistance. Despite many challenges, there is hope that immunotherapy will lead to breakthroughs that will revolutionize OS therapy.

Author contributions

LY, JZ, and YL substantially contributed to the conception, drafting, editing, and final approval of this manuscript. All authors contributed to the article and approved the submitted version.

Conflict of interest

The authors declare that the research was conducted in the absence of any commercial or financial relationships that could be construed as a potential conflict of interest.

Publisher's note

References

1. Mirabello L, Troisi RJ, Savage SA. International osteosarcoma incidence patterns in children and adolescents, middle ages and elderly persons. *Int J Cancer* (2009) 125(1):229–34. doi: 10.1002/ijc.24320

2. Siegel RL, Miller KD, Fuchs HE, Jemal A. Cancer statistics, 2021. *CA: Cancer J Clin* (2021) 71(1):7–33. doi: 10.3322/caac.21654

3. Mirabello L, Troisi RJ, Savage SA. Osteosarcoma incidence and survival rates from 1973 to 2004: data from the surveillance, epidemiology, and end results program. *Cancer* (2009) 115(7):1531–43. doi: 10.1002/cncr.24121

4. Savage SA, Mirabello L. Using epidemiology and genomics to understand osteosarcoma etiology. *Sarcoma* (2011) 2011:548151. doi: 10.1155/2011/548151

5. Rickel K, Fang F, Tao J. Molecular genetics of osteosarcoma. *Bone* (2017) 102:69–79. doi: 10.1016/j.bone.2016.10.017

6. Savage SA, Mirabello L, Wang Z, Gastier-Foster JM, Gorlick R, Khanna C, et al. Genome-wide association study identifies two susceptibility loci for osteosarcoma. *Nat Genet* (2013) 45(7):799–803. doi: 10.1038/ng.2645

7. Casali PG, Bielack S, Abecassis N, Aro HT, Bauer S, Biagini R, et al. Bone sarcomas: ESMO-PaedCan-EURACAN clinical practice guidelines for diagnosis, treatment and follow-up. *Ann Oncol* (2018) 29:79–95. doi: 10.1093/annonc/mdy310

8. Ferrari S, Briccoli A, Mercuri M, Bertoni F, Picci P, Tienghi A, et al. Postrelapse survival in osteosarcoma of the extremities: Prognostic factors for long-term survival. *J Clin Oncol* (2003) 21(4):710–5. doi: 10.1200/JCO.2003.03.141

9. DeLaney TF, Park L, Goldberg SI, Hug EB, Liebsch NJ, Munzenrider JE, et al. Radiotherapy for local control of osteosarcoma. *Int J Radiat Oncol Biol Physics* (2005) 61(2):492–8. doi: 10.1016/j.ijrobp.2004.05.051

10. Schwarz R, Bruland O, Cassoni A, Schomberg P, Bielack S eds. *The role of radiotherapy in oseosarcoma. symposium on pediatric and adolescent osteosarcoma*. Houston: Univ Texas, MD Anderson Canc Ctr (2008). p. TX2009.

11. Isakoff MS, Bielack SS, Meltzer P, Gorlick R. Osteosarcoma: Current treatment and a collaborative pathway to success. *J Clin Oncol Off J Am Soc Clin Oncol* (2015) 33(27):3029–35. doi: 10.1200/JCO.2014.59.4895

12. Wojtkowiak JW, Verduzco D, Schramm KJ, Gillies RJ. Drug resistance and cellular adaptation to tumor acidic pH microenvironment. *Mol Pharmaceut* (2011) 8(6):2032–8. doi: 10.1021/mp200292c

13. Wu T, Dai Y. Tumor microenvironment and therapeutic response. *Cancer Lett* (2017) 387:61–8. doi: 10.1016/j.canlet.2016.01.043

14. Murciano-Goroff YR, Warner AB, Wolchok JD. The future of cancer immunotherapy: microenvironment-targeting combinations. *Cell Res* (2020) 30 (6):507–19. doi: 10.1038/s41422-020-0337-2

15. Xiao Y, Yu D. Tumor microenvironment as a therapeutic target in cancer. *Pharmacol Ther* (2021) 221:107753. doi: 10.1016/j.pharmthera.2020.107753

16. Casazza A, Di Conza G, Wenes M, Finisguerra V, Deschoemaeker S, Mazzone M. Tumor stroma: a complexity dictated by the hypoxic tumor microenvironment. *Oncogene* (2014) 33(14):1743–54. doi: 10.1038/onc.2013.121

17. Multhoff G, Vaupel P. Hypoxia compromises anti-cancer immune responses. In: Ryu PD, LaManna JC, Harrison DK, Lee SS, editors. *Oxygen transport to tissue xli. advances in experimental medicine and biology* (Advances in experimental medicine and biology) (2020) 12322020:131–43.

18. Giatromanolaki A, Harris AL. Tumour hypoxia, hypoxia signaling pathways and hypoxia inducible factor expression in human cancer. *Anticancer Res* (2001) 21 (6B):4317–24.

19. Choudhry H, Harris AL. Advances in hypoxia-inducible factor biology. *Cell Metab* (2018) 27(2):281–98. doi: 10.1016/j.cmet.2017.10.005

20. Daniel C, Bell C, Burton C, Harguindey S, Reshkin SJ, Rauch C. The role of proton dynamics in the development and maintenance of multidrug resistance in cancer. *Biochim Et Biophys Acta-Mol Basis Dis* (2013) 1832(5):606–17. doi: 10.1016/j.bbadis.2013.01.020

21. Avnet S, Chano T, Massa A, Bonuccelli G, Lemma S, Falzetti L, et al. Acid microenvironment promotes cell survival o human bone sarcoma through the activation of clAP proteins and NE-kappa b pathway. *Am J Cancer Res* (2019) 9 (6):1127–+.

22. Wang D, Qian G, Wang J, Wang T, Zhang L, Yang P, et al. Visfatin is involved in the cisplatin resistance of osteosarcoma cells *via* upregulation of snail and Zeb1. *Cancer Biol Ther* (2019) 20(7):999–1006. doi: 10.1080/15384047.2019.1591675

23. Keremu A, Aini A, Maimaitirexiati Y, Liang Z, Aila P, Xierela P, et al. Overcoming cisplatin resistance in osteosarcoma through the miR-199a-modulated inhibition of HIF-1α. *Biosci Rep* (2019) 39(11). doi: 10.1042/BSR20170080

24. Zheng D, Wu W, Dong N, Jiang X, Xu J, Zhan X, et al. Mxd1 mediates hypoxia-induced cisplatin resistance in osteosarcoma cells by repression of the PTEN tumor suppressor gene. *Mol Carcinog* (2017) 56(10):2234–44. doi: 10.1002/mc.22676

25. Guo X, Yu L, Zhang Z, Dai G, Gao T, Guo W. miR-335 negatively regulates osteosarcoma stem cell-like properties by targeting POU5F1. *Cancer Cell Int* (2017) 17:29. doi: 10.1186/s12935-017-0398-6

26. Ma Q, Zhang Y, Liu T, Jiang K, Wen Y, Fan Q, et al. Hypoxia promotes chemotherapy resistance by down-regulating SKA1 gene expression in human osteosarcoma. *Cancer Biol Ther* (2017) 18(3):177–85. doi: 10.1080/15384047.2017.1294285

27. Zhao CF, Zhang Q, Yu T, Sun SD, Wang WJ, Liu GY. Hypoxia promotes drug resistance in osteosarcoma cells *via* activating AMP-activated protein kinase (AMPK) signaling. *J Bone Oncol* (2016) 5(1):22–9. doi: 10.1016/j.jbo.2016.01.002

28. Zhou C, Tan W, Lv H, Gao F, Sun J. Hypoxia-inducible microRNA-488 regulates apoptosis by targeting bim in osteosarcoma. *Cell Oncol (Dordrecht)* (2016) 39(5):463–71. doi: 10.1007/s13402-016-0288-2

29. Wang GC, He QY, Tong DK, Wang CF, Liu K, Ding C, et al. MiR-367 negatively regulates apoptosis induced by adriamycin in osteosarcoma cells by targeting KLF4. *J Bone Oncol* (2016) 5(2):51–6. doi: 10.1016/j.jbo.2016.02.002

30. Lin Z, Song D, Wei H, Yang X, Liu T, Yan W, et al. TGF-beta1-induced miR-202 mediates drug resistance by inhibiting apoptosis in human osteosarcoma. *J Cancer Res Clin Oncol* (2016) 142(1):239–46. doi: 10.1007/s00432-015-2028-9

31. Xu RD, Liu SZ, Chen HH, Lao LF. MicroRNA-30a downregulation contributes to chemoresistance of osteosarcoma cells through activating beclin-1-mediated autophagy. *Oncol Rep* (2016) 35(3):1757–63. doi: 10.3892/or.2015.4497

32. Li C, Guo D, Tang B, Zhang Y, Zhang K, Nie L. Notch1 is associated with the multidrug resistance of hypoxic osteosarcoma by regulating MRP1 gene expression. *Neoplasma* (2016) 63(5):734–42. doi: 10.4149/neo_2016_510

33. Guo YQ, Huang CX, Li GW, Chen T, Li JX, Huang ZW. Paxilitaxel induces apoptosis accompanied by protective autophagy in osteosarcoma cells through hypoxia-inducible factor-1 alpha pathway. *Mol Med Rep* (2015) 12(3):3681–7. doi: 10.3892/mmr.2015.3860

34. Zhang Y, Duan G, Feng S. MicroRNA-301a modulates doxorubicin resistance in osteosarcoma cells by targeting AMP-activated protein kinase alpha 1. *Biochem Biophys Res Commun* (2015) 459(3):367–73. doi: 10.1016/j.bbrc.2015.02.101

35. Roncuzzi L, Pancotti F, Baldini N. Involvement of HIF-1α activation in the doxorubicin resistance of human osteosarcoma cells. *Oncol Rep* (2014) 32(1):389–94. doi: 10.3892/or.2014.3181

36. Scholten DJ2nd, Timmer CM, Peacock JD, Pelle DW, Williams BO, Steensma MR. Down regulation of wnt signaling mitigates hypoxia-induced chemoresistance in human osteosarcoma cells. *PloS One* (2014) 9(10):e111431. doi: 10.1371/journal.pone.0111431

37. Dong J, Qin Z, Zhang WD, Cheng G, Yehuda AG, Ashby CRJr., et al. Medicinal chemistry strategies to discover p-glycoprotein inhibitors: An update. *Drug Resist Updat* (2020) 49:100681. doi: 10.1016/j.drup.2020.100681

38. Liu X. ABC Family transporters. *Adv Exp Med Biol* (2019) 1141:13–100. doi: 10.1007/978-981-13-7647-4_2

39. Leandro K, Bicker J, Alves G, Falcao A, Fortuna A. ABC Transporters in drug-resistant epilepsy: mechanisms of upregulation and therapeutic approaches. *Pharmacol Res* (2019) 144:357–76. doi: 10.1016/j.phrs.2019.04.031

40. Ma Q, Zhang YL, Liu T, Jiang K, Wen YH, Fan QY, et al. Hypoxia promotes chemotherapy resistance by down-regulating SKA1 gene expression in human osteosarcoma. *Cancer Biol Ther* (2017) 18(3):177–85. doi: 10.1080/15384047.2017.1294285

41. Fallah J, Rini BI. HIF inhibitors: Status of current clinical development. *Curr Oncol Rep* (2019) 21(1). doi: 10.1007/s11912-019-0752-z

42. Amaravadi RK, Kimmelman AC, Debnath J. Targeting autophagy in cancer: Recent advances and future directions. *Cancer Discovery* (2019) 9(9):1167–81. doi: 10.1158/2159-8290.CD-19-0292

43. Yun CW, Jeon J, Go G, Lee JH, Lee SH. The dual role of autophagy in cancer development and a therapeutic strategy for cancer by targeting autophagy. *Int J Mol Sci* (2021) 22(1). doi: 10.3390/ijms22010179

44. White E, Mehnert JM, Chan CS. Autophagy, metabolism, and cancer. *Clin Cancer Res* (2015) 21(22):5037–46. doi: 10.1158/1078-0432.CCR-15-0490

45. Akin D, Wang SK, Habibzadegah-Tari P, Law B, Ostrov D, Li M, et al. A novel ATG4B antagonist inhibits autophagy and has a negative impact on osteosarcoma tumors. *Autophagy* (2014) 10(11):2021–35. doi: 10.4161/auto.32229

46. Camuzard O, Santucci-Darmanin S, Carle GF, Pierrefite-Carle V. Role of autophagy in osteosarcoma. *J Bone Oncol* (2019) 16:100235. doi: 10.1016/j.jbo.2019.100235

47. Nehme G, Gordon N. Autophagy in osteosarcoma. *Adv Exp Med Biol* (2020) 1258:167–75. doi: 10.1007/978-3-030-43085-6_11

48. Feng H, Wang J, Chen W, Shan B, Guo Y, Xu J, et al. Hypoxia-induced autophagy as an additional mechanism in human osteosarcoma radioresistance. *J Bone Oncol* (2016) 5(2):67–73. doi: 10.1016/j.jbo.2016.03.001

49. Zhang D, Zhao Q, Sun H, Yin L, Wu J, Xu J, et al. Defective autophagy leads to the suppression of stem-like features of CD271(+) osteosarcoma cells. *J Biomed Sci* (2016) 23(1):82. doi: 10.1186/s12929-016-0297-5

50. Jing X, Yang F, Shao C, Wei K, Xie M, Shen H, et al. Role of hypoxia in cancer therapy by regulating the tumor microenvironment. *Mol Cancer* (2019) 18(1):157. doi: 10.1186/s12943-019-1089-9

51. Qian BZ, Pollard JW. Macrophage diversity enhances tumor progression and metastasis. *Cell* (2010) 141(1):39–51. doi: 10.1016/j.cell.2010.03.014

52. Ostuni R, Kratochvill F, Murray PJ, Natoli G. Macrophages and cancer: from mechanisms to therapeutic implications. *Trends Immunol* (2015) 36(4):229–39. doi: 10.1016/j.it.2015.02.004

53. Duluc D, Corvaisier M, Blanchard S, Catala L, Descamps P, Gamelin E, et al. Interferon-gamma reverses the immunosuppressive and protumoral properties and prevents the generation of human tumor-associated macrophages. *Int J Cancer* (2009) 125(2):367–73. doi: 10.1002/ijc.24401

54. Sica A, Larghi P, Mancino A, Rubino L, Porta C, Totaro MG, et al. Macrophage polarization in tumour progression. *Semin Cancer Biol* (2008) 18(5):349–55. doi: 10.1016/j.semcancer.2008.03.004

55. Mantovani A, Biswas SK, Galdiero MR, Sica A, Locati M. Macrophage plasticity and polarization in tissue repair and remodelling. *J Pathol* (2013) 229(2):176–85. doi: 10.1002/path.4133

56. DeNardo DG, Brennan DJ, Rexhepaj E, Ruffell B, Shiao SL, Madden SF, et al. Leukocyte complexity predicts breast cancer survival and functionally regulates response to chemotherapy. *Cancer Discovery* (2011) 1(1):54–67. doi: 10.1158/2159-8274.CD-10-0028

57. Dijkgraaf EM, Heusinkveld M, Tummers B, Vogelpoel LT, Goedemans R, Jha V, et al. Chemotherapy alters monocyte differentiation to favor generation of cancer-supporting M2 macrophages in the tumor microenvironment. *Cancer Res* (2013) 73(8):2480–92. doi: 10.1158/0008-5472.CAN-12-3542

58. Mantovani A, Allavena P. The interaction of anticancer therapies with tumor-associated macrophages. *J Exp Med* (2015) 212(4):435–45. doi: 10.1084/jem.20150295

59. Shojaei F, Wu X, Malik AK, Zhong C, Baldwin ME, Schanz S, et al. Tumor refractoriness to anti-VEGF treatment is mediated by CD11b+Gr1+ myeloid cells. *Nat Biotechnol* (2007) 25(8):911–20. doi: 10.1038/nbt1323

60. Nakasone ES, Askautrud HA, Kees T, Park JH, Plaks V, Ewald AJ, et al. Imaging tumor-stroma interactions during chemotherapy reveals contributions of the microenvironment to resistance. *Cancer Cell* (2012) 21(4):488–503. doi: 10.1016/j.ccr.2012.02.017

61. Ruffell B, Chang-Strachan D, Chan V, Rosenbusch A, Ho CM, Pryer N, et al. Macrophage IL-10 blocks CD8+ T cell-dependent responses to chemotherapy by suppressing IL-12 expression in intratumoral dendritic cells. *Cancer Cell* (2014) 26(5):623–37. doi: 10.1016/j.ccell.2014.09.006

62. Shree T, Olson OC, Elie BT, Kester JC, Garfall AL, Simpson K, et al. Macrophages and cathepsin proteases blunt chemotherapeutic response in breast cancer. *Genes Dev* (2011) 25(23):2465–79. doi: 10.1101/gad.180331.111

63. Larionova I, Cherdyntseva N, Liu T, Patysheva M, Rakina M, Kzhyshkowska J. Interaction of tumor-associated macrophages and cancer chemotherapy. *Oncoimmunology* (2019) 8(7):1596004. doi: 10.1080/2162402X.2019.1596004

64. Jinushi M, Chiba S, Yoshiyama H, Masutomi K, Kinoshita I, Dosaka-Akita H, et al. Tumor-associated macrophages regulate tumorigenicity and anticancer drug responses of cancer stem/initiating cells. *Proc Natl Acad Sci U States A* (2011) 108(30):12425–30. doi: 10.1073/pnas.1106645108

65. Weizman N, Krelin Y, Shabtay-Orbach A, Amit M, Binenbaum Y, Wong RJ, et al. Macrophages mediate gemcitabine resistance of pancreatic adenocarcinoma by upregulating cytidine deaminase. *Oncogene* (2014) 33(29):3812–9. doi: 10.1038/onc.2013.357

66. Han Y, Guo W, Ren T, Huang Y, Wang S, Liu K, et al. Tumor-associated macrophages promote lung metastasis and induce epithelial-mesenchymal transition in osteosarcoma by activating the COX-2/STAT3 axis. *Cancer Lett* (2019) 440-441:116–25. doi: 10.1016/j.canlet.2018.10.011

67. Shao XJ, Xiang SF, Chen YQ, Zhang N, Cao J, Zhu H, et al. Inhibition of M2-like macrophages by all-trans retinoic acid prevents cancer initiation and stemness in osteosarcoma cells. *Acta Pharmacol Sinica* (2019) 40(10):1343–50. doi: 10.1038/s41401-019-0262-4

68. Ngambenjawong C, Gustafson HH, Pun SH. Progress in tumor-associated macrophage (TAM)-targeted therapeutics. *Adv Drug Deliv Rev* (2017) 114:206–21. doi: 10.1016/j.addr.2017.04.010

69. Meyers PA, Schwartz CL, Krailo M, Kleinerman ES, Betcher D, Bernstein ML, et al. Osteosarcoma: a randomized, prospective trial of the addition of ifosfamide and/or muramyl tripeptide to cisplatin, doxorubicin, and high-dose methotrexate. *J Clin Oncol Off J Am Soc Clin Oncol* (2005) 23(9):2004–11. doi: 10.1200/JCO.2005.06.031

70. Chou AJ, Kleinerman ES, Krailo MD, Chen Z, Betcher DL, Healey JH, et al. Addition of muramyl tripeptide to chemotherapy for patients with newly diagnosed metastatic osteosarcoma: a report from the children's oncology group. *Cancer* (2009) 115(22):5339–48. doi: 10.1002/cncr.24566

71. Meyers PA, Schwartz CL, Krailo MD, Healey JH, Bernstein ML, Betcher D, et al. Osteosarcoma: the addition of muramyl tripeptide to chemotherapy improves overall survival–a report from the children's oncology group. *J Clin Oncol Off J Am Soc Clin Oncol* (2008) 26(4):633–8. doi: 10.1200/JCO.2008.14.0095

72. Punzo F, Bellini G, Tortora C, Pinto DD, Argenziano M, Pota E, et al. Mifamurtide and TAM-like macrophages: effect on proliferation, migration and differentiation of osteosarcoma cells. *Oncotarget* (2020) 11(7):687–98. doi: 10.18632/oncotarget.27479

73. Pahl JH, Kwappenberg KM, Varypataki EM, Santos SJ, Kuijjer ML, Mohamed S, et al. Macrophages inhibit human osteosarcoma cell growth after activation with the bacterial cell wall derivative liposomal muramyl tripeptide in combination with interferon-γ. *J Exp Clin Cancer Res* (2014) 33(1):27. doi: 10.1186/1756-9966-33-27

74. Ando K, Mori K, Corradini N, Redini F, Heymann D. Mifamurtide for the treatment of nonmetastatic osteosarcoma. *Expert Opin Pharmacother* (2011) 12 (2):285–92. doi: 10.1517/14656566.2011.543129

75. Tap WD, Gelderblom H, Palmerini E, Desai J, Bauer S, Blay JY, et al. Pexidartinib versus placebo for advanced tenosynovial giant cell tumour (ENLIVEN): a randomised phase 3 trial. *Lancet* (2019) 394(10197):478–87. doi: 10.1016/S0140-6736(19)30764-0

76. Song YJ, Xu Y, Zhu X, Fu J, Deng C, Chen H, et al. Immune landscape of the tumor microenvironment identifies prognostic gene signature CD4/CD68/CSF1R in osteosarcoma. *Front Oncol* (2020) 10:1198. doi: 10.3389/fonc.2020.01198

77. Denny WA, Flanagan JU. Small-molecule CSF1R kinase inhibitors; review of patents 2015-present. *Expert Opin Ther Patents* (2021) 31(2):107–17. doi: 10.1080/13543776.2021.1839414

78. Lee JH, Chen TW, Hsu CH, Yen YH, Yang JC, Cheng AL, et al. A phase I study of pexidartinib, a colony-stimulating factor 1 receptor inhibitor, in Asian patients with advanced solid tumors. *Investigational New Drugs* (2020) 38(1):99–110. doi: 10.1007/s10637-019-00745-z

79. Liu JF, Lee CW, Lin CY, Chao CC, Chang TM, Han CK, et al. CXCL13/CXCR5 interaction facilitates VCAM-1-Dependent migration in human osteosarcoma. *Int J Mol Sci* (2020) 21(17). doi: 10.3390/ijms21176095

80. Chen Q, Zhang XH, Massagué J. Macrophage binding to receptor VCAM-1 transmits survival signals in breast cancer cells that invade the lungs. *Cancer Cell* (2011) 20(4):538–49. doi: 10.1016/j.ccr.2011.08.025

81. Liu X, Kwon H, Li Z, Fu YX. Is CD47 an innate immune checkpoint for tumor evasion? *J Hematol Oncol* (2017) 10(1):12. doi: 10.1186/s13045-016-0381-z

82. Horrigan SK. Replication study: The CD47-signal regulatory protein alpha (SIRPa) interaction is a therapeutic target for human solid tumors. *eLife* (2017) 6. doi: 10.7554/eLife.18173

83. Mohanty S, Yerneni K, Theruvath JL, Graef CM, Nejadnik H, Lenkov O, et al. Nanoparticle enhanced MRI can monitor macrophage response to CD47 mAb immunotherapy in osteosarcoma. *Cell Death Dis* (2019) 10(2):36. doi: 10.1038/s41419-018-1285-3

84. Xu JF, Pan XH, Zhang SJ, Zhao C, Qiu BS, Gu HF, et al. CD47 blockade inhibits tumor progression human osteosarcoma in xenograft models. *Oncotarget* (2015) 6(27):23662–70. doi: 10.18632/oncotarget.4282

85. Fang S, Yin H, Song Z, Li R, Xie X, Gu Z. Anti-CD47 antibody eliminates bone tumors in rats. *Saudi J Biol Sci* (2019) 26(8):2074–8. doi: 10.1016/j.sjbs.2019.09.011

86. Mohanty S, Aghighi M, Yerneni K, Theruvath JL, Daldrup-Link HE. Improving the efficacy of osteosarcoma therapy: combining drugs that turn cancer cell 'don't eat me' signals off and 'eat me' signals on. *Mol Oncol* (2019) 13 (10):2049–61. doi: 10.1002/1878-0261.12556

87. Ray M, Lee YW, Hardie J, Mout R, Tonga GY, Farkas ME, et al. CRISPRed macrophages for cell-based cancer immunotherapy. *Bioconjugate Chem* (2018) 29 (2):445–50. doi: 10.1021/acs.bioconjchem.7b00768

88. Luo ZW, Liu PP, Wang ZX, Chen CY, Xie H. Macrophages in osteosarcoma immune microenvironment: Implications for immunotherapy. *Front Oncol* (2020) 10:586580. doi: 10.3389/fonc.2020.586580

89. Gabrilovich DI, Ostrand-Rosenberg S, Bronte V. Coordinated regulation of myeloid cells by tumours. *Nat Rev Immunol* (2012) 12(4):253–68. doi: 10.1038/nri3175

90. Nagaraj S, Gupta K, Pisarev V, Kinarsky L, Sherman S, Kang L, et al. Altered recognition of antigen is a mechanism of CD8+ T cell tolerance in cancer. *Nat Med* (2007) 13(7):828–35. doi: 10.1038/nm1609

91. Rodriguez PC, Ernstoff MS, Hernandez C, Atkins M, Zabaleta J, Sierra R, et al. Arginase I-producing myeloid-derived suppressor cells in renal cell carcinoma are a subpopulation of activated granulocytes. *Cancer Res* (2009) 69(4):1553–60. doi: 10.1158/0008-5472.CAN-08-1921

92. Lau EY, Ho NP, Lee TK. Cancer stem cells and their microenvironment: Biology and therapeutic implications. *Stem Cells Int* (2017) 2017:3714190. doi: 10.1155/2017/3714190

93. Bertagnolli MM. Chemoprevention of colorectal cancer with cyclooxygenase-2 inhibitors: two steps forward, one step back. *Lancet Oncol* (2007) 8(5):439–43. doi: 10.1016/S1470-2045(07)70139-0

94. Ligon JA, Choi W, Cojocaru G, Fu W, Hsiue EH, Oke TF, et al. Pathways of immune exclusion in metastatic osteosarcoma are associated with inferior patient outcomes. *J Immunother Cancer* (2021) 9(5). doi: 10.1136/jitc-2020-001772

95. Deng C, Xu Y, Fu J, Zhu X, Chen H, Xu H, et al. Reprograming the tumor immunologic microenvironment using neoadjuvant chemotherapy in osteosarcoma. *Cancer Sci* (2020) 111(6):1899–909. doi: 10.1111/cas.14398

96. Jiang K, Li J, Zhang J, Wang L, Zhang Q, Ge J, et al. SDF-1/CXCR4 axis facilitates myeloid-derived suppressor cells accumulation in osteosarcoma microenvironment and blunts the response to anti-PD-1 therapy. *Int Immunopharmacol* (2019) 75:105818. doi: 10.1016/j.intimp.2019.105818

97. Shi X, Li X, Wang H, Yu Z, Zhu Y, Gao Y. Specific inhibition of PI3Kdelta/gamma enhances the efficacy of anti-PD1 against osteosarcoma cancer. *J Bone Oncol* (2019) 16:100206. doi: 10.1016/j.jbo.2018.11.001

98. Uehara T, Eikawa S, Nishida M, Kunisada Y, Yoshida A, Fujiwara T, et al. Metformin induces CD11b+-cell-mediated growth inhibition of an osteosarcoma: implications for metabolic reprogramming of myeloid cells and anti-tumor effects. *Int Immunol* (2019) 31(4):187–98. doi: 10.1093/intimm/dxy079

99. Guan Y, Zhang R, Peng Z, Dong D, Wei G, Wang Y. Inhibition of IL-18-mediated myeloid derived suppressor cell accumulation enhances anti-PD1 efficacy against osteosarcoma cancer. *J Bone Oncol* (2017) 9:59–64. doi: 10.1016/j.jbo.2017.10.002

100. Long AH, Highfill SL, Cui Y, Smith JP, Walker AJ, Ramakrishna S, et al. Reduction of MDSCs with all-trans retinoic acid improves CAR therapy efficacy for sarcomas. *Cancer Immunol Res* (2016) 4(10):869–80. doi: 10.1158/2326-6066.CIR-15-0230

101. Kumar V, Patel S, Tcyganov E, Gabrilovich DI. The nature of myeloid-derived suppressor cells in the tumor microenvironment. *Trends Immunol* (2016) 37(3):208–20. doi: 10.1016/j.it.2016.01.004

102. Acharyya S, Oskarsson T, Vanharanta S, Malladi S, Kim J, Morris PG, et al. A CXCL1 paracrine network links cancer chemoresistance and metastasis. *Cell* (2012) 150(1):165–78. doi: 10.1016/j.cell.2012.04.042

103. Finke J, Ko J, Rini B, Rayman P, Ireland J, Cohen P. MDSC as a mechanism of tumor escape from sunitinib mediated anti-angiogenic therapy. *Int Immunopharmacol* (2011) 11(7):856–61. doi: 10.1016/j.intimp.2011.01.030

104. Liu Y, Huang N, Liao S, Rothzerg E, Yao F, Li Y, et al. Current research progress in targeted anti-angiogenesis therapy for osteosarcoma. *Cell Prolif* (2021) 54(9):e13102. doi: 10.1111/cpr.13102

105. Goel S, Duda DG, Xu L, Munn LL, Boucher Y, Fukumura D, et al. Normalization of the vasculature for treatment of cancer and other diseases. *Physiol Rev* (2011) 91(3):1071–121. doi: 10.1152/physrev.00038.2010

106. Chim SM, Tickner J, Chow ST, Kuek V, Guo BS, Zhang G, et al. Angiogenic factors in bone local environment. *Cytokine Growth Factor Rev* (2013) 24(3):297–310. doi: 10.1016/j.cytogfr.2013.03.008

107. Alfranca A, Martinez-Cruzado L, Tornin J, Abarrategi A, Amaral T, de Alava E, et al. Bone microenvironment signals in osteosarcoma development. *Cell Mol Life Sci* (2015) 72(16):3097–113. doi: 10.1007/s00018-015-1918-y

108. Tan Q, Saggar JK, Yu M, Wang M, Tannock IF. Mechanisms of drug resistance related to the microenvironment of solid tumors and possible strategies to inhibit them. *Cancer J* (2015) 21(4):254–62. doi: 10.1097/PPO.0000000000000131

109. Zhao ZX, Li X, Liu WD, Liu XZ, Wu SJ, Hu XH. Inhibition of growth and metastasis of tumor in nude mice after intraperitoneal injection of bevacizumab. *Orthopaedic Surg* (2016) 8(2):234–40. doi: 10.1111/os.12236

110. Quan GM, Choong PF. Anti-angiogenic therapy for osteosarcoma. *Cancer Metastasis Rev* (2006) 25(4):707–13.

111. Scharf VF, Farese JP, Coomer AR, Milner RJ, Taylor DP, Salute ME, et al. Effect of bevacizumab on angiogenesis and growth of canine osteosarcoma cells xenografted in athymic mice. *Am J Veterinary Res* (2013) 74(5):771–8. doi: 10.2460/ajvr.74.5.771

112. Pignochino Y, Grignani G, Cavalloni G, Motta M, Tapparo M, Bruno S, et al. Sorafenib blocks tumour growth, angiogenesis and metastatic potential in preclinical models of osteosarcoma through a mechanism potentially involving the inhibition of ERK1/2, MCL-1 and ezrin pathways. *Mol Cancer* (2009) 8:118. doi: 10.1186/1476-4598-8-118

113. Kunz P, Fellenberg J, Moskovszky L, Sapi Z, Krenacs T, Machado I, et al. Improved survival in osteosarcoma patients with atypical low vascularization. *Ann Surg Oncol* (2015) 22(2):489–96. doi: 10.1245/s10434-014-4001-2

114. Navid F, Santana VM, Neel M, McCarville MB, Shulkin BL, Wu J, et al. A phase II trial evaluating the feasibility of adding bevacizumab to standard osteosarcoma therapy. *Int J Cancer* (2017) 141(7):1469–77. doi: 10.1002/ijc.30841

115. Grignani G, Palmerini E, Dileo P, Asaftei SD, D'Ambrosio L, Pignochino Y, et al. A phase II trial of sorafenib in relapsed and unresectable high-grade osteosarcoma after failure of standard multimodal therapy: an Italian sarcoma group study. *Ann Oncol Off J Eur Soc Med Oncol* (2012) 23(2):508–16. doi: 10.1093/annonc/mdr151

116. Xu H, Huang Z, Li Y, Zhang Q, Hao L, Niu X. Perioperative rh-endostatin with chemotherapy improves the survival of conventional osteosarcoma patients: a

prospective non-randomized controlled study. *Cancer Biol Med* (2019) 16(1):166–72.

117. Ebb D, Meyers P, Grier H, Bernstein M, Gorlick R, Lipshultz SE, et al. Phase II trial of trastuzumab in combination with cytotoxic chemotherapy for treatment of metastatic osteosarcoma with human epidermal growth factor receptor 2 overexpression: A report from the children's oncology group. *J Clin Oncol* (2012) 30(20):2545–51. doi: 10.1200/JCO.2011.37.4546

118. Schuetze SM, Zhao LL, Chugh R, Thomas DG, Lucas DR, Metko G, et al. Results of a phase II study of sirolimus and cyclophosphamide in patients with advanced sarcoma. *Eur J Cancer* (2012) 48(9):1347–53. doi: 10.1016/j.ejca.2012.03.022

119. Navid F, Santana VM, Neel M, McCarville MB, Shulkin BL, Wu JR, et al. A phase II trial evaluating the feasibility of adding bevacizumab to standard osteosarcoma therapy. *Int J Cancer* (2017) 141(7):1469–77. doi: 10.1002/ijc.30841

120. Casazza A, Laoui D, Wenes M, Rizzolio S, Bassani N, Mambretti M, et al. Impeding macrophage entry into hypoxic tumor areas by Sema3A/Nrp1 signaling blockade inhibits angiogenesis and restores antitumor immunity. *Cancer Cell* (2013) 24(6):695–709. doi: 10.1016/j.ccr.2013.11.007

121. Justus CR, Sanderlin EJ, Yang LV. Molecular connections between cancer cell metabolism and the tumor microenvironment. *Int J Mol Sci* (2015) 16 (5):11055–86. doi: 10.3390/ijms160511055

122. de Palma M, Biziato D, Petrova TV. Microenvironmental regulation of tumour angiogenesis. *Nat Rev Cancer* (2017) 17(8):457–74. doi: 10.1038/nrc.2017.51

123. Palazon A, Goldrath AW, Nizet V, Johnson RS. HIF transcription factors, inflammation, and immunity. *Immunity* (2014) 41(4):518–28. doi: 10.1016/j.immuni.2014.09.008

124. Eelen G, Treps L, Li X, Carmeliet P. Basic and therapeutic aspects of angiogenesis updated. *Circ Res* (2020) 127(2):310–29. doi: 10.1161/CIRCRESAHA.120.316851

125. Lane AN, Higashi RM, Fan TW. Metabolic reprogramming in tumors: Contributions of the tumor microenvironment. *Genes Dis* (2020) 7(2):185–98. doi: 10.1016/j.gendis.2019.10.007

126. Buechler MB, Turley SJ. A short field guide to fibroblast function in immunity. *Semin Immunol* (2018) 35(C):48–58. doi: 10.1016/j.smim.2017.11.001

127. Riera-Domingo C, Audige A, Granja S, Cheng WC, Ho PC, Baltazar F, et al. Immunity, hypoxia, and metabolism-the menage a trois of cancer: Implications for immunotherapy. *Physiol Rev* (2020) 100(1):1–102. doi: 10.1152/physrev.00018.2019

128. Taneja SS. Re: Safety and activity of anti-PD-L1 antibody in patients with advanced cancer editorial comment. *J Urol* (2012) 188(6):2148–9. doi: 10.1016/j.juro.2012.08.169

129. Grosso JF, Jure-Kunkel MN. CTLA-4 blockade in tumor models: an overview of preclinical and translational research. *Cancer Immun* (2013) 13:5.

130. Daskivich TJ, Belldegrun A. Re: Safety, activity, and immune correlates of anti-PD-1 antibody in cancer. *Eur Urol* (2015) 67(4):816–7. doi: 10.1016/j.eururo.2014.12.052

131. Chang CH, Qiu J, O'Sullivan D, Buck MD, Noguchi T, Curtis JD, et al. Metabolic competition in the tumor microenvironment is a driver of cancer progression. *Cell* (2015) 162(6):1229–41. doi: 10.1016/j.cell.2015.08.016

132. Geiger R, Rieckmann JC, Wolf T, Basso C, Feng YH, Fuhrer T, et al. L-arginine modulates T cell metabolism and enhances survival and anti-tumor activity. *Cell* (2016) 167(3):829–+. doi: 10.1016/j.cell.2016.09.031

133. Joyce JA, Fearon DT. T Cell exclusion, immune privilege, and the tumor microenvironment. *Sci (New York NY)* (2015) 348(6230):74–80. doi: 10.1126/science.aaa6204

134. Smyth MJ, Ngiow SF, Ribas A, Teng MW. Combination cancer immunotherapies tailored to the tumour microenvironment. *Nat Rev Clin Oncol* (2016) 13(3):143–58. doi: 10.1038/nrclinonc.2015.209

135. Baumeister SH, Freeman GJ, Dranoff G, Sharpe AH. Coinhibitory pathways in immunotherapy for cancer. In: Littman DR, Yokoyama WM, editors. *Annual review of immunology* (Annual review of immunology) (2016), vol. 34 . p. 539–73.

136. Wolchok JD, Chiarion-Sileni V, Gonzalez R, Rutkowski P, Grob JJ, Cowey CL, et al. Overall survival with combined nivolumab and ipilimumab in advanced melanoma. *New Engl J Med* (2017) 377(14):1345–56. doi: 10.1056/NEJMoa1709684

137. Herbst RS, Baas P, Kim DW, Felip E, Perez-Gracia JL, Han JY, et al. Pembrolizumab versus docetaxel for previously treated, PD-L1-positive, advanced non-small-cell lung cancer (KEYNOTE-010): a randomised controlled trial. *Lancet* (2016) 387(10027):1540–50. doi: 10.1016/S0140-6736(15)01281-7

138. Motzer RJ, Tannir NM, McDermott DF, Arén Frontera O, Melichar B, Choueiri TK, et al. Nivolumab plus ipilimumab versus sunitinib in advanced renal-cell carcinoma. *New Engl J Med* (2018) 378(14):1277–90. doi: 10.1056/NEJMoa1712126

139. Chen S, Guenther LM, Aronhalt A, Cardillo L, Janeway KA, Church AJ. PD-1 and PD-L1 expression in osteosarcoma: Which specimen to evaluate? *J Pediatr Hematol Oncol* (2020) 42(8):482–7. doi: 10.1097/MPH.0000000000001685

140. Thanindratarn P, Dean DC, Nelson SD, Hornicek FJ, Duan Z. Advances in immune checkpoint inhibitors for bone sarcoma therapy. *J Bone Oncol* (2019) 15:100221. doi: 10.1016/j.jbo.2019.100221

141. Mamalis A, Garcha M, Jagdeo J. Targeting the PD-1 pathway: a promising future for the treatment of melanoma. *Arch Dermatol Res* (2014) 306(6):511–9. doi: 10.1007/s00403-014-1457-7

142. Fife BT, Pauken KE, Eagar TN, Obu T, Wu J, Tang QZ, et al. Interactions between PD-1 and PD-L1 promote tolerance by blocking the TCR-induced stop signal. *Nat Immunol* (2009) 10(11):1185–U70. doi: 10.1038/ni.1790

143. Riley JL. PD-1 signaling in primary T cells. *Immunol Rev* (2009) 229:114–25. doi: 10.1111/j.1600-065X.2009.00767.x

144. Torabi A, Amaya CN, Wians FH, Bryan BA. PD-1 and PD-L1 expression in bone and soft tissue sarcomas. *Pathology* (2017) 49(5):506–13. doi: 10.1016/j.pathol.2017.05.003

145. Costa Arantes DA, Gonçalves AS, Jham BC, Duarte ECB, de Paula ÉC, de Paula HM, et al. Evaluation of HLA-G, HLA-e, and PD-L1 proteins in oral osteosarcomas. *Oral Surg Oral Med Oral Pathol Oral Radiol* (2017) 123(6):e188–e96.

146. Sundara YT, Kostine M, Cleven AH, Bovée JV, Schilham MW, Cleton-Jansen AM. Increased PD-L1 and T-cell infiltration in the presence of HLA class I expression in metastatic high-grade osteosarcoma: a rationale for T-cell-based immunotherapy. *Cancer Immunol Immunother CII* (2017) 66(1):119–28. doi: 10.1007/s00262-016-1925-3

147. Koirala P, Roth ME, Gill J, Piperdi S, Chinai JM, Geller DS, et al. Immune infiltration and PD-L1 expression in the tumor microenvironment are prognostic in osteosarcoma. *Sci Rep* (2016) 6. doi: 10.1038/srep30093

148. Lussier DM, O'Neill L, Nieves LM, McAfee MS, Holechek SA, Collins AW, et al. Enhanced T-cell immunity to osteosarcoma through antibody blockade of PD-1/PD-L1 interactions. *J Immunother (Hagerstown Md 1997)* (2015) 38(3):96–106. doi: 10.1097/CJI.0000000000000065

149. Chowdhury F, Dunn S, Mitchell S, Mellows T, Ashton-Key M, Gray JC. PD-L1 and CD8(+)PD1(+) lymphocytes exist as targets in the pediatric tumor microenvironment for immunomodulatory therapy. *Oncoimmunology* (2015) 4 (10). doi: 10.1080/2162402X.2015.1029701

150. Zheng WJ, Xiao H, Liu H, Zhou Y. Expression of programmed death 1 is correlated with progression of osteosarcoma. *Apmis* (2015) 123(2):102–7. doi: 10.1111/apm.12311

151. Shen JK, Cote GM, Choy E, Yang P, Harmon D, Schwab J, et al. Programmed cell death ligand 1 expression in osteosarcoma. *Cancer Immunol Res* (2014) 2(7):690–8. doi: 10.1158/2326-6066.CIR-13-0224

152. Chen S, Guenther LM, Aronhalt A, Cardillo L, Janeway KA, Church AJ. PD-1 and PD-L1 expression in osteosarcoma: Which specimen to evaluate? *J Pediatr Hematol/Oncol* (2020) 42(8):482–7. doi: 10.1097/MPH.0000000000001685

153. Dhupkar P, Gordon N, Stewart J, Kleinerman ES. Anti-PD-1 therapy redirects macrophages from an M2 to an M1 phenotype inducing regression of OS lung metastases. *Cancer Med* (2018) 7(6):2654–64. doi: 10.1002/cam4.1518

154. Skertich NJ, Chu F, Tarhoni IA, Szajek S, Borgia JA, Madonna MB. Expression of programmed death ligand 1 in drug-resistant osteosarcoma: An exploratory study. *Surg Open Sci* (2021) 6:10–4. doi: 10.1016/j.sopen.2021.07.001

155. Shen JK, Cote GM, Choy E, Yang P, Harmon D, Schwab J, et al. Programmed cell death ligand 1 expression in osteosarcoma. *Cancer Immunol Res* (2014) 2(7):690–8. doi: 10.1158/2326-6066.CIR-13-0224

156. Zheng BX, Ren TT, Huang Y, Sun KK, Wang SD, Bao X, et al. PD-1 axis expression in musculoskeletal tumors and antitumor effect of nivolumab in osteosarcoma model of humanized mouse. *J Hematol Oncol* (2018) 11.

157. Park JA, Cheung NV. GD2 or HER2 targeting T cell engaging bispecific antibodies to treat osteosarcoma. *J Hematol Oncol* (2020) 13(1):172. doi: 10.1186/s13045-020-01012-y

158. Liu Z, Wang H, Hu C, Wu C, Wang J, Hu F, et al. Targeting autophagy enhances atezolizumab-induced mitochondria-related apoptosis in osteosarcoma. *Cell Death Dis* (2021) 12(2):164. doi: 10.1038/s41419-021-03449-6

159. Tawbi HA, Burgess M, Bolejack V, Van Tine BA, Schuetze SM, Hu J, et al. Pembrolizumab in advanced soft-tissue sarcoma and bone sarcoma (SARC028): a multicentre, two-cohort, single-arm, open-label, phase 2 trial. *Lancet Oncol* (2017) 18(11):1493–501. doi: 10.1016/S1470-2045(17)30624-1

160. Boye K, Longhi A, Guren T, Lorenz S, Naess S, Pierini M, et al. Pembrolizumab in advanced osteosarcoma: results of a single-arm, open-label, phase 2 trial. *Cancer Immunol Immunother CII* (2021) 70(9):2617–24. doi: 10.1007/s00262-021-02876-w

161. Egen JG, Kuhns MS, Allison JP. CTLA-4: new insights into its biological function and use in tumor immunotherapy. *Nat Immunol* (2002) 3(7):611–8. doi: 10.1038/ni0702-611

162. Buchbinder E, Hodi FS. Cytotoxic T lymphocyte antigen-4 and immune checkpoint blockade. *J Clin Invest* (2015) 125(9):3377–83. doi: 10.1172/JCI80012

163. Lee KM, Chuang E, Griffin M, Khattri R, Hong DK, Zhang W, et al. Molecular basis of T cell inactivation by CTLA-4. *Sci (New York NY)* (1998) 282 (5397):2263–6. doi: 10.1126/science.282.5397.2263

164. He J, Wang J, Wang D, Dai S, Yv T, Chen P, et al. Association between CTLA-4 genetic polymorphisms and susceptibility to osteosarcoma in Chinese han population. *Endocrine* (2014) 45(2):325–30. doi: 10.1007/s12020-013-0050-8

165. Liu Y, He Z, Feng D, Shi G, Gao R, Wu X, et al. Cytotoxic T-lymphocyte antigen-4 polymorphisms and susceptibility to osteosarcoma. *DNA Cell Biol* (2011) 30(12):1051–5. doi: 10.1089/dna.2011.1269

166. Lussier DM, Johnson JL, Hingorani P, Blattman JN. Combination immunotherapy with alpha-CTLA-4 and alpha-PD-L1 antibody blockade prevents immune escape and leads to complete control of metastatic osteosarcoma. *J Immunother Cancer* (2015) 3. doi: 10.1186/s40425-015-0067-z

167. Nagamori M, Kawaguchi S, Murakami M, Wada T, Nagoya S, Yamashita T, et al. Intrinsic and extrinsic manipulation of B7/CTLA-4 interaction for induction of anti-tumor immunity against osteosarcoma cells. *Anticancer Res* (2002) 22(6a):3223–7.

168. Kawano M, Itonaga I, Iwasaki T, Tsumura H. Enhancement of antitumor immunity by combining anti-cytotoxic T lymphocyte antigen-4 antibodies and cryotreated tumor lysate-pulsed dendritic cells in murine osteosarcoma. *Oncol Rep* (2013) 29(3):1001–6. doi: 10.3892/or.2013.2224

169. Merchant MS, Wright M, Baird K, Wexler LH, Rodriguez-Galindo C, Bernstein D, et al. Phase I clinical trial of ipilimumab in pediatric patients with advanced solid tumors. *Clin Cancer Res Off J Am Assoc Cancer Res* (2016) 22 (6):1364–70. doi: 10.1158/1078-0432.CCR-15-0491

170. Liu J, Wang J, Jiang W, Tang Y. Effect of cytotoxic T-lymphocyte antigen-4, TNF-alpha polymorphisms on osteosarcoma: evidences from a meta-analysis. *Chin J Cancer Res Chung-kuo Yen Cheng Yen Chiu.* (2013) 25(6):671–8.

171. Kleinerman ES, Jia SF, Griffin J, Seibel NL, Benjamin RS, Jaffe N. Phase II study of liposomal muramyl tripeptide in osteosarcoma: the cytokine cascade and monocyte activation following administration. *J Clin Oncol Off J Am Soc Clin Oncol* (1992) 10(8):1310–6. doi: 10.1200/JCO.1992.10.8.1310

172. Chiu DK, Yuen VW, Cheu JW, Wei LL, Ting V, Fehlings M, et al. Hepatocellular carcinoma cells up-regulate PVRL1, stabilizing PVR and inhibiting the cytotoxic T-cell response *via* TIGIT to mediate tumor resistance to PD1 inhibitors in mice. *Gastroenterology* (2020) 159(2):609–23. doi: 10.1053/j.gastro.2020.03.074

173. Stamm H, Oliveira-Ferrer L, Grossjohann EM, Muschhammer J, Thaden V, Brauneck F, et al. Targeting the TIGIT-PVR immune checkpoint axis as novel therapeutic option in breast cancer. *Oncoimmunology* (2019) 8(12):e1674605. doi: 10.1080/2162402X.2019.1674605

174. Wang Z, Wu H, Chen Y, Chen H, Yuan W, Wang X. The heterogeneity of infiltrating macrophages in metastatic osteosarcoma and its correlation with immunotherapy. *J Oncol* (2021) 2021:4836292. doi: 10.1155/2021/4836292

175. Zhou Y, Yang D, Yang Q, Lv X, Huang W, Zhou Z, et al. Single-cell RNA landscape of intratumoral heterogeneity and immunosuppressive microenvironment in advanced osteosarcoma. *Nat Commun* (2020) 11(1):6322. doi: 10.1038/s41467-020-20059-6

176. Mellor AL, Munn DH. Tryptophan catabolism and T-cell tolerance: immunosuppression by starvation? *Immunol Today* (1999) 20(10):469–73. doi: 10.1016/S0167-5699(99)01520-0

177. Uyttenhove C, Pilotte L, Théate I, Stroobant V, Colau D, Parmentier N, et al. Evidence for a tumoral immune resistance mechanism based on tryptophan degradation by indoleamine 2,3-dioxygenase. *Nat Med* (2003) 9(10):1269–74. doi: 10.1038/nm934

178. Karanikas V, Zamanakou M, Kerenidi T, Dahabreh J, Hevas A, Nakou M, et al. Indoleamine 2,3-dioxygenase (IDO) expression in lung cancer. *Cancer Biol Ther* (2007) 6(8):1258–62. doi: 10.4161/cbt.6.8.4446

179. Brandacher G, Perathoner A, Ladurner R, Schneeberger S, Obrist P, Winkler C, et al. Prognostic value of indoleamine 2,3-dioxygenase expression in colorectal cancer: effect on tumor-infiltrating T cells. *Clin Cancer Res Off J Am Assoc Cancer Res* (2006) 12(4):1144–51. doi: 10.1158/1078-0432.CCR-05-1966

180. Speeckaert R, Vermaelen K, van Geel N, Autier P, Lambert J, Haspeslagh M, et al. Indoleamine 2,3-dioxygenase, a new prognostic marker in sentinel lymph nodes of melanoma patients. *Eur J Cancer (Oxford Engl 1990)* (2012) 48(13):2004–11. doi: 10.1016/j.ejca.2011.09.007

181. Liebau C, Baltzer AW, Schmidt S, Roesel C, Karreman C, Prisack JB, et al. Interleukin-12 and interleukin-18 induce indoleamine 2,3-dioxygenase (IDO) activity in human osteosarcoma cell lines independently from interferon-gamma. *Anticancer Res* (2002) 22(2a):931–6.

182. Urakawa H, Nishida Y, Nakashima H, Shimoyama Y, Nakamura S, Ishiguro N. Prognostic value of indoleamine 2,3-dioxygenase expression in high grade osteosarcoma. *Clin Exp Metastasis* (2009) 26(8):1005–12. doi: 10.1007/s10585-009-9290-7

183. Neelapu SS, Locke FL, Bartlett NL, Lekakis LJ, Miklos DB, Jacobson CA, et al. Axicabtagene ciloleucel CAR T-cell therapy in refractory Large b-cell lymphoma. *New Engl J Med* (2017) 377(26):2531–44. doi: 10.1056/NEJMoa1707447

184. Prasad V. Tisagenlecleucel - the first approved CAR-t-cell therapy: implications for payers and policy makers. *Nat Rev Clin Oncol* (2018) 15(1):11–+. doi: 10.1038/nrclinonc.2017.156

185. Ahmed N, Brawley VS, Hegde M, Robertson C, Ghazi A, Gerken C, et al. Human epidermal growth factor receptor 2 (HER2) -specific chimeric antigen receptor-modified T cells for the immunotherapy of HER2-positive sarcoma. *J Clin Oncol* (2015) 33(15):1688–+. doi: 10.1200/JCO.2014.58.0225

186. Norris S, Coleman A, Kuri-Cervantes L, Bower M, Nelson M, Goodier MR. PD-1 expression on natural killer cells and CD8(+) T cells during chronic HIV-1 infection. *Viral Immunol* (2012) 25(4):329–32. doi: 10.1089/vim.2011.0096

187. Stojanovic A, Fiegler N, Brunner-Weinzierl M, Cerwenka A. CTLA-4 is expressed by activated mouse NK cells and inhibits NK cell IFN-gamma production in response to mature dendritic cells. *J Immunol* (2014) 192 (9):4184–91. doi: 10.4049/jimmunol.1302091

188. Benson DMJr., Bakan CE, Mishra A, Hofmeister CC, Efebera Y, Becknell B, et al. The PD-1/PD-L1 axis modulates the natural killer cell versus multiple myeloma effect: a therapeutic target for CT-011, a novel monoclonal anti-PD-1 antibody. *Blood* (2010) 116(13):2286–94. doi: 10.1182/blood-2010-02-271874

189. Markiewicz K, Zeman K, Kozar A, Golebiowska-Wawrzyniak M, Wozniak W. Evaluation of selected parameters of cellular immunity in children with osteosarcoma at diagnosis. *Medycyna Wieku Rozwojowego* (2012) 16(3):212–21.

190. Kochin V, Nishikawa H. Meddling with meddlers: curbing regulatory T cells and augmenting antitumor immunity. *Nagoya J Med Sci* (2019) 81(1):1–18.

191. Fernandez L, Valentin J, Zalacain M, Leung W, Patino-Garcia A, Perez-Martinez A. Activated and expanded natural killer cells target osteosarcoma tumor initiating cells in an NKG2D-NKG2DL dependent manner. *Cancer Lett* (2015) 368 (1):54–63. doi: 10.1016/j.canlet.2015.07.042

192. Hermanson DL, Kaufman DS. Utilizing chimeric antigen receptors to direct natural killer cell activity. *Front Immunol* (2015) 6. doi: 10.3389/fimmu.2015.00195

193. Esser R, Müller T, Stefes D, Kloess S, Seidel D, Gillies SD, et al. NK cells engineered to express a GD2 -specific antigen receptor display built-in ADCC-like activity against tumour cells of neuroectodermal origin. *J Cell Mol Med* (2012) 16 (3):569–81. doi: 10.1111/j.1582-4934.2011.01343.x

194. Uherek C, Tonn T, Uherek B, Becker S, Schnierle B, Klingemann HG, et al. Retargeting of natural killer-cell cytolytic activity to ErbB2-expressing cancer cells results in efficient and selective tumor cell destruction. *Blood* (2002) 100(4):1265–73. doi: 10.1182/blood.V100.4.1265.h81602001265_1265_1273

195. Klingemann H. Challenges of cancer therapy with natural killer cells. *Cytotherapy* (2015) 17(3):245–9. doi: 10.1016/j.jcyt.2014.09.007

196. Floros T, Tarhini AA. Anticancer cytokines: Biology and clinical effects of interferon-alpha 2, interleukin (IL)-2, IL-15, IL-21, and IL-12. *Semin Oncol* (2015) 42(4):539–48. doi: 10.1053/j.seminoncol.2015.05.015

197. Meyers PA, Healey JH, Chou AJ, Wexler LH, Merola PR, Morris CD, et al. Addition of pamidronate to chemotherapy for the treatment of osteosarcoma. *Cancer* (2011) 117(8):1736–44. doi: 10.1002/cncr.25744

198. DuBois SG, Shusterman S, Ingle AM, Ahern CH, Reid JM, Wu B, et al. Phase I and pharmacokinetic study of sunitinib in pediatric patients with refractory solid tumors: A children's oncology group study. *Clin Cancer Res* (2011) 17 (15):5113–22. doi: 10.1158/1078-0432.CCR-11-0237

199. Keir ST, Morton CL, Wu JR, Kurmasheva RT, Houghton PJ, Smith MA. Initial testing of the multitargeted kinase inhibitor pazopanib by the pediatric preclinical testing program. *Pediatr Blood Cancer* (2012) 59(3):586–8. doi: 10.1002/pbc.24016

200. Safwat A, Boysen A, Lucke A, Rossen P. Pazopanib in metastatic osteosarcoma: Significant clinical response in three consecutive patients. *Acta Oncol* (2014) 53(10):1451–4. doi: 10.3109/0284186X.2014.948062

201. Navid F, Baker SD, McCarville MB, Stewart CF, Billups CA, Wu JR, et al. Phase I and clinical pharmacology study of bevacizumab, sorafenib, and low-dose cyclophosphamide in children and young adults with Refractory/Recurrent solid tumors. *Clin Cancer Res* (2013) 19(1):236–46. doi: 10.1158/1078-0432.CCR-12-1897

202. Grignani G, Palmerini E, Ferraresi V, D'Ambrosio L, Bertulli R, Asaftei SD, et al. Sorafenib and everolimus for patients with unresectable high-grade osteosarcoma progressing after standard treatment: a non-randomised phase 2 clinical trial. *Lancet Oncol* (2015) 16(1):98–107. doi: 10.1016/S1470-2045(14)71136-2

203. Fotia C, Avnet S, Kusuzaki K, Roncuzzi L, Baldini N. Acridine orange is an effective anti-cancer drug that affects mitochondrial function in osteosarcoma cells. *Curr Pharm Design* (2015) 21(28):4088–94. doi: 10.2174/1381612821666150918144953

204. Bond M, Bernstein ML, Pappo A, Schultz KR, Krailo M, Blaney SM, et al. A phase II study of imatinib mesylate in children with refractory or relapsed solid tumors: A children's oncology group study. *Pediatr Blood Cancer* (2008) 50(2):254–8. doi: 10.1002/pbc.21132

205. Aplenc R, Blaney SM, Strauss LC, Balis FM, Shusterman S, Ingle AM, et al. Pediatric phase I trial and pharmacokinetic study of dasatinib: A report from the children's oncology group phase I consortium. *J Clin Oncol* (2011) 29(7):839–44. doi: 10.1200/JCO.2010.30.7231

206. Maris JM, Courtright J, Houghton PJ, Morton CL, Kolb EA, Lock R, et al. Initial testing (stage 1) of sunitinib by the pediatric preclinical testing program. *Pediatr Blood Cancer* (2008) 51(1):42–8. doi: 10.1002/pbc.21535

207. Gopalakrishnan V, Spencer CN, Nezi L, Reuben A, Andrews MC, Karpinets TV, et al. Gut microbiome modulates response to anti-PD-1 immunotherapy in melanoma patients. *Sci (New York NY)* (2018) 359(6371):97–103. doi: 10.1126/science.aan4236

208. Chowell D, Morris LGT, Grigg CM, Weber JK, Samstein RM, Makarov V, et al. Patient HLA class I genotype influences cancer response to checkpoint blockade immunotherapy. *Sci (New York NY)* (2018) 359(6375):582–7. doi: 10.1126/science.aao4572

209. Rizvi NA, Hellmann MD, Snyder A, Kvistborg P, Makarov V, Havel JJ, et al. Mutational landscape determines sensitivity to PD-1 blockade in non-small cell lung cancer. *Sci (New York NY)* (2015) 348(6230):124–8. doi: 10.1126/science.aaa1348

210. Sade-Feldman M, Jiao YJ, Chen JH, Rooney MS, Barzily-Rokni M, Eliane JP, et al. Resistance to checkpoint blockade therapy through inactivation of antigen presentation. *Nat Commun* (2017) 8(1):1136. doi: 10.1038/s41467-017-01062-w

211. Leavy O. Therapeutic antibodies: past, present and future. *Nat Rev Immunol* (2010) 10(5):297. doi: 10.1038/nri2763

212. Ahmadzadeh M, Johnson LA, Heemskerk B, Wunderlich JR, Dudley ME, White DE, et al. Tumor antigen-specific CD8 T cells infiltrating the tumor express high levels of PD-1 and are functionally impaired. *Blood* (2009) 114(8):1537–44. doi: 10.1182/blood-2008-12-195792

213. Shi T, Ma Y, Yu L, Jiang J, Shen S, Hou Y, et al. Cancer immunotherapy: A focus on the regulation of immune checkpoints. *Int J Mol Sci* (2018) 19(5). doi: 10.3390/ijms19051389

frontiers | Frontiers in Immunology

TYPE Original Research
PUBLISHED 26 October 2022
DOI 10.3389/fimmu.2022.989972

OPEN ACCESS

EDITED BY
Marco Ponzetti,
University of L'Aquila, Italy

REVIEWED BY
Zihan Zhao,
Nanjing University, China
Jamshidkhan Chamani,
Islamic Azad University of Mashhad, Iran

*CORRESPONDENCE
Li Feng
fengli663@126.com

†These authors have contributed equally to this work

SPECIALTY SECTION
This article was submitted to Cancer Immunity and Immunotherapy, a section of the journal Frontiers in Immunology

RECEIVED 09 July 2022
ACCEPTED 07 October 2022
PUBLISHED 26 October 2022

CITATION
Chang J, Jiang Z, Ma T, Li J, Chen J, Ye P and Feng L (2022) Integrating transcriptomics and network analysis-based multiplexed drug repurposing to screen drug candidates for M2 macrophage-associated castration-resistant prostate cancer bone metastases. *Front. Immunol.* 13:989972. doi: 10.3389/fimmu.2022.989972

Integrating transcriptomics and network analysis-based multiplexed drug repurposing to screen drug candidates for M2 macrophage-associated castration-resistant prostate cancer bone metastases

Jinyuan Chang†, Zhenglong Jiang†, Tianyu Ma, Jie Li, Jiayang Chen, Peizhi Ye and Li Feng*

National Cancer Center/National Clinical Research Center for Cancer/Cancer Hospital, Chinese Academy of Medical Sciences and Peking Union Medical College, Beijing, China

Metastatic castration-resistant prostate cancer (CRPC) has long been considered to be associated with patient mortality. Among metastatic organs, bone is the most common metastatic site, with more than 90% of advanced patients developing bone metastases (BMs) before 24 months of death. Although patients were recommended to use bone-targeted drugs represented by bisphosphonates to treat BMs of CRPC, there was no significant improvement in patient survival. In addition, the use of immunotherapy and androgen deprivation therapy is limited due to the immunosuppressed state and resistance to antiandrogen agents in patients with bone metastases. Therefore, it is still essential to develop a safe and effective therapeutic schedule for CRPC patients with BMs. To this end, we propose a multiplex drug repurposing scheme targeting differences in patient immune cell composition. The identified drug candidates were ranked from the perspective of M2 macrophages by integrating transcriptome and network-based analysis. Meanwhile, computational chemistry and clinical trials were used to generate a comprehensive drug candidate list for the BMs of CRPC by drug redundancy structure filtering. In addition to docetaxel, which has been approved for clinical trials, the list includes norethindrone, testosterone, menthol and foretinib. This study provides a new scheme for BMs of CRPC from the perspective of M2 macrophages. It is undeniable that this multiplex

drug repurposing scheme specifically for immune cell-related bone metastases can be used for drug screening of any immune-related disease, helping clinicians find promising therapeutic schedules more quickly, and providing reference information for drug R&D and clinical trials.

KEYWORDS

drug repurposing, castration-resistant prostate cancer, bone metastases, network pharmacology, M2 macrophage

Introduction

It is undeniable that prostate cancer has become the second leading cause of death in men (1). Prostate cancer is characterized by hormone responsiveness, and androgen deprivation therapy can make tumor regression in prostate cancer patients (2). However, most patients progress to castration-resistant prostate cancer (CRPC) after a period of castration therapy, and 85% of patients with prostate cancer develop bone metastases (BMs) and are resistant to immunotherapy (3–5). To date, bone metastases remain an incurable form of prostate cancer with a significant impact on disease-specific morbidity and mortality (5), and represent a major challenge for advanced fatal prostate cancer.

Tumor-associated macrophages (TAMs) in the microenvironment have been proven to account for more than 50% of the tumor mass and are key drivers of tumor progression, metastasis and therapeutic resistance. M1-like TAMs with antitumor effects and M2-like TAMs with protumor effects coexist within the microenvironment, and the opposing effects of these M1/M2 subsets on tumors directly affect current strategies for antitumor immunotherapy. In addition, macrophages exhibit dynamic plasticity in the tumor microenvironment and can transform from an antitumor M1-like phenotype to an M2-like phenotype during certain specific immune responses, thus exerting a tumor-supporting influence (6). Studies have shown that macrophage infiltration is associated with poor prognosis in non-small cell lung cancer, hepatocellular carcinoma, pancreatic ductal adenocarcinoma (PDAC), glioblastoma, and bladder cancer (7). Stimulated by colony-stimulating factor, it increases the risk of BMs of lung cancer and breast cancer (8). In addition, osteoclasts formed by their differentiation are involved in bone remodeling, repair and homeostasis regulation, and are considered to be one of the driving factors of tumor BMs. Inhibiting or depleting macrophage infiltration in the bone microenvironment can effectively prevent BMs. Although CRPC patients with BMs also have features of immunosuppression, differences in macrophage phenotypes have rarely been reported in such patients, and it is unclear whether macrophages in the bone microenvironment are associated with the BMs of CRPC.

In terms of therapeutic drugs, the currently approved bone-targeted drugs, monoclonal antibodies (denosumab), and radiopharmaceuticals provide some benefits, effectively reducing bone pain and pathological fractures in patients with BMs of prostate cancer, and improving the overall quality of life in these patients (9, 10). However, a large proportion of patients still experience skeletal-related events (SREs) during treatment, and safety and tolerability issues often need to be considered. Adverse effects, represented by nephrotoxicity and severe hypocalcemia, usually limit the long-term use of drugs for BMs (11). In addition, immunotherapy, which plays a role in most solid tumors, showed dissatisfactory efficacy in patients with BMs, suggesting a state of immunosuppression in these patients (5). Therefore, the scientific community needs to identify, test and approve new therapeutic compounds targeting the specific relatively immunosuppressive bone microenvironment of patients with BMs to improve the symptoms of BMs in CRPC patients, overcome adverse drug reactions, and prolong patient survival.

However, drug research and development (R&D) is usually an energy-intensive, low-yield process. Therefore, prioritization of promising therapeutic drugs based on preclinical evaluation of pharmacoinformatics and repurposing of existing drugs are often worthwhile and necessary (12, 13). With the accumulation of available data, a variety of preclinical drug R&D methods have been proposed to assist researchers in making informed decisions. Computational chemistry-based ligand-receptor binding conformational modeling has been widely used in pharmacodynamics and pharmacokinetics studies, and has played a crucial role in understanding and identifying drug-target interactions (14–16), providing a method for micromechanics analysis in the complex stable system formed by small molecules and targets (17–19). For example, the study of the interaction between anthocyanins and human serum albumin transferrin complexes using spectral, calorimetric, stopped flow and molecular modeling approaches provides a new perspective for elucidating the cyclic distribution of anthocyanins (20). Here, by integrating transcriptomic and drug susceptibility data, and based on network analysis, a multiplex drug repurposing scheme was used to investigate

and comprehensively evaluate the immune infiltration landscape, differentially expressed genes (DEGs) mediating immune infiltration-related BMs, and promising candidate drugs in CRPC patients with BMs. To provide usable information for drug R&D and repurposing targeting DEGs of M2 macrophage-related BMs.

Methods

Patients and datasets

The microarray datasets GSE32269 (including 22 tumor samples and 29 BM samples) and GSE77930 (including 22 tumor samples and 20 BM samples) with clinical information were downloaded from Gene Expression Omnibus (GEO) (https://www.ncbi.nlm.nih.gov/gds) (21), and used as the discovery set and validation set, respectively. Specifically, the GEOquerry (22) package of R was used to download data, the hgu133a.db package of R was used to convert gene probe ID into gene symbol, and the Normalized between Arrays function in the limma (23) package of R was used for data normalization.

DEGs analysis and functional enrichment analysis

Genes with differential expression between the BM group and the primary group in the GSE32269 and GSE77930 cohorts were analyzed using the R package limma. And adjusted $p< 0.05$, and $|log2FoldChange| > 1$ were used as filter conditions. Functional enrichment analysis was performed using the R package clusterProfiler, and Gene Ontology (GO) and Kyoto Encyclopedia of Genes (KEGG) terms with adj $p<0.05$ were considered significant.

Transcriptome-based assessment of immune infiltration

The immune score, stromal score and tumor purity were calculated for each tumor sample in the primary and BM groups, using the ESTIMATE algorithm. Based on the ssGSEA method, the tumor immune microenvironment signatures of primary and BMs were inferred using a manually curated gene expression signature of 29 immune microenvironment functional genes by Alexander Bagaev et al. (24). The content of infiltrated immune cells in the tumor microenvironment of the primary and BM groups was calculated using the EPIC and Timer methods encapsulated by the R package IOBR and the CIBERSORT method provided online (25–27). The EPIC and Timer methods were executed with default parameters. For the CIBERSORT method, gene expression profiles prepared from standard annotation files were uploaded to the CIBERSORTx web portal (https://cibersortx.stanford.edu/) and run using the LM22 gene signature file and 1,000 permutations. To ensure the accuracy of the results, only samples with a CIBERSORT p value< 0.05 were retained for further analysis, and immune cells whose content was 0 in more than half of the samples were excluded. Immune cells with statistical significance and similar infiltration patterns in more than two algorithms were considered reliable.

Evaluation of DEGs and pathways in M2 macrophage-associated BMs

A random forest classifier was constructed using the randomForest package to identify the genes most associated with the BM phenotype of CRPC, ranking in importance according to the mean decrease accuracy value (28). Then, 5 times of ten-fold cross-validation were performed, and the number of important genes was selected according to the cross-validation curve. Permutation tests were performed on important genes using the rfPermute package, and significance information for each gene was obtained. Gene set enrichment analysis (GSEA) was performed with the R package Pi to explore the upregulation of pathways in the BMs group of CRPC (29). Specifically, the HALLMARK gene set was downloaded for quantification of pathway activity. The GSEA algorithm was run with 10,000 permutations using the gene list sorted by Log2FC as input, followed by the Benjamini-Hochberg method to control for FDR. Pathways with gene peaks greater than 30 and FDRs less than 0.05 were considered significantly enriched. Between each method, protein-protein interactions (PPI) based on the STRING database were used to screen for DEGs associated with M2 macrophages in BMs (30).

Transcriptome-based multiplex drug repurposing

The obtained prostate cancer BMs differential genes were input into the Connectivity Map (31), L1000CDS^2 (32) and L1000FWD (33) tools, respectively. Since the output of L1000CDS2 was limited to 50 drugs, the same cutoff was chosen for other databases, and the databases were sorted according to their reverse enrichment scores (inhibition scores). The drug scores from three different datasets were calculated with reference to the method proposed by the researcher Marios Tomazou to normalize the ranking of drugs using the weighting of the average ranking and the number of occurrences, which were used as input for the prior score of CoDReS. In this study, the weights of each part of CoDReS are defined as waS=0.45, wFS=0.45, and wStS=0.1 (34, 35).

Transcriptome-based repurposed drug structures were searched and downloaded, entered into the ChemBioServer 2.0 tool, used to calculate distance matrices for chemical and structural similarity, and clustered the drugs using the Ward method with a minimum Tanimoto similarity of 80% (36). The drug with the highest ranking according to the CoDReS normalized score in each cluster was selected to eliminate redundant structures in the drug list.

Transcriptome-based drug sensitivity analysis

The R package oncoPredict was used to assess the sensitivity of CRPC patients with BMs to chemotherapeutic drugs (37). The package was based on a ridge regression model that used expression data and drug response data from cancer cell lines to train the model to predict drug sensitivity from a patient's gene expression data. Drug response data for human cancer cell lines were obtained from Genomics of Drug Sensitivity in Cancer (GDSC1&2, https://www.cancerrxgene.org/), and expression data for GDSC1&2 cancer cell lines were obtained from the GDSC1000 resource (https://www.cancerrxgene.org/gdsc1000/). Drugs with NA values in more than 20% of cell lines were discarded. The k-nearest neighbors (KNN) method was used to estimate the remaining missing values.

Network-based natural compound screening

In the HERB database, the cell or tissue type was set to be derived from prostate cancer to screen the natural compounds, and the obtained compounds were used as the keyword input in the "Differentially expressed genes" module to obtain the potential action target of the compound (38). Cytoscape 3.7.2 was used to construct a natural compound-prostate cancer BMs network, calculating the criticality of natural compounds in the network according to the formula (1), and normalizing the ranking of key natural compounds within the unit interval (–1, 1) by dividing by the absolute maximum score. Key compounds were classified by structure, and extensive virtual screening of compounds in the same category was performed in the MedChemExpress library. ADMETLAB 2.0 was used to comprehensively evaluate the pharmacophysicochemical properties and pharmacokinetics of candidate compounds in the natural compound database, and molecules with reasonable conformations and low toxicities were considered as promising inhibitors (39).

$$ScoreBM_i = \frac{DegreeBM_{reverse_i} - DegreeBM_{mimic_i}}{N_{S_i \cap S_{BM}} \times \max|ScoreBM|}$$

$$ScoreM2_i = \frac{DegreeM2_{reverse_i} - DegreeM2_{mimic_i}}{N_{S_i \cap S_{GSEA}} \times \max|ScoreBM|}$$

$$i = 1, \ldots, N \quad \text{Drugs}$$

$$DR_i = \omega_{BM} \times ScoreBM_i + \omega_{M2} \times ScoreM2_i \qquad (1)$$

$Degree_{reverse}$ indicates that natural compounds regulate transcription in the reverse direction (with antagonistic effects) to BMs differential genes. $Degree_{mimic}$ indicates that natural compounds regulate transcription in the same direction (with synergistic effects) as BMs differential genes. S_i represents the gene set related to natural compounds. S_{GSEA} represents the gene set generated by GSEA. In this study, ω_{BM}=0.3 and ω_{M2} =0.7 were set respectively.

Molecular docking and virtual screening

The 3D structure of the compound was downloaded, and if only 2D structures were available, chem3D was used to draw the 3D structure and optimize the force field. The structural information of key targets was retrieved and predicted through the PDB database and AlphaFold Protein Structure Database, respectively. The most potential ligand binding sites were found based on the cocrystals, protein cavities and literature reports. The Arg-Gly-Asp (RGD) structure of SPP1 was the main site where it is bound by receptors and mediates signaling. The RGD polypeptide structure of SPP1 was obtained from a cocrystal of 1L5G (PDBID) (40).

The protein and compound structures were imported into AutoDock software. The compound was set to be flexible and the center coordinates were set according to the ligand binding site. The Lamarckian genetic algorithm was used to evaluate the binding ability between the ligand and the protein (41).

Allosteric sites of SPP1 receptor proteins based on D3pocket and DCC (dynamic cross-correlation matrices) analysis

The SPP1 receptor structure downloaded from PDB was used as input to the D3pocket and R package Bio3D tools (42, 43). The orthosteric and allosteric sites were represented using PyMOL in light blue and red, respectively. DCC was used to analyze the trajectory after Gromacs dynamics simulation.

Molecular dynamics

Gromacs was used for 10 ns molecular dynamics simulations of the candidate compounds and to perform an ensemble equilibration of temperature and pressure at 310 K and 1 Bar,

followed by positional confinement of proteins and small molecules, respectively (44, 45). The last frame structure after simulation equilibrium was used as the input of the allotype to predict the potential function of candidate compounds (46).

Comparison with ongoing clinical trials

Clinical studies related to castration-resistant prostate cancer bone metastases were obtained from ClinicalTrials.gov. Using "Prostate Cancer", "Castration resistant", and "Bone Metastasis" as keywords, the structures of small molecule drugs and drugs reported for clinical research were obtained from PubChem. All candidate compounds were further used as input to Chembioserver 2.0.

Result

Transcriptome-based DEGs analysis

To detect the dispersion between samples, PCA was conducted on the included microarray data. As shown in Figures 1A, S1D, samples can be clearly divided into two categories, indicating that the samples have good intragroup consistency and intergroup heterogeneity. By analyzing the differences in transcriptome expression between the two groups of patients, in the discovery set, a total of 229 genes with significant differences were finally obtained, of which 89 were upregulated and 140 were downregulated (Figure 1B). The biological process of differential genes was mainly enriched in the formation of extracellular matrix and extracellular structure, which was positively correlated with the maintenance of extracellular structure, and was involved in the signal transduction of integrin binding, cell adhesion and extracellular matrix receptor interaction pathway (Figure 1C).

Immune infiltration was further used to analyze the mechanism of BMs from the perspective of immune cell composition. The results showed that compared with the primary samples, the microenvironment of BMs contained more immune cells and stromal cells, and the tumor purity was relatively low (Figure 1D). Further analysis of immune cell composition revealed that based on the SSGSEA tool, a total of 11 significant changes in immune infiltration components were obtained. Among them, immune cells represented by macrophages and tumor-associated fibroblasts were significantly increased in BMs, while antitumor cytokines and MHC-I were significantly reduced (Figures 1E, F). Based on the EPIC and TIMER tools, four and two different abundances of infiltrating immune cells were obtained, respectively. Among them, the abundance of CD8+ T cells, macrophages and tumor-associated fibroblasts in BMs were significantly higher than that in the primary focus (Figures 1E, S1A, B). Based on the CIBERSORT tool, a total of 2 different types of immune cells were obtained, including activated NK cells elevated in the primary focus and M0 macrophages elevated in BMs. Meanwhile, in the discovery set, M2 macrophages, resting NK cells, and T regulatory cells were also enriched in BMs (Figure S1C). Interestingly, the validation set and the discovery set were highly consistent in the immune cell infiltration results, suggesting a certain degree of reliability and reproducibility of the above results (Figures S1F-H). The results of immune infiltration showed that BMs were enriched in macrophages and deficient in CD8+ T cells, and the results were mutually validated by more than two approaches in both the discovery set and the validation set. Due to the important role of macrophages in bone homeostasis, this study focused on the further exploration of their involvement in BMs from the perspective of macrophages.

The DEGs obtained by the TIMER and EPIC methods were correlated with macrophage phenotypes. As shown in Figure 2A, under the condition that the correlation is greater than 0.3 and is significant, 141 and 1466 macrophage-related DEGs were obtained in the discovery set and the validation set, respectively, of which a panel of 42 DEGs was simultaneously proven to be related to macrophage phenotype by two methods in the two datasets. The random forest method was further used to identify the genes with the ability to distinguish BMs in this collection. When the threshold was set to 5 (Figure 2B), the genes represented by COL11A1 were obtained, and the set constituted by them had the maximum discrimination ability (Figure 2C).

Generally, macrophages are divided into two subtypes, M1 and M2, with different biological functions. It is necessary to explore which subtypes are enriched in BMs. Although the content of M2 macrophages did not show differences in the validation set, the content of M2 macrophages in BMs showed an upward trend (Figure S1H), while it was significantly increased in the discovery set. Therefore, based on the WGCNA method, this study further explored the DEGs associated with M2 macrophages in the discovery set. Simultaneously, the correlation between each gene module and the abundance of macrophages obtained using the EPIC and TIMER methods was calculated based on the Pearson correlation coefficient. Finally, 699 genes related to macrophages (338 based on the EPIC method and 361 based on the TIMER method) and 147 genes related to M2 macrophage were extracted (Figures S2, S3). To further confirm the M2 macrophage-related genes, this study used the macrophage-related genes derived from the EPIC and TIMER methods as a universal set, including but not limited to the M0, M1 and M2 macrophage subtypes, and further intersected them with the related genes of M2 macrophages obtained by CIBERSORT analysis. A total of 104 genes with the potential to regulate M2 macrophages were identified based on WGCNA of the three immune infiltration algorithms (Figure 2D),

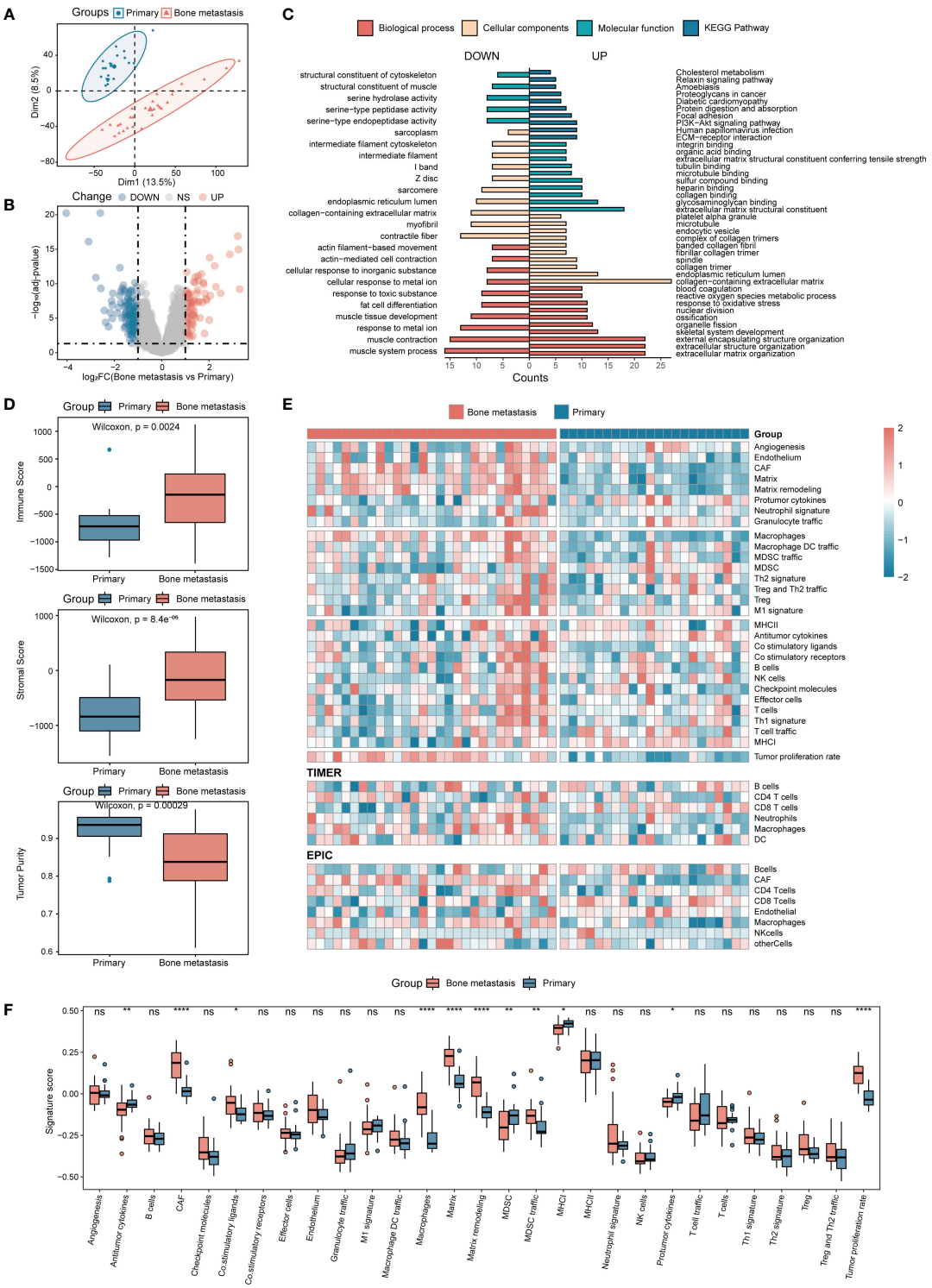

FIGURE 1
Analysis of DEGs and immune infiltration in CRPC with BMs. **(A)** Sample principal component analysis. **(B)** Analysis of DEGs in BMs. **(C)** DEGs of BMs enrichment analysis. **(D)** Immune, stromal, and tumor purity scores in patients between the primary focus and BMs. **(E)** Immune infiltration analysis. **(F)** Twenty-nine immune cell characteristics in patients with BMs. *P<0.05; **P<0.01; ****P<0.0001. ns, not significant.

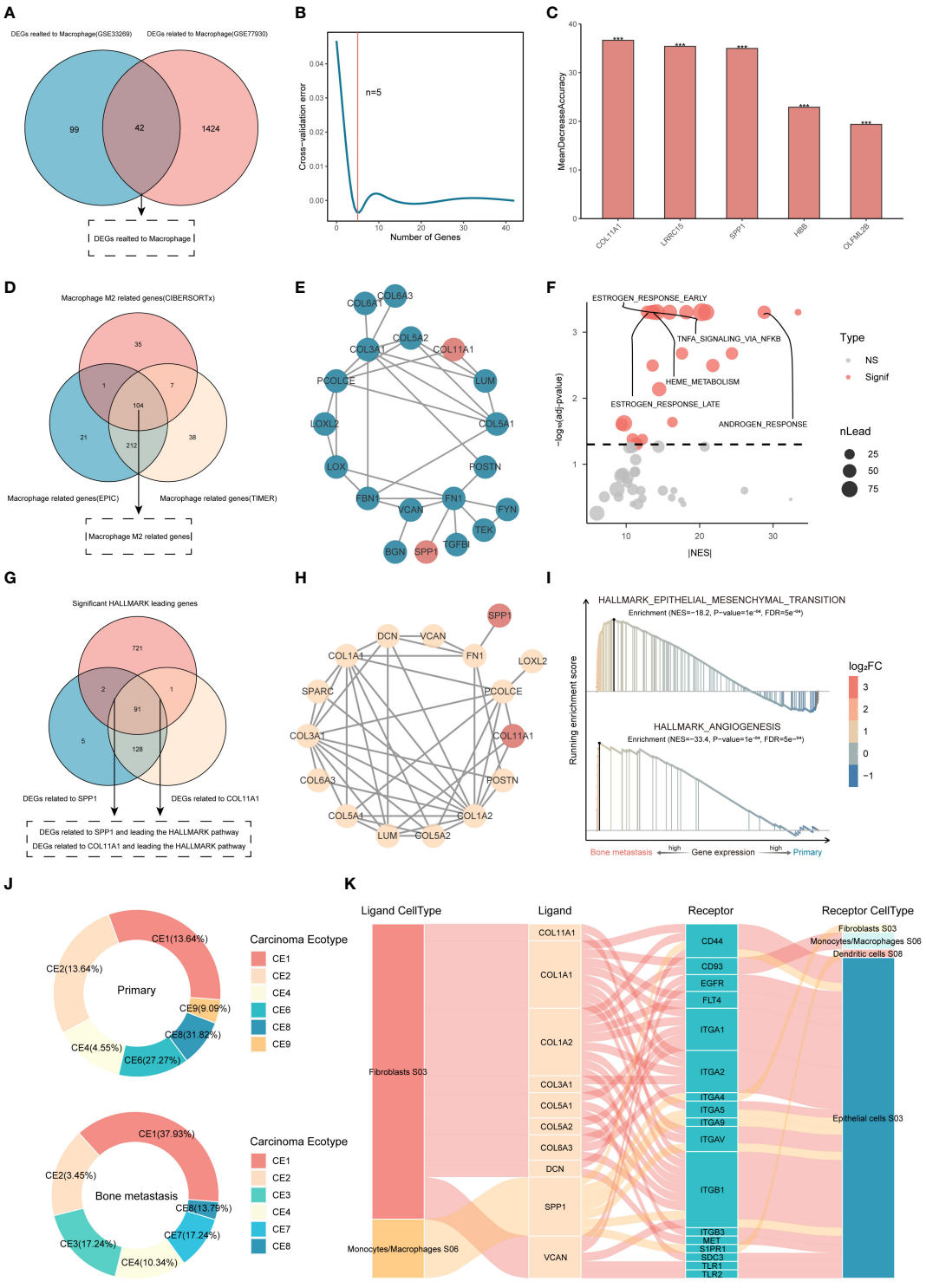

FIGURE 2
Identification of genes characteristic of M2 macrophage-associated BMs. **(A)** Macrophage-related DEGs. **(B, C)** Key gene identification based on random forest. ***P<0.001. ns, not significant. **(D)** Analysis of M2 macrophage-related DEGs based on WGCNA. **(E)** PPI between DEGs of BMs and M2 macrophage-related genes. **(F)** GSEA of SPP1 and COL11A1 proteins. **(G, H)** PPI analysis between proteins in enrichment pathways and key proteins. **(I)** GSEA of kernel targets. **(J, K)** Cancer ecotype analysis and cellular distribution of ligands and receptors.

suggesting that these genes play a crucial role in regulating the phenotype of M2 macrophages in CRPC.

To further explore the relevant genes that can predict BMs and participate in direct or indirect regulation of the M2 macrophage phenotype, 104 M2-related genes, 10 M2 macrophage markers (http://xteam.xbio.top/CellMarker/), and 5 macrophage-related genes with the ability to differentiate bone metastasis were used for PPI analysis, and the results showed that SPP1 and COL11A1 were considered to be the key DEGs with both the ability to differentiate between BMs and to regulate M2-macrophages (Figure 2E).

GSEA was further used to analyze genes related to SPP1 and COL11A1, and 22 pathways closely related to the BMs of CRPC were screened (Figure 2F). The enriched DEGs in the pathway were 93 and 92, with the ability to regulate BMs, related to SPP1 and COL11A1, respectively (Figure 2G). Interestingly, both had identical PPI networks under the set threshold, and the obtained set of 16 genes played a more central role in M2 macrophage-mediated BMs (Figure 2H), which were used as kernel inputs for subsequent drug repurposing studies. Functionally, it was mainly enriched in the pathways of epithelial-mesenchymal transition and angiogenesis (Figure 2I).

The results of cancer ecotype analysis showed that there were significant differences in the ecological composition. Compared with the primary focus, patients with BMs accounted for more CE1 and CE4, but less CE8, and had specific CE3 subtypes and lacked CE6 and CE9 subtypes. The 16 kernel genes represented by SPP1 and COL11A1 were mainly distributed in two ecological subtypes, CE1 rich in macrophages and CE3 rich in fibroblasts and epithelial cells (Figure 2J). Proteins represented by integrin, CD44 and S1PR1 distributed in fibroblasts, epithelial cells and dendritic cells were considered to be receptors for kernel genes (Figure 2K).

Drug sensitivity analysis

Hundreds of cancer cell line gene expression data and drug response data from GDSC1&2 were used to train a ridge regression model to infer the susceptibility of patients in primary focus versus BMs to different drugs. Since cancer cell lines in the blood system have different gene expression signatures from most other cancer cell lines (Figure 3A), they were excluded to ensure the reliability of the predicted results. Drugs with IC50 values less than 10 μM and repeated in GDSC1&2 were considered as potential drugs for the treatment of prostate cancer BMs. The results showed that GDSC1&2 included 138 and 51 BMs-sensitive drugs that met the screening conditions, respectively, of which 19 co-occurring drugs were repeatedly verified by two databases to have anti-CRPC and BMs potential (Figure 3B).

Further IC50 studies of the drugs showed that compared with primary focus, navitoclax was more sensitive to BMs (7.65 μM) and the efficacy was consistent in the GDSC1&2 databases ($P<0.05$). Patients were more sensitive to drugs represented by docetaxel (mean IC50 of 0.00857 μM and 0.0114 μM in patients with primary focus and BMs, respectively) and sepantronium bromide (mean IC50 of 0.0129 μM and 0.0155 μM, respectively) (Figure 3C).

Transcriptome-based multiplex drug repurposing

The transcriptome-based drug collection was sorted and normalized, and a total of 102 structurally-specific drugs with the potential to negatively regulate DEGs in the BMs of CRPC were obtained (Table S1). Hierarchical clustering analysis revealed that the input drugs spanned a broad diversity of chemical structures. Specifically, 38 clusters were obtained, of which 31 contained more than one drug (Figure 3D). By calculating the normalized CoDReS scores of the drugs, a total of 38 drugs represented by taxifolin were finally obtained. Combined with GDSC, 19 drugs with potential sensitivity to BMs were used as positive controls for the subsequent natural compound screening.

Screening of natural compounds based on network topology

According to the screening conditions, 10 natural compounds with potential regulation of prostate cancer were obtained. According to the constructed network, among the obtained natural compounds, testosterone had the most intersecting genes with a total of 134, followed by Withaferin A and Celastrol (Figure 3E). To standardize and normalize the number and regulation direction of DEGs contained in natural compounds, the obtained natural compounds were further calculated according to formula (1) in this study. Menthol, testosterone, luteolin and celastrol had higher scores and potential therapeutic effects on the BMs of prostate cancer (Table S2). Figure 3F also showed that more of the 16 kernel targets obtained by GSEA fall into regions with therapeutic potential. Although Withaferin A had more intersecting genes, it was excluded from subsequent studies due to its undesirable logFC value in GSEA-related targets.

To further clarify the role of natural compounds in macrophage-related BMs, the four natural compounds obtained in formula (1) were subjected to enrichment analysis, and a potential pathway map was drawn. As shown in Figure 3G, all four could regulate the expression of collagen or SPP1, thereby exerting regulatory effects on the invasion and metastasis of prostate cancer cells. Meanwhile, menthol, testosterone and luteolin could also regulate the differentiation of osteoclasts, participating in the regulation of bone remodeling

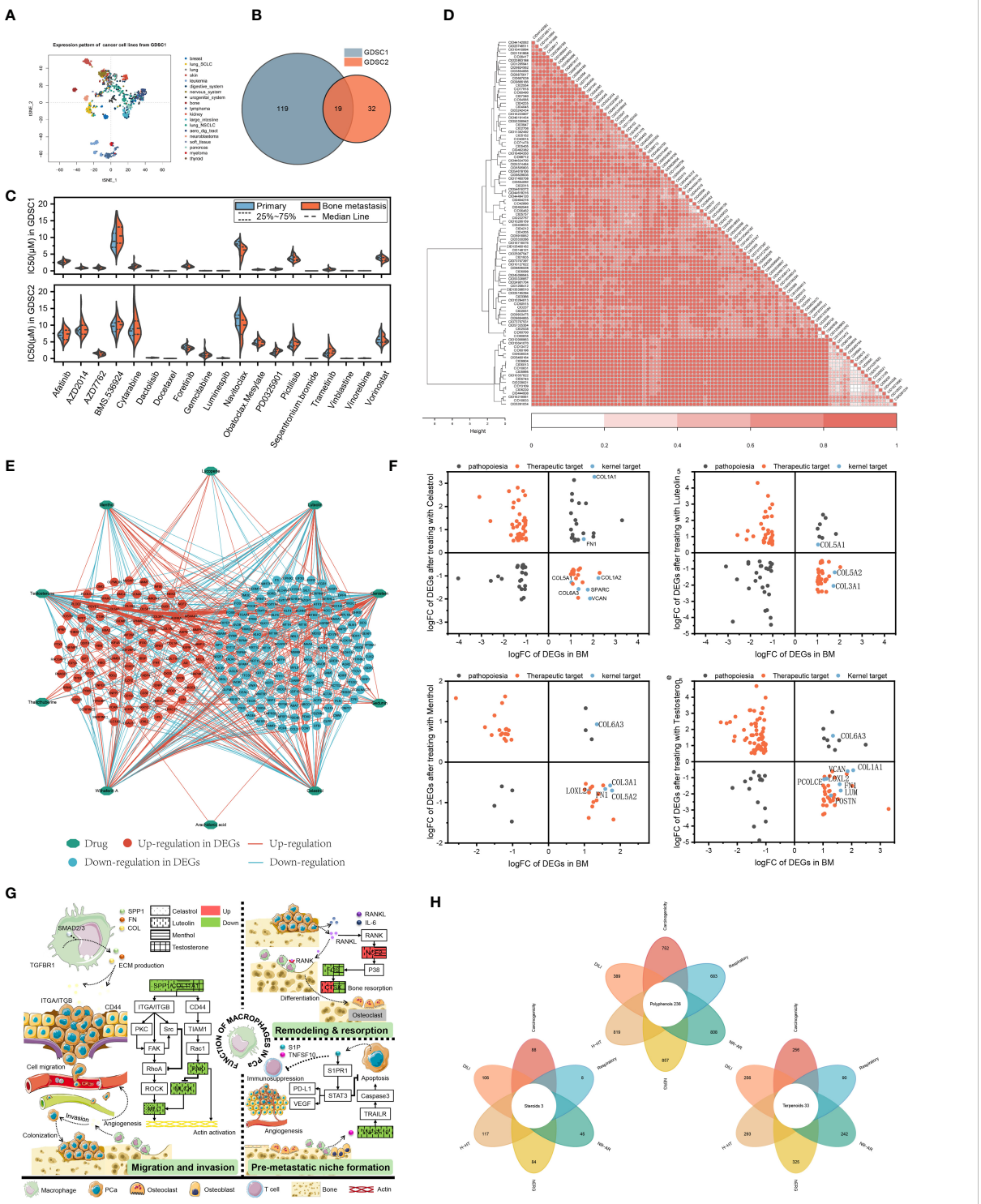

FIGURE 3
Integrating transcriptomes and network-based drug repurposing. **(A)** Cellular gene expression signature. **(B)** Sensitive drugs with co-occurrence in GDSC1&2. **(C)** IC50 of drugs in primary focus and BMs. **(D)** Structure-based drug cluster analysis. **(E)** Network pharmacology of natural compounds. **(F)** Topology-based candidate natural compounds. **(G)** Pathway patterns of candidate natural compounds. **(H)** Rational structure compounds in the MedChemExpress database.

and resorption balance. CTSK protein, as one of the specific markers of osteoclasts, testosterone and luteolin have diametrically opposite regulatory directions. As an androgen, testosterone can inhibit bone resorption, enhancing bone strength, which is the same as the potential function of androgen. Luteolin can inhibit the secretion of TNFSF10 from macrophages, regulating the formation of the pre-metastatic microenvironment.

Based on the assumption of structural similarity and functional similarity, 380 terpenoids, 124 steroids and 881 polyphenols in MedChemExpress were included for further investigation. ADMETLAB 2.0 was used to evaluate the structural plausibility of the included natural compounds. Among them, polyphenols, terpenoids and steroids had a total of 236, 33 and 3 candidate compounds that met the criteria, respectively (Figure 3H).

Mulberroside C and terrestrosin D have higher affinity

Molecular docking was performed on the candidate natural compounds, and the positive drugs obtained in the above process were used as controls (Figure 4A and Table S3). Two compounds were obtained (Figure 4B), CID 190453 (mulberroside C) and CID 78177919 (terrestrosin D), both of which had a higher affinity to the targets than the average value of the positive control. Determining the binding mechanism depends on fundamental thermodynamic parameters, such as binding free energy, which can be calculated from hydrogen bonds formed between ligands and proteins, electrostatic forces, van der Waals forces, and hydrophobic interactions (47, 48). To further quantify the binding ability of the ligand to the protein, this study further predicted the binding constant by AutoDock (Table 1), suggesting that the binding constants of mulberroside C and terrestrosin D to the receptors of SPP1 were both at the nanomolar level, showing good spontaneous binding ability.

Figure 4C showed that both have good safety profiles, among which mulberroside C has relatively excellent oral absorption and drug metabolism. Although terrestrosin D has poor oral absorption, which is the same as steroid drugs, it has the better plasma protein binding (PPB) and distribution ability, suggesting that mulberroside C can be administered orally, and terrestrosin D can be administered intravenously or intramuscularly.

Both of them can not only bind to CD44, ITGAV/ITGB3 and S1PR1 receptors through hydrophobic forces, but also form hydrogen bonds to improve the binding stability (Figures 4D, S4). In addition, the compounds occupied the residue site of SPP1 interacting with these three receptors, which affected the normal function of the signaling pathway.

Stability and activity analysis of mulberroside C and terrestrosin D based on dynamics and allotype tools

Dynamics simulations of CD44, ITGAV/ITGB3 and S1PR1 were performed using Gromacs, and the equilibrated trajectory files were used as input to D3Pocket and bio3D (Figure 4E).

Previous studies showed that hyaluronate binds to the far N-terminal domain of CD44 (the red pocket) and does not affect the OPN-CD44 interaction (Figure 4F). Throughout the trajectory, the dynamic correlation of residue sites where the red pocket was located showed a negative correlation with residues within the blue pocket (Figure 4G). Here, blue and red pockets were used to bind SPP1 and natural compounds, respectively. Similarly, as shown in Figures S5A–D, the red pocket residues of ITGAV/ITGB3 and S1PR1 exhibited a dynamic correlation with the residues in the blue pocket and were further investigated as allosteric and orthosteric sites, respectively.

Molecular dynamics studies of small molecules and receptors showed that in 10 ns simulations, both SPP1 and candidate compounds reached equilibrium, fluctuating root mean square deviation (RMSD) values over time compared to the position of the CD44 receptor pocket, fluctuating between 0.015 and 0.656 nm, with similar volatility (Figure 4H). Compared with the CD44 receptor, the RMSD fluctuation of candidate compound binding to the ITGAV/ITGB3 receptor was more stable. However, mulberroside C did not stably bind to the allosteric pocket of S1PR1 (Figures S5E, F).

In addition, after binding of mulberroside C and terrestrosin D, the fluctuation of residues had different peaks than those of SPP1 (Figures S5G–I). Taking CD44 as an example, compared with the binding of SPP1, the flexibility of receptor residues 40-60 was higher after binding to the candidate compound, and reached the peak around residues 111 and 165, while these residues showed lower flexibility when binding to SPP1. Similarly, after binding SPP1, CD44 was significantly more volatile at residue 95 than the allosteric site-binding candidate compound (Figure 4I). This may be related to the ligands occupying the receptor pocket, which affected the flexibility of the residue by forming an interaction force, thereby affecting the movement of the residue at the orthosteric site by binding to the allosteric site, and then hindering the function of proteins.

The rigidness of the compound in the system can be addressed through the inspection of the radius of gyration (Rg) value. As shown in Figures 4J, S5J, K, after the candidate compounds bound to CD44, the Rg remained at approximately 0.546 ± 0.023 nm and 0.771 ± 0.029 nm, and the SPP1 fluctuates around 0.572 ± 0.032 nm. Among them, the Rg of terrestrosin D was significantly larger than that of mulberroside C and SPP1, which may be related to its complex structure.

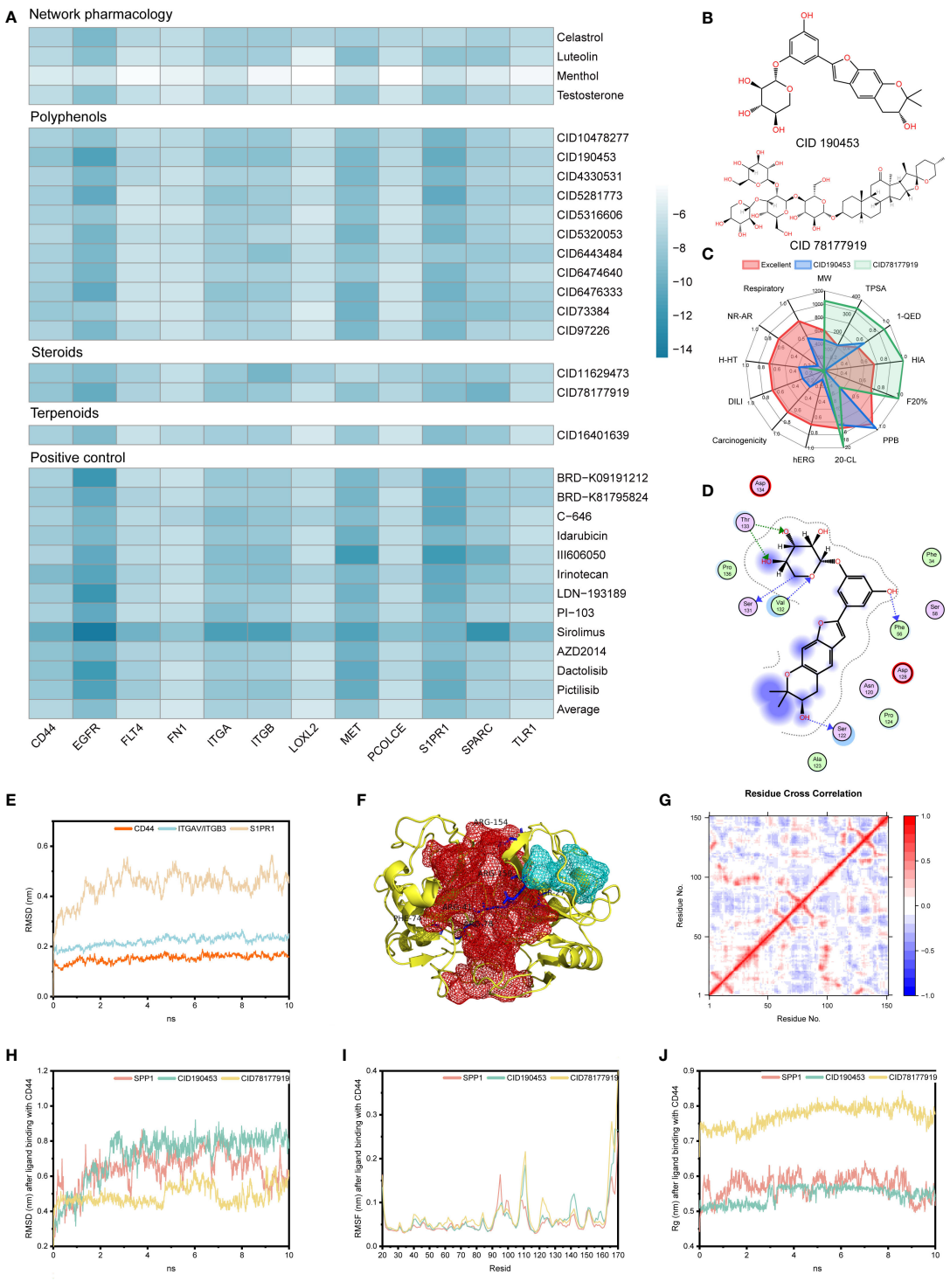

FIGURE 4
Stability evaluation of candidate compounds. **(A)** Docking simulation of candidate compounds. **(B)** Chemical formulas of CID 190453 and CID 78177919. **(C)** Evaluation of pharmacophysicochemical properties based on ADMETLAB2.0. **(D)** The docking pattern of CID 190453 with CD44. **(E)** Molecular dynamics simulation of SPP1 receptors. **(F)** Allosteric (red pocket) and orthosteric sites (blue pocket) of CD44. **(G)** DCC analysis of CD44. **(H-J)**. RMSD, RMSF and Rg analysis of candidate compounds after binding to the SPP1 receptor.

TABLE 1 Binding energies and binding constants of mulberroside C and terrestrosin D to the receptors of SPP1.

Target name	Compound name	Binding energy	Ki [Temperature = 298.15 K] (nM)
CD44	CID 190453	-8.5	589.94
	CID 78177919	-8.4	698.31
ITGAV/ITGB3	CID 190453	-8.8	355.72
	CID 78177919	-8.6	498.40
S1PR1	CID 190453	-10.3	28.35
	CID 78177919	-9	253.88

The last frame after 10 ns simulation was used as the input file of the allotype tool to predict the function after the receptor binds to the allosteric pocket. The results show that the ΔΔG values of the candidate compounds are all negative (Table 2), suggesting that the function of the candidate compounds is to inhibit the binding of the protein to SPP1, thereby inhibiting the pathway.

Evaluation of the integrated drug list with respect to ongoing clinical trials

Cluster analysis was performed on 62 drugs and clinical trials obtained from multiplex drug repurposing, and a total of 48 clusters were obtained, of which 2 drugs (docetaxel and sirolimus) were already in clinical trials. Eight structurally specific drugs (danazol, 3-Cl-AHPC, 5-fluorocytosine, rilmenidine, BRD-K09191212, SB-225002, PD-0325901, and obatoclax mesylate) were also obtained. Among them, PD-0325901 was reported to have BMs sensitivity in the GDSC database.

In the remaining clusters, structurally similar drugs to current clinical trials were highlighted (Figure S5L), and the most promising repurposing drugs that could play a role in the treatment of BMs of CRPC by interfering with M2 macrophages were further screened according to the following three principles: (a) drugs that were similar to phase 3 or 4 clinical trials and belonged to the same cluster, (b) drugs that have the ability to regulate the M2 macrophage-associated BMs genes obtained by modulating GSEA, and (c) drugs that have been reported in the literature to have prostate cancer therapeutic potential.

The criteria were met by 5 drugs on the list (norethindrone, testosterone, docetaxel, menthol, and foretinib). Among them, testosterone and docetaxel have been used in phase 2 and phase 3 clinical trials, respectively. Although experts still have concerns about the use of testosterone in prostate cancer, there have been several phase II clinical trials investigating "bipolar androgen therapy (BAT)" for CRPC (49). The five drugs mentioned above have the potential to further become clinical drugs for BMs of CRPC.

Discussion

The median overall survival in metastatic CRPC was only 13 months (50), underscoring the need for treatment. Immunotherapy has been successfully used in the treatment of a variety of tumors, however, accumulating evidence suggests that prostate cancer is a "cold" immune desert with low immune infiltration, low tumor mutational burden, and low antigen presentation. Therefore, prostate cancer does not respond as strongly to a single immune checkpoint inhibitor treatment as it does for immune "hot" tumors represented by non-small cell lung cancer, which leads to limited response to immunotherapy and suggests the immunosuppressive state of patients with BMs (51). Due to the dynamic balance between "osteoblasts" and "osteoclasts" inherent in bone, bone has a relatively unique immune microenvironment. Studies have shown that in the tissue samples of patients with osteolytic metastasis of prostate cancer, an increase in immune infiltration represented by macrophages and T cells was observed. Compared with osteolytic metastasis, the content of macrophages in osteogenic bone metastasis was significantly reduced. In addition, the

TABLE 2 Calculated ΔΔG Values for candidate compounds after binding to the SPP1 receptors using AlloType.

Protein	PDBID	Ligand	Predicted allsoteric type	ΔΔG (kcal/mol)
CD44	4PZ3	CID 190453	Inhibition	32.5070
		CID 78177919	Inhibition	41.7766
ITGAV/ITGB3	1L5G	CID 190453	Inhibition	39.1615
		CID 78177919	Inhibition	35.5584
S1PR1	3V2Y	CID 78177919	Inhibition	11.5344

immune checkpoint B7-H3 is upregulated in tissue samples from patients with BMs, suggesting that prostate cancer BMs have immunogenic characteristics distinct from those of the primary tumor (52). In particular, immune cells represented by macrophages not only play an important role in bone homeostasis, but also participate in the regulation of bone formation (11). Studies have shown that the number of M2 macrophages and the activity of inflammasomes were positively correlated with bone tumor burden (10).

The results of this study also showed that BMs of CRPC have higher immune scores and more macrophages than the primary focus, but the number of CD8+ T cells (EPIC & TIMER) and activated NK cells (CIBERSORT) in BMs is lower, with more M2 macrophages, T regulatory cells (CIBERSORT) and tumor related fibroblasts (ssGSEA & EPIC). Moreover, the abundance of MHC I-related antigen-presenting molecules (ssGSEA) was lower than that in the primary focus, which resulted in BMs with relatively low immunogenicity. Thus, the absence of such "cytotoxic" cells and the infiltration of "immune response suppressor" cells makes the microenvironment of CRPC patients with BMs more closely resemble those of cold immune tumors. Although BMs have significantly higher immune scores than primary tumors, immune checkpoint therapy for patients with BMs has not been successful. This is related to the unique composition of T cell populations and the infiltration of immunosuppressive cells in patients with BMs (5, 53). These findings underscore the importance of careful assessment of immune infiltration in CRPC patients with BMs to guide drug use.

Simultaneously, a collection of DEGs identified from CRPC with BMs highlighted in enrichment analysis extracellular matrix and integrin-related pathways that were strongly associated with prostate cancer metastasis. Specifically, among the DEGs, a total of 141 genes were involved in the regulation of macrophages. Through random forest, WGCNA, GSEA and PPI, it was finally determined that SPP1 and COL11A1 were related to M2 macrophages with the ability to predict BMs.

As a highly specific osteolysis biomarker, SPP1 and type I collagen have been previously shown to be expressed and secreted by a variety of cancers, and participate in cell adhesion, bone resorption, cell adhesion, metastasis and other processes by binding to CD44 and integrin receptors (54–58). As a major mediator of tumor-associated inflammation, SPP1 has been proven to be related to enzalutamide resistance by activating the PI3K/AKT and ERK1/2 signaling pathways in CRPC, and promoting the invasion and metastasis of CRPC (59). COL11A1 was shown to be involved in immune-related pathways and was significantly associated with RFS in patients (60). In consideration of their important roles in CRPC, both have been suggested by investigators as alternative prognostic assessments and new promising immunotherapy targets for drug development.

Based on the DEGs of the above two groups of patients, integrated transcriptomic and network-based analysis combined with existing clinical trials to screen promising drugs for repurposing, a total of 5 nonrepetitive drugs were obtained (norethindrone, testosterone, docetaxel, menthol, and foretinib), and should receive special attention.

As a progesterone derivative, norethindrone inhibits 5α-reductase, a key protease that converts testosterone to dihydrotestosterone, has been proven to reduce bone mineral loss in male castrated mice, and has been used in the treatment of hormone-refractory prostate cancer (61). Here, this study highlights its bone-protective effect through the M2 macrophages, which can be further used in the prevention and treatment of CRPC bone metastases.

Different from progesterone, testosterone, as an important androgen, has a role in promoting the occurrence and growth of prostate cancer. Although studies have shown that testosterone levels correlate with disease progression, and that androgen deprivation therapy can lead to prostate cancer tumor regression (2), patients inevitably enter a castration-resistant stage, where castration-resistant therapy is no longer effective. Studies have shown that in prostate cancer, the Gleason score is negatively correlated with testosterone dependence, and highly aggressive prostate cancer does not depend on testosterone. Artificial supplementation with exogenous testosterone can inhibit the further progression of such highly aggressive prostate cancer, thereby reducing prostate cancer invasion risk (62, 63). Several clinical trials have been conducted using BAT for CRPC. Considering the important role of testosterone in bone health, if exogenous testosterone supplementation is no longer a contraindication for CRPC, we have reason to believe that the application of testosterone will be a promising treatment for BMs of CRPC.

Docetaxel, a drug that has been clinically approved for CRPC treatment, has been shown to prolong the survival of prostate cancer patients with more than 4 BMs (64). It also shows that the drugs obtained based on integrated transcriptomic and network-based analysis have certain robustness and reproducibility.

As a multiple receptor tyrosine kinase inhibitor, foretinib exhibited potent inhibition of c-MET, vascular endothelial growth factor receptor 2 (KDR) and FLT4, and showed antitumor and antiangiogenic activities. High expression of c-MET was found in 83% of prostate cancer BMs, and inhibitors targeting this protein have been used in clinical trials at various stages (65).

As a terpenoid, menthol can bind to TRPM8 and has been approved for the treatment of bronchitis and rhinitis. TRPM8, as a member of the transient potential receptor family, has been shown to be highly expressed in androgen-sensitive cancer cells, is a potential prognostic marker for metastatic CRPC, and is also considered a promising druggability target for the treatment of

prostate cancer (66). Although prostate cancer cells depend on the Ca^{2+} infiltration of TRPM8 for invasion and metastasis, non-physiological activation of TRPM8 by menthol inhibits the proliferation and motility of CRPC (67, 68). Screening potent specific agonists for activating TRPM8 channels will be one of the strategies for future drug R&D.

Natural compounds are considered a treasure trove of drug discovery, with an estimated 25-38% of innovative FDA-approved chemical drugs derived from phytochemicals or their derivatives (69). Network-based and integration of existing natural compound transcriptome sequencing results of prostate cancer cells. Two of the four potential drug candidates (Menthol and Testosterone) were included in the final candidate list, showing the referential role of network pharmacology in drug R&D. Through further analysis of the natural compound database, two potential compounds were finally obtained, namely, mulberroside C and terrestrosin D. Both have greater affinities for receptor proteins than the average positive drugs in the virtual screening. In addition, in the follow-up molecular dynamics, except that mulberroside C and S1PR1 failed to bind stably, they all showed good stability in the 10 ns simulation.

Allostery is a phenomenon in proteins where functional changes in the active site result from distant perturbations (such as ligand binding and mutation). In general, allosteric can be analyzed as a thermodynamic energy cycle, and it is usually necessary to predict the allosteric ability of drugs before R&D. In 2021, Professor Lai's research group from Peking University proposed a tool called allotype to predict the direction of allosteric regulation based on the force distribution in the binding site, which is used to calculate the allosteric coupling strength $\Delta\Delta G$ (46). The results of Allotype also showed that both have the ability to inhibit the binding of SPP1 to the receptor, thereby inhibiting the activation of downstream pathways. In terms of inhibitory ability, compared with terrestrosin D, which has a greater inhibitory ability against CD44, mulberroside C has a stronger inhibitory ability against ITGAV/ITGB3. Among the three receptors, the inhibitory ability of CD44 and ITGAV/ITGB3 was stronger, but that of S1PR1 was weaker. However, this study was mainly based on theoretical calculations, and the binding energy of the drugs were not measured experimentally, which may result in a discrepancy between the two. The main reasons for the difference may be as follows (70): (a) the sampling strategies and scoring criteria for Lamarck genetic algorithms and grid calculations used in the molecular docking process limit the increase in accuracy. (b) The molecular weight of the ligand is too large or contains multiple polar groups, which participate in the formation of various electrostatic interactions. (c) Insufficient sampling of ligand parameters such as spatial position, orientation, distance and conformation resulted in the failure to fully consider the effect of the internal energy contained in the candidate compounds on the binding energy during the docking process. Despite the problem of false positives or false negatives during virtual screening, hit quality improves with the number of compounds screened (71). A total of 1686 compounds were included in this study, and 328 small molecules were evaluated by molecular docking simulation. The ligand pose after binding of protein was dynamically evaluated by molecular docking and molecular dynamics. It is possible to eliminate false positives or false negatives for binding energies caused by incorrect ligand posture. Although they were not included in the list of the most promising repurposed drugs through the final screening conditions, there were also experimental studies showing that terrestrosin D has the effect of inhibiting the growth of prostate cancer and anti-angiogenesis (72).

Drug repurposing is used to rapidly identify and develop therapeutics for unmet needs. However, the plasma concentrations of many newly discovered compounds are lower than the required drug concentrations, limiting their direct clinical use (73). Combinations in tumor therapy, originally proposed to overcome drug resistance and provide new treatment options (74), have been used as a way to increase the success rate of drug repurposing. Two drugs that exhibit synergistic effects in clinical treatment allow the drug to achieve the same level of efficacy as a high-dose single drug at a lower dose, thereby reducing the dose of one drug and improving clinical safety. Tumor pathogenesis usually involves pathological features characterized by redundancy and versatility, limiting the clinical efficacy of single-target drugs. However, drug combination therapy often results in complex pharmacodynamic or pharmacokinetic interactions, or both, due to individual differences and other factors, which makes it difficult to describe the effectiveness and side effects of combined drugs, and may bring additional health issues (75). The evaluation of drug absorption, distribution, metabolism, excretion and toxicity characteristics is of great significance for predicting drug interactions. Most antitumor drugs need to undergo extensive liver metabolism, such as drugs metabolized by microsomal cytochrome P-450. When other drugs used in combination inhibit the activity of these enzymes, it is easy to cause drug interactions *in vivo* and affect drug efficacy. In this study, through the multiplex drug repurposing method, among the five candidate compounds obtained, docetaxel combined with abiraterone was used for the first-line treatment of metastatic CRPC, with a lower rate of serious adverse events (76). Although the phase II clinical study of foretinib showed that all patients included experienced at least one adverse event (77), its combination with PD-1 has been shown to be applicable in the treatment of colorectal cancer (78), suggesting the value of candidate compounds in combined medication.

Naturally, this work still has certain limitations. At present, only two transcriptome dataset has been included for DEGs analysis, and were used as the discovery set and validation set. The results may have potential bias, which still needs the support and proof of a quantity of transcriptome data in the future. In addition, the transcriptome sequencing results of natural compounds against prostate cancer cells are limited. Although this study simulated the natural compound database with molecular docking and dynamics, the real situation may still differ from the simulation. Finally, we used a multiplex-drug repurposing approach integrating transcriptomes and network-based approaches to generate a drug candidate list. Although these drugs have demonstrated clinical or experimental antitumor effects, for bone metastases, the primary site of treatment is equally important, which requires consideration of the toxic and adverse reactions of combined pharmacotherapy in clinical use, and evaluation of drug safety. Here, the research based on the method of pharmacoinformatics provides new insights for the repurposing of drugs that are already in the experiment, exploring the new indications of drugs from the perspective of synthesis and prediction, and provides a new scheme for the treatment for BMs of CRPC.

Data availability statement

The datasets presented in this study can be found in online repositories. The names of the repository/repositories and accession number(s) can be found in the article/Supplementary Material.

Author contributions

LF is the corresponding author of this article, JCa and ZJ contributed equal. LF conceived the research. JCa collected the data and drafted the manuscript. ZJ analyzed the data and TM and JL provided valuable suggestions on the investigation. JCe and PY critically reviewed the manuscript and assisted in the final write-up of the manuscript. All authors contributed to the article and approved the submitted version.

Funding

This research was supported by the cancer discipline construction project of integrated traditional Chinese and Western medicine of Peking Union Medical College (20192010302), the Beijing Natural Science Foundation (7222293) and the special subject of research and evaluation of China Association of Chinese Medicine (CACMRE2021-A-05).

Acknowledgments

In this study, we sincerely thank Mr. Zixuan Chai from the Cancer Hospital Affiliated to Chongqing University for his guidance and help in the process of bioinformatics analysis.

Conflict of interest

The authors declare that the research was conducted in the absence of any commercial or financial relationships that could be construed as a potential conflict of interest.

Publisher's note

All claims expressed in this article are solely those of the authors and do not necessarily represent those of their affiliated organizations, or those of the publisher, the editors and the reviewers. Any product that may be evaluated in this article, or claim that may be made by its manufacturer, is not guaranteed or endorsed by the publisher.

Supplementary material

The Supplementary Material for this article can be found online at: https://www.frontiersin.org/articles/10.3389/fimmu.2022.989972/full#supplementary-material

References

1. Siegel RL, Miller KD, Fuchs HE, Jemal A. Cancer statistics, 2022. *CA Cancer J Clin* (2022) 72(1):7–33. doi: 10.3322/caac.21708

2. Desai K, Mcmanus JM, Sharifi N. Hormonal therapy for prostate cancer. *Endocr Rev* (2021) 42(3):354–73. doi: 10.1210/endrev/bnab002

3. Lokeshwar SD, Klaassen Z, Saad F. Treatment and trials in non-metastatic castration-resistant prostate cancer. *Nat Rev Urol* (2021) 18(7):433–42. doi: 10.1038/s41585-021-00470-4

4. Coleman RE, Croucher PI, Padhani AR, Clezardin P, Chow E, Fallon M, et al. Bone metastases. *Nat Rev Dis Primers* (2020) 6(1):83. doi: 10.1016/B978-0-323-47674-4.00056-6

5. Kfoury Y, Baryawno N, Severe N, Mei S, Gustafsson K, Hirz T, et al. Human prostate cancer bone metastases have an actionable immunosuppressive microenvironment. *Cancer Cell* (2021) 39(11):1464–78. doi: 10.1016/j.ccell.2021.09.005

6. Yunna C, Mengru H, Lei W, Weidong C. Macrophage M1/M2 polarization. *Eur J Pharmacol* (2020) 877:173090. doi: 10.1016/j.ejphar.2020.173090

7. Wu K, Lin K, Li X, Yuan X, Xu P, Ni P, et al. Redefining tumor-associated macrophage subpopulations and functions in the tumor microenvironment. *Front Immunol* (2020) 11:1731. doi: 10.3389/fimmu.2020.01731

8. Jiang P, Gao W, Ma T, Wang R, Piao Y, Dong X, et al. CD137 promotes bone metastasis of breast cancer by enhancing the migration and osteoclast

differentiation of monocytes/macrophages. *Theranostics* (2019) 9(10):2950–66. doi: 10.7150/thno.29617

9. Gillessen S, Attard G, Beer TM, Beltran H, Bjartell A, Bossi A, et al. Management of patients with advanced prostate cancer: Report of the advanced prostate cancer consensus conference 2019. *Eur Urol* (2020) 77(4):508–47. doi: 10.1016/j.eururo.2020.01.012

10. Hofbauer LC, Bozec A, Rauner M, Jakob F, Perner S, Pantel K. Novel approaches to target the microenvironment of bone metastasis. *Nat Rev Clin Oncol* (2021) 18(8):488–505. doi: 10.1038/s41571-021-00499-9

11. Zhang X. Interactions between cancer cells and bone microenvironment promote bone metastasis in prostate cancer. *Cancer Commun (Lond)* (2019) 39 (1):76. doi: 10.1186/s40880-019-0425-1

12. Pushpakom S, Iorio F, Eyers PA, Escott KJ, Hopper S, Wells A, et al. Drug repurposing: Progress, challenges and recommendations. *Nat Rev Drug Discovery* (2019) 18(1):41–58. doi: 10.1038/nrd.2018.168

13. Dareini M, Amiri TZ, Marjani N, Taheri R, Aslani-Firoozabadi S, Talebi A, et al. A novel view of the separate and simultaneous binding effects of docetaxel and anastrozole with calf thymus DNA: Experimental and in silico approaches. *Spectrochim Acta A Mol Biomol Spectrosc* (2020) 228:117528. doi: 10.1016/j.saa.2019.117528

14. Sadeghzadeh F, Entezari AA, Behzadian K, Habibi K, Amiri-Tehranizadeh Z, Asoodeh A, et al. Characterizing the binding of angiotensin converting enzyme I inhibitory peptide to human hemoglobin: Influence of electromagnetic fields. *Protein Pept Lett* (2020) 27:1007–21. doi: 10.2174/1871530320666200425203636

15. Beigoli S, Sharifi RA, Askari A, Assaran DR, Chamani J. Isothermal titration calorimetry and stopped flow circular dichroism investigations of the interaction between lomefloxacin and human serum albumin in the presence of amino acids. *J Biomol Struct Dyn* (2019) 37:2265–82. doi: 10.1080/07391102.2018.1491421

16. Marjani N, Dareini M, Asadzade-Lotfabad M, Pejhan M, Mokaberi P, Amiri-Tehranizadeh Z, et al. Evaluation of the binding effect and cytotoxicity assay of 2-Ethyl-5-(4-methylphenyl) pyramido pyrazole ophthalazine trione on calf thymus DNA: spectroscopic, calorimetric, and molecular dynamics approaches. *LUMINESCENCE* (2022) 37:310–22. doi: 10.1002/bio.4173

17. Zare-Feizabadi N, Amiri-Tehranizadeh Z, Sharifi-Rad A, Mokaberi P, Nosrati N, Hashemzadeh F, et al. Determining the interaction behavior of calf thymus DNA with anastrozole in the presence of histone H1: Spectroscopies and cell viability of MCF-7 cell line investigations. *DNA Cell Biol* (2021) 40:1039–51. doi: 10.1089/dna.2021.0052

18. Askari A, Mokaberi P, Dareini M, Medalian M, Pejhan M, Erfani M, et al. Impact of linker histone in the formation of ambochlorin-calf thymus DNA complex: Multi-spectroscopic, stopped-flow, and molecular modeling approaches. *Iran J Basic Med Sci* (2021) 24:1568–82. doi: 10.22038/IJBMS.2021.58829.13070

19. Chamani J, Moosavi-Movahedi AA. Effect of n-alkyl trimethylammonium bromides on folding and stability of alkaline and acid-denatured cytochrome c: a spectroscopic approach. *J Colloid Interface Sci* (2006) 297:561–9. doi: 10.1016/j.jcis.2005.11.035

20. Khashkhashi-Moghadam S, Ezazi-Toroghi S, Kamkar-Vatanparast M, Jouyaeian 0, Mokaberi P, Yazdyani H, et al. Novel perspective into the interaction behavior study of the cyanidin with human serum albumin-holo transferrin complex: Spectroscopic, calorimetric and molecular modeling approaches. *J Mol LIQ* (2022) 356, 119042. doi: 10.1016/j.molliq.2022.119042

21. Clough E, Barrett T. The gene expression omnibus database. *Methods Mol Biol* (2016) 1418:93–110. doi: 10.1007/978-1-4939-3578-9_5

22. Davis S, Meltzer PS. GEOquery: A bridge between the gene expression omnibus (GEO) and BioConductor. *Bioinformatics* (2007) 23(14):1846–7. doi: 10.1093/bioinformatics/btm254

23. Ritchie ME, Phipson B, Wu D, Hu Y, Law CW, Shi W, et al. Limma powers differential expression analyses for RNA-sequencing and microarray studies. *Nucleic Acids Res* (2015) 43(7):e47. doi: 10.1093/nar/gkv007

24. Bagaev A, Kotlov N, Nomie K, Svekolkin V, Gafurov A, Isaeva O, et al. Conserved pan-cancer microenvironment subtypes predict response to immunotherapy. *Cancer Cell* (2021) 39(6):845–65. doi: 10.1016/j.ccell.2021.04.014

25. Racle J, Gfeller D. EPIC: A tool to estimate the proportions of different cell types from bulk gene expression data. *Methods Mol Biol* (2020) 2120:233–48. doi: 10.1007/978-1-0716-0327-7_17

26. Li T, Fu J, Zeng Z, Cohen D, Li J, Chen Q, et al. TIMER2.0 for analysis of tumor-infiltrating immune cells. *Nucleic Acids Res* (2020) 48(W1):W509–14. doi: 10.1093/nar/gkaa407

27. Newman AM, Liu CL, Green MR, Gentles AJ, Feng W, Xu Y, et al. Robust enumeration of cell subsets from tissue expression profiles. *Nat Methods* (2015) 12 (5):453–7. doi: 10.1038/nmeth.3337

28. Wang X, Chai Z, Li Y, Long F, Hao Y, Pan G, et al. Identification of potential biomarkers for anti-PD-1 therapy in melanoma by weighted correlation network analysis. *Genes (Basel)* (2020) 11(4):435. doi: 10.3390/genes11040435

29. Subramanian A, Tamayo P, Mootha VK, Mukherjee S, Ebert BL, Gillette MA, et al. (2005). Gene set enrichment analysis: A knowledge-based approach for interpreting genome-wide expression profiles *Proc Natl Acad Sci U S A* 102. 15545–50. doi: 10.1073/pnas.0506580102.

30. Chang J, Liu L, Wang Y, Sui Y, Li H, Feng L. Investigating the multitarget mechanism of traditional chinese medicine prescription for cancer-related pain by using network pharmacology and molecular docking approach. *Evid Based Complement Alternat Med* (2020) 2020:7617261. doi: 10.1155/2020/7617261

31. Lamb J, Crawford ED, Peck D, Modell JW, Blat IC, Wrobel MJ, et al. The connectivity map: Using gene-expression signatures to connect small molecules. *Genes Disease Sci* (2006) 313(5795):1929–35. doi: 10.1126/science.1132939

32. Duan Q, Reid SP, Clark NR, Wang Z, Fernandez NF, Rouillard AD, et al. L1000CDS(2): LINCS L1000 characteristic direction signatures search engine. *NPJ Syst Biol Appl* (2016) 2:16015. doi: 10.1038/npjsba.2016.15

33. Wang Z, Lachmann A, Keenan AB, Ma'Ayan A. (2018). L1000FWD: Fireworks visualization of drug-induced transcriptomic signatures, *Bioinformatics* 34: 2150–2. doi: 10.1093/bioinformatics/bty060.

34. Tomazou M, Bourdakou MM, Minadakis G, Zachariou M, Oulas A, Karatzas E, et al. Multi-omics data integration and network-based analysis drives a multiplex drug repurposing approach to a shortlist of candidate drugs against COVID-19. *Brief Bioinform* (2021) 22(6):bbab114. doi: 10.1093/bib/bbab114.

35. Karatzas E, Minadakis G, Kolios G, Delis A, Spyrou GM (2019). A web tool for ranking candidate drugs against a selected disease based on a combination of functional and structural criteria *Comput Struct Biotechnol J*17:939–45. doi: 10.1016/j.csbj.2019.05.010

36. Karatzas E, Zamora JE, Athanasiadis E, Dellis D, Cournia Z, Spyrou GM. ChemBioServer 2.0: An advanced web server for filtering, clustering and networking of chemical compounds facilitating both drug discovery and repurposing. *Bioinformatics* (2020) 36(8):2602–4. doi: 10.1093/bioinformatics/btz976.

37. Maeser D, Gruener RF, Huang RS. OncoPredict: An r package for predicting *in vivo* or cancer patient drug response and biomarkers from cell line screening data. *Brief Bioinform* (2021) 22(6):bbab260. doi: 10.1093/bib/bbab260

38. Fang S, Dong L, Liu L, Guo J, Zhao L, Zhang J, et al. HERB: A high-throughput experiment- and reference-guided database of traditional Chinese medicine. *Nucleic Acids Res* (2021) 49(D1):D1197–206. doi: 10.1093/nar/gkaa1063

39. Xiong G, Wu Z, Yi J, Fu L, Yang Z, Hsieh C, et al. ADMETlab 2.0: An integrated online platform for accurate and comprehensive predictions of ADMET properties. *Nucleic Acids Res* (2021) 49(W1):W5–14. doi: 10.1093/nar/gkaa1063

40. Park D, Park CW, Choi Y, Lin J, Seo DH, Kim HS, et al. A novel small-molecule PPI inhibitor targeting integrin alphavbeta3-osteopontin interface blocks bone resorption *in vitro* and prevents bone loss in mice. *Biomaterials* (2016) 98:131–42. doi: 10.1016/j.biomaterials.2016.05.007

41. Trott O, Olson AJ. AutoDock vina: Improving the speed and accuracy of docking with a new scoring function, efficient optimization, and multithreading. *J Comput Chem* (2010) 31(2):455–61. doi: 10.1002/jcc.21334

42. Chen Z, Zhang X, Peng C, Wang J, Xu Z, Chen K, et al. D3Pockets: A method and web server for systematic analysis of protein pocket dynamics. *J Chem Inf Model* (2019) 59(8):3353–8. doi: 10.1021/acs.jcim.9b00332

43. Grant BJ, Skjaerven L, Yao XQ. The Bio3D packages for structural bioinformatics. *Protein Sci* (2021) 30(1):20–30. doi: 10.1002/pro.3923

44. Tian R, Li Y, Wang X, Li J, Li Y, Bei S, et al. A pharmacoinformatics analysis of artemisinin targets and *de novo* design of hits for treating ulcerative colitis. *Front Pharmacol* (2022) 13:843043. doi: 10.3389/fphar.2022.843043

45. Chang J, Jiang Z, Jin W, Wang Y, Li J, Chen J, et al. The molecular mechanism of traditional Chinese medicine prescription: Gu-tong formula in relieving osteolytic bone destruction. *BioMed Res Int* (2022) 2022:4931368. doi: 10.1155/2022/4931368

46. Huang Q, Song P, Chen Y, Liu Z, Lai L. Allosteric type and pathways are governed by the forces of protein-ligand binding. *J Phys Chem Lett* (2021) 12 (22):5404–12. doi: 10.1021/acs.jpclett.1c01253

47. Vahedian-Movahed H, Saberi MR, Chamani J. Comparison of binding interactions of lomefloxacin to serum albumin and serum transferrin by resonance light scattering and fluorescence quenching methods. *J Biomol Struct Dyn* (2011) 28:483–502. doi: 10.1080/07391102.2011.10508590

48. Hosseinzadeh M, Nikjoo S, Zare N, Delavar D, Beigoli S, Chamani J, et al. Characterization of the structural changes of human serum albumin upon interaction with single-walled and multi-walled carbon nanotubes: spectroscopic and molecular modeling approaches. *Res Chem Intermed* (2019) 45:401–23. doi: 10.1007/s11164-018-3608-5

49. Denmeade SR, Isaacs JT. Bipolar androgen therapy: The rationale for rapid cycling of supraphysiologic androgen/ablation in men with castration resistant prostate cancer. *Prostate* (2010) 70(14):1600–7. doi: 10.1002/pros.21196

50. Moreira DM, Howard LE, Sourbeer KN, Amarasekara HS, Chow LC, Cockrell DC, et al. Predicting time from metastasis to overall survival in castration-resistant prostate cancer: Results from SEARCH. *Clin Genitourin Cancer* (2017) 15:60–6. doi: 10.1016/j.clgc.2016.08.018

51. Beer TM, Kwon ED, Drake CG, Fizazi K, Logothetis C, Gravis G, et al. Randomized, double-blind, phase III trial of ipilimumab versus placebo in asymptomatic or minimally symptomatic patients with metastatic chemotherapy-naive castration-resistant prostate cancer. *J Clin Oncol* (2017) 35 (1):40–7. doi: 10.1200/JCO.2016.69.1584

52. Ihle CL, Provera MD, Straign DM, Smith EE, Edgerton SM, Van Bokhoven A, et al. Distinct tumor microenvironments of lytic and blastic bone metastases in prostate cancer patients. *J Immunother Cancer* (2019) 7:293. doi: 10.1186/s40425-019-0753-3

53. Idorn M, Kollgaard T, Kongsted P, Sengelov L, Thor SP. Correlation between frequencies of blood monocytic myeloid-derived suppressor cells, regulatory T cells and negative prognostic markers in patients with castration-resistant metastatic prostate cancer. *Cancer Immunol Immunother* (2014) 63:1177–87. doi: 10.1007/s00262-014-1591-2

54. Klement JD, Paschall AV, Redd PS, Ibrahim ML, Lu C, Yang D, et al. An osteopontin/CD44 immune checkpoint controls CD8+ T cell activation and tumor immune evasion. *J Clin Invest* (2018) 128(12):5549–60. doi: 10.1172/JCI123360

55. Pang X, Gong K, Zhang X, Wu S, Cui Y, Qian BZ. Osteopontin as a multifaceted driver of bone metastasis and drug resistance. *Pharmacol Res* (2019) 144:235–44. doi: 10.1016/j.phrs.2019.04.030

56. Hall CL, Dubyk CW, Riesenberger TA, Shein D, Keller ET, van Golen KL. Type I collagen receptor (alpha2beta1) signaling promotes prostate cancer invasion through RhoC GTPase. *Neoplasia* (2008) 10(8):797–803. doi: 10.1593/neo.08380

57. Paolillo M, Schinelli S. Extracellular matrix alterations in metastatic processes. *Int J Mol Sci* (2019) 20(19):4947. doi: 10.3390/ijms20194947

58. Yu L, Sui B, Fan W, Lei L, Zhou L, Yang L, et al. (2021). Exosomes derived from osteogenic tumor activate osteoclast differentiation and concurrently inhibit osteogenesis by transferring COL1A1-targeting miRNA-92a-1-5p. *J Extracell Vesicles.* 10:e12056. doi: 10.1002/jev2.12056

59. Pang X, Zhang J, He X, Gu Y, Qian BZ, Xie R, et al. SPP1 promotes enzalutamide resistance and epithelial-Mesenchymal-Transition activation in castration-resistant prostate cancer *via* PI3K/AKT and ERK1/2 pathways. *Oxid Med Cell Longev* (2021) 2021:5806602. doi: 10.1155/2021/5806602

60. Zhang Y, Fu Y. Comprehensive analysis and identification of an immune-related gene signature with prognostic value for prostate cancer. *Int J Gen Med* (2021) 14:2931–42. doi: 10.2147/IJGM.S321319

61. Kaore SN, Langade DK, Yadav VK, Sharma P, Thawani VR, Sharma R. Novel actions of progesterone: What we know today and what will be the scenario in the future? *J Pharm Pharmacol* (2012) 64(8):1040–62. doi: 10.1111/j.2042-7158.2012.01464.x

62. Kaplan AL, Hu JC, Morgentaler A, Mulhall JP, Schulman CC, Montorsi F. Testosterone therapy in men with prostate cancer. *Eur Urol* (2016) 69(5):894–903. doi: 10.1016/j.eururo.2015.12.005

63. Loeb S, Folkvaljon Y, Damber JE, Alukal J, Lambe M, Stattin P. Testosterone replacement therapy and risk of favorable and aggressive prostate cancer. *J Clin Oncol* (2017) 35(13):1430–6. doi: 10.1200/JCO.2016.69.5304

64. Kyriakopoulos CE, Chen YH, Carducci MA, Liu G, Jarrard DF, Hahn NM, et al. Chemohormonal therapy in metastatic hormone-sensitive prostate cancer: Long-term survival analysis of the randomized phase III e3805 CHAARTED trial. *J Clin Oncol* (2018) 36(11):1080–7. doi: 10.1200/JCO.2017.75.3657

65. Zhang L, Barritt GJ. TRPM8 in prostate cancer cells: A potential diagnostic and prognostic marker with a secretory function? *Endocr Relat Cancer* (2006) 13 (1):27–38. doi: 10.1677/erc.1.01093

66. Yee NS. Roles of TRPM8 ion channels in cancer: Proliferation, survival, and invasion. *Cancers (Basel)* (2015) 7(4):2134–46. doi: 10.3390/cancers7040882

67. Naziroglu M, Blum W, Josvay K, Cig B, Henzi T, Olah Z, et al. Menthol evokes Ca(2+) signals and induces oxidative stress independently of the presence of TRPM8 (menthol) receptor in cancer cells. *Redox Biol* (2018) 14:439–49. doi: 10.1016/j.redox.2017.10.009

68. Enioutina EY, Job KM, Krepkova LV, Reed MD, Sherwin CM. How can we improve the safe use of herbal medicine and other natural products? a clinical pharmacologist mission. *Expert Rev Clin Pharmacol* (2020) 13(9):935–44. doi: 10.1080/17512433.2020.1803739

69. Ferreira RS, Simeonov A, Jadhav A, Eidam O, Mott BT, Keiser MJ, et al. Complementarity between a docking and a high-throughput screen in discovering new cruzain inhibitors. *J Med Chem* (2010) 53:4891–905. doi: 10.1021/jm100488w

70. Gorgulla C, Boeszoermenyi A, Wang ZF, Fischer PD, Coote PW, Padmanabha DK, et al. An open-source drug discovery platform enables ultra-large virtual screens. *Nature* (2020) 580:663–8. doi: 10.1038/s41586-020-2117-z

71. Wei S, Fukuhara H, Chen G, Kawada C, Kurabayashi A, Furihata M, et al. A steroidal saponin from tribulus terrestris l., inhibits growth and angiogenesis of human prostate cancer *in vitro* and *in vivo*. *Pathobiology* (2014) 81(3):123–32. doi: 10.1159/000357622

72. Sun W, Sanderson PE, Zheng W. Drug combination therapy increases successful drug repositioning. *Drug Discovery Today* (2016) 21:1189–95. doi: 10.1016/j.drudis.2016.05.015

73. Jaaks P, Coker EA, Vis DJ, Edwards O, Carpenter EF, Leto SM, et al. Effective drug combinations in breast, colon and pancreatic cancer cells. *Nature* (2022) 603:166–73. doi: 10.1038/s41586-022-04437-2

74. Li P, Huang C, Fu Y, Wang J, Wu Z, Ru J, et al. Large-Scale exploration and analysis of drug combinations. *Bioinformatics* (2015) 31:2007–16. doi: 10.1093/bioinformatics/btv080

75. Chen J, Zhang Y, Zhang X, Zhao J, Ni Y, Zhu S, et al. Comparison of systemic treatments for metastatic castration-resistant prostate cancer after docetaxel failure: A systematic review and network meta-analysis. *Front Pharmacol* (2021) 12:789319. doi: 10.3389/fphar.2021.789319

76. Seiwert T, Sarantopoulos J, Kallender H, McCallum S, Keer HN, Blumenschein GJ. Phase II trial of single-agent foretinib (GSK1363089) in patients with recurrent or metastatic squamous cell carcinoma of the head and neck. *Invest New Drugs* (2013) 31:417–24. doi: 10.1007/s10637-012-9861-3

77. Fu Y, Peng Y, Zhao S, Mou J, Zeng L, Jiang X, et al. Combination foretinib and anti-PD-1 antibody immunotherapy for colorectal carcinoma. *Front Cell Dev Biol* (2021) 9:689727. doi: 10.3389/fcell.2021.689727

78. Varkaris A, Corn PG, Gaur S, Dayyani F, Logothetis CJ, Gallick GE. The role of HGF/c-met signaling in prostate cancer progression and c-met inhibitors in clinical trials. *Expert Opin Investig Drugs* (2011) 20(12):1677–84. doi: 10.1517/13543784.2011.631523

frontiers | Frontiers in Immunology

TYPE Review
PUBLISHED 05 July 2023
DOI 10.3389/fimmu.2023.1121878

OPEN ACCESS

EDITED BY
Jawed A. Siddiqui,
University of Nebraska Medical Center,
United States

REVIEWED BY
Sofia Sousa,
NovaRock Biotherapeutics Ltd,
United States
Marco Ponzetti,
University of L'Aquila, Italy

*CORRESPONDENCE
Tiina E. Kähkönen
tiina.kahkonen@oncobone.com

RECEIVED 12 December 2022
ACCEPTED 19 June 2023
PUBLISHED 05 July 2023

CITATION
Kähkönen TE, Halleen JM, MacRitchie G, Andersson RM and Bernoulli J (2023) Insights into immuno-oncology drug development landscape with focus on bone metastasis. *Front. Immunol.* 14:1121878. doi: 10.3389/fimmu.2023.1121878

Insights into immuno-oncology drug development landscape with focus on bone metastasis

Tiina E. Kähkönen[1]*, Jussi M. Halleen[1], Gary MacRitchie[2], Ronnie M. Andersson[2] and Jenni Bernoulli[3]

[1]OncoBone Ltd, Oulu, Finland, [2]1stOncology, BioSeeker Group AB, Stockholm, Sweden, [3]University of Turku, Institute of Biomedicine, Turku, Finland

Bone is among the main sites of metastasis in breast, prostate and other major cancers. Bone metastases remain incurable causing high mortality, severe skeletal-related effects and decreased quality of life. Despite the success of immunotherapies in oncology, no immunotherapies are approved for bone metastasis and no clear benefit has been observed with approved immunotherapies in treatment of bone metastatic disease. Therefore, it is crucial to consider unique features of tumor microenvironment in bone metastasis when developing novel therapies. The vicious cycle of bone metastasis, referring to crosstalk between tumor and bone cells that enables the tumor cells to grow in the bone microenvironment, is a well-established concept. Very recently, a novel osteoimmuno-oncology (OIO) concept was introduced to the scientific community. OIO emphasizes the significance of interactions between tumor, immune and bone cells in promoting tumor growth in bone metastasis, and it can be used to reveal the most promising targets for bone metastasis. In order to provide an insight into the current immuno-oncology drug development landscape, we used 1stOncology database, a cancer drug development resource to identify novel immunotherapies in preclinical or clinical development for breast and prostate cancer bone metastasis. Based on the database search, 24 immunotherapies were identified in preclinical or clinical development that included evaluation of effects on bone metastasis. This review provides an insight to novel immuno-oncology drug development in the context of bone metastasis. Bone metastases can be approached using different modalities, and tumor microenvironment in bone provides many potential targets for bone metastasis. Noting current increasing interest in the field of OIO, more therapeutic opportunities that primarily target bone metastasis are expected in the future.

KEYWORDS

cancer, bone metastasis, immuno-oncology, osteoimmuno-oncology, immunotherapies, drug development, 1st oncology, database

1 Introduction

Metastases are the main cause of cancer-related deaths and bone is among the major sites of metastasis in many cancers such as breast, prostate, lung, renal, colon and bladder cancer and melanoma (1). Notably, when bone metastases are observed, the 5-year survival rate drops to 5% as there are no effective treatments available (2). Therefore, bone metastases are incurable and induce severe skeletal-related effects such as pathological fractures, spinal cord compression, bone pain and decreased quality of life (3).

Immunotherapies may give hope for bone metastatic patients (4). Bone marrow is an important secondary lymphoid organ and bone metastases develop a unique immune microenvironment. Bone is a highly immunosuppressed microenvironment, as recently demonstrated for prostate cancer (5), which may explain why immunotherapies have not produced promising effects on bone metastatic patients (6). Factors behind the development of the immunosuppressed bone metastatic microenvironment include: 1) in the process of metastasis formation, cancer cells need to have properties that allow them to avoid elimination by immune cells, 2) even at healthy state, bone marrow has a lower number of cytotoxic cells than other tissues, 3) immunomodulation of the pre-metastatic niche to allow seeding of cancer cells to the growth-supporting microenvironment, and 4) modulation of the metastatic microenvironment through interactions of stromal cells.

The role of stromal cells in modulating the microenvironment is often neglected. Stromal cell effects are especially important in bone metastasis because bone cells are important regulators in promoting tumor growth in a process called vicious cycle of bone metastasis (7). The vicious cycle explains how cancer cells regulate the number and activity of bone resorbing cells, which in turn results in increased bone resorption and release of factors that promote growth of bone metastases. Furthermore, stromal cells have a role in modulating immune microenvironment (8). For example, bone-resorbing osteoclasts can present antigens, inhibit T cells and express immunosuppressive factors (9), which also occurs in bone metastases (10).

A recently established novel osteoimmuno-oncology (OIO) concept refers to interactions between cancer, bone and immune cells (11). It is essential to understand these interactions in order to develop effective and safe therapies for cancer patients with bone metastases. The OIO concept is supported by years of research on the role of interactions between cancer, bone and immune cells, and also by observations in patients treated with different immunotherapies who developed skeletal-related adverse events (SRAEs) such as resorptive bone lesions, spinal cord compression and even fractures (12). A recent study indicated that many musculoskeletal adverse effects are observed in immunotherapy-treated patients, but interestingly, patients experiencing musculoskeletal adverse effects had a good anti-tumor response (13). This could be explained by changes in the immune microenvironment that make the tumors responsive to immunotherapies but at the same time disturb the immune homeostasis in bone, leading to above-described adverse events. Therefore, development of novel therapies with confirmed efficacy on bone metastasis and without causing SRAEs should be prioritized especially for bone metastatic patients who already have compromised bone health.

This review summarizes current immuno-oncology drug development landscape for bone metastatic breast and prostate cancer. Using a comprehensive oncology-focused drug development database we identified drugs with preclinical or clinical data in the context of bone metastasis. Approved immunotherapies were excluded from this review as they have recently been discussed elsewhere (4). Current treatment options for bone metastasis, all with limited efficacy, include radium-223 dichloride, bisphosphonates such as zoledronic acid, and the anti-RANKL antibody denosumab, that can be applied in combination with standard-of-care cancer therapies.

2 Database search for immuno-oncology drugs in development for bone metastatic breast and prostate cancer

This unique and comprehensive data review was performed using 1stOncology database that contains detailed scientific, clinical and commercial drug information on almost 20,000 oncology drugs and 1,877 targets and covers more than 21,000 interventional clinical trials in 391 indications (search results on November 18, 2022). The research concentrated on breast and prostate cancers that have the highest incidence of bone metastases (14).

The search of active studies for breast cancer resulted in 1,498 drugs and 537 targets. Addition of 'bone metastasis' in the search resulted in 242 drugs and 178 targets. Of these drugs, 67 were immuno-oncology drugs that are of interest to this review, of which 36 were in clinical and 1 in preclinical development. In prostate cancer, there were 746 drugs in active research, covering 356 targets. Limiting down to those associated with bone metastasis resulted in 206 drugs and 180 targets. Of these drugs, 73 were in the immuno-oncology category, of which 47 in clinical and 2 in preclinical development. These search results are summarized in Table 1, and these 86 drugs (36 + 1 for breast and 47 + 2 for prostate cancer) were the starting population for a more detailed search for efficacy data on bone metastasis. The more detailed search included relevant scientific results published in major scientific events. After going through all drugs identified in the initial search it was concluded that 20 drugs in clinical development had published data available about effects on bone metastasis that can be discussed in this review.

3 Immuno-oncology drug development for bone metastasis

3.1 Overview of immuno-oncology drugs in clinical development

Table 2 lists the 20 prostate cancer therapies in clinical development with published data on bone metastasis effects. Notably, even though the initial search identified therapies also

TABLE 1 Database searches performed to narrow the scope of this review.

Database search	Breast cancer	Prostate cancer
All drugs in active development	1,498 drugs	746 drugs
Limiting to drugs with development related to bone metastasis	242 drugs	206 drugs
Further Limiting to immuno-oncology drugs only	67 drugs	73 drugs
Further Limiting to immuno-oncology drugs in clinical development (phase 1-3)	36 drugs	47 drugs
Drugs with published data available about effects on bone metastasis	0 drugs	20 drugs*

* Of the 20 drugs, 6 included both breast and prostate cancer as indication, but bone metastasis data is published only in prostate cancer bone metastasis.

TABLE 2 Immuno-oncology drugs in clinical development for prostate cancer in the context of bone metastasis.

ASSET NAME	TARGET (S)	MODALITY	TRIAL	SELECTED ELIGIBILITY CRITERIA AND OUTCOME MEASUREMENT		TRIAL STATUS	DEVELOPER/ SPONSOR
				INCLUSION	OUTCOME		
Imifoplatin (PT-112)	Pyrophosphate-platinum conjugate	Small molecule	NCT02266745, ph1/2	Progressive disease measured by physical examination or imaging (RECIST v1.1 or PCWG3 or by informative tumor markers)	Secondary: rPFS, disease control rate, objective response rate, duration of response, OS	Recruiting	Promontory Therapeutics/ Pfizer, EMD Serono
P-PSMA-101	PSMA	CAR-T	NCT04249947, ph1 (in combination with rimiducid)	Measurable disease by RECIST 1.1 or bone only metastases with measurable PSA	Overall response rate, percentage of patients with complete or partial response	Recruiting	Poseida Therapeutics
Pasotuximab (BAY2010112)	PSMAxCD3	Bispecific antibody	NCT01723475, ph1	Appearance of one more new lesions in bone scan	Secondary: Tumor and PSA response	Completed	Bayer
MGC018	B7-H3	Antibody-drug conjugate	NCT03729596, ph1/2 (combination with anti-PD-1 will not enroll) NCT05551117, ph2/3	In prostate cancer cohort, patients with bone only disease are eligible One or more metastatic lesion, present MRI, CT or bone scan	Secondary: OS, PFS, rPFS, response rate Primary: rPFS	Active, not recruiting Not yet recruiting	MacroGenics
DS-7300a	B7-H3	Antibody-drug conjugate	NCT04145622, ph1/2	CRPC participants with bone only disease may be eligible on a case-by-case basis	Anti-tumor activity	Recruiting	Daiichi Sankyo
MVI-118	Encode AR LBD	DNA vaccine	NCT02411786, ph1 (+/- GM-CSF)	Soft tissue and/or bone metastases by radiographic imaging	Secondary: Median and 18-month PFS	Completed	Madison Vaccines
MVI-816 (pTVG-HP)	Encode AR LBD	DNA vaccine	NCT01706458, ph2 (in combination with sipuleucel-T) NCT02499835, ph1/2 (in combination with pembrolizumab)	Soft tissue and/or bone metastases in imaging studies	Secondary: PFS, time to radiographic progression	Completed Active, not recruiting	Madison Vaccines
Recombinant Ad5 vaccine	PSA/MUC-1/brachyury	Virus vaccine	NCT03481816, ph1	Metastatic bone disease in an imaging study	Secondary: OS, PFS	Completed	ImmunityBio/ NCI
Rilimogene glafolivec	PSA, CD48, CD80, ICAM1, KLK3	Virus vaccine	NCT01322490, ph3 (+/- GM-CSF)	Radiological progression (new or growing bone metastases or new/enlarging lymph node disease)	Primary: OS, number alive without event after 6 months (event is two new bone lesions or other metastases)	Completed	Bavarian Nordic

(Continued)

TABLE 2 Continued

ASSET NAME	TARGET (S)	MODALITY	TRIAL	SELECTED ELIGIBILITY CRITERIA AND OUTCOME MEASUREMENT		TRIAL STATUS	DEVELOPER/ SPONSOR
				INCLUSION	OUTCOME		
Bintrafusp alfa (M7824) and M9241	PD-L1-TGFβ NHS-IL12A	Fusion protein Fusion protein	NCT04633252, ph1/2 (in combination with androgen deprivation therapy, prednisone and docetaxel)	Metastatic disease, defined as at least one lesion on TC99 bone scan or at least one measurable lesion per RECIST 1.1.	Secondary: Radiographic response rates, radiographic and biochemical time to progression	Recruiting	Merck KGaA/ NCI
Vudalimab (XmAb20717)	PD-1 x CTLA-4	Bispecific antibody	NCT05005728, ph2 (in combination with carboplatin, cabazitaxel, olaparib	Progression of bone disease (evaluable disease) or 2 or more new bone lesions by bone scan	Secondary: Objective response rate by PCWG3, bone scan and rPFS, duration of response	Recruiting	Vencor
Tremelimumab	CTLA-4	Monoclonal antibody	NCT03204812, ph2 (in combination with durvalumab)	Evidence of metastatic disease to the bone seen in most recent bone scan, CT scan and/or MRI	Secondary: rPFS, median OS	Completed	Pfizer/MDA
BMS-986249	CTLA-4	Conditionally activated antibody	NCT03369223, ph 1/2 (in combination with nivolumab)	Measurable disease or metastatic disease documented by bone lesions in radionuclide bone scan	Secondary: PFS, overall response, duration of response	Recruiting	CytomX Therapeutics/ Bristol-Myers Squibb
Epacadostat and MVA-BN Brachyury	IDO1 TBXT	Small molecule Protein	NCT03493945, ph1/2 (in combination with M7824 and N-803)	Radiographically proven metastatic or locally advanced solid tumor of any type	Secondary: PFS	Recruiting	Incyte/NCI Bavarian Nordic
Talabostat mesylate (BXCL701)	DPP4, DPP8, DPP9, FAP	Small molecule	NCT03910660, ph1/2 (in combination with pembrolizumab)	RECIST 1.1 measurable disease or detectable bone metastases by whole body bone scintigraphy	Secondary: rPFS, median OS, duration of response	Recruiting	BioXcel Therapeutics
Dendritic cell vaccine	CTAG1B, MAGEC2, MUC1	Cell vaccine	NCT02692976, ph2	Bone disease progression defined by two or more new lesions in bone scan as described in PCWG2 criteria	Secondary: rPFS, OS	Completed	Radbound University
MB-105	PSCA	CAR-T	NCT03873805, ph1	Radiographic evidence of new metastatic foci in computed CT or bone scan	Secondary: rPFS, OS	Recruiting	Fortress Biotech/City of Hope Med Cent
Reolysin (pelareorep)	N/A	Virus	NCT01619813, ph2 (in combination with docetaxel and prednisone)	Metastatic or locally recurrent disease, clinically and/or radiologically documented disease	Primary: Disease progression, OS	Completed	Oncolytic Biotech

"Developer" refers to the original developer/owner, "Stage" refers to the highest development stage. "Inclusion" and "Outcome" columns include selected parameters relevant in the context of bone metastasis. Detailed description of the drugs and the results are provided in the chapters below. All listed trials are for prostate cancer. AR, androgen receptor; B7-H3, B7 homolog 3; CAR-T, chimeric antigen receptor, T cell; CD, cluster of differentiation; CRPC, castration-resistant prostate cancer; CTAG1B, cancer/testis antigen 1B; CTLA-4, cytotoxic T-lymphocyte-associated protein 4; DPP, dipeptidyl peptidase; FAP, fibroblast activation protein; ICAM 1, intracellular adhesion molecule 1; IL12A, interleukin 12 A; KLK3, kallikrein related peptidase 3; LBD, ligand binding domain; MAGEC2, MAGE family member C2; MRI, magnetic resonance imaging; MUC-1, mucin-1; OS, overall survival; PCWG3, prostate cancer working group 3; PD-1, programmed cell death 1; PD-L1, programmed death-ligand 1; PFS, progression-free survival; PSA, prostate-specific antigen; PSCA, prostate stem cell antigen; PSMA, prostate-specific membrane antigen; RECIST, response evaluation criteria in solid tumors; rPFS, radiographic progression-free survival; TBTX, T-box transcription factor T; TGFβ, transforming growth factor beta. N/A, Not available.

for breast cancer, none of the clinical trials in breast cancer specifically addressed effects on bone metastasis. Inclusion criteria for the trials listed bone metastases evaluated by imaging, and outcome measurements varied largely between studies. Most of the listed trials are currently in phase 1 or 2. Description of the main findings in the context of bone metastasis for all listed therapies is provided in the chapters below.

3.2 Imifoplatin

Imifoplatin (PT-112) is a platinum-pyrophosphate compound studied for the treatment of cancer. Due to the pyrophosphate presence, imifoplatin localizes to bone tissues in high concentration (15). Imifoplatin has been studied in patients with advanced solid tumors including bone metastatic prostate cancer (clinical trial

identifier NCT02266745). The results were published in ASCO Genitourinary Cancers Symposium 2020 (16, 17), showing decrease in bone pain and reduction of serum alkaline phosphatase (ALP, bone biomarker) in 9/10 and PSA in 3/10 patients. In a combination study (NCT03409458) with avelumab in a cohort of metastatic castration-resistant prostate cancer (mCRPC), 24/32 patients showed reduction in serum ALP and improvement in patient-reported pain and quality of life (18), suggesting marked therapeutic activity for imifoplatin in bone metastasis.

3.3 P-PSMA-101

P-PSMA-101 is an autologous prostate-specific membrane antigen (PSMA) -targeting Chimeric Antigen Receptor T cell (CAR-T) therapy with a high percentage of stem cell memory T cell (TSCM) phenotype initially associated with efficacy, safety and bone homing. TSCM cells remain viable in hostile bone microenvironment and the bone homing attribute makes it a promising candidate treatment for bone metastasis. After promising preclinical data in prostate cancer models, a phase I clinical study (NCT04249947) was started in mCRPC patients. The results were reported in ASCO Genitourinary Symposium 2022 (19). The study included 10 heavily pretreated patients, of which 7 had decreased PSA levels. Four patients showed marked CAR-T uptake in bone metastases and post-treatment biopsy of one patient showed infiltration of P-PSMA-101 CAR-T cells into the tumor, the patient experiencing pathologic complete response. However, enrollment was stopped in the study in November 2022 when the company focused on developing their allogeneic platform.

3.4 Pasotuxizumab

Pasotuxizumab (BAY2010112) is a PSMA-targeting bispecific T-cell engager (BiTE) antibody. BiTE molecules bind to both the target cells and T cells, and they can recruit and activate T cells without the need of any co-stimulatory signals. Phase I dose escalation results in CRPC (NCT01723475) have been published (20). The study does not state the exact number of patients with bone metastases, but the majority of patients had advanced or metastatic stage IV disease. When PSMA BiTE was administered to patients intravenously, altogether 14/16 patients experienced a PSA response. Two patients had a long-term PSA response in the study. The first patient had a long-term stable disease, and the second patient had a marked PSA decrease and experienced a near-complete regression of lymph node lesions and bone metastases with 500 days to disease progression.

3.5 MGC018

MGC018 is an anti-B7-H3 antibody-drug conjugate (ADC). B7-H3, a member of the B7 family of immunomodulatory molecules, is overexpressed in a wide range of solid tumors (21). MGC018 is comprised of the cleavable linker-duocarmycin payload, valine-citrulline-*seco* duocarmycin hydroxybenzamide azaindole (vc-*seco*-DUBA), conjugated to an anti-B7-H3 humanized IgG1/kappa monoclonal antibody (22). A phase I/II study (NCT03729596) will evaluate the effects of MGC018 in patients with advanced solid tumors, including mCRPC with bone only metastases. Preliminary results of the trial presented in ESMO 2021 congress indicated that 55% of the patients experienced over 50% decrease in PSA levels (23). The study included only mCRPC patients with bone metastases, indicating a significant bone metastasis anti-tumor effect for MGC018. The effects of MGC018 are currently evaluated in advanced solid tumors, and a phase II/III trial (NCT05551117) in mCRPC patients evaluating radiographic progression free survival (rPFS) as a primary endpoint will be initiated.

B7-H3 is an interesting target for bone metastasis. A study in patients with the primary bone cancer osteosarcoma demonstrated that soluble B7-H3 levels were increased in patients with osteosarcoma compared to healthy individuals, and high levels of soluble B7-H3 correlated with tumor stage, metastases and shorter overall survival (OS) (24). Also, high levels of B7-H3 correlated with low number of CD8+ tumor-infiltrating lymphocytes (25). Importantly for bone metastasis, B7-H3 has been shown to regulate the differentiation and activity of bone-forming osteoblast cells that are overactive in prostate cancer (26, 27).

3.6 DS-7300a

DS-7300a is an anti-B7-H3 antibody conjugated to DXd (MAAA-1181), a novel derivate of a topoisomerase I inhibitor exatecan (DX-8951f). The first results of the ongoing phase I/II trial (NCT04145622) were presented in ASCO Genitourinary symposium in 2022. Out of 29 patients treated with 6.4 to 16 mg/kg of DS-7300, six patients experienced partial response and 15 resulted in stable disease with improvements in PSA and bone metastases (28).

3.7 MVI-118

MVI-118 (pTVG-AR) is a plasmid DNA vaccine encoding the ligand-binding domain of the human androgen receptor. In a phase I study (NCT02411786), 55% of metastatic castration-sensitive prostate cancer (mCSPC) patients had bone metastases and 68% of the patients were progression-free at 18 months in groups receiving the vaccine with or without granulocyte-macroghage colony-stimulating factor (GM-CSF) adjuvant (29). Patients who had immunological response with interferon gamma (IFNγ) and/or granzyme B had prolonged time to develop castration resistance. The study did not include radiographic evaluation of patients even though it included a high number of patients with bone metastases. MVI-118 is currently evaluated in prostate cancer patients in combination with pembrolizumab (NCT04090528) in a study enrolling patients with bone metastases.

3.8 MVI-816 (pTVG-HP)

MVI-816 (pTVG-HP) is an intradermal prostatic acid phosphatase (PAP) encoding DNA plasmid vaccine. Eighteen mCRPC patients were included in a phase II study (NCT01706458) evaluating effects of sipuleucel T alone (Arm 1) or in combination with pTVG-HP (Arm 2). The patients underwent CT/bone scan in 3 months intervals for the two years follow-up period. Patients with bone metastases were unevenly distributed between the two treatment arms (22% vs 56% in Arms 1 and 2, respectively) and there were no differences between the treatment arms in median time to radiographic progression (30). However, two patients in Arm 2 seemed to be progression free until 9 to 12 months. Overall, the number of responders was low and the study was unable to recruit enough patients, and it was closed early as it was unlikely to meet the primary immunological endpoint.

In another phase II study (NCT02499835) the effects of MVI-816 and pembrolizumab were evaluated in mCRPC patients on 6 months progression-free survival (PFS) and time to radiographic progression. In the study, 80-100% of patients had bone metastases and 32% remained on trial without radiographic progression after 6 months. Estimated rPFS rate was 44% and 62% in patients receiving a combination of MVI-816 and pembrolizumab in two dosing sequences (31). In the same study, the effects of pTVG-HP in combination with pembrolizumab were studied by FLT PET/CT imaging and different metastases were analyzed (32). Unfortunately, bone metastases were not analyzed in this study due to high background FLT uptake in PET/CT imaging from the proliferating bone marrow. If it would have been possible to image bone metastases, the study would have given important metastasis-specific information.

3.9 Recombinant Ad5 vaccine

A novel Ad5 vaccine uses adenovirus 5 vectors targeting tumor-associated antigens PSA, MUC-1 and brachyury. The first-in-human trial (NCT03481816) was performed in mCRPC patients that needed to have incurable disease with radiographic progression defined either by new or growing bone lesions or growing lymph node disease with increasing PSA levels (33). Seventeen patients were included in the study, of which one patient had a partial response, five had stable disease for over six months, and five patients had confirmed decline in PSA. The study did not outline what metastases the responders had, which would have been helpful for better interpretation of the results. Median PFS was 22 weeks. All patients experienced mounted T cell responses to at least one tumor-associated antigen, whereas about half of the patients mounted immune responses to all three tumor-associated antigens. Surprisingly, despite the promising anti-cancer results, almost all currently active clinical trials of the Ad5 vaccine are related to COVID-19 research.

3.10 Rilimogene glafolivec

Rilimogene glafolivec (PROSTVAC) is a therapeutic cancer vaccine for mCRPC patients (34). It is a combination of two viruses encoding PSA and TRICOM co-stimulatory molecules (CD80), leukocyte function associated antigen-3 (LFA-3) and intracellular adhesion molecule-1 (ICAM-1 or CD54). The patients are first given a vaccinia virus -based vector (rilimogene galvacirepvec, PROSTVAC-V) for priming and later a recombinant fowlpox virus -based vector (rilimogene glafolivec, PROSTVAC-F) for boosting the immunity. A phase III study (NCT01322490) evaluated efficacy of PROSTVAC alone and in combination with GM-CSF over placebo in mCPRC patients. About 75% of the patients had bone metastases in each cohort but there was no effect in OS, and the most common event in patients was radiographic progression and bone pain (35). Combinations with rilimogene glafolivec are currently evaluated in 7 clinical trials for different subsets of prostate cancer.

3.11 Bintrafusp alfa and M9241

Bintrafusp alfa (M7824) is a first-in-class bifunctional agent targeting programmed death ligand 1 (PD-L1) moiety fused with peptide linkers to 'trap' transforming growth factor beta (TGFβ) in the tumor microenvironment (36). In preclinical studies, bintrafusp alfa inhibited breast cancer metastasis to lungs and its effects were more profound than those of PD-L1 or TGFβ alone, and it is also an effective combination partner with chemo- and radiation therapy (37), vaccines (38) and M9241 (NHS-IL12), an immunocytokine composed of two IL-12 heterodimers fused to an antibody with high affinity to DNA (39). Phase I clinical trials in advanced solid tumors have been reported (40, 41).

As the role of TGFβ is well established in regulating growth of bone metastases (42), it would be of interest to evaluate if bintrafusp alfa affects also bone metastasis. A trial evaluating effects of binstrafusp alfa in combination with other therapies including M9241 in mCSPC and mCRPC (NCT04633252) will perform Tc99 imaging to confirm the extent of bone metastases and follow up radiographic response rates and time to radiographic progression with estimated study completion in 2023.

3.12 Vudalimab

Vudalimab (XmAb20717) is a bispecific antibody that engages programmed cell death 1 (PD-1) and cytotoxic T-lymphocyte antigen-4 (CTLA-4) with limited amount of published data available. Results presented in SITC 2020 concluded a preliminary clinical finding of vudalimab in advanced solid tumors (43). This study also included CRPC patients, and 2/7 patients responded to the treatment with a more than 50% decrease in PSA and no progression in bone scans. The effects of vudalimab will be studied in combination with chemo- or targeted therapy in a phase II trial in mCRPC patients (NCT05005728). In this trial, the patients will be categorized into treatment groups based on molecular characteristics of the tumors or previous treatment history. The study will evaluate effects on bone metastases by evaluating rPFS, with expected study completion in 2024.

3.13 Tremelimumab

Tremelimumab is a fully-human IgG2 monoclonal antibody targeting CTLA-4 and directed to treatment of advanced melanoma, prostate, breast, colorectal and renal cancer. Especially in combination with PD-1 targeting antibodies, tremelimumab has produced long-term survival benefits in advanced patients (44). Of interest to this review, tremelimumab has been studied in combination with PD-1 targeting durvalumab in bone metastatic CRPC (45, NCT03204812). rPFS was assessed with CT and Tc-99m-MDP bone scintigraphy, and bone biopsies were collected to evaluate immune cells at baseline and after 2 and 4 doses of treatment. The study reported a rPFS of 3.7 months, and 1-, 2-, and 3-year OS were 96%, 55% and 35%, respectively. Stable disease lasting at least 6 months was observed in 6/25 patients (disease control rate of 35%). Analysis of immune cell subsets in bone metastases showed no difference in T cell populations, but the number of macrophages and neutrophils was increased during the treatment period.

Effects of tremelimumab are currently evaluated in 112 clinical studies in different cancer indications, and it was approved by FDA in combination with durvalumab for unresectable hepatocellular carcinoma in October 2022. Tremelimumab in combination with durvalumab is currently studied in bone metastatic NSCLC patients (46) and metastatic urothelial carcinoma (mUC) (47). In the NSCLC study (NCT03057106), bone metastases were associated with lower OS and PFS in patients, but the treatment had no beneficial effect. The mUC study (NCT02516241) also confirmed that patients with bone metastases had lower OS and PFS, and patients with PD-L1 -high bone metastases treated with tremelimumab, durvalumab or their combination had numerically higher OS than patients with PD-L1 -low bone metastases.

3.14 BMS-986249

BMS-986249 is a probody composed of ipilimumab (anti-CTLA-4 antibody) linked to a proprietary masking peptide that covers the active antigen-binding site of the antibody through a protease-cleavable linker (48). BMS-986249 is currently evaluated in a phase I clinical study (NCT03369223) including patients with advanced cancer in combination with nivolumab. Results published in ESMO 2022 congress demonstrated that regardless of cancer indication, 26/39 patients treated with BMS-986249 received partial response and 16 or 38 out of 64 patients received complete or partial response, respectively, when treated with combination of BMS-986249 and nivolumab (49). The study is currently recruiting patients, and one of the cohorts will be mCRPC patients where bone metastases will be evaluated at inclusion by radionuclide bone scan. The study is expected to complete in 2024.

3.15 MVA-BN Brachyury and epacadostat

MVA-BN Brachyury is a recombinant vaccine under development for the treatment of patients with advanced cancers. Brachyury is a transcription factor expressed in many cancers and associated with metastatic process and chemotherapy resistance (50). The vaccine is modified from two viruses encoding a transgene for brachyury and it induces T cell responses against CEA and MUC1. QuEST1 study (NCT03493945) evaluated effects of MVA-BN Brachyury combined with M7824 (bintrafusp alfa, discussed above), M7824 and ALT-803 (IL-15 superagonist), or M7824, ALT-803 and epacadostat (discussed below) in CRPC patients who had radiologically confirmed bone metastases or PSA progression (51). Results of the QuEST1 study published in ESMO 2020 congress indicated that 4/9 asymptomatic or minimally symptomatic CRPC patients receiving the triple combination of the vaccine, bintrafusp alfa and the IL-15 superagonist sustained PSA responses and 2/4 of them had radiographic response, whereas a similar response was only observed in 1/13 patients receiving the vaccine and bintrafusp alfa (52). Furthermore, analysis of peripheral blood mononuclear cells from these two study groups showed increase in NK cells, TCR diversity and absolute lymphocyte count together with increased serum levels of granzyme B, CD27 and CD40L, indicating an established immune reaction to the vaccination (53). Also, patients who experienced a PSA response had higher numbers of CD4+ and CD8+ cells and decreased number of immunosuppressive cells such as myeloid-derived suppressor cells and monocytes, which could partially explain the observed anti-tumor effects.

Epacadostat is an indoleamine 2,3-dioxygenase (IDO) inhibitor intended to be used for treatment of cancer (54). Results of phase I/II trials for epacadostat (55) and its combination with pembrolizumab (56) in advanced solid tumors have been published. As mentioned above, the effects of epacadostat are evaluated in Arm 3 of QuEST1 trial (NCT03493945) for mCRPC patients with the inclusion criteria metastasis to bone, organs or lymph nodes, and will follow radiographic progression of the disease with expected results by the end of 2023. We have previously performed a preclinical bone metastasis study in triple-negative breast cancer where epacadostat alone or in combination with pembrolizumab had no effect on growth of bone metastases (57). However, these results do not directly translate to prostate cancer bone metastases as they may differ immunologically from breast cancer bone metastases.

3.16 Talabostat mesylate

Talabostat mesylate is a small-molecule inhibitor of dipeptidyl peptidases (DPPs) 4, 8 and 9, and fibroblast activation protein that activates innate immunity (58). Effects of talabostat mesylate were studied in combination with pembrolizumab in a phase II trial in mCRPC patients (NCT03910660). In this study, 40% of the patients had bone metastases, and even after a short 9-week follow-up time, 27% of the patients showed PSA reduction (59). Further results were reported in ASCO genitourinary meeting in 2022 with similar findings, demonstrating that in a mCRPC cohort that included 44% of patients with bone metastases, 23% of all mCRPC patients had complete response and 16% had partial response (60). Even though the data does not yet indicate response rates separately for bone metastatic patients, the observed 40% of patients with bone

metastases will hopefully lead to discussing the issue when the full results of the phase II study are published.

3.17 Dendritic cell vaccine

Radboud University is developing a novel dendritic cell vaccine with subpopulations of myeloid dendritic cells (mDC) and plasmacytoid dendritic cells (pDC) targeting CTAG1B, MAGEC2 and MUC1. Results presented in ASCO Genitourinary Cancers Symposium 2018 reported rPFS data in mCRPC patients with localized, lymph node and bone metastasis positive disease (61). In this trial (NCT02692976) mCRPC patients received either mDC, pDC or combined vaccination and their radiological responses were assessed on 68GA-PSMA-PET-CT and MRI imaging for bone metastases. The results showed that overall, 13/21 patients had no radiological disease progression and at 12 months follow-up time 5/11 patients had stable disease. Mean rPFS was 6.1 months. Results published in ESMO 2019 congress reported that patients who had non-progressive disease had more antigen-specific T cells (IFNγ+) compared to progressed patients (62). rPFS was 18.8 months in patients with high IFNγ+ cells and 5.1 months in patients with low IFNγ+ cells, indicating that immune activation as seen by an elevated amount of IFNγ+ cells would mediate prolonged rPFS in patients.

3.18 MB-105

MB-105 is a prostate stem cell antigen (PSCA) -CAR T cell therapy currently studied in mCRPC. Prostate cancer is an immunologically cold tumor often infiltrated with abundant macrophages, and infiltration of M2 macrophages correlates with metastasis and poor prognosis. To study the effects of MB-105 at preclinical stages, prostate cancer cells were intratibially injected into 'humanized mice' with human immune cells to model the immunosuppressed microenvironment in a bone metastatic disease (63). PD-L1 expression was observed in tumor-associated macrophages infiltrating tumors following the PSCA-CAR T cell therapy. Importantly, treatment with anti-PD-L1 monoclonal antibodies rescued anti-tumor activity of PSCA-CAR T cells in the presence of M2 macrophages, suggesting that PD-L1 is a mediator of M2 macrophage -driven immune suppression in prostate cancer. PSCA-CAR T cell therapy is currently evaluated in a phase 1 clinical trial (NCT03873805) in mCRPC patients with PSCA-positive tumors. Results presented in ASCO Genitourinary Symposium in 2022 (64) indicated that when given with prior lymphodepletion at an optimized dose level, 3/3 patients had stable disease. More patients need to be treated before making conclusions about efficacy of the therapy.

3.19 Reolysin

Pelareorep (Reolysin), a naturally occurring oncolytic reovirus is developed for treatment of cancer. The reovirus infects and kills cancer cells with activated Ras pathway (65). A phase II study (NCT01656538) that included patients with bone metastases showed 7 months improved OS in patients receiving combination of pelareorep and paclitaxel compared to paclitaxel alone (66). A previous study had already indicated safety in patients with advanced solid tumors (67).

Pelareorep received Fast Track Designation from FDA in 2017 for metastatic breast cancer, and its effects are currently evaluated for other metastatic cancers. Pelareorep was studied in mCRPC (NCT01619813) by CT, bone scans and bone biomarkers to evaluate the extent and response on bone metastases (68). The results were negative, and patients receiving pelareorep, docetaxel and prednisone vs patients receiving docetaxel and prednisone had no effect on survival. A recent meta-analysis in advanced or metastatic cancer patients indicated that other oncolytic virotherapies may be more effective than pelareorep (69).

3.20 IMM-101

IMM-101 is a vaccine derived from heat killed mycobacterium and developed for the treatment of cancer, including prostate cancer (70). A summary of case reports of 6 prostate cancer patients treated with IMM-101 demonstrated decreased PSA levels in 3 patients with symptomatic bone metastases after starting IMM-101 treatment (71). Bone metastases remained stable, or decreased in one patient who also received zoledronic acid. In these patients the disease remained stable for 2 to 9 years. These results showed that at least some patients do respond to IMM-101 with a positive response. Current clinical development of IMM-101 seems to be directed to melanoma, pancreatic and colorectal cancers.

3.21 Preclinical-stage assets

Database search identified three preclinical-stage therapies showing effects in bone metastasis models, rAd.DCN, EMU-116 and DUET-02. To the best of our knowledge, no clinical studies have been posted for these therapies up to date.

University of Illinois at Chicago develops an oncolytic adenovirus-expressing decorin, rAd.DCN, for the treatment of cancer. Decorin is a natural inhibitor of TGFβ that has multiple pro-metastatic and immunomodulatory properties (72). Studies of rAd.DCN in breast cancer bone metastasis models indicated that the treatment did not prevent colonization to bones but significantly decreased tumor growth in bone (73).

EMU-116 is an orally bioavailable small-molecule CXCR4 antagonist under development for the treatment of cancer. CXCR4 has been a promising cancer target for years and it is an especially interesting anti-metastatic target as it is one of the factors involved in bone-homing of cancer cells (74). Recent preclinical data shows that EMU-116 was effective in a prostate cancer bone metastasis model when combined with docetaxel (75).

DUET-02 (CpG-STAT3ASO) is a Signal Transducer and Activator of Transcription 3 (STAT3) antisense oligonucleotide

(STAT3ASO) conjugated to immunostimulatory CpG oligodeoxynucleotides that is currently being explored for the treatment of cancer. STAT3 is an oncogenic transcription factor that plays an important role in both prostate cancer progression and sustaining immune suppression in the tumor microenvironment. At preclinical stages, DUET-02 effectively prevented tumor growth and improved survival in an intratibial (tumor growing in bone) bone metastasis model (76).

4 Discussion

Based on the database search we identified 24 therapies in development that were evaluated in the context of bone metastasis. It is challenging to draw conclusions of which therapies could be most successful in the future, because these experimental therapies are in different stages of development, they have been tested in different patient populations, different modalities have been studied, and some of them are evaluated in combination with other therapies.

Three of the identified therapies were specifically related to tumor growing in bone metastatic microenvironment and their clinical evaluation followed outcomes in bone metastatic patients with relevant outcome measurements. These therapies included a first-in-class platinum-pyrophosphate conjugate small molecule imifoplatin (see chapter 4.2), an autologous PSMA-targeting CAR-T therapy P-PSMA-101 (chapter 4.3), and a B7-H3 targeting ADC MGC018 (chapter 4.5). Imifoplatin has affinity for bone (osteotropism) ensuring specific accumulation to bone metastases. It causes immunogenic cell death leading to recruitment of tumor-infiltrating lymphocytes (17) and it has been studied in combination with anti-PD-L1 in mCRPC patients, highlighting the rationale for the studied combination (18 ASCO). P-PSMA-101 has TSCM phenotype (19), which has been considered important for its bone marrow homing, surviving and tumor eliminating properties in mCRPC patients with bone metastases. The properties of bone homing and survival can be considered essential features for an effective therapy. However, despite of the promising phase I results, winding down was recently announced for this autologous CAR-T program and transition to an allogeneic platform. B7-H3 is a cell surface immunomodulatory glycoprotein expressed during prostate cancer progression and in the majority of patients with mCRPC (77). Interestingly, B7-H3 has been reported also to affect differentiation and activity of bone-forming osteoblast cells that are overactive in osteoblastic bone metastases typical for prostate cancer (26, 27). This indicates that targeting B7-H3 could potentially prevent the formation of pathologic osteoblastic bone lesions in mCRPC, currently an unmet medical need. Taking into account B7-H3 expression in tumor and immune cells with potential activity also in osteoblasts, B7-H3 can be considered as a potential OIO target in prostate cancer patients with bone metastases.

Some other clinical-stage therapies identified in this review have shown potential efficacy on bone metastases, including for example MVI-118, the dendritic cell vaccine and pasotuximab. However, comparison of these therapies is very difficult as the studies evaluated responders differently and used different outcomes, for example PFS or OS that do not evaluate efficacy for bone metastases as such. It is also important to acknowledge that not all therapies have shown good effects on bone metastases. For example, the study of rilimogene glafolivec addressed efficacy on bone metastases but failed to show effects on survival, bone metastasis progression or bone pain. Furthermore, different bone metastatic cancers can have differential efficacy on a therapy as shown in the case of reolysin that received fast track designation from the FDA for metastatic breast cancer but showed no efficacy on metastatic prostate cancer when both studies included patients with bone metastases. The immune microenvironment can be very different in breast and prostate cancer bone metastases, being affected by the osteolytic or osteoblastic nature, respectively, which could explain the results. These findings highlight the heterogeneity of bone metastases and the need to study effects on different cancer types separately, and not only rely on data obtained from one cancer type.

This data search resulted only in three preclinical-stage immunotherapies that have been tested in preclinical bone metastasis models. These therapies include rAD.DCN, DUET-02, and EMU-116 in combination with docetaxel that decreased bone metastasis growth in animal models. None of these experimental therapies appear to have proceeded to clinical trials yet. It will be interesting to see how the preclinical efficacy translates to clinical effectiveness on bone metastases. On the other hand, almost none of the clinical-stage therapies listed in this review have published results available on preclinical data supporting continuation to clinical studies for treatment of patients with bone metastases, with the exception of MB-105 that has reported data available from bone metastasis animal models and early data from a phase 1 clinical trial. Some other drugs had data showing effects for inhibiting or decreasing growth of lymph node or lung metastases, but these metastases are very different from bone metastases and results obtained on other metastases are usually not translatable to bone metastases. One reason for the lack of preclinical studies in bone metastasis models could be the special expertise needed to carry out studies in these technically challenging models (78). We have recently published results on how effects of immunotherapies can be addressed in proper metastasis models (79, 80) and we hope that metastasis models would be extensively used at preclinical development stages to confirm the efficacy before initiating clinical studies. This approach would lead to selecting most promising drug candidates for bone metastases to proceed to clinical trials, which would decrease the currently very high 97% failure rate in oncology clinical trials (81), and allow faster entrance of truly efficacious new oncology drugs to the market.

Considering that bone metastases are a high unmet medical need, it is surprising how few relevant studies finally address the efficacy of novel therapies on bone metastases either in preclinical or clinical studies. In fact, the efficacy of novel therapies on bone metastases should be specifically addressed as bone metastases are associated with very low response rates to therapies and shorter PFS and OS rates (46). For this reason, it has been proposed that bone metastases should be considered as a new important stratification factor for clinical trials evaluating effects of immunotherapies (46). Guidance on how to study and evaluate effects of therapies on bone metastases in clinical trials is not well established. The RECIST criteria often advise to exclude bone metastases in monitoring the response of experimental therapies. PCWG3 criteria, that are often used to evaluate responses in prostate

cancer, advise bone imaging as part of evaluating effects on bone metastases, but states that more data is needed to understand the data collected by imaging tools in evaluating responses on bone metastases. In fact, results of bone scans can be sometimes misleading. New bone scan lesions may represent osteoblastic bone healing defined as bone pseudoprogression and mistakenly diagnosed as disease progression (82). Bone-related biomarkers have been developed and used in bone-related diseases for a long time, but they remain mainly unexplored with bone metastases (83). In our opinion, bone turnover markers should be more widely studied and used in clinical trials for early detection of bone metastases and evaluating efficacy of therapies. Furthermore, there are some promising developments for bone metastasis -specific biomarkers such as DKK-1 (84). The use of hormone-deprivation therapies, either anti-estrogens or anti-androgens, induces bone changes in patients, further complicating the analysis of bone metastasis results. These and other complexities in the follow-up together with the limited guidance are probably among the main reasons why there are so few studies evaluating specific effects on bone metastases. In this review we identified concrete evidence on these issues. The initial data search was performed for breast and prostate cancer, but a more detailed evaluation of the data showed that only clinical trials in prostate cancer studied effects on bone metastases. Besides breast and prostate cancer, many other common cancers such as lung, colon and bladder cancer and melanoma have a high incidence of bone metastases, and bone metastasis -specific evaluation should be applied to all these cancer indications in studies that include bone metastatic patients.

This review provides important timely insights to new and emerging immunotherapies with evidence for effects on bone metastases. Publication strategies of drug development companies heavily depend on intellectual property right issues. Therefore, studies are often published during later development phases and data sources are important tools to follow real-time drug development. Most of the data that was used for preparing this manuscript was obtained from non-peer-reviewed sources such as meeting abstracts, and readers should consider this when making interpretations of the data presented. We previously performed a search for clinical bone metastasis studies and immuno-oncology drug development publications and concluded that the number of peer-reviewed publications in this area is very low (85). However, considering importance of this topic and knowing there are opportunities in development, we wanted to perform an expanded data search using a database with a tailor-made filter for finding therapies with data available for bone metastasis from more abundant information sources such as news, patents and meeting abstracts that include latest published data available.

In summary, this review provides insights to novel immuno-oncology drug development for bone metastasis. Because OIO is still a largely unexplored area, conducting clinical trials in bone metastasis setting is challenging. Publication practices during drug development provide their own challenges for obtaining information, but we were able to identify novel therapies with targets or properties relevant to bone metastasis with promising data obtained during early-stage development. According to this review, bone metastases can be approached using different modalities and the tumor microenvironment in bone provides many potential targets in immune, bone and tumor cells. In the future, we will hopefully see more therapies with bone metastasis specific targets that have provided both preclinical and clinical proof-of-concept for efficacy on bone metastases.

Author contributions

TK: writing the first version of the manuscript, manuscript modification and finalization. GM: adaptation of the database machine learning algorithms to identify associations and relationships to bone metastasis within IO drug trials. RA: subject expertise on the database, commenting and confirming that statements related to the database are correctly presented. JH: commenting and modifying the manuscript, language corrections. JB: concept for the manuscript, commenting and confirming that the data is properly presented. All authors contributed to the article and approved the submitted version.

Conflict of interest

Authors GM and RA are employees of BioSeeker Group AB who has developed the 1stOncology database that was used to generate the data described in the manuscript. Authors TK and JH are employed by the company OncoBone Ltd.

The remaining authors declare that the research was conducted in the absence of any commercial or financial relationships that could be construed as a potential conflict of interest.

Publisher's note

References

1. Coleman RE, Croucher PI, Padhani AR, Clézardin P, Chow E, Fallon M, et al. Bone metastases. *Nat Rev Dis Primers* (2020) 6(1):83. doi: 10.1038/s41572-020-00216-3

2. Svensson E, Christiansen CF, Ulrichsen SP, Rørth MR, Sørensen HT. Survival after bone metastasis by primary cancer type: a Danish population-based cohort study. *BMJ Open* (2017) 7(9):e016022. doi: 10.1136/bmjopen-2017-016022

3. Yang M, Liu C, Yu X. Skeletal-related adverse events during bone metastasis of breast cancer: current status. *Discovery Med* (2019) 27(149):211–20.

4. Liu C, Wang M, Xu C, Li B, Chen J, Chen J, et al. Immune checkpoint inhibitor therapy for bone metastases: specific microenvironment and current situation. *J Immunol Res* (2021) 2021:8970173. doi: 10.1155/2021/8970173

5. Kfoury Y, Baryawno N, Severe N, Mei S, Gustafsson K, Hirz T, et al. Human prostate cancer bone metastases have an actionable immunosuppressive microenvironment. *Cancer Cell* (2021) 39(11):1464–1478.e8. doi: 10.1016/j.ccell.2021.09.005

6. Xiang L, Gilkes DM. The contribution of the immune system in bone metastasis pathogenesis. *Int J Mol Sci* (2019) 20(4):999. doi: 10.3390/ijms20040999

7. Tahara RK, Brewer TM, Theriault RL, Ueno NT. Bone metastasis of breast cancer. *Adv Exp Med Biol* (2019) 1152:105–29. doi: 10.1007/978-3-030-20301-6_7

8. Owen KL, Parker BS. Beyond the vicious cycle: the role of innate osteoimmunity, automimicry and tumor-inherent changes in dictating bone metastasis. *Mol Immunol* (2019) 110:57–68. doi: 10.1016/j.molimm.2017.11.023

9. Li H, Hong S, Qian J, Zheng Y, Yang J, Yi Q. Cross talk between the bone and immune systems: osteoclasts function as antigen-presenting cells and activate CD4+ and CD8+ T cells. *Blood* (2010) 116(2):210–7. doi: 10.1182/blood-2009-11-255026

10. Monteiro AC, Bonomo A. CD8+ T cells from experimental *in situ* breast carcinoma interfere with bone homeostasis. *Bone* (2021) 150:116014. doi: 10.1016/j.bone.2021.116014

11. Kähkönen TE, Halleen JM, Bernoulli J. Osteoimmuno-oncology: therapeutic opportunities for targeting immune cells in bone metastasis. *Cells* (2021) 10(6):1529. doi: 10.3390/cells10061529

12. Moseley KF, Naidoo J, Bingham CO, Carducci MA, Forde PM, Gibney GT, et al. Immune-related adverse events with immune checkpoint inhibitors affecting the skeleton: a seminal case series. *J Immunother Cancer* (2018) 6(1):104. doi: 10.1186/s40425-018-0417-8

13. Angelopoulou F, Bogdanos D, Dimitroulas T, Sakkas L, Daoussis D. Immune checkpoint inhibitor-induced musculoskeletal manifestations. *Rheumatol Int* (2021) 41(1):33–42. doi: 10.1007/s00296-020-04665-7

14. Hofbauer LC, Bozec A, Rauner M, Jakob F, Perner S, Pantel K. Novel approaches to target the microenvironment of bone metastasis. *Nat Rev Clin Oncol* (2021) 18(8):488–505. doi: 10.1038/s41571-021-00499-9

15. Ames TD, Sharik ME, Rather GM, Hochart G, Bonnel D, Linehan S, et al. Translational research of PT-112, a clinical agent in advanced phase I development: evident bone tropism, synergy *In vitro* with bortezomib and lenalidomide , and potent efficacy in the Vk*MYC mouse model of multiple myeloma. *Blood* (2017) 130 (Supplement 1):1797.

16. Bryce AH, Dronca RS, Costello BA, Infante JR, Ames TD, Jimeno J, et al. PT-112 in advanced metastatic castrate-resistant prostate cancer (mCRPC), as monotherapy or in combination with PD-L1 inhibitor avelumab: findings from two phase I studies. *J Clin Oncol* (2020) 38(suppl 6; abstr 83). doi: 10.1200/JCO.2020.38.6_suppl.83

17. Karp DD, Camidge DR, Infante JR, Ames TD, Price MR, Jimeno J, et al. Phase I study of PT-112, a novel pyrophosphate-platinum immunogenic cell death inducer, in advanced solid tumours. *EClinicalMedicine* (2022) 49:101430. doi: 10.1016/j.eclinm.2022.101430

18. Bryce AH, Dronca RS, Costello BA, Aparicio A, Subudhi SK, O'Donnell JF, et al. A phase 1b study of novel immunogenic cell death inducer PT-112 plus PD-L1 inhibitor avelumab in metastatic castrate-resistant prostate cancer (mCRPC) patients. *J Clin Oncol* (2021) 39(suppl 15; abstr e17025). doi: 10.1200/JCO.2021.39.15_suppl.e17025

19. Slovin SF, Dorff TB, Falchook GS, Wei XX, Gao X, McKay RR, et al. Phase 1 study of p-PSMA-101 CAR-T cells in patients with metastatic castration-resistant prostate cancer (mCRPC). *J Clin Oncol* (2022) 40(suppl 6; abstr 98). doi: 10.1200/JCO.2022.40.6_suppl.098

20. Hummel HD, Kufer P, Grüllich C, Seggewiss-Bernhardt R, Deschler-Baier B, Chatterjee M, et al. Pasotuxizumab, a BiTE® immune therapy for castration-resistant prostate cancer: phase I, dose-escalation study findings. *Immunotherapy* (2021) 13(2):125–41. doi: 10.2217/imt-2020-0256

21. Scribner JA, Brown JG, Son T, Chiechi M, Li P, Sharma S, et al. Preclinical development of MGC018, a duocarmycin-based antibody-drug conjugate targeting B7-H3 for solid cancer. *Mol Cancer Ther* (2020) 19(11):2235–44. doi: 10.1158/1535-7163.MCT-20-0116

22. Scribner JA, Chiechi M, Li P, Son T, Hooley J, Li Y, et al. MGC018, a duocarmycin-based antibody-drug conjugate targeting B7-H3, exhibits immunomodulatory activity and enhanced antitumor activity in combination with checkpoint inhibitors. *Cancer Research* (2020) 80(16, Suppl):Abstract 5203.

23. Shenderov E, Mallesara GHG, Wysocki PJ, Xu W, Ramlau R, Weickhardt AJ, et al. 620P - MGC018, an anti-B7-H3 antibody-drug conjugate (ADC), in patients with advanced solid tumors: preliminary results of phase I cohort expansion. *Ann Oncol* (2021) 32(suppl_5):S626–77. doi: 10.1016/annonc/annonc702

24. Wang L, Kang FB, Zhang GC, Wang J, Xie MF, Zhang YZ. Clinical significance of serum soluble B7-H3 in patients with osteosarcoma. *Cancer Cell Int* (2018) 18:115. doi: 10.1186/s12935-018-0614-z

25. Wang L, Zhang Q, Chen W, Shan B, Ding Y, Zhang G, et al. B7-H3 is overexpressed in patients suffering osteosarcoma and associated with tumor aggressiveness and metastasis. *PloS One* (2013) 8(8):e70689. doi: 10.1371/journal.pone.0070689

26. Suh WK, Wang SX, Jheon AH, Moreno L, Yoshinaga SK, Ganss B, et al. The immune regulatory protein B7-H3 promotes osteoblast differentiation and bone mineralization. *Proc Natl Acad Sci U S A* (2004) 101(35):12969–73. doi: 10.1073/pnas.0405259101

27. Xu L, Zhang G, Zhou Y, Chen Y, Xu W, Wu S, et al. Stimulation of B7-H3 (CD276) directs the differentiation of human marrow stromal cells to osteoblasts. *Immunobiology* (2011) 216(12):1311–7. doi: 10.1016/j.imbio.2011.05.013

28. Patel MR, Johnson ML, Falchook GS, Doi T, Friedman CF, Piha-Paul SA, et al. DS-7300 (B7-H3 DXd-ADC) in patients (pts) with metastatic castration-resistant prostate cancer (mCRPC): a subgroup analysis of a phase 1/2 multicenter study. *J Clin Oncol* (2022) 40(suppl 6; abstr 87). doi: 10.1200/JCO.2022.40.6_suppl.087

29. Kyriakopoulos CE, Eickhoff JC, Ferrari AC, Schweizer MT, Wargowski E, Olson BM, et al. Multicenter phase I trial of a DNA vaccine encoding the androgen receptor ligand-binding domain (pTVG-AR, MVI-118) in patients with metastatic prostate cancer. *Clin Cancer Res* (2020) 26(19):5162–71. doi: 10.1158/1078-0432.CCR-20-0945

30. Wargowski E, Johnson LE, Eickhoff JC, Delmastro L, Staab MJ, Liu G, et al. Prime-boost vaccination targeting prostatic acid phosphatase (PAP) in patients with metastatic castration-resistant prostate cancer (mCRPC) using sipuleucel-T and a DNA vaccine. *J Immunother Cancer* (2018) 6(1):21. doi: 10.1186/s40425-018-0333-y

31. McNeel DG, Eickhoff JC, Wargowski E, Johnson LE, Kyriakopoulos CE, Emamekhoo H, et al. Phase 2 trial of T-cell activation using MVI-816 and pembrolizumab in patients with metastatic, castration-resistant prostate cancer (mCRPC). *J Immunother Cancer* (2022) 10(3):e004198. doi: 10.1136/jitc-2021-004198

32. Scarpelli M, Zahm C, Perlman S, McNeel DG, Jeraj R, Liu G. FLT PET/CT imaging of metastatic prostate cancer patients treated with pTVG-HP DNA vaccine and pembrolizumab. *J Immunother Cancer* (2019) 7(1):23. doi: 10.1186/s40425-019-0516-1

33. Bilusic M, McMahon S, Madan RA, Karzai F, Tsai YT, Donahue RN, et al. Phase I study of a multitargeted recombinant Ad5 PSA/MUC-1/brachyury-based immunotherapy vaccine in patients with metastatic castration-resistant prostate cancer (mCRPC). *J Immunother Cancer* (2021) 9(3):e002374. doi: 10.1136/jitc-2021-002374

34. Lasek W, Zapała Ł. Therapeutic metastatic prostate cancer vaccines: lessons learnt from urologic oncology. *Cent Eur J Urol* (2021) 74(3):300–7. doi: 10.5173/ceju.2021.0094

35. Gulley JL, Borre M, Vogelzang NJ, Ng S, Agarwal N, Parker S, et al. Phase III trial of PROSTVAC in asymptomatic or minimally symptomatic metastatic castration-resistant prostate cancer. *J Clin Oncol* (2019) 37:1051–61. doi: 10.1200/JCO.18.02031

36. Gameiro SR, Strauss J, Gulley JL, Schlom J. Preclinical and clinical studies of bintrafusp alfa, a novel bifunctional anti-PD-L1/TGFβRII agent: current status. *Exp Biol Med (Maywood)* (2022) 247(13):1124–34. doi: 10.1177/15353702221089910

37. Lan Y, Zhang D, Xu C, Hance KW, Marelli B, Qi J, et al. Enhanced preclinical antitumor activity of M7824, a bifunctional fusion protein simultaneously targeting PD-L1 and TGF-β. *Sci Transl Med* (2018) 10(424):eaan5488. doi: 10.1126/scitranslmed.aan5488

38. Knudson KM, Hicks KC, Luo X, Chen JQ, Schlom J, Gameiro SR. M7824, a novel bifunctional anti-PD-L1/TGFβ trap fusion protein, promotes anti-tumor efficacy as monotherapy and in combination with vaccine. *Oncoimmunology* (2018) 7(5):e1426519. doi: 10.1080/2162402X.2018.1426519

39. Xu C, Marelli B, Qi J, Qin G, Yu H, Wang H, et al. NHS-IL12 and bintrafusp alfa combination therapy enhances antitumor activity in preclinical cancer models. *Transl Oncol* (2022) 16:101322. doi: 10.1016/j.tranon.2021.101322

40. Strauss J, Heery CR, Schlom J, Madan RA, Cao L, Kang Z, et al. Phase I trial of M7824 (MSB0011359C), a bifunctional fusion protein targeting PD-L1 and TGFβ, in advanced solid tumors. *Clin Cancer Res* (2018) 24(6):1287–95. doi: 10.1158/1078-0432.CCR-17-2653

41. Doi T, Fujiwara Y, Koyama T, Ikeda M, Helwig C, Watanabe M, et al. Phase I study of the bifunctional fusion protein bintrafusp Alfa in Asian patients with advanced solid tumors, including a hepatocellular carcinoma safety-assessment cohort. *Oncologist* (2020) 25(9):e1292–302. doi: 10.1634/theoncologist.2020-0249

42. Juárez P, Guise TA. TGF-β in cancer and bone: implications for treatment of bone metastases. *Bone* (2011) 48(1):23–9. doi: 10.1016/j.bone.2010.08.004

43. Shum E, Daud A, Reilley M, Najjar Y, Thompson J, Baranda J, et al. Preliminary safety, pharmacokinetics/pharmacodynamics, and antitumor activity of XmAb20717, a PD-1 x CTLA-4 bispecific antibody, in patients with advanced solid tumors. *JITC* (2020) 8(3):A247–8. doi: 10.1136/jitc-2020-SITC2020.0407

44. Comin-Anduix B, Escuin-Ordinas H, Ibarrondo FJ. Tremelimumab: research and clinical development. *Onco Targets Ther* (2016) 9:1767–76. doi: 10.2147/OTT.S65802

45. Subudhi SK, Siddiqui BA, Aparicio AM, Yadav SS, Basu S, Chen H, et al. Combined CTLA-4 and PD-L1 blockade in patients with chemotherapy-naïve metastatic castration-resistant prostate cancer is associated with increased myeloid and neutrophil immune subsets in the bone microenvironment. *J Immunother Cancer* (2021) 9(10):e002919. doi: 10.1136/jitc-2021-002919

46. Leitzel K, Ali AM, Ding K, Leighl NB, Badillo FEV, Gaudreau P-O, et al. Treatment with or without chemotherapy in high-risk, stage IVA/B NSCLC. *J Clin Oncol* (2022) 40(16_suppl):9067–7. doi: 10.1200/JCO.2022.40.16_suppl.9067

47. Stecca C, Abdeljalil O, Lu C, Zhang H, Goluboff ET, Sridhar SS. Prognostic impact of bone metastasis in patients with metastatic urothelial carcinoma (mUC) treated with durvalumab (D) with or without tremelimumab (T) in the DANUBE study. *J Clin Oncol* (2022) 40(16_suppl):4564–4. doi: 10.1200/JCO.2022.40.16_suppl.4564

48. Engelhardt J, Akter R, Loffredo J, Bezman N, So P, Tipton K, et al. Preclinical characterization of novel anti-CTLA-4 prodrug antibodies with an enhanced therapeutic index. *Cancer Research* (2020) 80(16, Suppl):Abstract 4551.

49. Gutierrez M, Friedman CF, Long GV, Ascierto PA, Melero I, Richards D, et al. 740P - anti-cytotoxic T-lymphocyte antigen-4 (CTLA 4) probody BMS-986249 ±

nivolumab (NIVO) in patients (pts) with advanced cancers: updated phase I results. *Ann Oncol* (2022) 33(suppl_7):S331–55. doi: 10.1016/annonc/annonc1058

50. Collins JM, Donahue RN, Tsai YT, Manu M, Palena C, Gatti-Mays ME, et al. Phase I trial of a modified vaccinia Ankara priming vaccine followed by a fowlpox virus boosting vaccine modified to express brachyury and costimulatory molecules in advanced solid tumors. *Oncologist* (2020) 25(7):560–e1006. doi: 10.1634/theoncologist.2019-0932

51. Redman JM, Steinberg SM, Gulley JL. Quick efficacy seeking trial (QuEST1): a novel combination immunotherapy study designed for rapid clinical signal assessment metastatic castration-resistant prostate cancer. *J Immunother Cancer* (2018) 6(1):91. doi: 10.1186/s40425-018-0409-8

52. Redman JM, Madan RA, Karzai F, Bilusic M, Cordes L, Marte J, et al. Efficacy of BN-brachyury (BNVax) + bintrafusp alfa (BA) + N-803 in castration-resistant prostate cancer (CRPC): Results from a preliminary analysis of the Quick Efficacy Seeking Trial (QuEST1). *Annals of Oncol* (2020) 31(Suppl 4):Abstract 616MO.

53. Toney N, Tsai Y, Redman J, Gulley J, Schlom J, Donahue R. 582 immune correlates from QuEST1 in men with castration-resistant prostate cancer. *J ImmunoTherapy Cancer* (2021) 9. doi: 10.1136/jitc-2021-SITC2021.582

54. Prendergast GC, Malachowski WJ, Mondal A, Scherle P, Muller AJ. Indoleamine 2,3-dioxygenase and its therapeutic inhibition in cancer. *Int Rev Cell Mol Biol* (2018) 336:175–203. doi: 10.1016/bs.ircmb.2017.07.004

55. Beatty GL, O'Dwyer PJ, Clark J, Shi JG, Bowman KJ, Scherle PA, et al. First-in-Human phase I study of the oral inhibitor of indoleamine 2,3-Dioxygenase-1 epacadostat (INCB024360) in patients with advanced solid malignancies. *Clin Cancer Res* (2017) 23(13):3269–76. doi: 10.1158/1078-0432.CCR-16-2272

56. Mitchell TC, Hamid O, Smith DC, Bauer TM, Wasser JS, Olszanski AJ, et al. Epacadostat plus pembrolizumab in patients with advanced solid tumors: phase I results from a multicenter, open-label phase I/II trial (ECHO-202/KEYNOTE-037). *J Clin Oncol* (2018) 36(32):3223–30. doi: 10.1200/JCO.2018.78.9602

57. Kähkönen TE, Suominen MI, Mäki-Jouppila JH, Halleen JM, Bernoulli J. Efficacy of anti-PD-1, IDO inhibitor, chemotherapy and bone-targeting agent on tumor growth in a syngeneic bone metastasis model of triple-negative breast cancer. *Cancer Res* (2020) 80(16, Suppl):Abstract 5026.

58. Cunningham CC. Talabostat. *Expert Opin Investig Drugs* (2007) 16(9):1459–65. doi: 10.1517/13543784.16.9.1459

59. Monk P, Zhang J, Costin D, Petrylak DP, Tagawa ST, Karsh LI, et al. BXCL701 - 1st-in-class oral activator of systemic innate immunity-combined with pembrolizumab, in men with metastatic castration-resistant prostate cancer (mCRPC): phase II results. *Ann Oncol* (2021) 32(suppl_5):S626–77. doi: 10.1016/annonc/annonc702

60. Zhang Y, Liu C, Wang T, Kong F, Zhang H, Yi J, et al. Therapeutic effects of mesenchymal stem cells loaded with oncolytic adenovirus carrying decorin on a breast cancer lung metastatic mouse model. *Mol Ther Oncolytics* (2022) 24:486–96. doi: 10.1016/j.omto.2022.01.007

61. Westdorp H, van Oort IM, Creemers JHA, Schreibelt G, Mehra N, de Goede AL, et al. Myeloid and plasmacytoid dendritic cell vaccinations for castration-resistant prostate cancer patients. *J Clin Oncol* (2018) 36(suppl 6S; abstr 219). doi: 10.1200/JCO.2018.36.6_suppl.219

62. Creemers J, Westdorp H, van Oort I, Schreibelt G, Gorris M, Mehra N, et al. 1523 - natural dendritic cell vaccinations generate immune responses that correlate with clinical outcome in patients with chemo-naive castration-resistant prostate cancer. *Ann Oncol* (2019) 30(suppl_5):v475–532. doi: 10.1093/annonc/mdz253

63. Yamaguchi Y, Gibson J, Ou K, Priceman S. M2 macrophage-mediated immune suppression of chimeric antigen receptor T cells *via* PD-L1 signaling in prostate cancer. *J Immunother Cancer* (2021) 9(Suppl 2):Abstract 224. doi: 10.1136/jitc-2021-SITC2021.224

64. Dorff TB, Blanchard S, Martirosyan H, Adkins L, Dhapola G, Moriarty A, et al. Phase 1 study of PSCA-targeted chimeric antigen receptor (CAR) T cell therapy for metastatic castration-resistant prostate cancer (mCRPC). *J Clin Oncol* (2022) 40(suppl 6; abstr 91). doi: 10.1200/JCO.2022.40.6_suppl.091

65. Stoeckel J, Hay JG. Drug evaluation: reolysin–wild-type reovirus as a cancer therapeutic. *Curr Opin Mol Ther* (2006) 8(3):249–60.

66. Bernstein V, Ellard SL, Dent SF, Tu D, Mates M, Dhesy-Thind SK, et al. A randomized phase II study of weekly paclitaxel with or without pelareorep in patients with metastatic breast cancer: final analysis of Canadian cancer trials group IND.213. *Breast Cancer Res Treat* (2018) 167(2):485–93. doi: 10.1007/s10549-017-4538-4

67. Gollamudi R, Ghalib MH, Desai KK, Chaudhary I, Wong B, Einstein M, et al. Intravenous administration of reolysin, a live replication competent RNA virus is safe in patients with advanced solid tumors. *Invest New Drugs* (2010) 28(5):641–9. doi: 10.1007/s10637-009-9279-8

68. Eigl BJ, Chi K, Tu D, Hotte SJ, Winquist E, Booth CM, et al. A randomized phase II study of pelareorep and docetaxel or docetaxel alone in men with metastatic castration resistant prostate cancer: CCTG study IND 209. *Oncotarget* (2018) 9 (8):8155–64. doi: 10.18632/oncotarget.24263

69. Xie R, Bi X, Shang B, Zhou A, Shi H, Shou J. Efficacy and safety of oncolytic viruses in advanced or metastatic cancer: a network meta-analysis. *Virol J* (2021) 18 (1):158. doi: 10.1186/s12985-021-01630-z

70. Stavrinides V, Dalgleish A, Copier JP, Moore CM. Mycobacterial immunotherapy for prostate cancer: where can we go from here? *Nat Rev Urol* (2020) 17(4):189–90. doi: 10.1038/s41585-020-0283-2

71. Dalgleish AG, Liu WM. The role of immune modulation and anti-inflammatory agents in the management of prostate cancer: a case report of six patients. *Oncol Lett* (2022) 24(2):247. doi: 10.3892/ol.2022.13367

72. Zhang J, Aggarwal RR, Tagawa ST, Linch MD, Petrylak DP, Costin D, et al. BXCL701: first-in-class oral activator of systemic innate immunity combined with pembrolizumab, in patients with metastatic castration-resistant prostate cancer (mCRPC) of adenocarcinoma phenotype–phase 2a results. *J Clin Oncol* (2022) 40 (6_suppl):125–5. doi: 10.1200/JCO.2022.40.6_suppl.125

73. Yang Y, Xu W, Neill T, Hu Z, Wang CH, Xiao X, et al. Systemic delivery of an oncolytic adenovirus expressing decorin for the treatment of breast cancer bone metastases. *Hum Gene Ther* (2015) 26(12):813–25. doi: 10.1089/hum.2015.098

74. Chatterjee S, Behnam Azad B, Nimmagadda S. The intricate role of CXCR4 in cancer. *Adv Cancer Res* (2014) 124:31–82. doi: 10.1016/B978-0-12-411638-2.00002-1

75. Miller EJ, Sun CQ, Gregorova P, Jecs E, Tahirovic YA, Wilson RJ, et al. Orally bioavailable small molecule CXCR4 antagonists with enhanced efficacy in mouse models of genitourinary cancers. *Cancer Res* (2022) 82(12, Suppl):Abstract 2649.

76. Moreira D, Adamus T, Zhao X, Su YL, Zhang Z, White SV, et al. STAT3 inhibition combined with CpG immunostimulation activates antitumor immunity to eradicate genetically distinct castration-resistant prostate cancers. *Clin Cancer Res* (2018) 24(23):5948–62. doi: 10.1158/1078-0432.CCR-18-1277

77. Guo C, Figueiredo I, Gurel B, Neeb A, Seed G, Crespo M, et al. B7-H3 as a therapeutic target in advanced prostate cancer. *Eur Urol* (2023) 83(3):224–38. doi: 10.1016/j.eururo.2022.09.004

78. Kähkönen TE, Bernoulli J, Halleen JM, Suomienen M. Novel and conventional preclinical models to investigate bone metastasis. *Curr Mol Bio Rep* (2019) 5:48–54. doi: 10.1007/s40610-019-0114-5

79. Kähkönen TE, Halleen JM, Bernoulli J. Immunotherapies and metastatic cancers: understanding utility and predictivity of human immune cell engrafted mice in preclinical drug development. *Cancers (Basel)* (2020) 12(6):1615. doi: 10.3390/cancers12061615

80. Kähkönen TE, Halleen JM, Bernoulli J. Preclinical osteoimmuno-oncology models to study effects of immunotherapies on bone metastasis. In: *Animal Models for the Development of Cancer Immunotherapy*. Hoboken (NJ), USA: John Wiley & Sons, Inc (2022). p. 167–209.

81. Wong CH, Siah KW, Lo AW. Estimation of clinical trial success rates and related parameters. *Biostatistics* (2019) 20(2):273–86. doi: 10.1093/biostatistics/kxx069

82. Lin M, Jin Y, Yang Z, Hu X, Zhang J. Determination and clinical significance of bone pseudoprogression in hormone receptor-positive metastatic breast cancer. *Ther Adv Med Oncol* (2021) 13:17588359211022881. doi: 10.1177/17588359211022881

83. Yamamichi G, Kato T, Yumiba S, Tomiyama E, Koh Y, Nakano K, et al. Diagnostic and prognostic significance of tartrate-resistant acid phosphatase type 5b in newly diagnosed prostate cancer with bone metastasis: a real-world multi-institutional study. *Int J Urol* (2022) 28. doi: 10.1111/iju.15063

84. Shi T, Liang K, Zhou X, Song X, Wang H, Zhang Y, et al. 1382 DKK1 is a biomarker and immunotherapeutic target for bone metastases in malignant cancers. *J ImmunoTherapy Cancer* (2022) 10. doi: 10.1136/jitc-2022-SITC2022.1382

85. Kähkönen TE, Halleen JM, Bernoulli J. Limited data from clinical trials assessing immunotherapy effects on bone metastases. *Cancer Res* (2021) 81(13, Suppl):Abstract 2870.

Frontiers in Immunology

Explores novel approaches and diagnoses to treat immune disorders.

The official journal of the International Union of Immunological Societies (IUIS) and the most cited in its field, leading the way for research across basic, translational and clinical immunology.

Discover the latest Research Topics

See more →

Frontiers

Avenue du Tribunal-Fédéral 34
1005 Lausanne, Switzerland
frontiersin.org

Contact us

+41 (0)21 510 17 00
frontiersin.org/about/contact